STRUCTURAL EFFECTS OF AMMONIUM AND HYDRONIUM IN JAROSITE MINERALS

HENRY JOSEPH SPRATT

Bachelor of Applied Science (Honours, Chemistry)

A thesis submitted in fulfilment of the requirements for the degree of Doctor of Philosophy

School of Chemistry, Physics and Mechanical Engineering

Science and Engineering Faculty

Queensland University of Technology

2015

“Some men are born mediocre, some men achieve mediocrity, and some men have mediocrity thrust upon them.”

Joseph Heller

ABSTRACT

Various crystal structure models for hydronium jarosite [$H_3OFe_3(SO_4)_2(OH)_6$] and ammoniojarosite [$NH_4Fe_3(SO_4)_2(OH)_6$] were refined and compared. There was no evidence for a lowering of the space group symmetry from $R\bar{3}m$ that has been suggested but infrequently modelled by previous studies. After successful location of all hydrogen atoms from difference Fourier methods, it was found the hydronium and ammonium ions are disordered over at least two orientations, either statically or dynamically; this disorder ensures there is no loss of symmetry compared to other jarosite minerals when averaged over time and space.

While adequate crystal structures were determined for hydronium jarosite and ammoniojarosite, they were not appropriate for vibrational spectroscopic purposes. This thesis argues the local configuration of the hydronium and ammonium ions at a finite point in time is more relevant for vibrational spectroscopy as structural averaging does not occur. Due to the ions' disorder, Davydov splitting cannot occur and vibrational modes follow site symmetry selection rules. The development of an improved procedure to determine the highest effective symmetry and likely normal modes of orientationally disordered molecules in ordered crystals is proposed using jarosites as a case study.

This thesis found that hydrogen bonding subtleties are the major structural differences between hydronium and ammonium ion substitution in jarosite minerals. All characterisation techniques employed in this thesis show that hydrogen bonds involving the hydronium and ammonium ions are predominantly towards hydroxyl groups. However, lower dehydroxylation temperatures, and significantly broader hydroxyl vibrational spectroscopic bands for hydronium jarosite, suggest hydronium hydrogen atoms are more mobile and/or form stronger hydrogen bonds when compared to ammonium hydrogen atoms. This is a contributing factor to the differing magnetic behaviours of the two minerals, despite both minerals containing orientationally disordered molecules.

KEYWORDS

Alunite supergroup of minerals · ammoniojarosite · crystal structure · difference Fourier methods · dynamic disorder · factor group analysis · far infrared spectroscopy · hydronium jarosite · infrared emission spectroscopy · infrared spectroscopy · jarosite · mass spectrometry · mineralogy · neutron powder diffraction · orientational disorder · Raman spectroscopy · Rietveld refinement · single crystal X-ray diffraction · static disorder · symmetry analysis · thermal decomposition · thermogravimetric analysis · vibrational spectroscopy · X-ray powder diffraction

LIST OF PUBLICATIONS

Spratt, H.J.; Rintoul, L.; Avdeev, M.; Martens, W.N. The crystal structure and vibrational spectroscopy of jarosite and alunite minerals. *American Mineralogist*, 2013, v. 98, pp. 1633-1643. *(Chapter 2)*

Spratt, H.J.; Rintoul, L.; Avdeev, M.; Martens, W.N. The thermal decomposition of hydronium jarosite and ammoniojarosite. *Journal of Thermal Analysis and Calorimetry*, 2014, v. 115, pp. 101-109. *(Chapter 4)*

Spratt, H.J.; Avdeev, M.; Pfrunder, M.C.; McMurtrie, J.; Rintoul, L.; Martens, W.N. Location of hydrogen atoms in hydronium jarosite. *Physics and Chemistry of Minerals*, 2014, v. 41, pp. 505-517. *(Chapter 5)*

Spratt. H.J.; Avdeev, M.; Jensen, J.R.; Martens, W.N. A neutron powder diffraction study of the crystal structure of ammoniojarosite: New ammonium ion orientation model. *American Mineralogist.* SUBMITTED MAY 2014, CURRENTLY UNDERGOING PEER REVIEW. *(Chapter 6)*

Spratt, H.J.; Rintoul, L.; Avdeev, M.; Martens, W.N. On the orientational disorder of hydronium jarosite and ammoniojarosite in comparison to jarosite: A vibrational spectroscopic study. *Mineralogical Magazine*. ACCEPTED PENDING REVISIONS. *(Chapter 7)*

TABLE OF CONTENTS

Abstract i

Keywords ii

List of Publications iii

Table of Contents iv

List of Figures x

List of Tables xiii

Abbreviations xiv

Statement of Original Authorship xv

Acknowledgements xvi

Chapter 1 Introduction 1

1.1 Introduction 2

1.2 Description of the Scientific Problems Investigated 3

1.3 Overall Objectives of the Study 5

1.4 Specific Aims of the Study 6

1.5 Account of the Scientific Process Linking the Scientific Papers 7

Chapter 2 The Crystal Structure and Vibrational Spectroscopy of Jarosite and Alunite Minerals 11

Statement of Contribution 12

Synopsis 13

Abstract 15

An Introduction to the Alunite Supergroup of Minerals: Nomenclature, Formation and Applications 16

Synthesis 18

Crystal Structure of the Jarosite and Alunite Mineral Subgroups 19

General Description of the Structure 19

Structural Variations in the Supergroup: Symmetry Lowering 21

Non-stoichiometry of Synthesised Jarosites and Alunites 22

Magnetic Structure and Proton Mobility 23

Structural Variation in the Supergroup: Members with a Super Cell 26

Vibrational Spectroscopy of the Alunite and Jarosite Mineral Subgroups 32

General Description of the Vibrational Spectra of Jarosite and Alunite Minerals.... 32

Factor Group Analysis of the Alunite Supergroup 33

Jarosite and Alunite Subgroup Band Assignments 35

Applications of Jarosite and Alunite Vibrational Spectroscopy 38

The Splitting of Sulfate Bands and Plumbojarosite 39

Symmetry Problems with Hydronium and Ammonium Ions 41

Implications 43

References Cited 44

Chapter 3 Orientational Disorder in Jarosite Minerals 55

Preface 56

3.1 Disorder in Crystalline Solids 57

3.1.1 Introduction 57

3.1.2 Orientational Disorder in Solids and Crystals 59

3.1.2.1 Crystal Structure Effects 59

3.1.2.2 Vibrational Spectroscopic Effects 62

3.1.2.3 Group Theory and Symmetry Considerations 62

3.2 Orientational Disorder in the Alunite Supergroup of Minerals 65

3.2.1 Hydronium and Ammonium Ion Substitution Background 65

3.2.2 Crystal Structure Investigations 67

3.2.3 Vibrational Spectroscopic Investigations 69

3.2.4 Investigations Using Other Characterisation Techniques 70

3.2.5 Symmetry Analysis: Inadequacy of Previous Methods for Orientational Disorder in the Alunite Supergroup of Minerals 71

3.3 Concluding Remarks 73

3.4 References 74

Chapter 4 The Thermal Decomposition of Hydronium Jarosite and Ammoniojarosite 81

Statement of Contribution 82

Synopsis 83

Abstract 85

Introduction 86

Experimental 89

Synthesis 89

Chemical Composition 89

Thermogravimetric Analysis 90

Infrared Emission Spectroscopy 90

Synchrotron X-Ray Diffraction 90

Results and Discussion 92

Hydronium Jarosite Thermal Decomposition 92

Ammoniojarosite Thermal Decomposition 98

Conclusions 105

References 106

Chapter 5 Location of Hydrogen Atoms in Hydronium Jarosite 111

Statement of Contribution 112

Synopsis 113

Abstract 115

Introduction 116

Experimental 120

Synthesis 120

Inductively Coupled Plasma – Optical Emission Spectrometry (ICP-OES) 120

Single Crystal X-Ray Diffraction 121

Neutron Powder Diffraction 121

Single Crystal Structure Refinement 121

Rietveld Refinement of Powder Diffraction Data 122

Results and Discussion 123

Single Crystal X-Ray Diffraction 123

Location of Hydrogen Atoms from Neutron Diffraction 127

Investigation of Lower Site Symmetry for the Hydronium Oxygen Atom in Space Group $R\bar{3}m$ 132

Investigation of a Lower Symmetry Space Group 135

Investigation of Hydronium Ion Geometry 140

Conclusions 145

References 146

Chapter 6 A Neutron Powder Diffraction Study of the Crystal Structure of Ammoniojarosite 153

Statement of Contribution 154

Synopsis 155

Abstract 157

Introduction 158

Experimental 160

Synthesis 160

Chemical Composition 160

Powder X-Ray Diffraction 161

Neutron Powder Diffraction 161

Rietveld Refinement of Neutron Powder Diffraction Patterns 161

Whole Powder Pattern Decomposition 162

Results and Discussion 163

Implications 173

References Cited 174

Chapter 7 On the Orientational Disorder of Hydronium Jarosite and Ammoniojarosite in Comparison to Jarosite 177

Statement of Contribution 178

Synopsis 179

Abstract 181

Introduction 182

Experimental 185

Synthesis 185

Powder X-Ray Diffraction 185

Fourier Transform Infrared Absorbance Spectroscopy 185

Low Temperature and Room Temperature Raman Spectroscopy of Hydronium Jarosite, Jarosite and Ammoniojarosite 186

Raman Spectroscopy at Room Temperature in Comparison to Deuterated Analogues 186

Spectral Manipulation and Analysis 187

Results and Discussion 188

Phase Identification 188

Spectroscopic Space Group Choice 188

Hydronium and Ammonium Ion Spectroscopic Site Symmetry 190

Spectral Interpretation and Analysis 193

Implications 207

References 209

Chapter 8 Conclusions 217

Preface 218

8.1 Original Contribution 219

8.2 General Discussion 224

8.3 Implications 229

8.4 Future Work 233

8.5 References 238

LIST OF FIGURES

Figure 1-1: Flow chart showing the arrangement and interactions of the thesis' chapters. Dashed arrows indicate indirectly related scientific papers. Dash-dotted arrows indicate directly related chapters 9

Figure 2-1: The crystal structure of jarosite projected down the a axis showing sulfate tetrahedra and FeO_6 octahedra 20

Figure 2-2: Magnetic structure of jarosites showing a) the impossibility of all moments coupling antiferromagnetically in a triangular array, b) one of the many degenerate ground states that is obtained by rotating the moments 120 ° and c) the q = 0 array of magnetic moments that is at T < 70 K. Adapted from Wills and Harrison (1996) 24

Figure 2-3: The crystal structure of super cell plumbojarosite projected down the a axis showing SO_4 and FeO_6 as polyhedra 29

Figure 2-4: Typical Raman spectrum of jarosite [$KFe_3(SO_4)_2(OH)_6$].....32

Figure 2-5: Typical infrared spectrum of jarosite [$KFe_3(SO_4)_2(OH)_6$] 33

Figure 2-6: Raman and infrared spectra of super cell plumbojarosite from 900 – 1300 cm^{-1} 40

Figure 3-1: Diagram showing the major types of disorder. Different localised configurations for all the types of disorder are shown in either red or blue 58

Figure 3-2: Example of a split atom model (right) for borane (BH_3) disordered around an inversion centre. Red and orange, and blue and purple in the split atom model approximate the red and blue orientations respectively in the higher symmetry model (left) 61

Figure 3-3: Ammonium and hydronium symmetry showing lack of an inversion centre.....65

Figure 3-4: Diagram showing the orientational disorder of the ammonium ion as determined by Wills *et al.* (2000). The two orientations are indicated as dark circles and open circles for both nitrogen and hydrogen atoms for position 2 68

Figure 4-1: TG/DTG curves for hydronium jarosite.....92

Figure 4-2: MS of evolved gases for hydronium jarosite 93

Figure 4-3: Significant *in situ* synchrotron XRD patterns (converted to 1.54056 Å) of hydronium jarosite as a function of temperature. Most intense hematite peaks are marked by a dashed line 95

Figure 4-4: IES spectra of hydronium jarosite (4,000-650 cm^{-1}).....95

Figure 4-5: TG/DTG curves for ammoniojarosite.....98

Figure 4-6: MS of evolved gases for hydronium jarosite 99

Figure 4-7: Significant *in situ* synchrotron XRD patterns of ammoniojarosite (converted to 1.54056 Å) as a function of temperature. Peaks marked with an asterisk at 421 °C are from $FeSO_4$ and those at 571 °C are from $Fe_2(SO_4)_3$. Most intense hematite peaks are marked with a dashed line 101

Figure 4-8: IES spectra of ammoniojarosite (4,000–650 cm^{-1})..... 102

Figure 5-1: Crystal structure of hydronium jarosite refined from single crystal XRD data showing 80% thermal ellipsoids. Note the lack of thermal motion of O4 parallel to unit cell parameter c. Hydrogen bonds involving hydroxyl groups appear to restrict the disorder of the hydronium ion (green), so that regions of concentrated electron density appear in positions labelled H2 124

Figure 5-2: Difference Fourier maps ($F_{obs} - F_{calc}$) with F_{calc} values obtained using all atomic sites for hydronium jarosite. Solid lines show positive contours while broken lines show negative and zero contours 128

Figure 5-3: Typical Rietveld refinement profile fit (unrestrained model) against the neutron powder diffraction pattern collected from hydronium jarosite 129

Figure 5-4: Structure of hydronium jarosite with the hydronium ion described by RB1 a) viewing direction is along a with FeO_6 and SO_4 groups shown as polyhedra b) viewing direction along the [110] axis with atoms shown as 50 % ellipsoids..... 142

Figure 5-5: Geometry of the hydronium ion described by RB1. Viewing direction is along c..... 143

Figure 6-1: Powder X-ray diffraction pattern (Cu Kα1 and Kα2) of the deuterated ammoniojarosite 163

Figure 6-2: Typical Rietveld refinement profile fit to the deuterated ammoniojarosite (unconstrained model at 298 K)..... 164

Figure 6-3: Difference Fourier maps at 298 K (top) and 3 K (bottom) at approximately +1σ contour levels. Cuts taken after refinement of the jarosite framework with no ammonium ^2H atoms (left), and after refinement to convergence including the previously found ^2H atoms (right) 166

Figure 6-4: Crystal structure of deuterated ammoniojarosite at 3 K viewed down [110]. All atoms are shown as 50 % probability ellipsoids. FeO_6 and SO_4 are shown as polyhedra 167

Figure 6-5: Hydrogen bonding scheme involving the ammonium ion. Hydrogen bonds are shown as thin orange lines 171

Figure 7-1: Crystal structure of jarosite projected down the a axis..... 182

Figure 7-2: a) XRD patterns of hydronium jarosite, ammoniojarosite and jarosite, b) XRD patterns of their respective deuterated analogs 188

Figure 7-3: Raman spectra collected with 633 nm excitation of a) hydronium jarosite at 82 K, b) hydronium jarosite at 298 K, c) ammoniojarosite at 82 K, d) ammoniojarosite at 298 K and e) jarosite at 298 K..... 189

Figure 7-4: Raman spectra collected with 633 nm excitation in the 1500 to 4000 cm^{-1} region of a) hydronium jarosite at 82 K, b) hydronium jarosite at 298 K, c) ammoniojarosite at 82 K, d) ammoniojarosite at 298 K and e) jarosite at 298 K..... 194

Figure 7-5: MIR (left) and 532 nm Raman (right) in the 1500 to 4000 cm^{-1} region for a) hydronium jarosite, b) deuteronium jarosite, c) ammoniojarosite, d) deuterated ammoniojarosite, e) jarosite and f) deuterated jarosite.....195

Figure 7-6: MIR (left) and 785 nm Raman (right) spectra in the 600 to 1500 cm^{-1} region for a) hydronium jarosite, b) deuteronium jarosite, c) ammoniojarosite, d) deuterated ammoniojarosite, e) jarosite and f) deuterated jarosite 198

Figure 7-7: Hydronium ion surrounding environment, showing possible hydrogen bonds to hydroxyl oxygen atoms (O3) or basal sulfate oxygen atoms (O2). Structural data from Wills and Harrison (1996).....198

Figure 7-8: Raman spectra collected with 633 nm excitation in the 1500 to 4000 cm^{-1} region of a) hydronium jarosite at 82 K, b) hydronium jarosite at 298 K, c) ammoniojarosite at 82 K, d) ammoniojarosite at 298 K and e) jarosite at 298 K 200

Figure 7-9: MIR spectra of low iron ammoniojarosite (black) compared to the ammoniojarosite previously analyzed (grey). Inset shows an expanded view of the sulfate stretching mode region.....202

Figure 7-10: Raman spectra collected with 633 nm excitation in the 100 to 700 cm^{-1} region of a) hydronium jarosite at 82 K, b) hydronium jarosite at 298 K, c) ammoniojarosite at 82 K, d) ammoniojarosite at 298 K and e) jarosite at 298 K 203

Figure 7-11: FIR (left) and 785 nm Raman (right) in the 200 to 700 cm^{-1} region for a) hydronium jarosite, b) deuteronium jarosite, c) ammoniojarosite, d) deuterated ammoniojarosite, e) jarosite and f) deuterated jarosite 204

LIST OF TABLES

Table 2-1: Factor group splitting of the internal modes for TO_4 groups 34

Table 5-1: List of atomic sites for the alunite supergroup in space group $R\bar{3}m$ 117

Table 5-2: Results from the refinement of hydronium jarosite from single crystal XRD data 126

Table 5-3: Positional and anisotropic ADPs from the single crystal XRD refinement of hydronium jarosite 127

Table 5-4: Results from the unrestrained refinement of hydronium jarosite 130

Table 5-5: Refined positional and isotropic ADPs from the unrestrained refinement of hydronium jarosite 131

Table 5-6: Select inter-atomic distances and angles from the unrestrained refinement of hydronium jarosite 131

Table 5-7: Results from an unrestrained refinement of hydronium jarosite with O4 displaced from the $\bar{3}m$ site 134

Table 5-8: Refined positional and isotropic ADPs from the unrestrained refinement of hydronium jarosite with O4 displaced from the $\bar{3}m$ site 134

Table 5-9: Results from an unrestrained refinement of hydronium jarosite in a lower symmetry space group 136

Table 5-10: Refined positional and isotropic ADPs from an unrestrained refinement of hydronium jarosite in space group $R3m$ 137

Table 5-11: Select inter-atomic distances and angles from an unrestrained refinement of hydronium jarosite in space group $R3m$ 138

Table 5-12: Results from the Rietveld refinement of the hydronium ion described by RB1 141

Table 5-13: Refined positional and isotropic ADPs from the refinement of the hydronium ion described by RB1. Atoms O4 through H4 form the rigid body and their coordinates are reported without e.s.d.s 141

Table 6-1: Unconstrained refinement results of deuterated ammoniojarosite 165

Table 6-2: Unconstrained refined positional parameters and isotropic ADPs ($\times 10^2$) of deuterated ammoniojarosite at 3 K. Isotropic ADPs at 298 K are shown for comparison 168

Table 6-3: Select inter-atomic distances and angles from the unconstrained refinement of ammoniojarosite at 3 K. Hydrogen bonds shown as dotted lines 170

Table 7-1: Symmetry of atomic sites for jarosite minerals in space group $R\bar{3}m$ 183

Table 7-2: Splitting of hydronium and ammonium ion internal modes in the alunite supergroup at a C_{3v} site 192

Table 7-3: Lattice modes of hydronium and ammonium ions in the alunite supergroup at a C_{3v} site 192

Table 7-4: Raman and MIR isotopic shifts upon deuteration 197

ABBREVIATIONS

°C	Degrees Celsius
°2θ	Degrees two theta
ADP	Atomic displacement parameter
ca	Circa
DTG	Differential thermogravimetric
FIR	Far infrared
h or hrs	Hours
IES	Infrared emission spectroscopy
IR	Infrared
ICP-OES	Inductively coupled plasma optical emission spectroscopy
K	Kelvin
min	Minutes
MIR	Mid infrared
NPD	Neutron powder diffraction
TG	Thermogravimetric analysis
s	Seconds
XRD	X-Ray diffraction

STATEMENT OF ORIGINAL AUTHORSHIP

The work contained in this thesis has not been previously submitted for a degree or diploma at this or any other educational institution. To the best of my knowledge and belief, this thesis contains no material previously published or written by another person, except where due reference is made.

QUT Verified Signature

19/02/15

Henry Joseph Spratt *19/02/15*

ACKNOWLEDGEMENTS

There are many people who ensured the success of this project over the years and/or went out of their way to help a sad post grad. Firstly, I must thank my primary supervisor, Dr Wayde Martens, for his advice, support, and friendship over the years. All this despite our tendency to be on opposite wavelengths, or realise we were saying the same thing after ~1 hr of discussion. My associate supervisor, Dr Llew Rintoul, is thanked for his assistance and expertise with all aspects of vibrational spectroscopy, and also for insightful comments and criticisms of my work. Dr Maxim (Max) Avdeev at the Bragg Institute of ANSTO has been a massive help. I thank him immensely for his helpful advice and support with neutron powder diffraction and Rietveld refinement, despite my long, (probably) annoying, and persistent emails. The numerous tech staff (particularly Dr Peter Hines, Mr Shane Russell, Mr Tri Nguyen, and Mr Tony Raftery) at QUT are thanked for their assistance and help with instrumentation. The Australian Government, QUT, and the Australian Institute of Nuclear Science and Engineering (AINSE) are gratefully acknowledged for ensuring my survival and ability to pay rent and bills for 3.5 years. Most chemistry post grads and members of my research group have made the PhD experience ~~bearable~~ more enjoyable. However, in particular, I must thank my fellow partners in procrastination: Jasmine Jensen, Kate Brough, Chris East, Mitch de Bruyn, Ashley Locke (before and after he ventured into the real world), James Brady, and Adrian Baker; for their friendship, help and support, advice, proof reading, reciprocity in vents/rants/whinges, extended lunch breaks, coffee breaks, and lolly shop visits. Cheers to my non-postgraduate friends for their sage advice of “just finish.” It never occurred to me. And lastly, I thank my family for their love and support; particularly dad for proof reading, and trying fairly successfully to organise me.

CHAPTER 1 INTRODUCTION

1.1 INTRODUCTION

This thesis, "Structural Effects of Hydronium and Ammonium in Jarosite Minerals," investigated the vibrational spectroscopic and crystallographic behaviour of jarosite minerals containing hydronium and ammonium ions – which are examples of crystals that have molecules located at sites that are not a subgroup of their molecular symmetry – at ambient, low and elevated temperatures. This thesis will argue that the spin glass behaviour of hydronium jarosite cannot be solely due to orientational disorder as the orientationally disordered ammoniojarosite undergoes long range magnetic ordering at low temperature. Hence, the aim of this thesis is to determine the crystal structures of hydronium and ammoniojarosite that are consistent with both magnetic and vibrational spectroscopic data. This thesis will show that hitherto overlooked hydrogen bonding differences between hydronium jarosite and ammoniojarosite offer an explanation for the anomalous magnetic behaviour between these two minerals.

This chapter outlines: the objectives and aims of the study; the scientific problems that were investigated during the course of this study; the structure of the thesis and lastly, how the scientific papers published by the author during the course of the study that address the scientific problems are linked together and overall, support the argument of the thesis. This thesis is a collection of published works submitted by the author to various scientific journals. Thus, the general formatting follows the style of the journal except for the appearance of headings, and figure and table labels, which follow the style in this chapter and Chapter 3. References and scientific and spelling conventions follow the style of the journal to which the corresponding work was submitted. Repetition and redundancy in the introductory sections of each chapter is unavoidable owing to the close relationships between the subject matter published.

1.2 DESCRIPTION OF THE SCIENTIFIC PROBLEMS INVESTIGATED

The crystal structures of jarosite ($AFe_3(SO_4)_2(OH)_6$, where A is a cation) minerals containing hydronium (H_3O^+) and ammonium (NH_4^+) ions are ambiguous. The ambiguity stems from the difficulty in locating the hydrogen atoms associated with the hydronium and ammonium ions. In addition, the molecular symmetries of hydronium (C_{3v}) and ammonium (T_d) ions are not a subgroup of their projected crystallographic site (D_{3d}), leading to the suggestion they are orientationally disordered, either statically or dynamically. This symmetry mismatch and orientational disorder imparts another important problem: how can the vibrational spectra of jarosite minerals containing hydronium and ammonium be rationalised when no molecular symmetry to site symmetry to crystallographic symmetry correlation can be established? This problem is not trivial and has been largely ignored for not only jarosite minerals, but also for other similar crystal structures where there are molecules located at crystallographic sites which are not a subgroup of their molecular symmetry.

To uncover structural nuances that can account for the anomalous magnetic behaviour of hydronium jarosite, this thesis reports the crystal structures of hydronium jarosite and ammoniojarosite, and aimed to locate all hydrogen atoms so that not only the vibrational spectra of hydronium jarosite and ammoniojarosite can be rationalised, but also other similarly disordered molecules in crystals. This structural investigation was achieved through a variety of characterisation techniques at ambient, low and elevated temperatures. A thorough investigation of crystal structure is required to understand vibrational spectra as they are inextricably linked; the crystal structure (time and spatially averaged structure) determines the selection rules and the expected modes of vibration and conversely, the vibrational spectra (structure at the molecular level) can determine the crystal structure when diffraction methods are ambiguous. This investigation into the crystal structure and vibrational spectroscopy of hydronium jarosite and ammoniojarosite

was designed and undertaken in order to: resolve debates concerning the most appropriate description of these two minerals crystal structures; accurately interpret, assign and rationalise these two minerals vibrational spectra; using these two minerals as a basis, suggest how the vibrational spectra of other similarly disordered crystals can be interpreted. If successful, such a study will fundamentally increase the knowledge of jarosite minerals and the symmetry analysis of orientationally disordered molecules in crystals; the cumulative effect being an account for the differing magnetic behaviour of ammoniojarosite and hydronium jarosite despite both being orientationally disordered.

1.3 OVERALL OBJECTIVES OF THE STUDY

The overall objective of this study was to account for the differing magnetic behaviour of ammoniojarosite and hydronium jarosite through rigorous structural characterisation methods. A primary aim was to locate all hydrogen atoms in hydronium and ammoniojarosite as this accomplishment would allow for: the most appropriate description of the crystal structure; the geometry of the hydronium and ammonium ions in the jarosite subgroup of minerals to be modelled; new insights into the magnetic behaviour of both minerals as bond distances and angles involving the missing hydrogen atoms can be determined; and, their vibrational spectra to be properly interpreted and related back to the crystal structure. Previous work in the field has rarely considered different structural models for hydronium jarosite and ammoniojarosite, as it is simply suggested the structure of these two minerals might be different.

The current study was conceived to rigorously examine the vibrational spectra and crystal structure of hydronium jarosite and ammoniojarosite at various temperatures so as to determine the structural effects the hydronium and ammonium ions impart on the jarosite crystal and magnetic structures. The results of this investigation will allow for the most appropriate method to rationalise the vibrational spectra of disordered molecules in otherwise ordered crystals, where the site symmetry is not a subgroup of the molecular symmetry. To achieve these goals, hydronium jarosite and ammoniojarosite were synthesised and compared to jarosite (the potassium end member), which is well characterised and has no orientational disorder. This study used neutron powder diffraction, X-ray diffraction (both powder and single crystal), infrared emission spectroscopy, thermogravimetric analysis, and vibrational spectroscopy (Raman, MIR, FIR) as the main structural probes of the synthesised jarosite minerals.

1.4 SPECIFIC AIMS OF THE STUDY

- Review the pertinent literature of the alunite supergroup of minerals and suggest research pathways that should be investigated further, and also, to clarify controversial topics in the relevant literature.

- Determine whether dehydroxylation and deammoniation are separate events or concurrent with desulfonation during the decomposition of hydronium and ammoniojarosite. Identify the intermediate phases that are formed during the thermal decomposition of hydronium and ammoniojarosite.

- Locate hydrogen atoms in hydronium jarosite and ammoniojarosite and thus, determine their crystal structures through the investigation of various models.

- Propose how the vibrational spectra of hydronium jarosite can be rationalised, given that factor group analysis cannot adequately predict the number of allowed modes of vibration due to orientational disorder arising from the hydronium and ammonium ions being located at a crystallographic site of higher symmetry than its molecular symmetry. Then, using hydronium jarosite and ammoniojarosite as a basis, outline general principles for the normal mode determination of similarly disordered materials.

- Accurately interpret jarosite mineral vibrational spectra and assign bands.

- Account for the long-range magnetic ordering of ammoniojarosite.

1.5 ACCOUNT OF THE SCIENTIFIC PROCESS LINKING THE SCIENTIFIC PAPERS

In order to rationalise the vibrational spectra of hydronium jarosite, ammoniojarosite, and crystals containing other orientationally disordered molecules, it is first necessary to understand what orientational disorder actually is and the effects it has on crystal structure and vibrational spectra. In addition, how orientational disorder relates to the jarosite minerals must be established before the crystallographic and spectroscopic study at various temperatures can be undertaken. Thus, the chapters of this thesis are arranged to:

- Critically evaluate the literature regarding the alunite and jarosite groups of minerals, and introduce the previous work on the crystallographic and spectroscopic studies of jarosite minerals that this thesis builds upon. *(Chapter 2).*

- Introduce the concept of orientational disorder, examine the previous literature on the problems caused by orientational disorder and the success or failure of their solutions, and finally explain how orientational disorder relates to jarosite minerals and how the previous literature on orientational disorder is not directly applicable to jarosite minerals. *(Chapter 3).*

- Study the infrared spectra and crystallographic behaviour of hydronium jarosite and ammoniojarosite at elevated temperatures, with the aim of identifying intermediate compounds. *(Chapter 4).*

- Locate hydrogen atoms in hydronium jarosite, determine the correct model for the crystal structure of hydronium jarosite, and model the geometry of the hydronium ion. *(Chapter 5).*

- Locate hydrogen atoms in ammoniojarosite, determine the correct model for the crystal structure of ammoniojarosite, and model the geometry of the ammonium ion. *(Chapter 6).*

- Rationalise the crystal structure of hydronium and ammoniojarosite with their vibrational spectra, clarify band assignment in the vibrational spectra, and determine the effects that the orientationally disordered hydronium and ammonium ions have on the jarosite framework at the molecular level compared to the ordered jarosite. Then, propose a method for the normal mode determination of other similarly disordered molecules in crystals using the jarosite minerals as a basis. *(Chapter 7).*

- Determine the important conclusions of each individual scientific paper, and lastly, show how the synergy between the scientific papers leads to the same conclusions and argument presented by the author in this thesis. In other words, the cumulative effect of the scientific papers, their individual contribution to the literature and hence, their cohesive research narrative is established. *(Chapter 8).*

The flow chart in Figure 1-1 on the next page is a graphical representation of how this thesis is structured. Figure 1-1 also illustrates the relationships between the aims and outcomes of the scientific papers written by the author, as previously discussed.

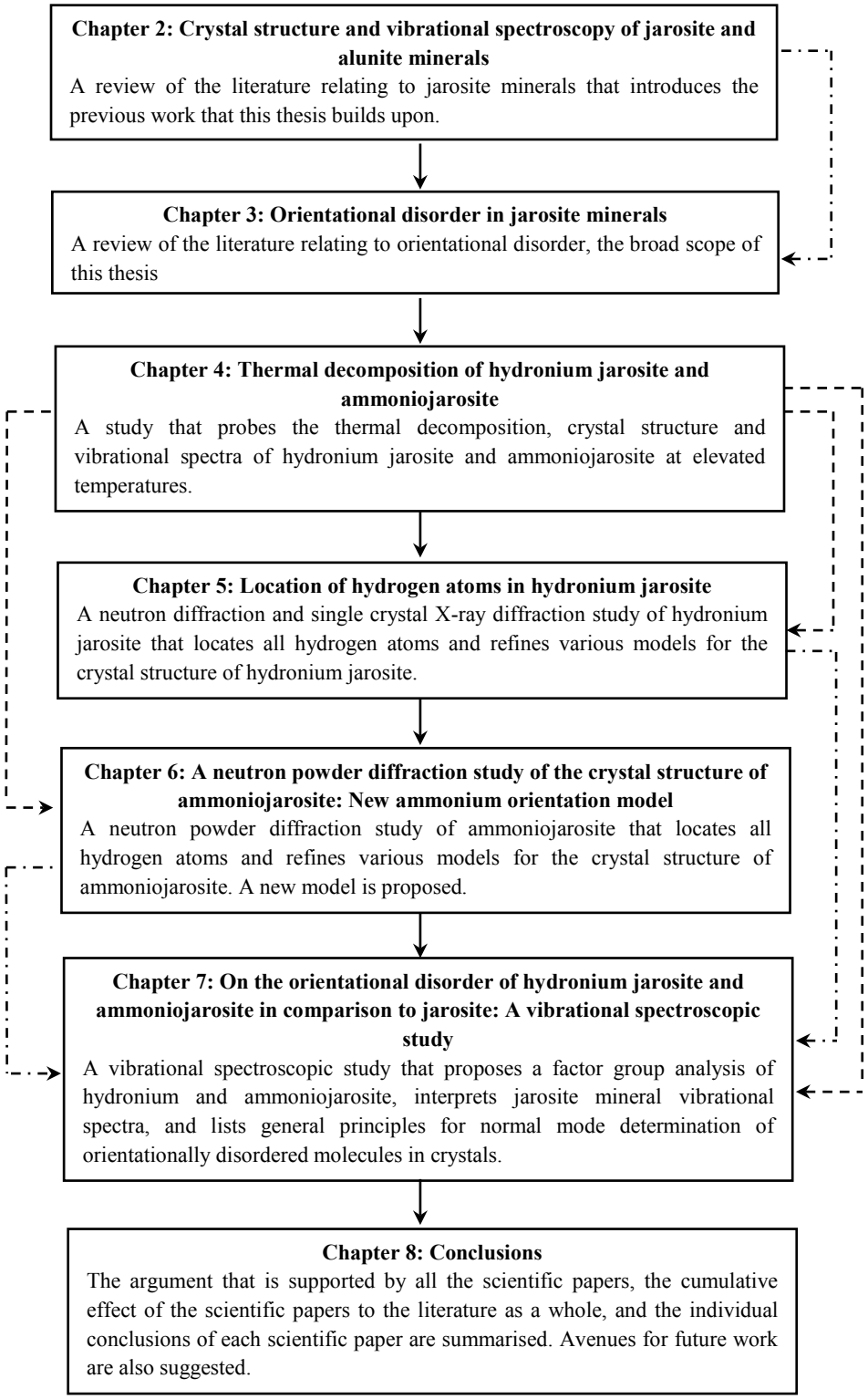

Figure 1-1: Flow chart showing the arrangement and interactions of the thesis' chapters. Dashed arrows indicate indirectly related scientific papers. Dash-dotted arrows indicate directly related chapters

CHAPTER 2 THE CRYSTAL STRUCTURE AND VIBRATIONAL SPECTROSCOPY OF JAROSITE AND ALUNITE MINERALS

REVIEW ARTICLE

Reproduced with permission from:

Spratt, H.J.; Rintoul, L.; Avdeev, M.; Martens, W.N. *American Mineralogist* 2013

© American Mineralogical Society 1997 – 2013

STATEMENT OF CONTRIBUTION

The authors listed below have certified* that:

1. They meet the criteria for authorship in that they have participated in the conception, execution, or interpretation, of at least that part of the publication in their field of expertise;
2. They take public responsibility for their part of the publication, except for the responsible author who accepts overall responsibility for the publication;
3. There are no other authors of the publication who meet these criteria;
4. Potential conflicts of interests have been disclosed to a) granting bodies, b) the editor or publisher of journals or other publications, and c) the head of the responsible academic unit, and
5. They agree to the use of the publication in the student's thesis and its publication on the Australasian Digital Thesis Database consistent with any limitations set by the publisher requirements.

In the case of this chapter:

The crystal structure and vibrational spectroscopy of jarosite and alunite minerals

Contributor	*Statement of Contribution**
Henry J. Spratt	Reviewed, compiled, and interpreted the literature; wrote the manuscript
Llew Rintoul	Supervision, editing
Maxim Avdeev	Supervision, editing
Wayde N. Martens	Overall supervisor, editing

Principal Supervisor Confirmation

I have sighted email or other correspondence from all co-authors confirming their certifying authorship.

Name	Signature	Date

SYNOPSIS

The current chapter reviews, analyses and reinterprets select literature relating to the more controversial aspects of the crystal structure and vibrational spectroscopy of the alunite and jarosite minerals, which culminates in a number of outstanding questions. This chapter also serves as an introduction to jarosite minerals themselves, their crystal structure, and vibrational spectroscopy, before the main thrust of the thesis. This review was written because there was found to be a lack of spectroscopic and crystallographic reviews of the alunite supergroup of minerals and their subgroups: most previously published reviews focus on their formation and nomenclature.

As a result of the review, it is proposed by the authors that the spin glass behaviour of hydronium jarosite is due to proton mobility and not just orientational disorder. Whilst the crystal structure of plumbojarosite and other members with a super cell is well known, the actual synthetic cause is not and requires investigation as each explanation for the observation of a super cell is met by a conflicting study. Confusion regarding vibrational spectroscopic band assignments due to significant overlap of different types of bands was found to plague the alunite supergroup of minerals. In some studies, more bands than what are allowed from theory are assigned. As a result of critically evaluating the published literature, new insights, research avenues, and conclusions were presented. This original interpretation of the published literature found numerous unanswered questions which warrant further investigation.

THE CRYSTAL STRUCTURE AND VIBRATIONAL SPECTROSCOPY OF JAROSITE AND ALUNITE MINERALS

Henry Spratt, Llew Rintoul and Wayde Martens

Chemistry, Physics and Mechanical Engineering, Science and Engineering Faculty, Queensland University of Technology, Brisbane, QLD, 4001 Australia

Maxim Avdeev

Bragg Institute, Australian Nuclear Science and Technology Organisation, Lucas Heights, NSW, 2234 Australia

Keywords: alunite supergroup · vibrational spectroscopy · Raman spectroscopy · infrared spectroscopy · crystal structure · magnetic structure · super cell

ABSTRACT

The alunite supergroup of minerals are a large hydroxy-sulfate mineral group which has seen renewed interest following their discovery on Mars. Numerous reviews exist which are concerned with the nomenclature, formation and natural occurrence of this mineral group. Sulfate minerals in general are widely studied and their vibrational spectra are well characterized. However, no specific review concerning alunite and jarosite spectroscopy and crystal structure has been forthcoming. This review focuses on the controversial aspects of the crystal structure and vibrational spectroscopy of jarosite and alunite minerals. Inconsistencies regarding band assignments especially in the 1000-400 cm^{-1} region plague these two mineral groups and result in different band assignments amongst the various spectroscopic studies. There are significant crystallographic and magnetic structure ambiguities with regards to ammonium and hydronium end members, namely, the geometry these two ions assume in the structure and the fact that hydronium jarosite is a spin glass. It was also found that the synthetic cause/s for the super cell in plumbojarosite, minamiite, huangite and walthierite are not known.

AN INTRODUCTION TO THE ALUNITE SUPERGROUP OF MINERALS: NOMENCLATURE, FORMATION AND APPLICATIONS

The large alunite supergroup of minerals can be described by the general formula $AB_3(TO_4)_2(OH)_6$. The A site is most commonly occupied by a monovalent cation but divalent cations can also occupy this site. If the B site is predominantly aluminum, the mineral is classified as an alunite; if iron (III) predominates at the B site, the mineral is a jarosite. Other trivalent cations and some divalent cations can also occupy the B site. The T site is typically occupied by sulfur, but arsenic and phosphorus are common at this site as well. The alunite supergroup is further divided into subgroups based on the occupation of the T and B sites. The supergroup forms extensive solid solutions at one or all crystallographic sites, leading to a vast number of chemical formulae and possible minerals (Brophy and Sheridan 1965; Brophy *et al.* 1962; Scott 1987; Stoffregen *et al.* 2000). Jarosites and alunites are also able to accommodate many elements from the periodic table in their flexible crystal structure (Becker and Gasharova 2001). However, the basic topology and structure remains the same despite the large array of potential compositions (Jambor 1999; Stoffregen *et al.* 2000). This review focuses on the jarosite (sulfur at the T site and iron at the B site) and alunite (sulfur at the T site and aluminum at the B site) subgroups. Titular jarosite and alunite, refer to the end members with potassium at the A site.

Jarosite, a mineral belonging to the alunite supergroup, was discovered on Mars at Meridiani Planum in 2004 by the Mars Exploration Rover Opportunity (Elwood Madden *et al.* 2004; Klingelhöfer 2004). This discovery suggested that the Martian atmosphere was once wet and that aqueous processes occurred on Mars at some point in the planet's history. Terrestrially, jarosite type minerals are found in sulfate-rich and oxidizing environments (Baron and Palmer 1996). Examples of these environments

include: the weathering and oxidation of sulfide ore deposits and sulfide-bearing sediments, especially those of pyrite (Baron and Palmer 1996; Becker and Gasharova 2001; Desborough *et al.* 2010; Lueth *et al.* 2005); acid-hypersaline lake sediments (Alpers *et al.* 1992); the oxidation of hydrogen sulfide in epithermal areas and hot springs (Lueth *et al.* 2005); acid-sulfate soils (Desborough *et al.* 2010); and by products of metal processing industries and acid-generating mining wastes (Desborough *et al.* 2010; Hochella *et al.* 2005).

The most important application of this mineral group is the removal of iron from process solutions in the zinc, copper and lead industries (Desborough *et al.* 2010; Dutrizac 2008). The supergroup could also be used for the long-term storage and immobilization of toxic and radioactive metal ions (Kolitsch and Pring 2001). The suitability of the alunite supergroup for this purpose is due to their thermal and chemical stability. Jarosites have been shown to act as a sink for arsenic (Savage *et al.* 2005) and can also adsorb arsenic (Asta *et al.* 2009). As alunite supergroup minerals form in acidic, aqueous environments, their chemical composition can be used to place constraints on fluid conditions such as pH and Eh in the environment (Burger *et al.* 2009). This review focuses on the controversial and debated aspects of the crystal structure and vibrational spectroscopy concerning the jarosite and alunite subgroups of the alunite supergroup of minerals.

SYNTHESIS

Alunite supergroup minerals can be synthesized in a variety of ways. Hydrothermal methods using elevated temperatures and pressures (~150 °C) in a sealed vessel are the most common. Synthesis is also possible at atmospheric pressure under reflux at 100 °C. There are many reagents that can be used but essentially, a source of B site sulfate (or phosphate and arsenate depending on the composition) and a soluble form of the A site (such as nitrates, sulfates or chlorides for example) is required. Jarosites can also be prepared from the biological oxidation of Fe^{2+} to Fe^{3+} by bacteria such as *T. ferrooxidans* or the chemical oxidation of Fe^{2+} using hydrogen peroxide (Sasaki and Konno 2000). Redox based hydrothermal methods using iron wire have also been employed (Bartlett and Nocera 2005). It is believed that the use of chlorides at a high concentration during the synthesis of these minerals suppresses the substitution of hydronium (H_3O^+) at the A site (Basciano and Peterson 2007b; Dutrizac 1991). Hydronium is a common impurity due to the acidic, aqueous conditions needed for synthesis. Synthesized and natural alunite supergroup minerals are usually poorly crystalline and do not readily form single crystals (Nocera *et al.* 2004). Indeed, there are only a handful of single crystal diffraction studies. This has resulted in a reliance on powder based techniques for structure determination.

CRYSTAL STRUCTURE OF THE JAROSITE AND ALUNITE MINERAL SUBGROUPS

GENERAL DESCRIPTION OF THE STRUCTURE

The A site is 12 coordinate, the B site is octahedral and the T site is a distorted tetrahedron with three of the four oxygen atoms bonding to the A and B sites (Scott 2000). The other bonds to the A and B site are from the oxygen atoms of hydroxyl groups. The apical oxygen atom from the TO_4 groups points either "up" or "down," and has a different bond length than the other three oxygen atoms (Papike *et al.* 2006). The crystal structure is highly symmetrical as no general positions are occupied (Papike *et al.* 2006). The A site is D_{3d} (3a site), the B site is C_{2h} (9d site), the TO_4 groups are C_{3v} (6c site) and the OH groups are C_s (18h site). The crystal structure can be described as alternating layers of the B site, and those comprised of A and T sites (Papike *et al.* 2006). This layer structure is seen more clearly when the crystal structure is projected down the **a** axis (Figure 2-1).

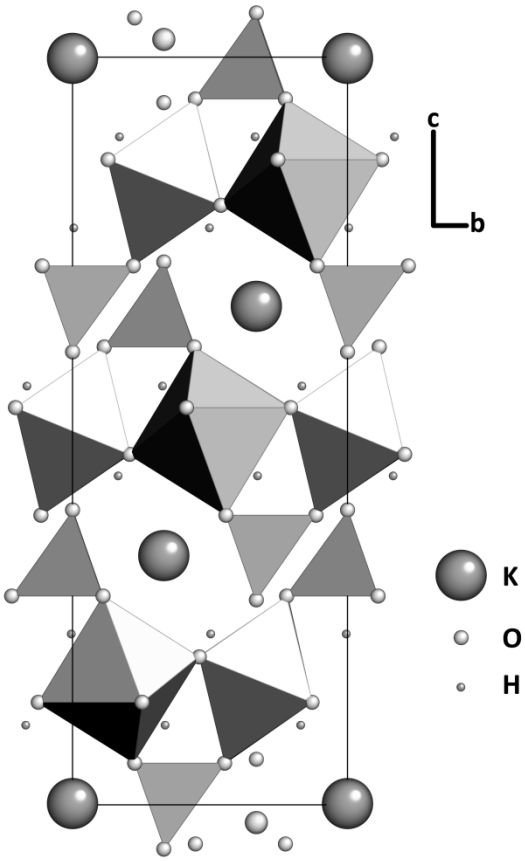

Figure 2-1: The crystal structure of jarosite projected down the **a** axis showing sulfate tetrahedra and FeO_6 octahedra

The majority of alunite supergroup minerals crystallize as the rhombohedral space group $R\bar{3}m$ (no. 166) and are described by a hexagonal axis with the number of formula units in the unit cell (Z) equal to 3 (Arkhipenko and Bokii 1979; Papike *et al.* 2006). The **a** and **b** axes are identical (*ca* 7 Å) while the **c** axis is unique (*ca* 17 Å) (Stoffregen *et al.* 2000). Some studies have suggested that the structure could be described by the non-centrosymmetric space group R3*m* (no. 160) on the basis of pyroelectricity (Hendricks 1937) and the detection of optical second harmonic generation (Loiacono *et al.* 1982). Recent measurements on a jarosite single crystal found no evidence for pyroelectricity and therefore, the space group remained centrosymmetric (Buurma *et al.* 2012). The overwhelming consensus in the literature is that the space

group should be treated as $R\bar{3}m$. In fact, it has been recommended that all jarosites and alunites be refined as belonging to space group $R\bar{3}m$ unless significant structural evidence is provided to the contrary (Menchetti and Sabelli 1976). It is well known that substitutions at the A site have the greatest effect upon the **c** axis whilst substitutions at the B site influence the **a** axis the most (Basciano and Peterson 2007a, 2007b; Brophy and Sheridan 1965; Brophy *et al.* 1962; Menchetti and Sabelli 1976; Sato *et al.* 2009; Stoffregen *et al.* 2000).

STRUCTURAL VARIATIONS IN THE SUPERGROUP: SYMMETRY LOWERING

As stated in the previous section, most alunite supergroup minerals belong to the rhombohedral space group $R\bar{3}m$. However, there are a significant number of alunite supergroup minerals which have been successfully refined in lower symmetry space groups. Gorceixite ($BaAl_3[PO_3\ (O, OH)]_2(OH)_6$) has been observed to crystallize in the monoclinic space group C*m*, but is strongly pseudorhombohedral (Blanchard 1989; Radoslovich 1982). The lowering of symmetry from rhombohedral to monoclinic was assigned to ordered protonation of one of the phosphate groups. However, a more recent investigation of the same mineral determined that $R\bar{3}m$ was the most appropriate space group choice (Dzikowski *et al.* 2006), but the authors noted that this may not be the case for all natural gorceixite samples and that the mechanism for symmetry lowering is unclear. Careful analysis of diffraction data and Rietveld refinement is needed to discern whether a lowering of symmetry is justified.

Segnitite, $PbFe_3(AsO_4)_2(OH, H_2O)_6$, is a member of the crandallite subgroup and belongs to space group $R\bar{3}m$. A segnitite related mineral with composition $Pb[Zn_{0.5}\square_{0.5}]Fe_3(AsO_4)_2(OH)_6$ where □ = vacancy, v space group *C*2/*c* with *Z* = 16 (Grey *et al.* 2008). The basic structure was found to be similar to the normal rhombohedral structure of the alunite supergroup. However, this

particular sample is unique in that there is a new site occupied: Zn is located within six membered rings formed by iron octahedra and is trigonal bipyramidal in coordination as a result of being displaced ~0.8 Å from the center of the ring. The Zn is ordered across only half of these sites and this leads to ordered displacements of Pb atoms. Ordering of partially occupied Fe^{3+} cations and their vacancies has been attributed to a lowering of symmetry for jarosite subgroup minerals (Grey *et al.* 2011; Scarlett *et al.* 2010). In these studies, natrojarosite, titular jarosite and natrojarosite-hydronium jarosite solid solutions were prepared with ordered iron vacancies which lead to a lowering of symmetry to the monoclinic space group C2/*m*. Further study into the properties of alunite supergroup minerals with lower symmetry and not just their crystal structure, is required, especially their magnetic properties (Scarlett *et al.* 2010). In addition, other examples of symmetry lowered alunite supergroup minerals as a result of ordering of different atomic sites and atomic sites and their vacancies may be discovered.

NON-STOICHIOMETRY OF SYNTHESISED JAROSITES AND ALUNITES

Most synthesized alunite supergroup minerals are not stoichiometric. The non-stoichiometry probably results from deficiencies at the A and B site rather than the T site as this makes the most structural sense (Jambor 1999; Szymanski 1985). Hence, the TO_4 groups are assumed to be fully occupied when calculating chemical compositions. In the majority of cases where a non-stoichiometric alunite supergroup mineral is synthesized, an excess of water/oxygen (not from OH groups) is usually observed along with an A site deficiency. This excess water is commonly attributed to the presence of the hydronium ion (H_3O^+) at the A site (Brophy and Sheridan 1965; Drouet and Navrotsky 2003; Ripmeester *et al.* 1986; Serna *et al.* 1986; Stoffregen and Alpers 1992; Stoffregen *et al.* 2000; Wilkins *et al.* 1974). In addition to deficiencies at the A site, the B site is also usually not fully occupied (Basciano and Peterson 2007b; Dutrizac and Kaiman 1976; Nielsen *et al.* 2008; Nielsen *et al.* 2011). Vacancies at the B site of up to 30% are not

uncommon. The B site vacancies are charge compensated by protonation of hydroxyl groups in the structure to form water.

The actual presence of the hydronium ion and the nature that the excess water assumes in the crystal structure is difficult to prove and has been the subject of much debate in the literature. The existence of both H_3O^+ and OH^- in the same crystal may seem surprising, especially when it is considered that H_3O^+ is surrounded by OH^- groups. It might be thought that these two groups would neutralize each other to form water molecules in the structure. Microprobe, wet chemistry and spectroscopic techniques have not conclusively shown that the hydronium ion exists in the supergroup (Stoffregen *et al.* 2000; Wilkins *et al.* 1974). However, ^{1}H NMR (Ripmeester *et al.* 1986), ^{2}H NMR (Nielsen *et al.* 2011) and neutron diffraction (Wills and Harrison 1996) studies have provided strong evidence for the presence of H_3O^+ in alunites and jarosites, and that protonation of the framework by hydronium does not occur.

MAGNETIC STRUCTURE AND PROTON MOBILITY

Alunite supergroup minerals with magnetic ions such as Fe^{3+} and V^{3+} at the B site undergo long-range magnetic ordering at low temperature (Grohol *et al.* 2003; Matan *et al.* 2009). These minerals are an ideal form of the rare Kagomé lattice which is composed of magnetic ions at the corners of triangles that are connected through their vertices (Grohol *et al.* 2003; Matan *et al.* 2009; Nocera *et al.* 2004). For a triangular array, it is impossible for all moments to couple antiferromagnetically and a non-collinear 120° structure is typically realized (Wills *et al.* 2000). In all jarosites except hydronium jarosite, long range magnetic order with the q = 0 structure is observed with a transition temperature below about 70 K (Inami *et al.* 2000; Matan *et al.* 2009; Wills *et al.* 2000). Hydronium jarosite on the other hand, is a spin glass with a freezing temperature at approximately 17 K (Fåk *et al.* 2008; Wills and Harrison 1996; Wills *et al.* 2000; Wills *et al.* 1998). The magnetic structure is shown in Figure 2-2. A review on the magnetic

structure of jarosite minerals has been published previously and the reader is directed there for further information (Wills 2001).

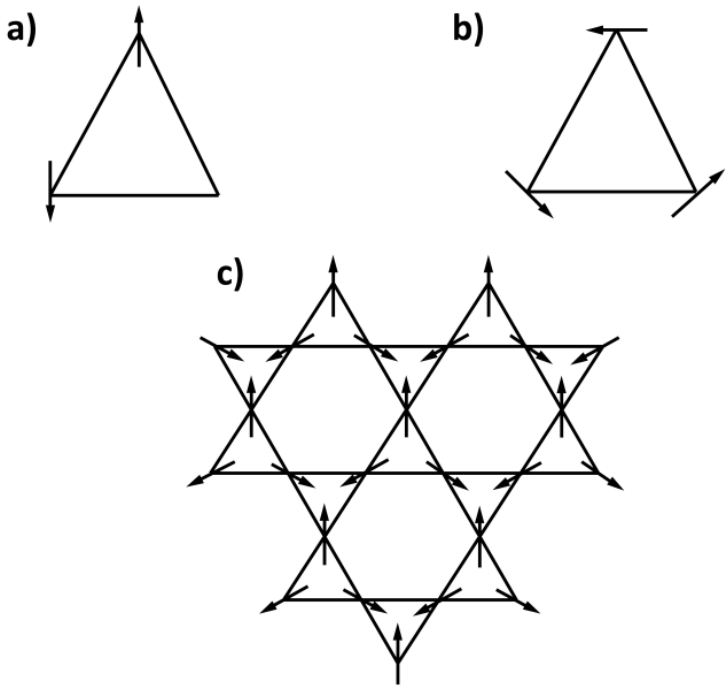

Figure 2-2: Magnetic structure of jarosites showing a) the impossibility of all moments coupling antiferromagnetically in a triangular array, b) one of the many degenerate ground states that is obtained by rotating the moments 120 ° and c) the q = 0 array of magnetic moments that is at T < 70 K. Adapted from Wills and Harrison (1996)

The long range magnetic ordering has been attributed to the fact that Fe^{3+} in jarosites has a weak single-ion-type anisotropy (Inami *et al.* 2000). However, the cause for the spin glass behavior of hydronium jarosite is under debate. It has been proposed that hydronium jarosite is a spin glass due to: structural disorder involving hydronium, different forms of further-neighbor inter- and/or intra-plane exchange (Frunzke *et al.* 2001); random disorder of hydronium due to its position and/or transfer of hydrogen through the structure (Fåk *et al.* 2008); a more ordered FeO_6 octahedra such that the other jarosites are more disordered and have higher antiferromagnetic transition temperatures (Bisson and Wills 2008); or the intrinsic reaction chemistry of hydronium jarosite which

facilitates proton transfer from hydronium to bridging hydroxyl groups (Nocera *et al.* 2004), this reaction is given below in equation 1:

$$(H_3O)Fe_3(OH)_6(SO_4)_2 \rightarrow (H_3O)_{1-x}(H_2O)_xFe_3(OH)_{6-x}(H_2O)_x(SO_4)_2 \qquad (1)$$

Nuclear magnetic resonance (NMR) is another method to probe magnetic structure and the spin glass behavior of hydronium jarosite. The first NMR study on hydronium alunite, although undertaken to confirm the existence of hydronium in the mineral group, showed that the hydronium ion has a high degree of mobility and that it is not annihilated by the surrounding hydroxyl groups (Ripmeester *et al.* 1986). Subsequent studies have also shown that the hydronium ion is highly mobile and that neutralization to water does not occur (Nielsen *et al.* 2008; Nielsen *et al.* 2011). However, it has been found that there is an interaction between hydronium ions and bridging hydroxyl groups from infrared spectroscopy (Grohol and Nocera 2007). Thus, the literature suggests that potential proton exchange and also proton mobility are the main reasons why hydronium jarosite is a spin glass, and for reasons that will be explained in the following paragraph, are linked to the orientational disorder of the hydronium ion.

Ammoniojarosite, despite also having orientational disorder of the A site cation (Basciano and Peterson 2007a), shows long range magnetic order like other jarosites. In this study of ammoniojarosite, the authors were able to locate the ammonium hydrogen atoms by single crystal X-ray diffraction at room temperature (Basciano and Peterson 2007a). It was found that the ammonium ion is disordered across two orientations with equal probability. A comparable single crystal X-ray diffraction study of hydronium jarosite, also at room temperature, failed to locate the hydronium hydrogen atoms (Majzlan *et al.* 2004). To the best of the authors' knowledge, only one study has successfully located the hydronium hydrogen positions and even then, the exact geometry was said to be uncertain (Wills and Harrison 1996). Given that the pKa of H_3O^+ is 0 and the pKa of NH_4^+ is 9.25 (Atkins and De Paula 2006), it can be said that the ammonium

ion is relatively unreactive with respect to the surrounding hydroxyl groups when compared to the hydronium ion. It has been shown that transfer of hydrogen atoms from hydronium ions to the surrounding hydroxyl groups is not impossible, but if it occurs, does not result in complete neutralization to water; H_3O^+ and OH^- both exist in the structure over time. Thus, it is argued that transfer of hydrogen to the hydroxyl groups may be a contributing mechanism by which the dynamically disordered hydronium ion reorients itself in the A site cavity. Such proton mobility would explain why the hydronium hydrogen atoms are more difficult to locate by diffraction techniques when compared to the ammonium hydrogen atoms, and also the observation that the hydronium ion is highly mobile from NMR studies.An NMR study comparing ammonioalunite or ammoniojarosite to hydronium jarosite or hydronium alunite could serve to clarify these issues. To date, no NMR study of ammonioalunite or ammoniojarosite has been undertaken.

Incoherent inelastic neutron scattering (IINS) can be used to determine proton dynamics in materials and has been used to assign bands to the hydronium ion for hydronium substituted mordenite (Jobic *et al.* 1992). We are aware of only one IINS study on hydronium containing alunite supergroup minerals with a view to determining proton dynamics and identifying the hydronium ion. This study analyzed alunite and hydronium alunite (Lager *et al.* 2001) but distinct peaks corresponding to hydronium were not observed. This was attributed to peaks due to hydronium, hydroxyl groups and hydrogen bonded water not being to be distinguished. Further IINS investigations into comparing hydronium and ammonium containing jarosite or alunite minerals with their potassium counterparts are warranted.

STRUCTURAL VARIATION IN THE SUPERGROUP: MEMBERS WITH A SUPER CELL

Despite the supergroup being largely isostructural, some members have a super cell with plumbojarosite, or lead jarosite [$Pb_{0.5}Fe_3(SO_4)_2(OH)_6$], being the most well known and characterized example (Hendricks 1937; Szymanski 1985). In this case, the

super cell structure is a maximal isomorphic subgroup of lowest index (Klassengleiche type IIc) of space group $R\bar{3}m$. This means that in order for the space group and symmetry operations to be preserved when Pb^{2+} occupies the A site, the unit cell must enlarge. The super cell for plumbojarosites manifests as a doubling of the **c** axis from ~17 Å to ~34 Å (Hendricks 1937; Szymanski 1985). The super cell can be detected in X-ray diffraction by a peak at approximately 7 – 9 °2θ when using Cu Kα1 radiation (Jambor and Dutrizac 1983). Additional peaks are present at higher diffraction angles, but this low angle peak is the most intense and is diagnostic of the super cell.

Other alunite supergroup minerals which possess a super cell are minamiite [(Na, Ca, K)$Al_3(SO_4)_2(OH)_6$], huangite [$Ca_{0.5}Al_3(SO_4)_2(OH)_6$] and walthierite [$Ba_{0.5}Al_3(SO_4)_2(OH)_6$] (Jambor 1999; Ossaka *et al.* 1982). These minerals also have divalent cations at the A site. Thus, one might think that the presence of a divalent cation automatically results in a super cell. However, there are a number of supergroup minerals with divalent cations at the A site which have no super cell (Sato *et al.* 2009). Examples of these minerals include beaverite [Pb(Fe, Cu)$_3(SO_4)_2(OH)_6$], beudantite [$PbFe_3(AsO_4)(SO_4)(OH)_6$], osarizawaite [Pb(Al, Cu)$_3(SO_4)_2(OH)_6$], schlossmacherite [(H_3O, Ca)$Al_3(AsO_4, SO_4)_2(OH)_6$] and most crandallite subgroup minerals (Jambor 1999).

As the general formula for jarosites and alunites has the A site being monovalent, a divalent cation (such as Pb^{2+}, Ca^{2+} and Ba^{2+}) at this site brings additional positive charge to the structure which must be mitigated. For those minerals which possess a super cell, charge balance is achieved by 50% occupancy of the A site. This results in two different species at the A site: the A^{2+} cation and a vacancy. When the distribution of vacancies and A^{2+} cations is ordered (repeating in a regular fashion), a super cell forms (Hendricks 1937; Jambor 1999; Jambor and Dutrizac 1983). It has been suggested that simply ordering amongst A site cations, even without the presence of vacancies, can result in a super cell (Jambor 1999).

Such ordering of A site cations and vacancies is clearly seen for plumbojarosite (Szymanski 1985). This study found that there were two different A site positions with significantly different fractional occupancies with respect to lead: one with a lead occupation of 0.961 (termed "occupied") and one with a lead occupation of 0.039 (termed "vacant"). This ordering results in alternate A sites along the *z* axis of the crystal, i.e. vacant at the Wyckoff site 3a (0, 0, 0) and occupied at the Wyckoff site 3b (0, 0, ½). To account for the doubled **c** axis and hence, twice as many atoms in the unit cell (Z = 6), the site symmetry of iron changes to C_s and there now two crystallographically independent sulfate (6c) and hydroxyl (18h) groups. Similar ordering of A site cations in minamiite was observed, such that Ca^{2+} and Na^{+} occupy one site whilst K^{+} and Na^{+} occupy the other with vacancies distributed across both (Ossaka *et al.* 1982). The plumbojarosite structure (Szymanski 1985) with doubled **c** axis is shown in Figure 2-3.

A different charge balance mechanism could explain why a super cell is not observed for some members of the super group despite divalent cations substituting at the A site. Beaverite, beudantite, osarizawaite, schlossmacherite and the crandallite subgroup have phosphorus or arsenic at the T site or a divalent cation at the B site. Hence, there is either additional negative charge from the TO_4^{3-} groups or less positive charge at the B site to counteract the substitution of a divalent ion at the A site. Therefore, charge balance is achieved without vacancies (or another species at the A site) and subsequent ordering at the A site cannot occur (a cation cannot order with itself if its site is fully occupied). Ordering of cations at the A site has been previously discussed in a review (Jambor 1999). An extensive analysis of the crystal structure of various alunite and beudantite group minerals with divalent cations at the A site and either divalent cations at the B site or TO_4^{3-} ions at the T site found no evidence for any super cell formation (Sato *et al.* 2009).

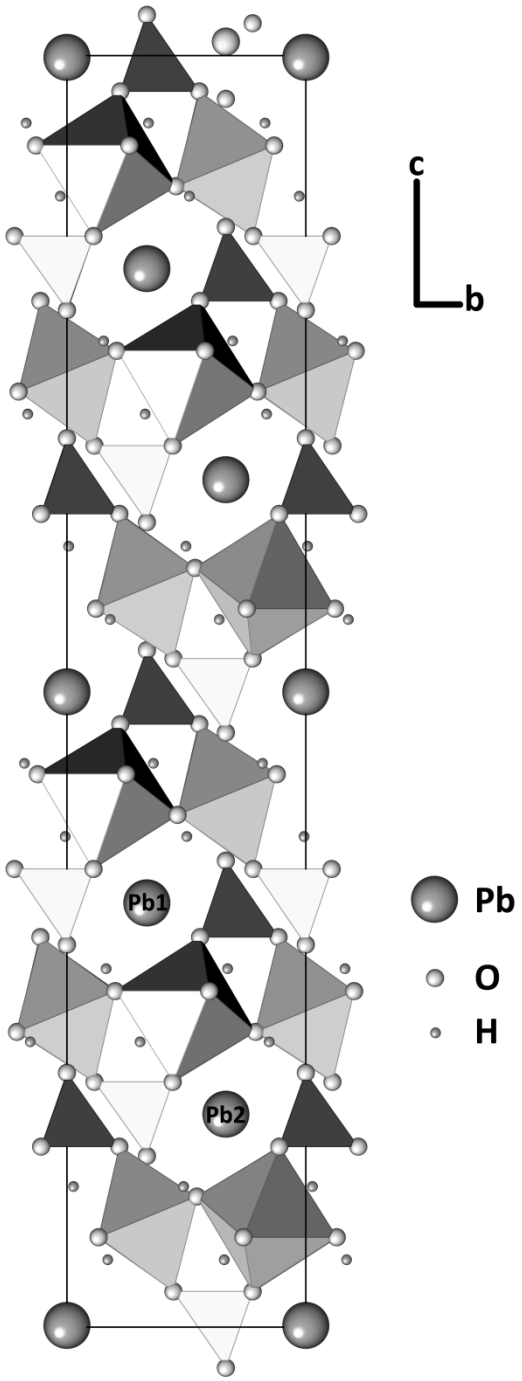

Figure 2-3: The crystal structure of super cell plumbojarosite projected down the **a** axis showing SO_4 and FeO_6 as polyhedra

However, to complicate things further, some studies have found or synthesized plumbojarosite without a super cell (Bartlett and Nocera 2005; Forray *et al.* 2010; Smith *et al.* 2006). No impurities were present that could have resulted in charge balance at the T or B sites in these studies. Thus, it can be said that the distribution of vacancies and

lead in these cases was random and not ordered. In addition, some of these studies (Forray *et al.* 2010; Smith *et al.* 2006) used a synthesis route that was previously found to yield plumbojarosite with a super cell (Dutrizac and Kaiman 1976).

Given the ubiquitous presence of hydronium in the alunite supergroup, hydronium substitution or chemical composition differences may be the cause of the discrepancies in **c** axis length for these plumbojarosite specimens. It has been argued that the doubled **c** axis is only observed in plumbojarosite when the composition approaches that of the end member (Mumme and Scott 1966). For those plumbojarosites that did not possess a doubled **c** axis, hydronium at the A site would mean that these plumbojarosites were actually an intermediate composition between a plumbojarosite-hydronium jarosite solid solution and ordering would need to occur between three A site species (Pb^{2+}, vacancy, H_3O^+). Indeed, 74% hydronium at the A site was found for one of the plumbojarosites with no doubled **c** axis (Forray *et al.* 2010). Minamiite has ordering between three species: Ca^{2+}, Na^+ and K^+ (Ossaka *et al.* 1982) so ordering between more than two species at the A site is not impossible. Stoichiometric plumbojarosite, with respect to both Fe^{3+} and Pb^{2+}, has been prepared with no doubled **c** axis (Bartlett and Nocera 2005), which suggests that composition and/or hydronium content does not influence the doubling of the **c** axis in plumbojarosite.

A study of the beaverite – plumbojarosite solid solution found that **c** axis length did not correlate with composition and that a specific lead composition was not necessary to form the doubled **c** axis (Jambor and Dutrizac 1983). Similar problems with **c** axis length have been observed for beaverite; a natural beaverite sample was found to have a doubled **c** axis while a synthetic sample did not (Hudson-Edwards *et al.* 2008). This was despite the natural beaverite's chemical composition not deviating significantly from the literature and other natural beaverite samples. Again, chemical composition and H_3O^+ contents do not appear to be the principle cause of **c** axis discrepancies. Therefore, it would seem that there is an unknown variable (or even variables) in the synthesis of plumbojarosite and beaverite which cause these variations in **c** axis length and the

presence of a super cell. A systematic study which synthesizes plumbojarosite and beaverite under various conditions may elucidate what causes the presence or absence of a super cell.

The fact that in some cases the same synthesis was carried out, but different **c** axis lengths reported, suggests that the X-ray data collection and/or refinement strategies are important. Thus, all X-ray diffraction patterns should be presented (not just refined parameters) when discussing plumbojarosite and other minerals which could potentially show the effects of a super cell. Careful inspection of diffraction patterns should be undertaken so as to ascertain whether the super cell peaks are present or missing. Patterns should be collected to as low a diffraction angle as possible so the first super cell peak can be observed, as has been recommended previously (Jambor 1999).

VIBRATIONAL SPECTROSCOPY OF THE ALUNITE AND JAROSITE MINERAL SUBGROUPS

GENERAL DESCRIPTION OF THE VIBRATIONAL SPECTRA OF JAROSITE AND ALUNITE MINERALS

Many extensive reviews and publications exist in the literature concerning the vibrational spectroscopy, especially that of infrared spectroscopy, for sulfate bearing minerals (Adler and Kerr 1965; Cloutis *et al.* 2006; Griffith 1970; Makreski *et al.* 2005; Omori and Kerr 1963). The free sulfate ion (T_d symmetry) has $1A_1 + 1E + 2T_2$ modes of vibration. The A_1 mode is the symmetric stretch (ν_1), the doubly degenerate E mode is the deformation vibration (ν_2) whilst the T_2 modes are the triply degenerate antisymmetric stretch (ν_3) and the triply degenerate bending vibration (ν_4) (Cloutis *et al.* 2006). For free sulfate ions in solution, the approximate positions of these modes are 1104 cm^{-1} (ν_3), 981 cm^{-1} (ν_1), 613 cm^{-1} (ν_4) and 451 cm^{-1} (ν_2) (Adler and Kerr 1965). These positions can be used as a general guide for the assignment of sulfate bands in vibrational spectroscopy.

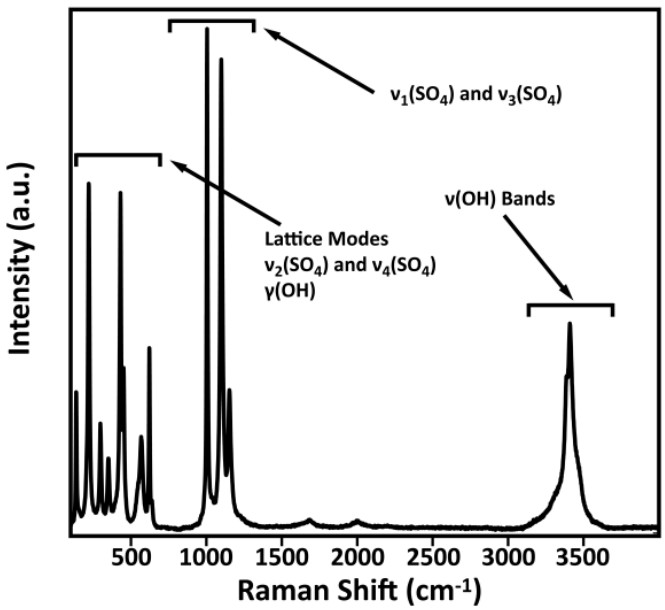

Figure 2-4: Typical Raman spectrum of jarosite [$KFe_3(SO_4)_2(OH)_6$]

The vibrational spectra of jarosites and alunites can be divided into three main groups of bands: those due to hydroxyl groups, internal modes of sulfate, and lattice modes (Chio *et al.* 2005; Murphy *et al.* 2009). Hydroxyl bands have been found to exhibit the highest sensitivity with respect to A site cation in Raman spectroscopy (Chio *et al.* 2005; Chio *et al.* 2010). The sulfate fundamental vibrations in Raman spectra, $\nu_1(SO_4)$ and $\nu_3(SO_4)$, correlate well with the **c** axis length (Sasaki *et al.* 1998) and in turn, the A site cation. Figures 2-4 and 2-5 are typical examples of Raman and infrared spectra of jarosites with monovalent cations at the A site.

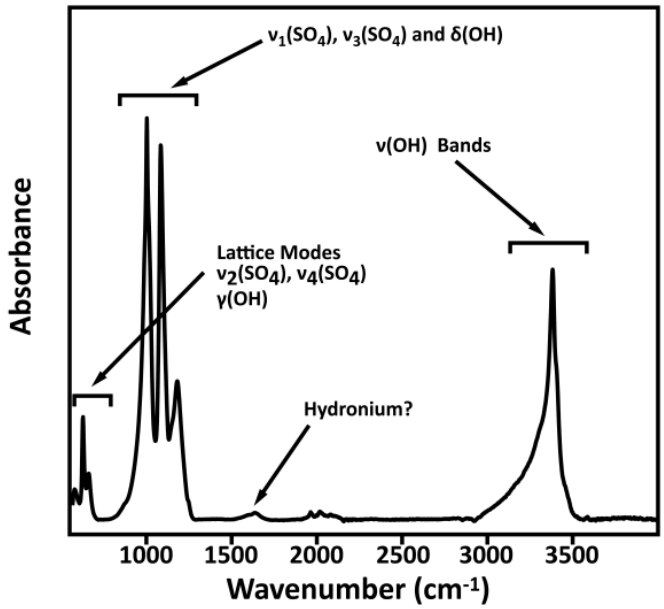

Figure 2-5: Typical infrared spectrum of jarosite [$KFe_3(SO_4)_2(OH)_6$]

FACTOR GROUP ANALYSIS OF THE ALUNITE SUPERGROUP

Factor group analysis (Adams 1973; DeAngelis *et al.* 1972; Rousseau *et al.* 1981) is necessary to understand the vibrational spectra of solids. Factor group analysis is essentially an extension of point group symmetry principles that are applied to molecules, except solids and minerals are under analysis (Rousseau *et al.* 1981). Factor group analysis allows one to determine the symmetry species of all expected vibrations for the

crystal of interest, assuming the chemical composition and crystal structure are known. It also facilitates accurate band assignment of vibrational spectra, especially when coupled to single crystal vibrational spectroscopic techniques (Beattie and Gilson 1968; Damen *et al.* 1966). A single crystal spectroscopic study has not been performed for any member of the alunite supergroup, probably due in part to the difficulty in obtaining adequate single crystal specimens, as alluded to earlier.

The following factor group analysis was performed using the tables in Farmer (Farmer 1974). The correlation diagram of the TO_4 groups, showing how the free (T_d) modes of vibration are affected by sitting at a lower symmetry C_{3v} site in a crystal of space group $R\bar{3}m$ (D_{3d}), is given in Table 2-1. The irreducible representation (total number of allowed modes), including lattice modes, is obtained after subtraction of the translational modes of the crystal ($1E_u + 1A_{2u}$) and is given by:

$$\Gamma_{irred} = 8A_{1g} + 3A_{2g} + 4A_{1u} + 10A_{2u} + 11E_g + 14E_u \text{ (75 modes total)}$$

Raman active modes: $8A_{1g} + 11E_g$

IR active modes: $10A_{2u} + 14E_u$

Inactive modes: $3A_{2g} + 4A_{1u}$

Table 2-1: Factor group splitting of the internal modes for TO_4 groups

Molecular symmetry (T_d)	Site symmetry (C_{3v})	Crystal symmetry (D_{3d})
		$3A_{1g}$ (Raman active)
A_1	$3A_1$	
		$3A_{2u}$ (IR active)
E		$3E_g$ (Raman active)
	$3E$	
$2T_2$		$3E_u$ (IR activce)

In the case of sulfate as the TO_4 group, Table 2-1 shows that: the ν_1 symmetric stretching mode (A_1) will split to give one Raman (A_{1g}) and one IR active band (A_{2u}); the

ν_2 deformation mode (E) will yield one Raman (E_g) and one IR (E_u) active band; whilst the ν_3 antisymmetric stretch and the ν_4 bending vibration (both T_2) will give rise to four vibrations each ($1A_{1g}$, $1A_{2u}$, $1E_g$ and $1E_u$). Thus, at least one band from all sulfate fundamental vibrations is expected in both Raman and IR spectra. Owing to the mutual exclusion principle, the gerade (g) modes are only Raman active and the ungerade (u) modes are only IR active.

JAROSITE AND ALUNITE SUBGROUP BAND ASSIGNMENTS

In most cases, the $\nu_3(SO_4)$ (1200-1000 cm^{-1}) and $\nu_4(SO_4)$ (700-600 cm^{-1}) modes should be easily assigned in infrared spectra as no other absorptions are expected in their spectral regions (Makreski *et al.* 2005). The $\nu_3(SO_4)$ bands are some of the strongest in the infrared spectrum (Bishop and Murad 2005). In Raman spectra the strong band at *ca* 1000 cm^{-1} is a $\nu_1(SO_4)$ mode and the strong bands around 1100 cm^{-1} are $\nu_3(SO_4)$ modes (Chio *et al.* 2005; Chio *et al.* 2010; Makreski *et al.* 2005). Bands above 3000 cm^{-1} are obviously due to ν(OH) modes of vibration originating from water, hydroxyl groups and hydronium ions. There are discrepancies involving the assignment of other bands in the infrared and Raman spectra. Indeed, this mineral group has an extended lattice nature and many bands overlap in the low wavenumber region (Breitinger *et al.* 1997; Powers *et al.* 1975; Toumi and Tlili 2008). The actual symmetry of bands in jarosite and alunite Raman and infrared spectra are yet to be assigned by a single crystal vibrational spectroscopic study. Such a study may help identify and correctly assign bands (Arkhipenko and Bokii 1975; Damen *et al.* 1966; Sacuto *et al.* 1996).

An infrared band at 1640 cm^{-1} which occurs in most hydronium substituted jarosites and alunites has been assigned to structural water molecules (Wilkins *et al.* 1974). This band has also been observed in all potassium-hydronium jarosite derivatives in a solid solution, but the intensity of this band did not increase as the hydronium content increased (Grohol and Nocera 2007). Other studies have either assigned it to be a result of structural water or surface adsorbed water (Bishop and Murad 2005; Makreski *et al.*

2005; Powers *et al.* 1975). However, it has also been argued that this band may be related to the use of KBr discs to collect infrared spectra (Toumi and Tlili 2008). This band is most likely an H–O–H deformation originating from structural water, in accordance with most literature on the subject. A band at ~1580 cm^{-1} has been assigned to the hydronium ion (Grohol and Nocera 2007; Kubisz 1972; Wilkins *et al.* 1974) as its intensity decreases as the alkali metal content at the A site increases (Grohol and Nocera 2007; Wilkins *et al.* 1974). Apart from this band, there is little vibrational spectroscopic proof for the existence of hydronium at the A site.

In an infrared study on alunite, jarosite and the deuterated analogue of jarosite, two bands above 3000 cm^{-1} (one intense and one shoulder) were observed and assigned to ν(OH) modes (Powers *et al.* 1975). A band at 1003 cm^{-1} was assigned to an OH deformation as it shifted to 761 cm^{-1} upon deuteration. Bands at 1181 and 1080 cm^{-1} were assigned to $\nu_3(SO_4)$ modes. A strong band at 626 cm^{-1} and a shoulder at 650 cm^{-1} were assigned to $\nu_4(SO_4)$ modes. A weak band at 1020 cm^{-1} was attributed to $\nu_1(SO_4)$. The remaining bands were attributed to lattice modes and metal – oxygen vibrations. In general, band positions for alunite were higher than jarosite, but no greater than 50 cm^{-1}. The $\nu_2(SO_4)$ mode went unassigned. However, this mode of vibration occurs in the low wavenumber region and may have overlapped with bands due to lattice modes (Bishop and Murad 2005). For example, a $\nu_2(SO_4)$ mode was assigned to a peak at 450 cm^{-1} in one infrared study (Sasaki *et al.* 1998).

Various jarosites with different A site cations have been studied by Raman spectroscopy (Chio *et al.* 2010; Sasaki *et al.* 1998). The position and number of the sulfate fundamentals were comparable, as were the lattice modes. Any minor variations in their band positions are explained by expected sample variation and collection of Raman spectra as well as the wavenumber cut-off at 200 cm^{-1} (Sasaki *et al.* 1998) and 100 cm^{-1} (Chio *et al.* 2010). However, differences between the two studies are found in: the hydroxyl stretching region with one, two or three bands being reported depending on hydronium content; a band at 1664 cm^{-1} which was assigned to $\nu_2(NH_4)$ (Chio *et al.* 2010)

but not observed in the other study; the number of γ(OH) modes at either two (Chio *et al.* 2010) or one (Sasaki *et al.* 1998); and the presence of a δ(OH) mode at 1021 cm^{-1} (Chio *et al.* 2010) that went unobserved in the other study.

The vibrational spectra of alunite and its deuterated analogue has been studied (Breitinger *et al.* 1997). Four bands between 1200-1000 cm^{-1} were observed in both infrared and Raman, whilst one at 1150 cm^{-1} shifted upon deuteration so it was ascribed to a δ(OH) mode. A Raman band at 655 cm^{-1} did not shift upon deuteration so it was assigned to $\nu_4(SO_4)$. In the infrared spectra, bands at 681, 631, 602, 529 and 432 cm^{-1} were assigned to lattice vibrations involving AlO_6 octahedra as they shifted by 15 cm^{-1} upon deuteration. It was thought that these bands obscure the δ(OH) and $\nu_4(SO_4)$ bands in this region, which were not assigned. An infrared and Raman study on a natural alunite specimen from El Gnater, Tunisia, resulted in very different band assignments in the region below 1000 cm^{-1} (Toumi and Tlili 2008).

In an infrared and Raman study focused on bands due to water and hydronium, bands at 1575 and 1175 cm^{-1} were assigned to $\nu(H_3O)$ and a band at 850 cm^{-1} to H_3O rotation, but other hydronium bands were believed to be obscured by ν(OH) (Kubisz 1972). The band at 1640 cm^{-1} was believed to be due to water which substitutes for B site cations. This study found that the infrared $\nu_1(SO_4)$ and $\nu_3(SO_4)$ bands shifted to higher wavenumber as the radius of the A site cation decreased. This study is very different to others due to more bands resulting from hydronium and water being assigned in the vibrational spectra.

Raman and infrared spectroscopy have shown that the space group for the jarosite and alunite subgroups is most likely $R\bar{3}m$ (Arkhipenko and Bokii 1979; Serna *et al.* 1986), as the predicted number of bands from factor group analysis for this space group matched the observed spectra for all end members. Unlike a more recent study on ammonium jarosites and alunites (Sasaki *et al.* 1998), bands at both 1650 and 1430 cm^{-1} were attributed to the NH_4^+ cation in infrared spectra (Serna *et al.* 1986). Like other

studies, there was difficulty in assigning δ(OH), γ(OH) and some sulfate fundamental modes due to overlap with metal – oxygen modes and other lattice vibrations (Serna *et al.* 1986). Similar band assignments and conclusions were also reached in the other study (Arkhipenko and Bokii 1979).

APPLICATIONS OF JAROSITE AND ALUNITE VIBRATIONAL SPECTROSCOPY

Given that the jarosite minerals are found on Mars, rapid identification of end members and solid solutions through vibrational spectroscopy is important. This is because compared to Mössbauer spectrometers (first used to detect jarosite minerals on Mars), vibrational spectrometers are inexpensive and handheld/portable vibrational spectrometers are available. Jarosite is stable under the surface conditions on Mars and should be able to be detected by reflectance spectroscopy as there are diagnostic bands in the 0.4-2.5 μm region (25000-4000 cm^{-1}) (Cloutis *et al.* 2008). Recently, jarosite was detected in the Mawrth Vallis region of Mars through the use of orbital visible to near infrared reflectance spectroscopy (Farrand *et al.* 2009). Alunite, also through the use of orbital reflectance spectroscopy, has been detected on Mars at Terra Sirenum (Swayze *et al.* 2008). Like the earlier studies in 2004, these discoveries provide further evidence for the existence of acidic, sulfur-rich water on Mars at some point in the planet's history given the different locations where jarosite and alunite minerals have been detected.

Different jarosite type minerals themselves can be identified from other minerals in complex environments (such as mine waste and other planets) from spectroscopic measurements (Das and Hendry 2011; Wray *et al.* 2011), but there are only few studies which investigate jarosite and alunite solid solutions and the effects of A, B and T site variation on vibrational spectra (Basciano and Peterson 2007a, 2007b; Drouet and Navrotsky 2003; Drouet *et al.* 2004). One study found that there are only subtle differences between hydronium jarosite and jarosite solid solution members with loss of detail of spectra being the only defining characteristic of hydronium content (Basciano and Peterson 2007b). They postulated that spectroscopy may be able to determine an

approximate hydronium content of jarosite minerals, including those from Mars. For instance, the lack of certain bands, those with low intensity or the comparison of intensities of two bands in the spectrum may provide an estimation of hydronium content (or other cations). Ammonium can be identified by the appearance of new bands such as an infrared band at 1423 cm^{-1} (Basciano and Peterson 2007a). Comparing the intensity of this band with another may provide an estimation of ammonium content. A significant wavenumber decrease for the ν(OH) bands occurs when sodium occupies the A site (Drouet and Navrotsky 2003). For jarosite-alunite and natrojarosite-natroalunite solid solutions, only the position and intensity of bands change (Drouet *et al.* 2004). Thus, the identification and rough estimation of A site cation occupancy for jarosite solid solution members through vibrational spectroscopy appears promising, but requires further study. Such a study may help resolve the ambiguity of band assignments in the 1000-400 cm^{-1} region.

THE SPLITTING OF SULFATE BANDS AND PLUMBOJAROSITE

It has been argued that the presence of non-equivalent ions in a crystal may enrich the vibrational spectrum beyond that allowed by the site symmetry (Adler and Kerr 1965). These same authors also write that the non-equivalent ions may have the same site symmetries as the non-equivalency could be due to different internuclear forces as a result of changes in the molecular surroundings. This is correct, and essentially what factor group analysis predicts for a molecule in a crystal. They then report that three fundamental $\nu_3(SO_4)$ and $\nu_4(SO_4)$ bands for jarosites and alunites can be allowed in the infrared spectrum. However, factor group analysis (Adams 1973; DeAngelis *et al.* 1972; Rousseau *et al.* 1981) predicts only two $\nu_3(SO_4)$ and $\nu_4(SO_4)$ modes of vibration in infrared spectra (Breitinger *et al.* 1997; Serna *et al.* 1986; Toumi and Tlili 2008). Nevertheless, assigning more sulfate fundamental modes of vibration than what would normally be allowed still persists (Chio *et al.* 2005; Cloutis *et al.* 2006; Murphy *et al.* 2009). In accordance with factor group analysis, those cases where three $\nu_3(SO_4)$ bands

are assigned, one of them has to be due to another vibrating unit, most likely an OH deformation, given that these modes of vibration occur in similar spectral regions (Sasaki *et al.* 1998; Serna *et al.* 1986).

It is correct to say that degenerate bands can split due to a lowering of symmetry, but this splitting does not exceed that allowed by factor group analysis. Obviously fewer bands than predicted can be observed due to resolution limitations, coincidence and overlap etc. Sometimes three bands in the hydroxide stretching region are observed, despite factor group analysis predicting two (Chio *et al.* 2010). The additional bands were explained due to the extra water or hydronium that is usually present in this mineral group (Chio *et al.* 2010).

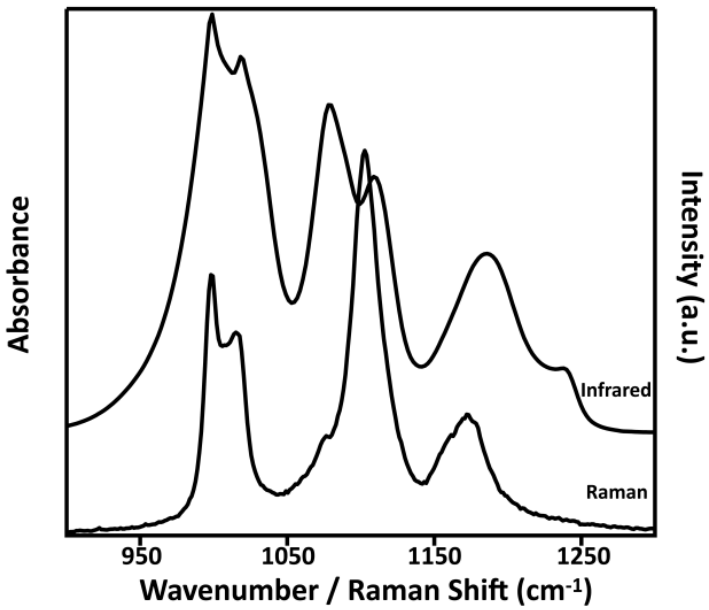

Figure 2-6: Raman and infrared spectra of super cell plumbojarosite from 900 – 1300 cm^{-1}

Plumbojarosite vibrational spectra are an interesting exception to other jarosites, as additional sulfate fundamental modes of vibration are actually observed (Sasaki *et al.* 1998). These additional bands were not observed for jarosites with a monovalent cation at the A site, and hence, those with no super cell. Similar results have been reported for beaverite and plumbojarosite (Hudson-Edwards *et al.* 2008). Figure 2-6 shows the Raman

and infrared spectra of plumbojarosite – the additional sulfate fundamental bands are clearly observed when compared to Figures 2-3 and 2-4. These extra sulfate bands were attributed to the fact that sulfate groups surrounding a vacancy are sufficiently different to those surrounding a Pb^{2+} cation (Sasaki *et al.* 1998). Thus, the two different sulfate groups (one surrounding a heavy Pb^{2+} ion and the other surrounding a vacancy) show the effects of additional Davydov/factor group splitting when compared to jarosite and alunite minerals with no super cell.

SYMMETRY PROBLEMS WITH HYDRONIUM AND AMMONIUM IONS

As mentioned previously, hydronium is known to substitute at the A site. However, the actual geometry that this ion assumes in the structure requires further investigation. Ammonium (NH_4^+) is another ion that can exist at the A site. The A site has D_{3d} symmetry and therefore, an inversion center. It seems surprising that H_3O^+ and NH_4^+ ions can be located at this site. This is because these two ions have no inversion center and it is well known that the site symmetry of a molecule must be a subgroup of the molecular symmetry (Jewess 1982; Petruševski *et al.* 1993; Schiebel *et al.* 2000); D_{3d} is not a subgroup of C_{3v} (free H_3O^+) or T_d (free NH_4^+). This fact is often glossed over, and has only been mentioned in some studies (Majzlan *et al.* 2004; Serna *et al.* 1986; Szymanski 1985) with no reference to how factor group analysis should be performed or vibrational spectra interpreted. If both ions are indeed located at the D_{3d} site as has been shown for ammoniojarosite (Basciano and Peterson 2007a), then factor group analysis cannot be performed under space group $R\bar{3}m$ with both ions at the D_{3d} site due to the inversion related symmetry mismatch between the free ions and the crystallographic site.

It has been suggested that H_3O^+ and NH_4^+ substitution at the A site would lower the symmetry to R3*m* or another lower symmetry space group (Majzlan *et al.* 2004; Serna *et al.* 1986; Szymanski 1985). However, vibrational spectroscopic studies clearly show that the spectra appear to be more in line with other jarosite and alunite minerals which

are $R\bar{3}m$ (Serna *et al.* 1986). These two minerals are frequently refined in space group $R\bar{3}m$. Thus, the actual geometry, and perhaps even space group, of jarosites and alunites with NH_4^+ and H_3O^+ ions at the A site requires further investigation as different models and structures have been proposed. For example, it has been argued based on a computational study, that the hydronium ion adopts a tilted configuration so that the 3-fold axis of the ion and the crystal are not coincident, resulting in more potential orientations and hydrogen bonds to the framework (Gale *et al.* 2010). An earlier study suggested that the hydronium oxygen instead occupies a C_{3v} (6c) site with 50% occupancy, and hydrogen atoms at a C_s (18h) site also with 50% occupancy. (Wills and Harrison 1996). Reconciliation of hydronium and ammoniojarosite's crystal structure with their vibrational spectra is needed.

IMPLICATIONS

Despite being studied for some time, there are still many unresolved questions surrounding the alunite supergroup of minerals, in particular:

- What causes the **c** axis to be doubled in plumbojarosite, minamiite, huangite and walthierite? In addition, can the doubling of the **c** axis be controlled synthetically?

- What is the geometry of the hydronium and ammonium ions in hydronium jarosite, hydronium alunite, ammoniojarosite and ammonioalunite, and how can this be reconciled with their vibrational spectra?

- What are the symmetry species of the observed bands in Raman and infrared spectra of jarosite and alunite minerals?

- Exactly why is hydronium jarosite a spin glass? Further NMR studies comparing hydronium jarosite to ammoniojarosite would be fruitful.

There is significant overlap of bands in the low wavenumber region of jarosite and alunite vibrational spectra. As a result, lattice modes, OH deformations and some sulfate fundamental modes of vibration (in particular ν_2 and ν_4) are difficult to positively identify. Care should be taken when interpreting vibrational spectra so that more bands than allowed by factor group analysis aren't assigned; only those minerals with a super cell are expected to have additional Raman and infrared bands for sulfate fundamental modes. Deuteration appears to be most useful for the alunite supergroup so that bands due to OH groups can be more clearly resolved from lattice and sulfate modes of vibration.

REFERENCES CITED

Adams, D. M., 1973: A descriptive introduction to analysis of the vibrational spectra of solids. *Coordination Chemistry Reviews*, **10,** 183-193.

Adler, H. H., and P. F. Kerr, 1965: Variations in infrared spectra, molecular symmetry and site symmetry of sulfate minerals. *American Mineralogist*, **50,** 132-147.

Alpers, C. N., R. O. Rye, D. K. Nordstrom, L. D. White, and B. S. King, 1992: Chemical, crystallographic, and isotopic properties of alunite and jarosite from acid hypersaline Australian lakes. *Chemical Geology*, **92,** 203-226.

Arkhipenko, D. K., and G. B. Bokii, 1975: Factor group analysis and X-ray diffraction study of crystals of vermiculite and talc. *Journal of Structural Chemistry*, **16,** 417-423.

——, 1979: Refinement of the alunite-jarosite space group by a vibrational spectroscopic method. *Soviet Physics, Crystallography*, **24,** 100-106.

Asta, M. P., J. Cama, M. Martínez, and J. Giménez, 2009: Arsenic removal by goethite and jarosite in acidic conditions and its environmental implications. *J. Hazard. Mat.*, **171,** 965-972.

Atkins, P., and J. De Paula, 2006: *Atkins' Physical Chemistry, 8th ed.* Oxford University Press.

Baron, D., and C. D. Palmer, 1996: Solubility of jarosite at 4-35 °C. *Geochimica et Cosmochimica Acta*, **60,** 185-195.

Bartlett, B. M., and D. G. Nocera, 2005: Long-Range Magnetic Ordering in Iron Jarosites Prepared by Redox-Based Hydrothermal Methods. *Journal of the American Chemical Society*, **127,** 8985-8993.

Basciano, L. C., and R. C. Peterson, 2007a: The crystal structure of ammoniojarosite, $(NH_4)Fe_3(SO_4)_2(OH)_6$ and the crystal chemistry of the

ammoniojarosite-hydronium jarosite solid-solution series. *Mineralogical Magazine*, **71,** 427-441.

——, 2007b: Jarosite-hydronium jarosite solid-solution series with full iron site occupancy: mineralogy and crystal chemistry. *American Mineralogist*, **92,** 1464-1473.

Beattie, I. R., and T. R. Gilson, 1968: Single crystal laser Raman spectroscopy. *Proceedings of the Royal Society of London. Series A, Mathematical and Physical Sciences*, **307,** 407-429.

Becker, U., and B. Gasharova, 2001: AFM observations and simulations of jarosite growth at the molecular scale: probing the basis for the incorporation of foreign ions into jarosite as a storage mineral. *Physics and Chemistry of Minerals*, **28,** 545-556.

Bishop, J. L., and E. Murad, 2005: The visible and infrared spectral properties of jarosite and alunite. *American Mineralogist*, **90,** 1100-1107.

Bisson, W. G., and A. S. Wills, 2008: Anisotropy-driven spin glass transition in the kagome antiferromagnet hydronium jarosite, $(H_3O)Fe_3(SO_4)_2(OH)_6$. *Journal of Physics: Condensed Matter*, **20,** 452204.

Blanchard, F. N., 1989: New X-ray powder data for gorceixite, $BaAl_3(PO_4)_2(OH_5)\bullet H_2O$, an evaluation of *d*-spacings and intensities, pseudosymmetry and its influence on the figure of merit. *Powder Diffraction*, **4,** 227-230.

Breitinger, D. K., R. Krieglstein, A. Bogner, R. G. Schwab, T. H. Pimpl, J. Mohr, and H. Schukow, 1997: Vibrational spectra of synthetic minerals of the alunite and crandallite type. *Journal of Molecular Structure*, **408-409,** 287-290.

Brophy, G. P., and M. F. Sheridan, 1965: Sulfate Studies IV: the jarosite-natrojarosite-hydronium jarosite solid solution series. *American Mineralogist*, **50,** 1595-1607.

Brophy, G. P., E. S. Scott, and R. A. Snellgrove, 1962: Sulfate studies II. Solid solution between alunite and jarosite. *American Mineralogist*, **47,** 112-126.

Burger, P. V., J. J. Papike, C. K. Shearer, and J. M. Karner, 2009: Jarosite growth zoning as a recorder of fluid evolution. *Geochimica et Cosmochimica Acta*, **73,** 3248-3259.

Buurma, A. J. C., I. P. Handayani, N. Mufti, G. R. Blake, P. H. M. van Loosdrecht, and T. T. M. Palstra, 2012: Spin-lattice coupling in iron jarosite. *Journal of Solid State Chemistry*, **195,** 50-54.

Chio, C. H., S. K. Sharma, and D. W. Muenow, 2005: Micro-Raman studies of hydrous ferrous sulfates and jarosites. *Spectrochimica Acta Part A: Molecular Spectroscopy*, **61,** 2428-2433.

Chio, C. H., S. K. Sharma, L.-C. Ming, and D. W. Muenow, 2010: Raman spectroscopic investigation on jarosite-yavapaiite stability. *Spectrochimica Acta Part A: Molecular Spectroscopy*, **75,** 162-171.

Cloutis, E. A., M. A. Craig, R. V. Kruzelecky, W. R. Jamroz, A. Scott, F. C. Hawthorne, and S. A. Mertzman, 2008: Spectral reflectance properties of minerals exposed to simulated Mars surface conditions. *Icarus*, **195,** 140-168.

Cloutis, E. A., and Coauthors, 2006: Detection and discrimination of sulfate minerals using reflectance spectroscopy. *Icarus*, **184,** 121-157.

Damen, T. C., S. P. S. Porto, and B. Tell, 1966: Raman Effect in Zinc Oxide. *Physical Review*, **142,** 570.

Das, S., and M. J. Hendry, 2011: Application of Raman spectroscopy to identify iron minerals commonly found in mine wastes. *Chemical Geology*, **290,** 101-108.

DeAngelis, B. A., R. E. Newnham, and W. B. White, 1972: Factor group analysis of the vibrational spectra of crystals: a review and consolidation. *American Mineralogist*, **57,** 255-268.

Desborough, G. A., and Coauthors, 2010: Mineralogical and chemical characteristics of some natural jarosites. *Geochimica et Cosmochimica Acta*, **74,** 1041-1056.

Drouet, C., and A. Navrotsky, 2003: Synthesis, characterization, and thermochemistry of K-Na-H3O jarosites. *Geochimica et Cosmochimica Acta*, **67,** 2063-2076.

Drouet, C., K. L. Pass, D. Baron, S. Draucker, and A. Navrotsky, 2004: Thermochemistry of jarosite-alunite and natrojarosite-natroalunite solid solutions. *Geochim. Cosmochim. Acta*, **68,** 2197-2205.

Dutrizac, J. E., 1991: The precipitation of lead jarosite from chloride media *Hydrometallurgy*, **26,** 327-346.

Dutrizac, J. E., 2008: Factors Affecting the Precipitation of Potassium Jarosite in Sulfate and Chloride Media. *Metallurgical and Materials Transactions B*, **39,** 771-783.

Dutrizac, J. E., and S. Kaiman, 1976: Synthesis and properties of jarosite-type compounds *Canadian Mineralogist*, **14,** 151-158.

Dzikowski, T. J., L. A. Groat, and J. L. Jambor, 2006: The symmetry and crystal structure of gorceixite, $BaAl_3[PO_3(O, OH)]_2(OH)_6$, a member of the alunite supergroup. *Canadian Mineralogist*, **44,** 951-958.

Elwood Madden, M. E., R. J. Bodnar, and J. D. Rimstidt, 2004: Jarosite as an indicator of water-limited chemical weathering on Mars. *Nature*, **431,** 821-823.

Fåk, B., F. C. Coomer, A. Harrison, D. Visser, and M. E. Zhitomirsky, 2008: Spin-liquid behavior in a kagomé antiferromagnet: deuteronium jarosite. *Europhysics Letters*, **81,** 17006.

Farmer, V. C., Ed., 1974: *The Infrared Spectra of Minerals*. Mineralogical Society.

Farrand, W. H., T. D. Glotch, J. W. Rice Jr, J. A. Hurowitz, and G. A. Swayze, 2009: Discovery of jarosite within the Mawrth Vallis region of Mars: Implications for the geologic history of the region. *Icarus*, **204,** 478-488.

Forray, F. L., A. M. L. Smith, C. Drouet, A. Navrotsky, K. Wright, K. A. Hudson-Edwards, and W. E. Dubbin, 2010: Synthesis, characterization and thermochemistry of a Pb-jarosite. *Geochimica et Cosmochimica Acta*, **74,** 215-224.

Frunzke, J., T. Hansen, A. Harrison, J. S. Lord, G. S. Oakley, D. Visser, and A. S. Wills, 2001: Magnetic ordering in diluted kagome antiferromagnets. *Journal of Materials Chemistry*, **11,** 179-185.

Gale, J. D., K. Wright, and K. A. Hudson-Edwards, 2010: A first-principles determination of the orientation of H_3O^+ in hydronium alunite. *American Mineralogist*, **95,** 1109-1112.

Grey, I. E., W. G. Mumme, P. Bordet, and S. J. Mills, 2008: A new crystal-chemical variation of the alunite-type structure in monoclinic $PbZn_{0.5}Fe_3(AsO_4)_2(OH)_6$. *Canadian Mineralogist*, **46,** 1355-1364.

Grey, I. E., N. V. Y. Scarlett, P. Bordet, and H. E. A. Brand, 2011: Jarosite-butlerite intergrowths in non-stoichiometric jarosites: crystal chemistry of monoclinic natrojarosite-hydronium jarosite phases. *Mineralogical Magazine*, **75,** 2775-2791.

Griffith, W. P., 1970: Raman studies on rock-forming minerals. Part II. Minerals containing MO_3, MO_4 and MO_6 groups. *Journal of the Chemical Society A*, 286-291.

Grohol, D., and D. G. Nocera, 2007: Magnetic disorder in the frustrated antiferromagnet jarosite arising from the H_3O^+•••OH^- interaction. *Chemistry of Materials*, **19,** 3061-3066.

Grohol, D., Q. Huang, B. H. Toby, J. W. Lynn, Y. S. Lee, and D. G. Nocera, 2003: Powder neutron diffraction analysis and magnetic structure of kagomé-type vanadium jarosite $NaV_3(OD_6)(SO_4)_2$. *Physical Review B*, **68,** 094404.

Hendricks, S. B., 1937: The crystal structure of alunite and the jarosites. *American Mineralogist*, **22,** 773-784.

Hochella, M. F., J. N. Moore, C. V. Putnis, A. Putnis, T. Kasama, and D. D. Eberl, 2005: Direct observation of heavy metal-mineral association from the Clark Fork River Superfund Complex: implications for metal transport and bioavailability. *Geochimica et Cosmochimica Acta*, **69,** 1651-1663.

Hudson-Edwards, K. A., A. M. L. Smith, W. E. Dubbin, A. J. Bennett, P. J. Murphy, and K. Wright, 2008: Comparison of the structures of natural and synthetic Pb-Cu-jarosite-type compounds. *European Journal of Mineralogy*, **20,** 241-252.

Inami, T., M. Nishiyama, S. Maegawa, and Y. Oka, 2000: Magnetic structure of the kagomé lattice antiferromagnetc potassium jarosite $KFe_3(OH)_6(SO_4)_2$. *Physical Review B*, **61,** 12181-12186.

Jambor, J. L., 1999: Nomenclature of the alunite supergroup. *Canadian Mineralogist*, **37,** 1323-1341.

Jambor, J. L., and J. E. Dutrizac, 1983: Beaverite-plumbojarosite solid solutions. *Canadian Mineralogist*, **21,** 101-113.

Jewess, M., 1982: A theoretical treatment of 'orientational' disorder for routine use. *Acta Crystallographer B*, **38,** 1418-1422.

Jobic, H., M. Czjzek, and R. A. Van Santen, 1992: Interaction of water with hydroxyl groups in H-mordenite: a neutron inelastic scattering study. *Journal of Physical Chemistry*, **96,** 1540-1542.

Klingelhöfer, G. M., R. V.; Bernhardt, B.; Schröder, C.; Rodionov, D. S.; de Souza Jr, P. A.; Yen, A.; Gellert, R.; Evlanov, E. N.; Zubkov, B.; Foh, J.; Bonnes, U.; Kankeleit, E.; Gütlich, P.; Ming, D. W.; Renz, F.; Wdowiak, T.; Squyres, S. W.;

Arvidson, R. E, 2004: Jarosite and hematite at Meridiani Planum from Opportunity's Mossbauer spectrometer. *Science*, **306,** 1740-1745.

Kolitsch, U., and A. Pring, 2001: Crystal chemistry of the crandallite, beudantite and alunite groups: a review and evaluation of the suitability as storage materials for toxic metals. *Journal of Mineralogical and Petrological Sciences*, **96,** 67-78.

Kubisz, J., 1972: Studies on synthetic alkali-hydronium jarosites III: infrared absorption study. *Mineralogia Polonica*, **3,** 23-37.

Lager, G. A., G. A. Swayze, C.-K. Loong, F. J. Rotella, J. W. Richardson, and R. E. Stoffregen, 2001: Neutron spectroscopic study of synthetic alunite and oxonium-substituted alunite. *Canadian Mineralogist*, **39,** 1131-1138.

Loiacono, G. M., G. Kostecky, and J. S. White, 1982: Resolution of space group ambiguities in minerals. *American Mineralogist*, **67,** 846-847.

Lueth, V. W., R. O. Rye, and L. Peters, 2005: "Sour gas" hydrothermal jarosite: ancient to modern acid-sulfate mineralization in the southern Rio Grande Rift. *Chemical Geology*, **215,** 339-360.

Majzlan, J., and Coauthors, 2004: Thermodynamic properties, low-temperature heat-capacity anomalies, and single-crystal X-ray refinement of hydronium jarosite, $(H_3O)Fe_3(SO_4)_2(OH)_6$. *Physics and Chemistry of Minerals*, **31,** 518-531.

Makreski, P., G. Jovanoski, and S. Dimitrovska, 2005: Minerals from Macedonia XIV. Identification of some sulfate minerals by vibrational (infrared and Raman) spectroscopy. *Vibrational Spectroscopy*, **39,** 229-239.

Matan, K., J. S. Helton, D. Grohol, D. G. Nocera, S. Wakimoto, K. Kakurai, and Y. S. Lee, 2009: Polarized neutron scattering studies of the kagomé lattice antiferromagnet $KFe_3(OH)_6(SO_4)_2$. *Physica B*, **404,** 2529-2531.

Menchetti, S., and C. Sabelli, 1976: Crystal chemistry of the alunite series: crystal structure refinement of alunite and synthetic jarosite. *Neues Jahrbuch für Mineralogie Monatshefte*, **9,** 406-417.

Mumme, W. G., and T. R. Scott, 1966: The relationship between basic ferric sulfate and plumbojarosite. *American Mineralogist*, **51,** 443-453.

Murphy, P. J., A. M. L. Smith, K. A. Hudson-Edwards, W. E. Dubbin, and K. Wright, 2009: Raman and IR spectroscopic studies of alunite-supergroup compounds containing, Al^{3+}, Cr^{3+} Fe^{3+} and V^{3+} at the B site. *Canadian Mineralogist*, **47,** 663-681.

Nielsen, U. G., J. Majzlan, and C. P. Grey, 2008: Determination and quantification of the local environments in stoichiometric and defect jarosite by solid-state ^2H NMR spectroscopy. *Chemistry of Materials*, **20,** 2234-2241.

Nielsen, U. G., I. Heinmaa, A. Samoson, J. Majzlan, and C. P. Grey, 2011: Insight into the local magnetic environments and deuteron mobility in jarosite ($AFe_2(SO_4)_2(OD,OD_2)_6$, A = K, Na, D_3O) and hydronium alunite ($(D_3O)Al_3(SO_4)_2(OD)_6$), from variable-temperature ^2H MAS NMR spectroscopy. *Chemistry of Materials*, **23,** 3176-3187.

Nocera, D. G., B. M. Bartlett, D. Grohol, D. Papoutsakis, and M. P. Shores, 2004: Spin frustration in 2D kagomé lattices: a problem for inorganic synthetic chemistry. *Chemistry A European Journal*, **10,** 3850-3859.

Omori, K., and P. F. Kerr, 1963: Infrared Studies of Saline Sulfate Minerals. *Geological Society of America Bulletin*, **74,** 709-734.

Ossaka, J., J.-I. Hirabayashi, K. Okada, and R. Kobayashi, 1982: Crystal structure of minamiite, a new mineral of the alunite group. *American Mineralogist*, **67,** 114-119.

Papike, J. J., J. M. Karner, and C. K. Shearer, 2006: Comparative planetary mineralogy: Implications of martian and terrestrial jarosite. A crystal chemical perspective. *Geochimica et Cosmochimica Acta*, **70,** 1309-1321.

Petruševski, V. M., B. Minčeva-Šukarova, and A. Džorovska, 1993: The vibrational species of molecules in disordered crystals: $M(NH_3)_2$ groups at C_{4h}

symmetry sites. *Bulletin of the Chemists and Technologists of Macedonia*, **12,** 31-34.

Powers, D. A., G. R. Rossman, H. J. Schugar, and H. B. Gray, 1975: Magnetic behavior and infrared spectra of jarosite, basic iron sulfate and their chromate analogies. *Journal of Solid State Chemistry*, **13,** 1-13.

Radoslovich, E. W., 1982: Refinement of gorceixite in C*m*. *Neues Jahrbuch für Mineralogie Monatshefte*, 446-464.

Ripmeester, J. A., C. I. Ratcliffe, J. E. Dutrizac, and J. L. Jambor, 1986: Hydronium ion in the alunite - jarosite group. *Canadian Mineralogist*, **24,** 435-447.

Rousseau, D. L., R. P. Bauman, and S. P. S. Porto, 1981: Normal mode determination in crystals. *Journal of Raman Spectroscopy*, **10,** 253-290.

Sacuto, A., A. Lebon, D. Colson, A. Bertinotti, J. F. Marucco, and V. Viallet, 1996: Normal-modes study of $HgBa_2Ca_2Cu_3O_8^+$[delta] single crystals by a micro-Raman analysis. *Physica C*, **259,** 209-217.

Sasaki, K., and H. Konno, 2000: Morphology of jarosite-group compounds precipitated from biologically and chemically oxidized Fe ions. *Canadian Mineralogist*, **38,** 45-56.

Sasaki, K., O. Tanaike, and H. Konno, 1998: Distinction of jarosite-group compounds by Raman spectroscopy. *Canadian Mineralogist*, **36,** 1225-1235.

Sato, E., I. Nakai, R. Miyawaki, and S. Matsubara, 2009: Crystal structures of alunite family minerals: beaverite, corkite, alunite, natroalunite, jarosite, svanbergite, and woodhouseite. *Neues Jahrbuch für Mineralogie Abhandlungen*, **185,** 313-322.

Savage, K. S., D. K. Bird, and P. A. O'Day, 2005: Arsenic speciation in synthetic jarosite. *Chemical Geology*, **215,** 473-498.

Scarlett, N. V. Y., I. E. Grey, and H. E. A. Brand, 2010: Ordering of iron vacancies in monoclinic jarosites. *American Mineralogist*, **95,** 1590-1593.

Schiebel, P., K. Burger, H. G. Büttner, G. J. Kearley, M. Lehmann, and W. Prandl, 2000: ND_3-Density distribution in orientationally disordered $Ni(ND_3)_6Cl_2$ observed by means of neutron Laue diffraction. *Journal of Physics: Condensed Matter*, **12,** 8567-8576.

Scott, K. M., 1987: Solid solution in, and classification of, gossan-derived members of the alunite-jarosite family, northwest Queensland, Australia. *American Mineralogist*, **72,** 178-187.

Scott, K. M., 2000: Nomenclature of the alunite supergroup: Discussion. *Canadian Mineralogist*, **38,** 1295-1297.

Serna, C. J., C. P. Cortina, and J. V. Garcia Ramos, 1986: Infrared and Raman study of alunite-jarosite compounds. *Spectrochimica Acta Part A: Molecular Spectroscopy*, **42A,** 729-734.

Smith, A. M. L., W. E. Dubbin, K. Wright, and K. A. Hudson-Edwards, 2006: Dissolution of lead- and lead-arsenic-jarosites at pH 2 and 8 and 20 °C: Insights from batch experiments. *Chem. Geol.*, **229,** 344-361.

Stoffregen, R. E., and C. N. Alpers, 1992: Observations on the unit-cell dimensions, H_2O contents and δD values of natural and synthetic alunite. *American Mineralogist*, **77,** 1092-1098.

Stoffregen, R. E., C. N. Alpers, and J. L. Jambor, 2000: Alunite-jarosite crystallography, thermodynamics, and geochronology. *Reviews in Mineralogy and Geochemistry*, **40,** 453-479.

Swayze, G. A., and Coauthors, 2008: Discovery of the acid-sulfate mineral alunite in Terra Sirenum, Mars, using MRO CRISM: possible evidence for acid-saline lacustrine deposits? *American Geophysical Union, Fall Meeting 2008, Abstract #P44A-04.*

Szymanski, J. T., 1985: The crystal structure of plumbojarosite. *Canadian Mineralogist*, **23,** 659-668.

Toumi, M., and A. Tlili, 2008: Rietveld refinement and vibrational spectroscopic study of alunite from El Gnater, central Tunisia. *Russian Journal of Inorganic Chemistry*, **53,** 1845-1853.

Wilkins, R. W. T., A. Mateen, and G. W. West, 1974: The spectroscopic study of oxonium ions in minerals. *American Mineralogist*, **59,** 811-819.

Wills, A. S., 2001: Conventional and unconventional orderings in the jarosites. *Canadian Journal of Physics*, **79,** 1501-1510.

Wills, A. S., and A. Harrison, 1996: Structure and magnetism of hydronium jarosite, a model Kagomé antiferromagnet. *Journal of the Chemical Society, Faraday Transactions*, **92,** 2161-2166.

Wills, A. S., A. Harrison, C. Ritter, and R. I. Smith, 2000: Magnetic properties of pure and diamagnetically doped jarosites: model kagomé antiferromagnets with variable coverage of the magnetic lattice. *Physical Review B*, **61,** 6156-6169.

Wills, A. S., A. Harrison, S. A. M. Mentink, T. E. Mason, and Z. Tun, 1998: Magnetic correlations in deuteronium jarosite, a model S = 5/2 Kagomé antiferromagnet. *Europhysics Letters*, **42,** 325-330.

Wray, J. J., and Coauthors, 2011: Columbus crater and other possible groundwater-fed paleolakes of Terra Sirenum, Mars. *Journal of Geophysical Research*, **116, E01001**.

CHAPTER 3 ORIENTATIONAL DISORDER IN JAROSITE MINERALS

PREFACE

This chapter is based on, and is closely related to the review article presented in Chapter 2. A thorough study of the vibrational spectra of hydronium jarosite and ammoniojarosite in relation to their crystal structure is lacking, due to orientational disorder, and the related ambiguous hydrogen atom location associated with the hydronium and ammonium ions. To account for these effects, it has been suggested the crystal structures of hydronium jarosite and ammoniojarosite may be different to other alunite supergroup minerals. This is disconcerting as an understanding of a solid's crystal structure is fundamental; all other properties must be in compliance. Additionally, the differing magnetic behaviour of hydronium jarosite and ammoniojarosite at low temperature is not adequately accounted for despite both minerals exhibiting orientational disorder. There must be a hitherto unaccounted for structural reason for this fact.

This chapter examines orientational disorder and how it affects the crystal structure of solids and minerals, which is an important concept in this thesis. Those cases where the disordered molecule is located at a crystallographic site that is not a subgroup of the molecule's symmetry are the main focus. The previous methods to overcome the problems associated with the prediction of the vibrational spectra of solids and minerals containing orientationally disordered molecules at symmetry disallowed sites are critically evaluated. This review culminates in a discussion of orientational disorder and its relationship to the jarosite group of minerals in terms of crystal structure and vibrational spectroscopy. It will be shown that so far, there is no adequate solution.

3.1 DISORDER IN CRYSTALLINE SOLIDS

3.1.1 INTRODUCTION

Disorder in crystallography can be considered as a breakdown of the local translational symmetry of the unit cell. However, the crystal's symmetry, when time and spatially averaged, is not destroyed. The breakdown of translational symmetry can apply to either the entire unit cell, or only one part. There are two main kinds of disorder in crystals: substitutional and orientational.

Substitutional disorder occurs when two or more elements occupy the same crystallographic site (Giacovazzo 2002). Both elements are either fractionally occupied so the multiplicity of their crystallographic site is preserved, or, when their valances are different, fractionally occupied so charge balance is achieved. Alternatively, the disorder may be between an element and a vacancy; in this case there is incomplete occupation and the multiplicity of the site is not preserved, but charge balance is still maintained. Substitutional disorder can be random or ordered. Clearly random substitutional disorder means the distribution of the two or more species occupying the same crystallographic site occurs in no regular repeating fashion. Ordered substitutional disorder means the distribution of species occupying the same crystallographic site occurs in a regular repeating fashion which often results in a superstructure, as is the case in plumbojarosite which exhibits ordering between Pb^{2+} and a vacancy to give a doubled **c** axis (Szymanski 1985).

Orientational disorder, sometimes called positional disorder, occurs when the local orientation or configuration of all or part of a molecule is ambiguous (Giacovazzo 2002; Massa 2004). This type of disorder commonly occurs in: molecular groups that have rotational freedom and can be found in different rotatmers such as *tert*-butyl groups (Müller 2009); molecules that can have different conformations due to rotation of one part of the molecule, such as crown ethers (Massa 2004); linear molecules than can coordinate at either end, and small high symmetry nearly spherical molecules (Massa

2004; Tilley 2013). Another type of disorder is when the entire molecule can assume two or more orientations (Cotton and Elgin 1992) related by a symmetry element (Massa 2004). An alternative way of thinking about orientational disorder is there exists more than one energy minimum for the molecule to occupy. Figure 3-1 below shows the different types of disorder.

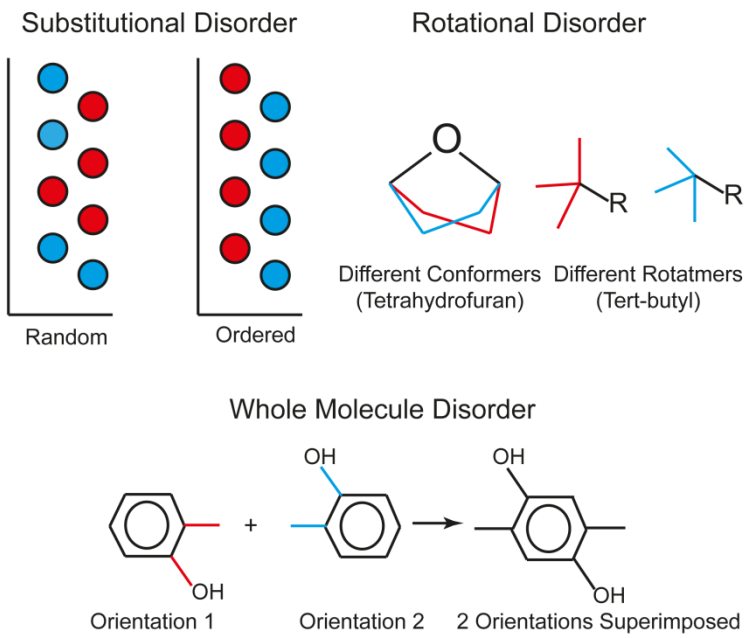

Figure 3-1: Diagram showing the major types of disorder. Different localised configurations for all the types of disorder are shown in either red or blue

Orientational disorder across two or more orientations can be static or dynamic. Static orientational disorder means the molecule may be found fixed in one of two or more orientations (often, but not always, equally distributed) across the unit cell. Dynamic orientational disorder means the molecule reorients itself between the available orientations over time. The mechanism for reorientation is dependent on the molecule and its surrounding environment. The reorientation mechanism, in general, cannot be determined from Rietveld refinement of diffraction data.

It is well known the site symmetry of a molecule in a crystal should be a subgroup of the molecular symmetry and the crystal symmetry (Jewess 1982; Petruševski

et al. 1993; Schiebel *et al.* 2000). However, there are numerous examples of molecules occupying crystallographic sites that are not a subgroup of their molecular symmetry, or, occupy a site of higher symmetry than their molecular symmetry (Boyle 1972; Catti and Ibberson 2002; Halford 1946; Oxton *et al.* 1976; Petruševski *et al.* 1993; Rudolf *et al.* 1985; Schiebel *et al.* 1996; Schiebel *et al.* 2000). Ammonium chloride (NH_4Cl) is perhaps the classic example whereby NH_4^+ ions are located at symmetry forbidden *m*3*m* sites (Levy and Peterson 1952). In such cases the molecule must be disordered across numerous orientations, freely rotating, or, the space group choice is wrong.

Orientational disorder is the focus of this review. Because static and dynamic disorder are both manifestations of orientational disorder, *static* or *dynamic* will only be referred to in the text when a clear distinction between these two types of disorder is necessary. For all intents and purposes, when *orientational disorder* is mentioned in the text, it refers to the situation where the local orientation of a molecule in a crystal is ambiguous, either statically or dynamically.

3.1.2 ORIENTATIONAL DISORDER IN SOLIDS AND CRYSTALS

3.1.2.1 Crystal Structure Effects

Static and dynamic disorders complicate the refinement of crystal structures and it is often necessary to choose between these two types of disorder. However, both static and dynamic orientational disorders have similar effects with regards to crystal structure refinement, especially on the atomic displacement parameters (ADPs) (Bürgi 2000). Indeed, it is not normally possible to differentiate between the two types of disorder from diffraction data alone (Dunitz *et al.* 1988; Giacovazzo 2002). If the ADPs of outer atoms of the disordered molecule are larger than the central atoms, then librations around the centre of mass are the probable motion (Pressprich *et al.* 2002). Both types of orientational disorder can lead to a foreshortening of bond distances involving the disordered molecule or atom (Dunitz *et al.* 1988). Some studies have shown excessive

rotation can cause a smearing of electron density in Fourier maps to give poorly resolved features or even circular contours (Dittrich *et al.* 2009; Rahman *et al.* 2003; Schiebel *et al.* 1996). In a related fashion, others believe that if the disordered atom is clearly resolved in a Fourier map then free rotation can be ruled out (Beintema 1965). It has been known for some time complete free rotation of a molecule in all dimensions of a crystal is rare (Staveley and Parsonage 1961), but there are some examples. Usually all that can be said from diffraction data is whether disorder is present.

Methods for modelling the crystal structures of orientationally disordered molecules, in particular those located at symmetry forbidden sites, are few and far between. When a disordered molecule appears to occupy a site higher than its molecular symmetry, it was suggested the proper description of the site symmetry for the disordered molecule can be derived by assuming stationary values of the potential energy are related to coincidences of the symmetry elements of the free ion with the symmetry elements of the crystal (Jewess 1982). The argument of Jewess (1982) is that only the coincidence of like symmetry elements of the molecule and the crystal are significant, and that principle rotation axes are the most important. He argues some atomic positions in disordered molecules (usually central atoms) should be displaced from high symmetry sites. However, if this displacement is minor, it may not be able to be modelled from diffraction data and actually be absorbed into the ADP (English and Heyns 1984; Müller 2009).

Alternatively, a "split atom model" may be appropriate for modelling a disordered molecule. In this instance the disordered parts of the molecule in question are shifted or "split" to occupy a lower symmetry site, often a general site (C_1) with appropriate fractional occupancy. See for example, refinements attempted by Schiebel et al. (1996). These models imply there are many orientations available to the disordered molecule (see Figure 3-2). However, the resolution of diffraction data may not permit the refinement of these models. Massa (2004) states atom positions for a split atom model must be at least 0.8 Å apart, and powder diffraction usually can't resolve atom positions

less than 0.6 Å from each other (Cotton and Elgin 1992). Thus, a split atom model should be applied with caution.

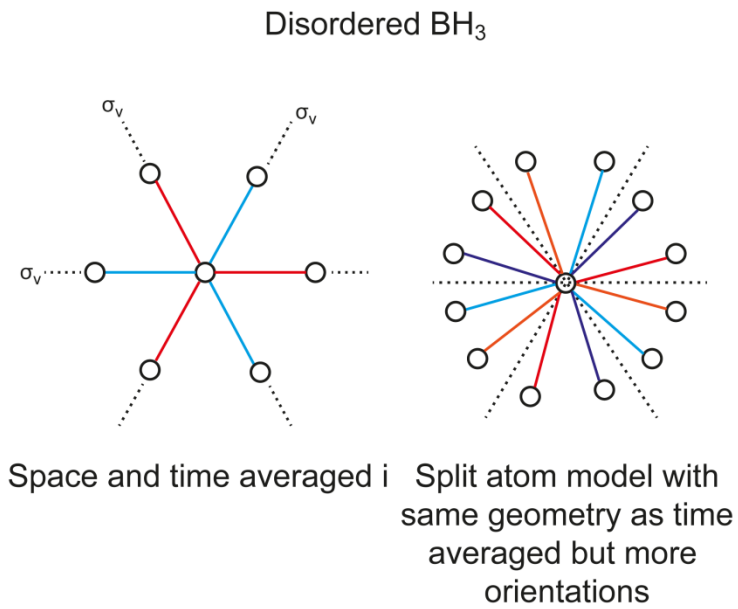

Figure 3-2: Example of a split atom model (right) for borane (BH_3) disordered around an inversion centre. Red and orange, and blue and purple in the split atom model approximate the red and blue orientations respectively in the higher symmetry model (left)

One other explanation for orientational disorder is the space group choice that results in disorder is incorrect (Harlow 1996; Massa 2004). There is often a related space group that lacks certain symmetry elements which results in no disorder. It has been said cases where the assigned space group symmetry is too high often result in disorder or large ADPs (Harlow 1996). Harlow (1996) also writes that a structure can actually be disordered and the structural problems misinterpreted. Indeed, a high symmetry disordered structure can be preferable to a low symmetry ordered structure (Marsh 1986; Marsh and Schomaker 1981).

Each situation is different and there appears to be no generally accepted rule for dealing with orientational disorder. A chemically feasible structure with acceptable inter-atomic distances and angles and reasonable ADPs, all of which may need restraining

(Watkin 2008), are perhaps the only criteria for a correct crystal structure model where disorder is involved.

3.1.2.2 Vibrational Spectroscopic Effects

Similar to structure refinement, static and dynamic disorder both have similar effects upon vibrational spectra, namely, bands broaden and there may be a breakdown of Davydov (factor group) splitting for the bands originating from the orientationally disordered molecule (Besbes *et al.* 1999; Dharmasena and Frech 1995; Fernandes *et al.* 1979; Pham-Thi *et al.* 1987). While both types of disorder affect Raman band widths, dynamic disorder shows greater temperature dependence such that band widths decrease rapidly with decreasing temperature (White 2005). However, broadening and no observable Davydov splitting in a spectrum does not automatically imply orientational disorder is present. Alternatively, depending on the crystal and the disordered molecule, the expected splitting of bands or other structural effects such as the mutual exclusion principle may be observed, as is the case for disordered $Zn(CN)_2$ (Ravindran *et al.* 2007). A crystal composed solely of a disordered molecule, such as the numerous phases of ice, only display broad and featureless bands (Bertie 1968; Pruzan *et al.* 1990). Free, or nearly free rotation, can manifest as rotation-like structure of the disordered molecule's stretching bands (Roberts *et al.* 1987). It has been said that vibrational spectroscopy is a responsive probe to slight changes in the molecular environment of molecules that reorient (Roberts 1990). Vibrational spectroscopy has also been used to rule out free rotation of ammonium in ammonium bromide (Wagner and Hornig 1950).

3.1.2.3 Group Theory and Symmetry Considerations

While orientational disorder poses some problems for structure refinement, it can be adequately modelled using the principles of crystallography by virtue of the fact that the most appropriate crystallographic model has the minimum number of assumptions (parameters) and the highest symmetry necessary to explain all diffraction and other data.

The prediction and interpretation of vibrational spectra of crystals containing orientationally disordered molecules using factor group analysis is more challenging. This is because no correlation between molecule and site and/or factor group symmetry can be established for the disordered molecule. A number of alternative methods have been derived and all have their advantages and disadvantages with none being applicable in all cases.

It is well known the spectroscopic space group for symmetry analysis can be different (either higher or lower symmetry) to the crystallographic space group (Buttery *et al.* 1969; Hollebone and Lever 1972; Kettle *et al.* 1984). Such differences are usually due to pseudo symmetry, or crystallisation in a lattice that is a small distortion of a high symmetry lattice. In these cases, the symmetry analysis is straightforward as an acceptable spectroscopic space group and site symmetry for the disordered molecule can be found.

In a study of orientationally disordered ice phases, it was suggested the identity operation is the only symmetry element a disordered crystal possesses, and factor group analysis based on the diffraction space group is not adequate for predicting IR activity (Bertie 1968). This theory[1] for orientationally disordered crystals is lattice vibrations due to both the factor group (order allowed) and every vibration whether optic, acoustic, transverse of longitudinal, regardless of wave vector (disorder allowed) are active in both the IR and Raman spectra (Bertie 1968; Whalley and Bertie 1967).

It was suggested that when the site symmetry is a higher order than the molecular symmetry, the ion interacts with the rest of the crystal as a point due to free rotation; special selection rules will apply (Halford 1946). However, no mention of these rules was given. Halford (1946) also stated that crystals containing freely rotating ions should not show the expected effects of orientation in single crystal Raman spectroscopy. The

[1]Note, this theory applies to *disordered crystals*, i.e. a crystal whose asymmetric unit is all or part of a disordered molecule. This situation is different to a crystal which contains a *disordered molecule,* in addition to other structural units that are not disordered.

present author suggests "free rotation" implies the molecule should be treated as though it were in the gas phase as it is able to rotate in all spatial dimensions in the crystal.

Orientation effects have been observed for orientationally disordered ammonium ions in ammonium perovskites (Auglló-Rueda *et al.* 1988). Thus, if the disorder is not so great that free rotation results, orientationally disordered molecules may still be influenced by the site and crystal symmetry. Furthermore, correlation through an infinite point group for molecules sitting at a higher symmetry site than their molecular symmetry has been successfully proposed (Petruševski *et al.* 1993). In this study, the crystal was built upon a disordered molecule of the type $H_3N–M–NH_3$ where M was Ni, Pt or Pd and so, assuming free rotation of the NH_3 groups, the point group $D_{\infty h}$ could be used to correlate between the forbidden site symmetry C_{4h} and the molecular symmetry D_{3d} or D_{3h}.

3.2 ORIENTATIONAL DISORDER IN THE ALUNITE SUPERGROUP OF MINERALS

3.2.1 HYDRONIUM AND AMMONIUM ION SUBSTITUTION BACKGROUND

Alunite supergroup minerals can be represented by the general formula $AB_3(SO_4)_2(OH)_6$, where B is mostly aluminium for alunites or mostly iron (III) for jarosites. Alunite supergroup minerals which have hydronium (H_3O^+) and ammonium (NH_4^+) ions occupying the A site are not often studied. Hydronium and ammonium alunite and jarosite minerals are the only end members which contain polyatomic ions at the A site. Hydronium and ammonium ions can easily substitute at the A site due to their comparable ionic radii, similar behaviour in aqueous solutions, and similar coordination numbers to alkali metal ions of potassium and sodium (Ross and Evans 1965).

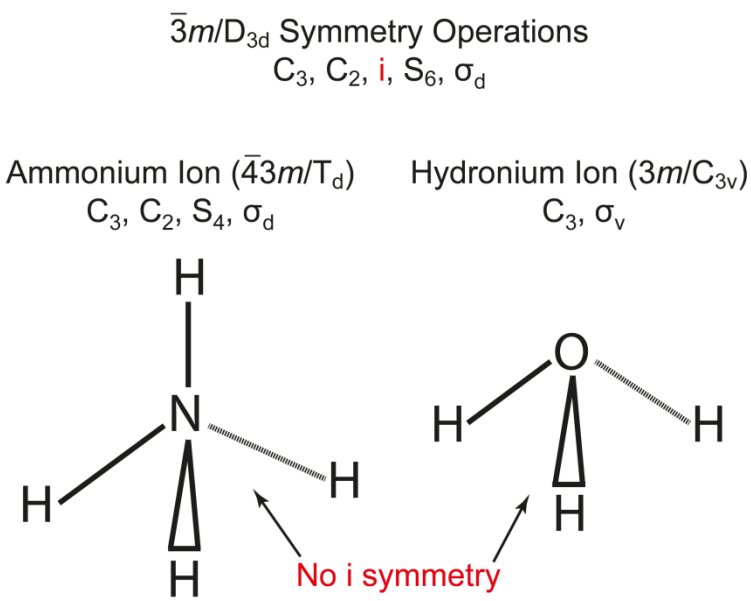

Figure 3-3: Ammonium and hydronium symmetry showing lack of an inversion centre

The symmetry of H_3O^+ and NH_4^+ ($3m$ and $\bar{4}3m$ respectively), is not a subgroup of the $\bar{3}m$ symmetry of the A site (see Figure 3-3). This led some to propose that the true

space group is not $R\bar{3}m$, but another lower symmetry space group (Majzlan *et al.* 2004; Serna *et al.* 1986; Szymanski 1985). Harlow (1996) writes that cases where the assigned space group symmetry is too high are quite rare and *R*-factors hang at unacceptably high values, but lowering the symmetry usually results in acceptable *R*-factors. However, he also says that examples of these structures will have high ADPs or appear disordered, the exact situation apparent in hydronium jarosite and ammoniojarosite. In general, the possibility of lower symmetry space groups has not been thoroughly investigated through refinement of crystal structure models for hydronium jarosite and ammoniojarosite. The hydronium and ammonium ions in jarosite minerals must be disordered, or, are occupying a lower symmetry site than other A site cations in the jarosite mineral group if the space group does not change as a result of these ions substitution at the A site. This orientational disorder and symmetry mismatch means that factor group analysis performed in the usual methods (Bhagavantam and Venkatarayudu 1939; Farmer 1974) cannot be employed for hydronium and ammonium containing alunite supergroup minerals.

Most jarosite minerals show long range magnetic ordering at low temperature, however, hydronium jarosite is a spin glass which freezes at about 17 K (Wills 2001; Wills *et al.* 2000). The spin glass behaviour of hydronium jarosite has been attributed to numerous mechanisms, including orientational disorder of the hydronium ion as orientational disorder is regarded as a prerequisite for spin glass behaviour (Fåk *et al.* 2008). However, if orientational disorder was significant then one would expect ammoniojarosite to also be a spin glass and not magnetically order. This fact has typically gone unnoticed, but it was suggested that the ammonium ion's hydrogen bonding is less disturbing or of a lesser consequence than the hydronium ion's (Wills 2001). A similar conclusion regarding the importance of the A site cation on magnetic structure was concluded from infrared spectroscopy (Grohol and Nocera 2007). Nevertheless, few direct comparisons using structural characterisation techniques between the two minerals

exist and the subtle differences between hydronium jarosite and ammoniojarosite are frequently ignored.

3.2.2 CRYSTAL STRUCTURE INVESTIGATIONS

There have been few crystal structure investigations of hydronium and ammoniojarosite. Considering the extra hydrogen atoms that are present in hydronium and ammoniojarosite, the lack of neutron diffraction studies is surprising. Unfortunately, jarosite minerals do not often form single crystals (Nocera *et al.* 2004), which means powder diffraction is the main structural characterisation technique. In addition, single crystals of hydronium jarosite (Majzlan *et al.* 2004) and ammoniojarosite (Basciano and Peterson 2007) which have been studied successfully by single crystal XRD are small (a lot less than 1.0 × 1.0 × 1.0 mm) and unsuitable for single crystal neutron diffraction.

There have been two main crystallographic studies of hydronium jarosite: one single crystal XRD study (Majzlan *et al.* 2004) and one neutron powder diffraction study (Wills and Harrison 1996). The former modelled the hydronium oxygen atom at the $\bar{3}m$ site as expected, while the latter modelled the hydronium oxygen atom at a 3*m* site with 50 % fractional occupancy. The single crystal XRD study could not locate hydronium hydrogen atoms. The neutron diffraction study located hydronium hydrogen atoms at an *m* site with 50 % fractional occupancy. The neutron diffraction study suggests the hydronium ion is disordered over at least two orientations in the unit cell. The structure determined by Wills and Harrison (1996) implies the two different oxygen positions can be resolved despite being less than 0.5 Å apart, while the structure refined by Majzlan et al. (2004) suggests any potential deviation from the $\bar{3}m$ site is included in the ADP. The different hydronium oxygen atom sites found by the two studies means further investigation and statistical tests on the *R*-factors of different crystallographic models is required.

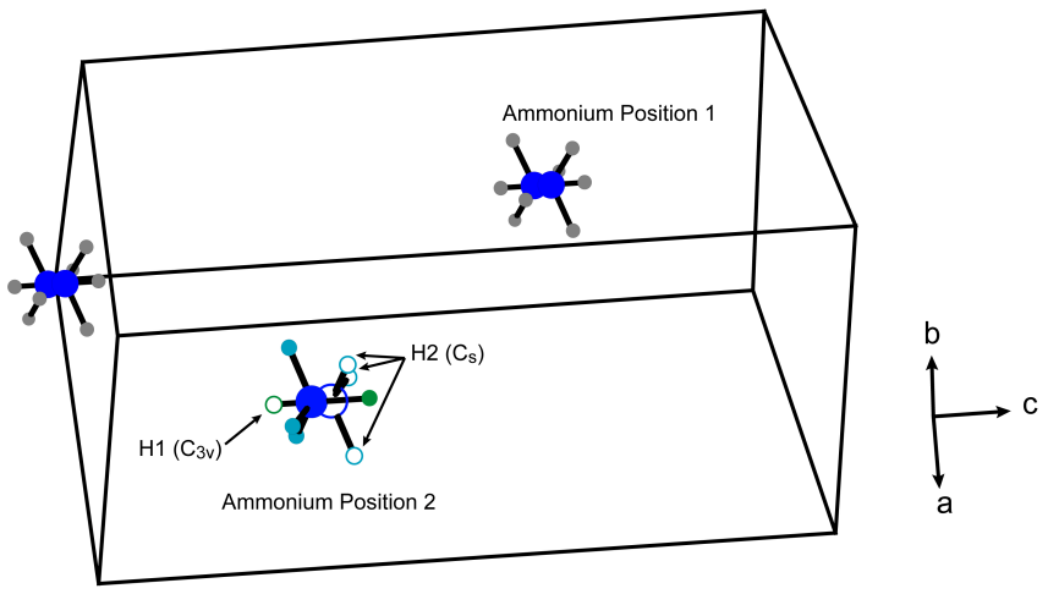

Figure 3-4: Diagram showing the orientational disorder of the ammonium ion as determined by Wills et al. (2000). The two orientations are indicated as dark circles and open circles for both nitrogen and hydrogen atoms for position 2

To the best of the author's knowledge, there exists only one in-depth study concerning the crystal structure of ammoniojarosite (Basciano and Peterson 2007). However, ammoniojarosite has also been studied via neutron powder diffraction in addition to other jarosite minerals (Wills *et al.* 2000). The main thrust of the latter paper however, was the magnetic structure of jarosite minerals. The single crystal XRD study managed to locate the disordered ammonium hydrogen atoms at a 3*m* and *m* site, both with 50 % fractional occupancy. This study also found no evidence for the ammonium nitrogen atom occupying a lower symmetry site than $\bar{3}m$. Thus, the ammonium ion was modelled as a tetrahedron with two orientations, up or down, with respect to the **c** axis. The structure refined by Wills et al. (2000) is essentially the same and the disorder of ammonium is shown in Figure 3-4. However, in this study, the authors shifted the ammonium nitrogen atom to a 3*m* site. They also found the refined ammoniojarosite structure when compared to the other jarosite minerals had higher *R*-factors, a higher χ^2,

and unstable ADPs. This was attributed to a possible small structural distortion from space group $R\bar{3}m$.

From the literature, any mention of a lower symmetry space group for ammoniojarosite and hydronium jarosite is merely mentioned and rarely investigated further, see for example, Majzlan et al. (2004) and Szymanski (1985). Wills et al. (2000) tried refining lower symmetry structures for ammoniojarosite but found no improvement in *R*-factors. These lower symmetry structures were maximal non-isomorphic subgroups of space group $R\bar{3}m$. The authors concluded that any distortion, if present, is small. It appears the most ambiguity is in the oxygen and nitrogen atom location for both ammonium and hydronium ions. Any shift of these two atoms to a lower symmetry site is not adequately accounted for and appears arbitrary.

3.2.3 VIBRATIONAL SPECTROSCOPIC INVESTIGATIONS

In-depth vibrational spectroscopic studies of hydronium and ammoniojarosite are few. Like crystallographic studies, some prior spectroscopic investigations simply noted the symmetry of hydronium and ammonium ions is not in agreement with the symmetry of the A site (Serna *et al.* 1986). In all earlier studies, the vibrational spectra of hydronium jarosite and ammoniojarosite are similar to other jarosite minerals with elemental cations at the A site (Chio *et al.* 2010; Powers *et al.* 1975; Sasaki *et al.* 1998; Serna *et al.* 1986); the only noticeable differences being NH_4^+ internal vibrations and a band at 1580 cm^{-1} due to hydronium. There is only one dedicated spectroscopic investigation of hydronium jarosite (Kubisz 1972), but band assignments differ significantly compared to other literature.

Serna et al. (1986) mentioned the space group of ammoniojarosite may be lower than $R\bar{3}m$, but interpreted the spectrum as though it were $R\bar{3}m$. A cold stage Raman study revealed no change in the vibrational spectrum of ammoniojarosite, even down to 8 K (Chio *et al.* 2010); the authors concluded no phase transition occurs for

ammoniojarosite or any jarosite mineral upon cooling. It seems likely that ordering of the orientations of ammonium does not occur and their orientational disorder remains even at low temperature. At least from a vibrational spectroscopic stand point, the space group of both hydronium jarosite and ammoniojarosite is not lower than $R\bar{3}m$. Small structural distortions alluded to in the crystallographic studies should be apparent in vibrational spectra.

3.2.4 INVESTIGATIONS USING OTHER CHARACTERISATION TECHNIQUES

Apart from vibrational spectroscopy and diffraction methods, nuclear magnetic resonance (NMR) has been used to investigate the hydronium ion in hydronium jarosite. There are no comparable studies for ammoniojarosite. An early NMR study of hydronium jarosite could not distinguish between D_2O or D_3O^+ at the A site and concluded the A site species has a high degree of mobility (Ripmeester *et al.* 1986). In fact, for many years it was debated whether the hydronium ion itself actually existed at the A site, or was neutralised to water. A Later NMR study found limited evidence for an intrinsic protonation reaction where D_3O^+ is neutralised by the surrounding hydroxyl groups (Nielsen *et al.* 2008). More recently, the existence of D_3O^+ was finally confirmed in stoichiometric regions of deuteronium jarosite and deuteronium alunite from variable temperature magic angle NMR (Nielsen *et al.* 2011). In this same study an activation energy for D_3O^+ motion was calculated at 6.3(4) kJ mol^{-1} and no evidence for proton transfer to the framework was observed. This activation energy is low and is suggestive of rapid motion as calculated from molecular dynamic simulations (Gale *et al.* 2010). Thus, NMR studies point towards dynamic orientational disorder of the hydronium ion, and by extension, the ammonium ion. Further study on the dynamics is required to determine its exact mechanism. Unfortunately, this is not possible from diffraction and spectroscopic methods as used in this thesis.

Incoherent inelastic neutron scattering (IINS) has been used to study hydronium alunite in comparison to alunite [$KAl_3(SO_4)_2(OH)_6$] (Lager *et al.* 2001). The present

author is not aware of a similar investigation of ammonium containing alunite supergroup minerals. IINS is very sensitive to hydrogen, and the technique offers complementary information to vibrational spectra. IINS is also sensitive to the motion of atoms (Kessel and Ben-Tal 2012), especially of the ^{1}H nucleus. The IINS study of hydronium alunite found a similar spectrum to alunite, with only the low energy range of the spectra being different. They found no clear evidence of vibrations that are solely related to hydronium and could not distinguish hydronium from hydroxyl groups and hydrogen bonded water. However, the authors noted they could only compare their spectra to a hydronium containing zeolite with a very different hydronium environment as few IINS studies of hydronium containing minerals exist. Nevertheless, IINS appeared inconclusive and did not offer significant extra information when compared to vibrational spectroscopy and neutron diffraction.

3.2.5 Symmetry Analysis: Inadequacy of Previous Methods for Orientational Disorder in the Alunite Supergroup of Minerals

As discussed in Section 1.2.3, the factor group analysis of orientationally disordered molecules at seemingly forbidden crystallographic site symmetries is not often investigated. It has been said that for these disordered structures, a precise determination of their modes is not permitted (Pruzan *et al.* 1990). Correlation through an infinite point group as suggested by Petruševski et al. (1993) will not work for hydronium jarosite and ammoniojarosite as the hydronium and ammonium ions are not linear, nor are any reasonable structural distortions, reorientations, or rotations of the ions. Indeed, the ions can only begin to reasonable linearity when at least two time and spatial orientations are considered as one: a localised orientation at a finite point in time is certainly not linear. Unlike the numerous disordered phases of ice, the majority of the repeat unit of hydronium jarosite and ammoniojarosite crystals is not disordered, only the ammonium and hydronium ions are disordered. Hence, the theory established for ice (see previous sections) whereby all vibrations are allowed, is not fully applicable to jarosite minerals.

All spectroscopic studies have shown the space group of ammoniojarosite and hydronium jarosite are best explained by $R\bar{3}m$. Even if there is a small structural distortion to a lower symmetry space group, the selection rules of the higher symmetry space group, i.e. $R\bar{3}m$, would apply to the vibrational spectra, as is the case for ammonium sulfate (Kettle *et al.* 1984). As diffraction experiments measure the time averaged structure across many unit cells, a small distortion to $R3m$ in reality would appear to be $R\bar{3}m$ when modelled. Similar effects have been observed for red mercuric iodide as its tetragonal structure is only a small distortion from octahedral (Hollebone and Lever 1972). There is overwhelming evidence the space group of hydronium jarosite and ammoniojarosite is $R\bar{3}m$, within the limits of current spectroscopic and diffraction based experiments. Any possible symmetry lowering is minor and cannot be detected or resolved.

Spherical symmetry resulting from free rotation is sometimes thought to be the reorientation mechanism for orientationally disordered molecules. However, hydrogen bonding can lead to partial ordering, the directional nature of N–H bonds, and isotopically dilute deuterated studies showing expected factor group splitting of $\nu(NH_3D^+)$ bands, has led others to believe that spherical symmetry is not always correct with respect to vibrational spectra (Fernandes *et al.* 1979; Mookherjee *et al.* 2002; Oxton *et al.* 1976). For jarosite minerals, spherical symmetry arising from free rotation of ammonium and hydronium ions in alunite supergroup minerals has to ignore the surrounding hydroxyl groups; it is unlikely that there would be no hydrogen bond formed or at least some weak electrostatic interaction. Prior studies have shown evidence for some interaction with the surrounding hydroxyl groups, but this interaction is such that complete neutralisation to water does not occur.

3.3 CONCLUDING REMARKS

The choice between static or dynamic disorder of an orientationally disordered molecule in a crystal presents many problems. Even if the disorder mechanism is known, the most appropriate way to model the relevant diffraction data, and interpret and predict vibrational spectra is not always clear. It has been shown that both ammoniojarosite and hydronium jarosite contain orientationally disordered molecules, but a thorough structural investigation these molecules impart on the jarosite framework is lacking. For example, both minerals have orientationally disordered molecules at seemingly symmetry forbidden crystallographic sites, yet display different magnetic ordering behaviour at low temperature. Hydronium jarosite is a spin glass whilst ammoniojarosite shows magnetic ordering. This is significant because orientational disorder is thought to be a prerequisite for spin glass behaviour.

Hydrogen atom location in these two jarosite minerals is controversial and alternative models for their crystal structure have not been adequately investigated. Explicit reasons for shifting the nitrogen and oxygen atoms of ammonium and hydronium ions respectively from the $\bar{3}m$ site have not been stated in all hitherto studies. A reinterpretation of hydronium jarosite and ammoniojarosite spectra that is also in agreement with diffraction methods, and predicts the number and symmetry of all bands is clearly needed. However, before a spectroscopic study and symmetry analysis, the crystal structures of hydronium jarosite and ammoniojarosite must be determined through the refinement and statistical comparison of various models. A thorough vibrational spectroscopic study of hydronium jarosite and ammoniojarosite may reveal previously unrecognised structural nuances. If successful, such a symmetry analysis would have implications for other similarly disordered structures and allow for symmetry analysis in complex cases. Ultimately, such an investigation may explain the conflicting magnetic structure and behaviour of the spin glass hydronium jarosite compared to other jarosites minerals, especially the similarly disordered ammoniojarosite.

3.4 REFERENCES

Auglló-Rueda, F., J. M. Calleja, and J. Bartolomé, 1988: Raman spectroscopy of the ammonium ion in NH_4MnF_3 and NH_4ZnF_3 perovskites: temperature dependence. *J. Phys. C.:* , **21,** 1287-1297.

Basciano, L. C., and R. C. Peterson, 2007: The crystal structure of ammoniojarosite, $(NH_4)Fe_3(SO_4)_2(OH)_6$ and the crystal chemistry of the ammoniojarosite-hydronium jarosite solid-solution series. *Min. Mag.*, **71,** 427-441.

Beintema, J., 1965: The crystal structure of 1,5-dimethylnaphthalene. *Acta. Cryst.*, **18,** 647-654.

Bertie, J. E., 1968: Far-infrared spectra of the ices. *Appl. Spectrosc.*, **22,** 634-640.

Besbes, H., T. Mhiri, and A. Daoud, 1999: Disorder study in triammonium hydrogen disulphate $(NH_4)_3H(SO_4)_2$ and its solid solutions $(NH_4)_{3-x}M_xH(SO_4)_2$. *Phase Transit.*, **70,** 183-195.

Bhagavantam, S., and T. Venkatarayudu, 1939: Raman effect in relation to crystal structure. *Proc. Indian Natl. Sci. Acad., A* **9,** 224-258.

Boyle, L. L., 1972: The method of ascent in symmetry-III application to lattice vibrations. *Spectrochim. Acta*, **A28,** 1355-1360.

Bürgi, H. B., 2000: Motion and disorder in crystal structure analysis: measuring and distinguishing them. *Annu. Rev. Phys. Chem.*, **51,** 275-296.

Buttery, H. J., G. Keeling, S. F. A. Kettle, I. Paul, and P. J. Stamper, 1969: Correlation between crystal structure and carbonyl-bond stretching vibrations of methyl benzene transition metal tricarbonyls. *Discuss. Faraday Soc.*, **47,** 48-52.

Catti, M., and R. M. Ibberson, 2002: Order-disorder of the hydronium ion and low-temperature phase transition of $(H_3O)Zr_2(PO_4)_3$ NASICON by neutron diffraction. *J. Phys. Chem. B.*, **106,** 11916-11921.

Chio, C. H., S. K. Sharma, L.-C. Ming, and D. W. Muenow, 2010: Raman spectroscopic investigation on jarosite-yavapaiite stability. *Spectrochim. Acta*, **A75,** 162-171.

Cotton, F. A., and J. L. Elgin, 1992: Crystallographic disorder in [M2X8]n-, M2X4L4 and related cmpounds: chemical and theoretical implications. *Inorg. Chem. Acta*, **198-200,** 13-22.

Dharmasena, G., and R. Frech, 1995: Orientational disorder in lithium sodium sulfate. *J. Chem. Phys.*, **102,** 6941-6945.

Dittrich, B., J. E. Warren, F. P. A. Fabbiani, W. Morgenroth, and B. Corry, 2009: Temperature dependence of rotational disorder in a non-standard amino acid from X-ray crystallography and molecular dynamics simulation. *Phys. Chem. Chem. Phys.*, **11,** 3601-2609.

Dunitz, J. D., V. Schomaker, and K. N. Trueblood, 1988: Interpretation of atomic displacement parameters from diffraction studies of crystals. *J. Phys. Chem.*, **92,** 856-867.

English, R. B., and A. M. Heyns, 1984: An infrared, Raman, and single crystal X-ray study of cesium hexafluorophosphate. *J. Cryst. Spectrosc.*, **14,** 531-540.

Fåk, B., F. C. Coomer, A. Harrison, D. Visser, and M. E. Zhitomirsky, 2008: Spin-liquid behavior in a kagomé antiferromagnet: deuteronium jarosite. *Europhys. Lett.*, **81,** 17006.

Farmer, V. C., Ed., 1974: *The infrared spectra of minerals*. Mineralogical Society.

Fernandes, J. R., S. Ganguly, and C. N. R. Rao, 1979: Infrared spectroscopic study of the phase transitions in $CsNO_3$, $RbNO_3$ and NH_4NO_3. *Spectrochim. Acta*, **A35,** 1013-1020.

Gale, J. D., K. Wright, and K. A. Hudson-Edwards, 2010: A first-principles determination of the orientation of H_3O^+ in hydronium alunite. *Am. Mineral.*, **95,** 1109-1112.

Giacovazzo, C., Ed., 2002: *Fundamentals of crystallography*. 2nd ed. Oxford University Press.

Grohol, D., and D. G. Nocera, 2007: Magnetic disorder in the frustrated antiferromagnet jarosite arising from the H_3O^+•••OH^- interaction. *Chem. Mater.*, **19,** 3061-3066.

Halford, R. S., 1946: Motions of molecules in condensed systems: I. Selection rules, relative intensities, and orientation effects for Raman and infrared spectra. *J. Chem. Phys.*, **14,** 8-15.

Harlow, R. L., 1996: Troublesome crystal structures: prevention, detection and resolution. *J. Res. Natl. Inst. Stand. Technol.*, **101,** 327-339.

Hollebone, B. R., and A. B. P. Lever, 1972: The application of symmetry ascent selection rules to a factor group analysis of red mercuric iodide. *Inorg. Chem.*, **11,** 1158-1160.

Jewess, M., 1982: A theoretical treatment of 'orientational' disorder for routine use. *Acta Cryst.*, **B38,** 1418-1422.

Kessel, A., and N. Ben-Tal, 2012: *Introduction to proteins: structure, function, and motion*. CRC Press.

Kettle, S. F. A., U. A. Jayasooriya, and L.-J. Norrby, 1984: Reinterpretation of the internal mode vibrational spectra of ammonium sulfate (phase I). *J. Phys. Chem.*, **88,** 5971-5975.

Kubisz, J., 1972: Studies on synthetic alkali-hydronium jarosites III: infrared absorption study. *Mineral. Pol.*, **3,** 23-37.

Lager, G. A., G. A. Swayze, C.-K. Loong, F. J. Rotella, J. W. Richardson Jr, and R. E. Stoffregen, 2001: Neutron spectroscopic study of synthetic alunite and oxonium-substituted alunite. *Can. Mineral.*, **39,** 1131-1138.

Levy, H. A., and S. W. Peterson, 1952: Neutron diffraction study of the crystal structure of ammonium chloride. *Phys. Rev.*, **86,** 766-770.

Majzlan, J., and Coauthors, 2004: Thermodynamic properties, low-temperature heat-capacity anomalies, and single-crystal X-ray refinement of hydronium jarosite, $(H_3O)Fe_3(SO_4)_2(OH)_6$. *Phys. Chem. Min.*, **31,** 518-531.

Marsh, R., 1986: Centrosymmetric or noncentrosymmetric? *Acta Cryst.*, **B42,** 193-198.

Marsh, R. E., and V. Schomaker, 1981: Some incorrect space groups: an update. *Inorg. Chem.*, **20,** 299-303.

Massa, W., Ed., 2004: *Crystal structure determination*. 2nd ed. Springer-Verlag.

Mookherjee, M., S. A. T. Redfern, M. Zhang, and D. S. Harlov, 2002: Orientational order-disorder of ND_4^+/NH_4^+ in synthetic ND_4/NH_4-phlogopite: a low temperature infrared study. *Eur. J. Min.*, **14,** 1033-1039.

Müller, P., 2009: Practical suggestions for better crystal structures. *Crystallogr. Rev.*, **15,** 57-83.

Nielsen, U. G., J. Majzlan, and C. P. Grey, 2008: Determination and quantification of the local environments in stoichiometric and defect jarosite by solid-state ^2H NMR spectroscopy. *Chem. Mater.*, **20,** 2234-2241.

Nielsen, U. G., I. Heinmaa, A. Samoson, J. Majzlan, and C. P. Grey, 2011: Insight into the local magnetic environments and deuteron mobility in jarosite ($AFe_2(SO_4)_2(OD,OD_2)_6$, A = K, Na, D_3O) and hydronium alunite ($(D_3O)Al_3(SO_4)_2(OD)_6$), from variable-temperature ^2H MAS NMR spectroscopy. *Chem. Mater.*, **23,** 3176-3187.

Nocera, D. G., B. M. Bartlett, D. Grohol, D. Papoutsakis, and M. P. Shores, 2004: Spin frustration in 2D kagomé lattices: a problem for inorganic synthetic chemistry. *Chem. Eur. J.*, **10,** 3850-3859.

Oxton, I. A., O. Knop, and M. Falk, 1976: Determination of the symmetry of the ammonium ion in crystals from the infrared spectra of the isotopically dilute NH_3D^+ species. *J. Phys. Chem.* , **80,** 1212-1217.

Petruševski, V. M., B. Minčeva-Šukarova, and A. Džorovska, 1993: The vibrational species of molecules in disordered crystals: $M(NH_3)_2$ groups at C_{4h} symmetry sites. *Bull. Chem. Technol. Macedonia*, **12,** 31-34.

Pham-Thi, M., P. Colomban, A. Novak, and R. Blinc, 1987: Vibrational spectra and phase transitions in caesium hydrogen sulphate. *J. Raman. Spectrosc.*, **18,** 185-194.

Powers, D. A., G. R. Rossman, H. J. Schugar, and H. B. Gray, 1975: Magnetic behavior and infrared spectra of jarosite, basic iron sulfate, and their chromate analogs. *J. Sol. State Chem.*, **13,** 1-13.

Pressprich, M. R., M. R. Bond, and R. D. Willett, 2002: Structures of $[(CH_3)_4P]_2CoCl_4$, $[(CH_3)_4Sb]_2CuCl_4$ and $[CH_3)_4Sb]_2ZnBr_4$ and a correlation of psuedo-antifluorite $[(CH_3)_4Pn]_2MX_4$ salts. *J. Phys. Chem. Solids*, **63,** 79-88.

Pruzan, P., J. C. Chervin, and M. Gauthier, 1990: Raman spectroscopy investigation of ice VII and deuterated ice VII to 40 GPa. Disorder in ice VII. *Europhys. Lett.*, **13,** 81-87.

Rahman, A. A., A. Usman, S. Chantrapromma, and H.-K. Fun, 2003: Redetermination of hydronium perchlorate at 193 and 293 K. *Acta Cryst.*, **C59,** 92-94.

Ravindran, T. R., A. K. Arora, and T. N. Sairam, 2007: A spectroscopic resolution of the structure of $Zn(CN)_2$. *J. Raman. Spectrosc.*, **38,** 283-287.

Ripmeester, J. A., C. I. Ratcliffe, J. E. Dutrizac, and J. L. Jambor, 1986: Hydronium ion in the alunite-jarosite group. *Can. Mineral.*, **24,** 435-447.

Roberts, M. P., 1990: The crystalline site symmetry and its effect on the vibrational spectra of a weakly hindered molecule. V. Crystallization effects in $NH_4B(C_5H_5)_4$. *J. Chem. Phys.*, **12,** 8524-8534.

Roberts, M. P., D. Clavell-Grunbaum, and H. L. Strauss, 1987: The libration-vibration bands of the ammonium ion in ammonium tetraphenylborate: evidence for nearly free rotation. *J. Chem. Phys.*, **11,** 6393-6404.

Ross, M., and H. T. Evans, 1965: Studies of the torbernite minerals (III): role of the interlayer oxonium, potassium, and ammonium ions, and water molecules. *Am. Mineral.*, **50,** 1-12.

Rudolf, P. R., M. A. Subramanian, A. Clearfield, and J. D. Jorgensen, 1985: The crystal structures of the ion conductors $(NH_4^+)Zr_2(PO_4)_3$ and $(H_3O^+)Zr_2(PO_4)_3$. *Solid State Ionics*, **17,** 337-342.

Sasaki, K., O. Tanaike, and H. Konno, 1998: Distinction of jarosite-group compounds by Raman spectroscopy. *Can. Mineral.*, **36,** 1225-1235.

Schiebel, P., W. Prandl, R. Papoular, and W. Paulus, 1996: Amost free rotation of NH_3 molecules in crystals: observation from a maximum-entropy reconstruction of the proton density in $[Co(NH_3)_6](PF_6)_2$. *Acta Cryst.*, **A52,** 189-197.

Schiebel, P., K. Burger, H. G. Büttner, G. J. Kearley, M. Lehmann, and W. Prandl, 2000: ND_3-density distribution in orientationally disordered $Ni(ND_3)_6Cl_2$ observed by means of neutron Laue diffraction. *J. Phys.: Condens. Matter*, **12,** 8567-8576.

Serna, C. J., C. P. Cortina, and J. V. Garcia Ramos, 1986: Infrared and Raman study of alunite-jarosite compounds. *Spectrochim. Acta*, **A42,** 729-734.

Staveley, L. A. K., and N. G. Parsonage, 1961: Ionic and molecular rotation in ammonium salts and clathrate compounds. *Pure Appl. Chem.*, **2,** 271-274.

Szymanski, J. T., 1985: The crystal structure of plumbojarosite. *Can. Mineral.*, **23,** 659-668.

Tilley, R. J. D., 2013: *Understanding solids: The science of materials*. 2nd ed. John Wiley & Sons.

Wagner, E. L., and D. F. Hornig, 1950: The vibrational spectra of molecules and complex ions in crystals IV. Ammonium bromide and deutero-ammonium bromide. *J. Chem. Phys.*, **18,** 305-312.

Watkin, D., 2008: Structure refinement: some background theory and practical strategies. *J. Appl. Cryst.*, **41,** 491-522.

Whalley, E., and J. E. Bertie, 1967: Optical spectra of orientationally disordered crystals. I. Theory for translational lattice vibrations. *J. Chem. Phys.*, **46,** 1264-1270.

White, W. B., 2005: The structure of particles and the structure of crystals: information from vibrational spectroscopy. *J. Ceram. Process. Res.*, **6,** 1-9.

Wills, A. S., 2001: Conventional and unconventional orderings in the jarosites. *Can. J. Phys.*, **79,** 1501-1510.

Wills, A. S., and A. Harrison, 1996: Structure and magnetism of hydronium jarosite, a model Kagomé antiferromagnet. *J. Chem. Soc., Faraday Trans.*, **92,** 2161-2166.

Wills, A. S., A. Harrison, C. Ritter, and R. I. Smith, 2000: Magnetic properties of pure and diamagnetically doped jarosites: model kagomé antiferromagnets with variable coverage of the magnetic lattice. *Phys. Rev. B.*, **61,** 6156-6169.

CHAPTER 4 THE THERMAL DECOMPOSITION OF HYDRONIUM JAROSITE AND AMMONIOJAROSITE

Reproduced with permission from:

Spratt, H.; Rintoul, L.; Avdeev, M.; Martens, W. *Journal of Thermal Analysis and Calorimetry* 2014

© Akadémiai Kiadó, Budapest, Hungary 2014

STATEMENT OF CONTRIBUTION

The authors listed below have certified* that:

1. They meet the criteria for authorship in that they have participated in the conception, execution, or interpretation, of at least that part of the publication in their field of expertise;
2. They take public responsibility for their part of the publication, except for the responsible author who accepts overall responsibility for the publication;
3. There are no other authors of the publication who meet these criteria;
4. Potential conflicts of interests have been disclosed to a) granting bodies, b) the editor or publisher of journals or other publications, and c) the head of the responsible academic unit, and;
5. They agree to the use of the publication in the student's thesis and its publication on the Australasian Digital Thesis database consistent with any limitations set by the publisher requirements.

In the case of this chapter:

The thermal decomposition of hydronium jarosite and ammoniojarosite

Contributor	*Statement of Contribution**
Henry J. Spratt	Experimental design, conducted experiments, data analysis/interpretation, wrote the manuscript,
Llew Rintoul	Supervision, aided experiments and data analysis/interpretation, editing
Maxim Avdeev	Supervision, editing
Wayde N. Martens	Overall supervisor, aided experimental design, aided experiments and data analysis/interpretation, editing

Principal Supervisor Confirmation

I have sighted email or other correspondence from all co-authors confirming their certifying authorship.

Name	Signature	Date

SYNOPSIS

This chapter examines the thermal decomposition of hydronium and ammoniojarosite via *in situ* synchrotron X-ray diffraction, infrared emission spectroscopy and thermogravimetric analysis coupled with evolved gas analysis. This study was undertaken due to the various conflicting mechanisms reported in the literature concerning the thermal decomposition of hydronium and ammoniojarosite. The dehydroxylation and dehydration stages that involve the hydronium and ammonium ions were of particular interest, as some studies claim that hydrogen atoms persist in the structure at high temperatures so that water is lost in tandem with SO_3 at ~560 °C. In addition, intermediate compounds formed during the thermal decomposition of hydronium and ammoniojarosite are rarely identified through diffraction methods; intermediates are merely proposed with little evidence for their existence from thermogravimetric analysis data alone.

This study found conclusive evidence that all hydrogen atoms are lost during dehydroxylation, dehydration and deammoniation and that these steps occur separately to desulfonation. Dehydroxylation occurs at lower temperatures for hydronium jarosite than ammoniojarosite and can be attributed to increased proton mobility of hydronium hydrogen atoms and a stronger attraction to the surrounding hydroxyl groups. Although intermediate compounds were not positively identified, the previously proposed intermediates from the literature were not detected in their normal crystalline phases and may exist as different phases or are amorphous. Thus, this study has resolved the disputed aspects of hydronium and ammoniojarosite thermal decomposition in the literature. It is suggested that further *in situ* diffraction experiments are needed under controlled atmospheres if intermediate compounds are to be successfully identified.

THE THERMAL DECOMPOSITION OF HYDRONIUM JAROSITE AND AMMONIOJAROSITE

Henry J. Spratt, Llew Rintoul and Wayde N. Martens

Chemistry, Physics and Mechanical Engineering, Science and Engineering Faculty,

Queensland University of Technology, Brisbane, QLD, 4001 Australia

Maxim Avdeev

Bragg Institute, Australian Nuclear Science and Technology Organisation, Lucas Heights,

NSW, 2234 Australia

Keywords: hydronium jarosite · ammoniojarosite · thermal decomposition · iron(III) reduction

ABSTRACT

The thermal decomposition of hydronium jarosite and ammoniojarosite was studied using thermogravimetric analysis and mass spectrometry, *in situ* synchrotron X-ray diffraction and infrared emission spectroscopy. There was no evidence for the simultaneous loss of water and sulfur dioxide during the desulfonation stage as has previously been reported for hydronium jarosite. Conversely, all hydrogen atoms are lost during the dehydration and dehydroxylation stage from 270 to 400 °C and no water, hydroxyl groups or hydronium ions persist after 400 °C. The same can be said for ammoniojarosite. The first mass loss step during the decomposition of hydronium jarosite has been assigned to the loss of the hydronium ion via protonation of the surrounding hydroxyl groups to evolve two water molecules. For ammoniojarosite, this step corresponds to the protonation of a hydroxyl group by ammonium, so that ammonia and water are liberated simultaneously. Iron(II) sulfate was identified as a possible intermediate during the decomposition of ammoniojarosite (421-521 °C) due to a redox reaction between iron(III) and the liberated ammonia during decomposition. Iron(II) ions were also confirmed with the 1,10-phenanthroline test. Iron(III) sulfate and other commonly suggested intermediates for hydronium and ammoniojarosite decomposition are not major crystalline phases; if they are formed, then they most likely exist as an amorphous phase or a different low temperature phases than usual.

INTRODUCTION

The alunite supergroup of minerals has the general formula $AB_3(SO_4)_2(OH)_6$ and is a large group of minerals. The A site is typically occupied by a monovalent cation, while a trivalent cation is commonly at the B site. Jarosites (Fe^{3+} at the B site) are used to precipitate iron (Fe) and alkali metals from metallurgical solutions in the zinc, copper, and lead industries [1]. Jarosite minerals are also by-products of some metal processing industries and the mining industry [2]. As hydronium jarosite (H_3O^+ at the A site) and ammoniojarosite (NH_4^+ at the A site) contain no alkali metals, they could be used to produce pure hematite (Fe_2O_3) via calcination for applications such as pigments, catalysts, magnetic materials, and clinker production [3-5].

The thermal decomposition of sulfate minerals, including jarosites, has been studied for some time using thermogravimetric analysis (TG) [6-9]. In many cases, X-ray diffraction (XRD) patterns are also collected [10-13], but these patterns are frequently complex, and phase identification is not always possible [8]. The intermediate products formed during the decomposition of other jarosite minerals are well characterized [12-14]. Infrared emission spectroscopy (IES), though infrequently used, has been shown to be useful for the study of sulfate minerals at high temperature and offers additional information to TG and XRD [15].

The decomposition of jarosite minerals proceeds in two distinct steps: dehydration and dehydroxylation at temperatures between 250 and 450 °C via the loss of H_2O; and desulfonation at temperatures between 600 and 800 °C via the loss of SO_3 which then decomposes to SO_2 and SO. The onset temperature of dehydroxylation and dehydration is dependent on the A site cation [3]. The final decomposition product depends on the A site cation, but is usually hematite [5, 7], hematite and ASO_4 where A is the A site cation [7, 13, 16], or hematite and the A site metal as is the case with argentojarosite [$AgFe_3(SO_4)_2(OH)_6$] [8].

Different mechanisms for the thermal decomposition of hydronium jarosite have been proposed in the few studies, which focuses on this mineral [3, 17-19]. Frost *et al.* [17] and Šolc *et al.* [19] believe that the hydronium ion (H_3O^+) persists in the structure at high temperature and that one mol of both H_2O and SO_3 are lost simultaneously at ~557 °C [17, 19]. This is in contrast with other results from the literature, which suggest that the first decomposition step is the loss of H_3O^+ from the crystal structure and the dehydration and desulfonation occur in two distinct steps [3, 18]. The intermediate compounds after dehydroxylation and dehydration proposed by these two authors also differ.

Kubisz [3] argued that there are four types of dehydration and dehydroxylation reactions: deprotonation, dehydration, main dehydroxylation, and final dehydroxylation which form a variety of Fe oxy/hydroxy/hydrated sulfate complexes and/or hematite. Deprotonation i.e, $H_3O^+ \rightarrow H_2O + H^+$, occurs at about 320 °C and movement of the proton to hydroxyl oxygen atoms is more likely than the protonation of sulfate oxygen atoms (assuming an analogy to $[H_3OGa_3(SO_4)_2(OH)_6]$) [3]. This mechanism differs to Frost *et al.* [17] who have this particular proton moving to sulfate groups to evolve H_2O and SO_2 at 557 °C. There is also another dehydration reaction that occurs between 520 and 550 °C [3]. This reaction is the dehydration of hydroxyl containing Fe sulfate compounds formed during the main dehydroxylation/dehydration stage and liberation of H_2O that is trapped in the jarosite structure. Following this, desulfonation occurs as usual with the eventual product being hematite.

The decomposition of ammoniojarosite has been studied [4, 5, 7, 11, 12, 20, 21], but more work is needed to identify intermediate products from its thermal decomposition. There is agreement in the literature [5, 7, 11] that the general scheme for the decomposition of ammoniojarosite is as follows: evolution of coordinated water; decomposition of ammoniojarosite to ferric sulfate and hematite via the loss of water and ammonia (NH_3); and lastly, formation of hematite as a result of the decomposition of Fe(III) sulfate.

This study examines the thermal analysis of ammoniojarosite and hydronium jarosite using IES, *in situ* synchrotron XRD and TG/MS. The dehydration and dehydroxylation stages as well as the loss of H_3O^+ from hydronium jarosite are of particular interest. This is due to the varying mechanisms presented during this stage of thermal decomposition. In addition it remains to be seen whether there is diffraction evidence for the intermediate compounds that have been previously proposed.

EXPERIMENTAL

SYNTHESIS

Hydronium jarosite and ammoniojarosite were synthesized hydrothermally in Teflon-lined pressure vessels and heated in a microwave reactor for 3 h at 150 °C under autogenous water vapor pressure (4 bar). The synthesis of hydronium jarosite employed hydrous ferric sulfate ($Fe_2(SO_4)_3 \cdot 7H_2O$, 9 g) which was dissolved in H_2O (18.2 MΩ, 65 mL). The synthesis of ammoniojarosite used a high chloride concentration which has been shown to inhibit H_3O^+ substitution [22]. In this synthesis, ammonium chloride (NH_4Cl, 0.36 g) was added to a saturated lithium chloride (LiCl, 18 mL) and 1.23 M ferric chloride ($FeCl_3$, 7.5 mL) solution. Then, an excess of $Fe_2(SO_4)_3 \cdot 7H_2O$ (9 g) was dissolved in H_2O (18.2 MΩ, 38 mL) and added to the previous solution. After synthesis the products were thoroughly washed with water and dried in an oven overnight at 100 °C.

CHEMICAL COMPOSITION

Iron (Fe) and sulfur (S) contents were determined using a Varian inductively coupled plasma optical emission spectrometer (ICP-OES). Samples (*ca* 0.0072 g) were dissolved in concentrated nitric acid (HNO_3, 2.15 mL) at 120 °C followed by dilution to 50 mL with water (18.2 MΩ). Various Fe (500 ppm) and S (1000 ppm) standards were prepared by serial dilution and made up in 3% HNO_3 for analysis. The S standard was spec pure sulfuric acid (H_2SO_4) and an ACR multi element standard was used as the Fe standard. The errors in the Fe and S contents are reported as the standard deviation from triplicate analyses. The S content was normalized to two in accordance with the literature for chemical formula calculations [23].

The nitrogen content of ammoniojarosite (*ca* 0.6 g) was determined using a Leco Trumac CN Analyzer operating at ~1,150 °C. Ceramic boats were used for the analysis with empty boats as a blank to check for drift. Ethylenediaminetetraacetic acid (EDTA,

ca 0.2 g) was used as a standard. All measurements were run in triplicate and the error in nitrogen content reported as the standard deviation.

THERMOGRAVIMETRIC ANALYSIS

Thermogravimetric analysis was conducted on a TA instruments Q500 thermogravimetric analyzer under a nitrogen (N_2) atmosphere for hydronium jarosite and an argon (Ar) atmosphere for ammoniojarosite. An Ar atmosphere was used for ammoniojarosite analyses to enable detection of nitrogen had it been evolved. In both cases, the furnace was purged at 10 mL min^{-1}. Approximately 45 mg of hydronium jarosite and 36 mg of ammoniojarosite were heated in a platinum (Pt) crucible from ambient temperature (*ca* 25 °C) to 1,000 °C at a rate of 5 °C min^{-1}. Evolved gas analysis was performed with a Balzers (Pfeiffer) mass spectrometer (MS).

INFRARED EMISSION SPECTROSCOPY

Infrared emission spectroscopy was performed using a Nicolet Nexus FTIR spectrometer which was modified to include an emission cell. Heating was conducted *in situ* under a flowing N_2 atmosphere. Emission spectra were collected in the temperature range of 100–750 °C in 50 °C increments on a Pt stage. Details of the technique and the instrumentation employed in this study have been previously published [24, 17].

SYNCHROTRON X-RAY DIFFRACTION

Synchrotron XRD patterns were collected at the powder diffraction beam line of the Australian Synchrotron. Samples were loaded into quartz capillaries (0.5 mm) and patterns were collected in the temperature range of 25 °C–700 °C in 50 °C increments with heating provided by a hot air blower *in situ*. The detector was a Mythen microstrip detector. Unlike TGA and IES experiments, the atmosphere was not controlled and is best described as a closed air environment. The wavelength was determined to be 0.77308 Å via refinement of a LaB_6-660c/diamond standard. The data were then converted into

intensity versus Cu Kα1 °2θ for phase analysis and identification purposes using the Bragg equation.

RESULTS AND DISCUSSION

HYDRONIUM JAROSITE THERMAL DECOMPOSITION

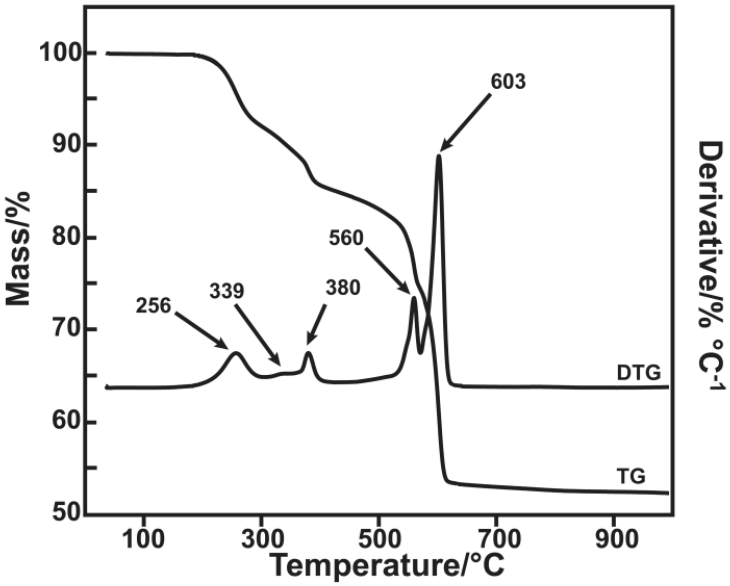

Figure 4-1: TG/DTG curves for hydronium jarosite

ICP-OES gave a Fe content of 3.13 ± 0.01 in the chemical formula after S normalization to two. The additional 0.13 (~4%) iron content is most likely due to another iron containing phase in the sample. However, such a phase is below the level of detection of the diffractometer employed as no impurities are detected from room temperature to 218 °C, or the extra phase is amorphous. Thus, the authors consider that the hydronium jarosite phase in this sample has no iron vacancies. Thermogravimetric (TG) and differential thermogravimetric (DTG) curves (Fig. 4-1) indicate that the decomposition of hydronium jarosite occurs in five main steps: 256; 339; 380; 560; and 603 °C. The mass losses associated with these temperatures are 8, 2, 5, 10 and 20% respectively, resulting in a total mass loss of 45%. The theoretical decomposition of hydronium jarosite to hematite results in a mass loss of 50%, which is a difference of 5%

from the observed. Thus, the extra 5% mass remaining from the observed TG results agrees with an amorphous iron containing phase.

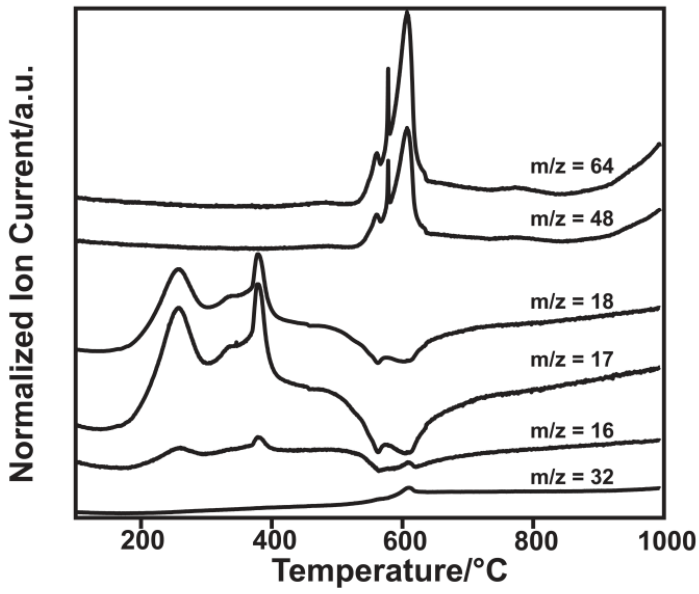

Figure 4-2: MS of evolved gases for hydronium jarosite

From the mass spectra of evolved gases (Fig. 4-2), it is clear that the mass loss steps at 256, 339 and 380 °C are due to dehydroxylation and dehydration as H_2O (*m/z* = 18), OH (*m/z* = 17) and O (*m/z* = 16) are detected in this range by MS. From Fig. 4-2, it is also clear that desulfonation occurs at 560 and 603 °C due to the detection of SO_2 (*m/z* = 64), SO (*m/z* = 48), O and S (*m/z* = 32). Full decomposition is completed by 700 °C with dehydroxylation completed by 450 °C.

Figure 4-3 shows those XRD patterns where there is a change in the diffracting material for hydronium jarosite. At 720 °C, only hematite remains as the pattern is due solely to this phase. From the temperatures examined, hydronium jarosite is stable up to 218 °C before peaks due to another phase are seen at 270 °C, along with some unreacted hydronium jarosite. At 321 °C (after the first mass loss event, but before the second from TG), the pattern is solely due to this new phase.

The mass loss of 8 % at 256 °C can be assigned to the loss of $2H_2O$ from hydronium jarosite (theoretical mass loss 7.5 %). This is most likely due to the protonation of a surrounding hydroxyl group by H_3O^+ which evolves $2H_2O$, in accordance with Kubisz [3]. The phase formed after the loss of $2H_2O$ was not positively identified using the PDF-4 database. However, this phase is most likely an Fe(III) hydroxy-sulfate of some description. Assuming the pattern at 321 °C is due to this phase alone, indexing of the first 24 significant peaks using the DICVOL 91 program within the Reflex module of Materials Studio (version 6) suggests that this phase is monoclinic with figures of merit (FOM) > 10. The first mass loss is tentatively assigned to the following reaction:

$$H_3OFe_3(SO_4)_2(OH)_6 \xrightarrow{256^\circ C} Fe_3(SO_4)_2(OH)_5 + 2H_2O$$

The theoretical loss of $1H_2O$ from hydronium jarosite is 3.75 %. The mass loss steps at 340 and 380 °C (2 and 5 % respectively) most likely represent the evolution of ~$0.5H_2O$ and $2H_2O$ as the total mass loss due to dehydroxylation and dehydration (15 %) agrees well with the theoretical loss of $4.5H_2O$ from hydronium jarosite (16.9 %). The five OH groups that remain after the first mass loss event would logically decompose and evolve $2.5H_2O$ to maintain charge balance. From Fig. 4-2 it is clear that no H_2O or OH is released after 450 °C. This suggests that dehydroxylation is separate to desulfonation.

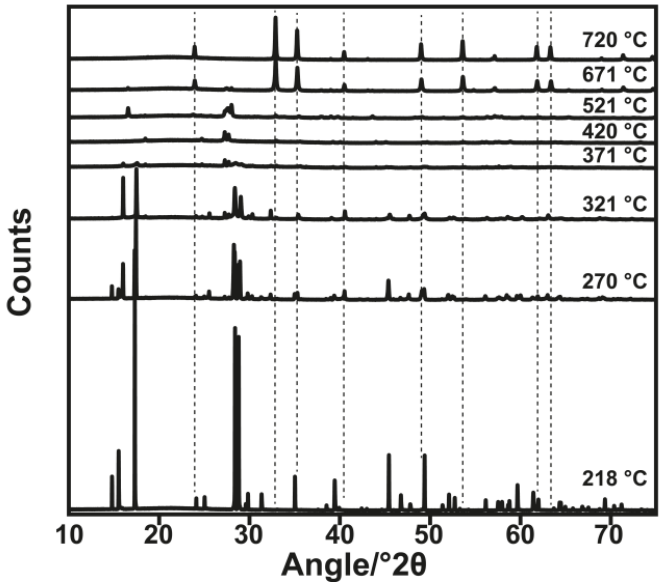

Figure 4-3: Significant *in situ* synchrotron XRD patterns (converted to 1.54056 Å) of hydronium jarosite as a function of temperature. Most intense hematite peaks are marked by a dashed line

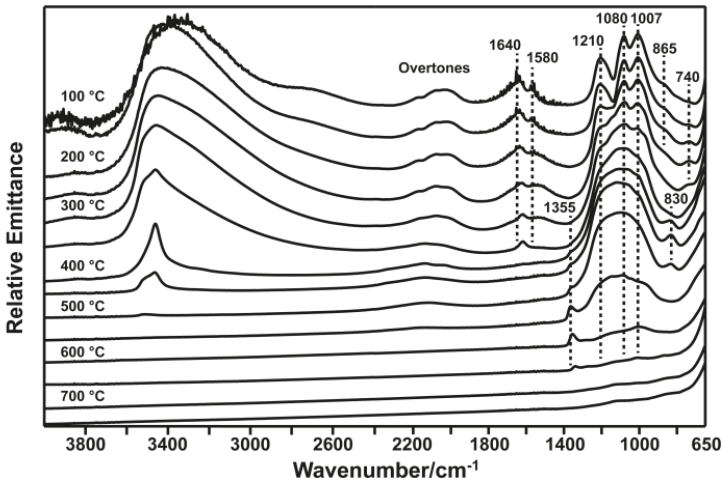

Figure 4-4: IES spectra of hydronium jarosite (4,000-650 cm^{-1})

Figure 4-4 shows that there are no OH stretching bands present past 500 °C for OH bands. In addition, the bands at 1,640 and 1,580 cm^{-1} which have been attributed to O–H vibrations with the latter from H_3O^+ [25-27], have disappeared by 400 °C. As desulfonation begins at about 500 °C, there is little evidence for the persistence of hydronium ions and hydrogen atoms past dehydroxylation and dehydration as seen in

some mechanisms [17, 19]. There is a gradual rise in the DTG curve from 400 to 500 °C and some weak OH IES bands in this temperature range. The extra step in hydronium jarosite decomposition proposed by Kubisz [3] most likely accounts for these two observations i.e., the gradual release of H_2O trapped in the jarosite structure and the full dehydroxylation/dehydration of any unreacted intermediates due to temperature differences in the sample [3].

Previous studies indicate that what remains after dehydroxylation/dehydration (typically temperatures between 400 and 500 °C) is hematite, Fe(III) sulfate [$Fe_2(SO_4)_3$], Fe(II) sulfate ($FeSO_4$), $Fe_2O(SO_4)_2$ and/or various hydroxy-sulfate intermediates [3, 17-19]. Given the limited evidence for the presence of hydrogen atoms after dehydroxylation, hydroxy-sulfate compounds can be ruled out. Interestingly, the synchrotron XRD patterns provide evidence for the formation of only a minor amount of crystalline Fe(III) sulfate or hematite directly after the dehydroxylation and dehydration of hydronium jarosite. An *ex situ* XRD study of selected products of the thermal decomposition of hydronium jarosite also failed to positively identify crystalline intermediates [28].

It is possible that any Fe(III) sulfate formed is amorphous. The IES spectra in Fig. 4-4 clearly show evidence of sulfate bands (1210, 1080 and 1007 cm^{-1}), indicating that the sulfate group has not been changed by thermal treatment at these temperatures. If any hematite is present it is not the major phase, as hematite does not predominate in the XRD patterns until 571 °C. The presence of crystalline $Fe_2O(SO_4)_2$ was not detected. The phases remaining after dehydroxylation and dehydration are most likely an Fe(III) oxy-sulfate compound (stoichiometry unknown) along with a minor amount of hematite. A potential reaction for the decomposition of hydronium jarosite between 300 and 400 °C is given below, along with the empirical formula of the crystalline Fe(III) oxy-sulfate compound:

$$2Fe_3(SO_4)_2(OH)_5 \xrightarrow{300-400^\circ C} 2Fe_3O_{2.5}(SO_4)_2 + 5H_2O$$

Decomposition during the desulfonation stage (500–650 °C) is relatively straightforward in that diffraction peaks for what is presumed to be the Fe(III) oxy-sulfate phase gradually weaken in intensity, while those due to hematite increase in intensity. The major sulfate stretching bands (1210, 1080 and 1007 cm^{-1}) broaden and decrease in intensity until they are no longer detected at 650 °C. It should be noted that librational modes of hydroxyl groups among other modes of vibration also appear in this region and can overlap with the sulfate bands [29]. A band at 1,355 cm^{-1} in the 550 °C spectra, which began as a shoulder in the 350/400 °C spectra becomes more intense. This band is most likely a sulfate band as it is not present in the 700 °C spectra where all sulfate have been decomposed. Thus, the corresponding sulfate group that gives rise to this band at 1,355 cm^{-1} is from a different crystalline phase than the sulfate bands that are observed below 350 °C; most likely what is formed after dehydroxylation and dehydration or an intermediate compound during desulfonation.

The total mass loss due to desulfonation is 30 %, which agrees well with the loss of $2SO_3$ from hydronium jarosite (theoretical mass loss 33 %). Although SO_3 (m/z = 80) is not detected by MS, it breaks down to SO_2 (m/z = 64) and O_2. Some SO_2 also breaks down to SO (m/z = 48) and O_2. Thus, the decomposition of hydronium jarosite between 500 and 650 °C is represented by the following reaction:

$$2Fe_3O_{2.5}(SO_4)_2 \xrightarrow{500-650^\circ C} 3Fe_2O_3 + 4SO_2 + 2O_2$$

This reaction assumes that the material formed after dehydroxylation exists as an oxy-sulfate phase. It should be noted that the hematite bands are located beyond the wavenumber cut-off of the IES employed in this study and are not observed.

AMMONIOJAROSITE THERMAL DECOMPOSITION

ICP-OES gave an iron content of 3.01 ± 0.01 in the chemical formula, which is essentially stoichiometric. The N content was determined to be 2.46 % (theoretical 2.92 %). Thus, the amount of NH_4^+ in the chemical formula is 0.88 ± 0.03, with the remainder of the A site assumed to be occupied by hydronium or vacant.

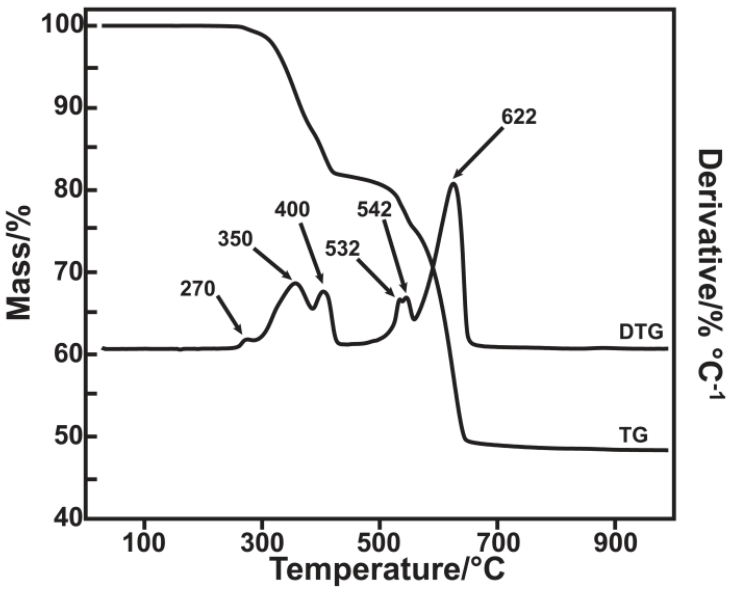

Figure 4-5: TG/DTG curves for ammoniojarosite

Thermogravimetric (TG) and differential thermogravimetric (DTG) curves (Fig. 4-5) indicate that the decomposition of ammoniojarosite occurs in six main steps: 270, 350, 400, 532, 542, and 622 °C. The mass losses are 1, 12, 5, 6 and 27 % (532 and 542 °C combined) respectively. The mass spectra of evolved gases (Fig. 4-6) shows that the mass loss steps at 350 and 400 °C are due to the simultaneous loss of H_2O (*m/z* = 18) and NH_3 (*m/z* = 15). The ion current curve for *m/z* = 17 originates from both NH_3 and OH^- evolution. The ion current curve *m/z* = 15 which is due to NH^+ and unique to NH_3, clearly shows that NH_3 is lost simultaneously with H_2O at 350 and 400 °C. Simultaneous evolution of NH_3 and H_2O has been reported for other ammonium-containing minerals such as NH_4^+-vermiculite [30]. Desulfonation occurs at 532, 542 and 622 °C as SO_2, SO,

O and S are detected at these temperatures. Full decomposition is completed by 700 °C. Dehydroxylation, dehydration and deammoniation are completed by about 450 °C. The total mass loss is 51 %.

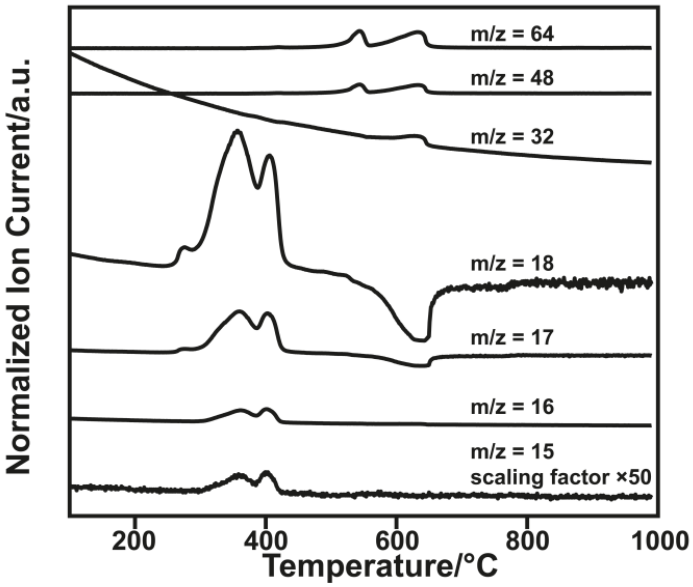

Figure 4-6: MS of evolved gases for hydronium jarosite

The temperature maxima of mass loss steps in the dehydration and dehydroxylation region (300–400 °C) for ammoniojarosite are higher than hydronium jarosite by about 20 °C. This could be due to greater proton mobility of hydronium hydrogen atoms compared to ammonium hydrogen atoms. For instance, the hydronium ion has been found to be highly mobile with low activation energy of motion (6.3 kJ mol^{-1}) [31, 32]. Compared to other jarosite minerals, hydronium jarosite is the only end member, which does not show long-range magnetic ordering and is instead, a spin glass [33] which is also related to proton disorder. Given that the pKa of H_3O^+ (0) is much lower than NH_4^+ (9) and both ions surround hydroxyl groups, it is not unreasonable that hydronium jarosite would undergo dehydration and dehydroxylation before ammoniojarosite as the ammonium hydrogen atoms are less mobile and experience less attraction to the surrounding hydroxyl groups.

The small mass loss of 1 % at 270 °C has been assigned to the dehydration of coordinated water, in accordance with the literature [5, 11, 21]. The structure is preserved upon loss of coordinated water, as the diffraction pattern of ammoniojarosite at this temperature shows no evidence for the formation of another phase. While the exact nature of the coordinated water is unknown, the current authors argue that it is related to water or hydronium located at the A site given that there is no signal from *m/z* = 15 at 270 °C. The moles of coordinated water were determined to be 0.26 (~0.25).

The TG/DTG curves presented in Fig. 4-6 are quite different from those reported in another study by Frost *et al.* [21] for ammoniojarosite. In fact, the TG/DTG curves in the other study are more similar to curves for hydronium jarosite both in this study, and an investigation into hydronium jarosite decomposition also by Frost *et al.* [17]. The difference in TG/DTG curves could be due to either ammonium or Fe content. This is because the synthesis employed by Frost *et al.* [21] used a low concentration of Fe and a high concentration of ammonium ions when compared to the synthesis employed in the current study. Thus, another ammoniojarosite was synthesized using the regime outlined by Frost *et al.* [21]. The CN analyzer gave a nitrogen content of 0.92 ± 0.04 at the A site (2.69 %); an Fe content of 2.79 ± 0.01 in the chemical formula was found from ICP-OES. Water is known to substitute for Fe^{3+} vacancies in order to maintain charge balance via protonation of OH^- groups [34, 31]. It is proposed that due to extra water being liberated from sites of iron vacancies, the curves reported by Frost *et al.* [21] appear to be more like hydronium jarosite.

The XRD patterns where there was a change in the diffracting material for ammoniojarosite are shown in Fig. 4-7. Ammoniojarosite is stable up to 271 °C before a new phase is detected at 321 °C. The pattern at 321 °C also contains some unreacted ammoniojarosite. Like hydronium jarosite, at 720 °C only hematite remains as the pattern is solely due to this phase. The theoretical mass loss with full decomposition of ammoniojarosite to hematite is 50 %, which is in strong agreement with the TG data (a difference of 1 %).

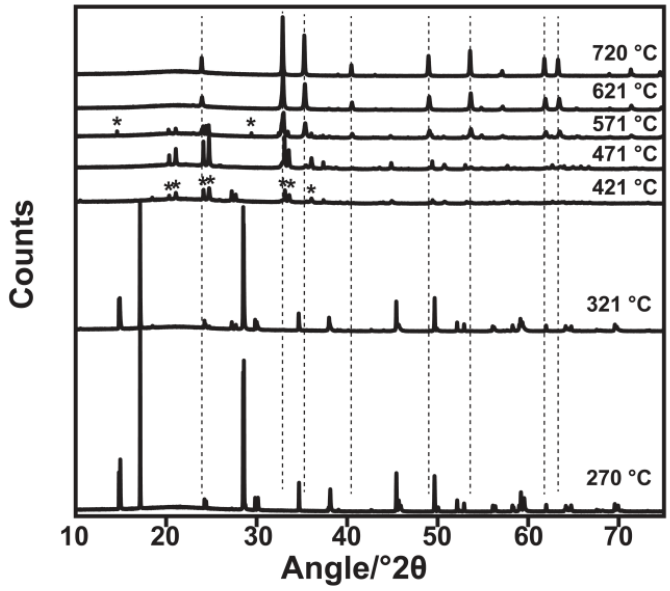

Figure 4-7: Significant *in situ* synchrotron XRD patterns of ammoniojarosite (converted to 1.54056 Å) as a function of temperature. Peaks marked with an asterisk at 421 °C are from $FeSO_4$ and those at 571 °C are from $Fe_2(SO_4)_3$. Most intense hematite peaks are marked with a dashed line

IES spectra of ammoniojarosite at various temperatures are shown in Fig. 4-8. The band at 1,420 cm^{-1} is assigned to an NH_4^+ deformation vibration in agreement with other spectroscopic studies of ammoniojarosite [35, 36]. This band persists until 350 °C but completely disappears by 400 °C. A band at 1,640 cm^{-1} is most likely due to an O–H bending vibration [27, 29, 37, 38] as this band is also in the hydronium jarosite spectra. The O–H and N–H stretching vibrations are gone by 500 °C. The IES spectra of O–H and N–H bending modes are in agreement with the simultaneous loss of NH_3 and H_2O as argued from the MS analysis of evolved gases, and also the IES spectra of Frost *et al.* [21].

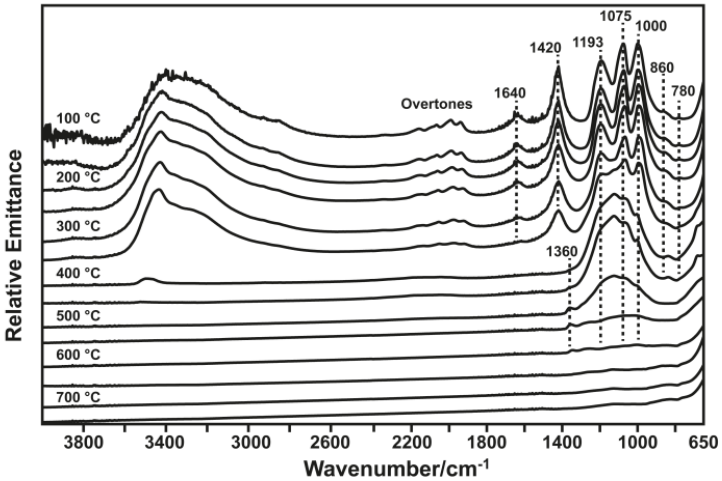

Figure 4-8: IES spectra of ammoniojarosite (4,000–650 cm^{-1})

If ammoniojarosite decomposes to release $3.5H_2O$ and $1NH_3$ [7] by 400 °C, then the theoretical mass loss is 16.9 % which is in close agreement with the observed mass loss of 17 %. Thus, dehydroxylation and dehydration are completed before desulfonation as all hydrogen atoms have been lost from the structure. The exact mechanism by which this occurs is unclear from synchrotron XRD as the phases formed were not positively identified. It is argued that the evolution of NH_3 would happen similar to the first mass loss step of hydronium jarosite: NH_4^+ protonates a surrounding hydroxyl group to form NH_3 and H_2O which are then liberated. An overall equation for the dehydroxylation, dehydration and deammoniation of ammoniojarosite is given by:

$$2NH_4Fe_3(SO_4)_2(OH)_6 \xrightarrow{300-400^\circ C} 7H_2O + 2NH_3 + 2Fe_3O_{2.5}(SO_4)_2$$

The 532 and 542 °C steps in desulfonation (Fig. 4-5) correspond to a two step degradation of the oxy-sulfate phase/s remaining after dehydration, dehydroxylation, and deammoniation. Similar to hydronium jarosite, crystalline Fe(III) sulfate is not detected directly after deammoniation and dehydroxylation. A sulfate band due to different crystalline phases is also seen at 1,360 cm^{-1}. At 421 °C iron (II) sulfate ($FeSO_4$) was

identified. It is also present until 521 °C before Fe(III) sulfate [$Fe_2(SO_4)_3$] is detected at 571 °C. Hematite predominates at 621 °C, but unlike hydronium jarosite where the most intense hematite peaks are only just resolved above background, in ammoniojarosite they are clearly present at 521 °C. The detection of $FeSO_4$ is unexpected as well as the subsequent transformation to $Fe_2(SO_4)_3$. However, as the atmosphere in the capillary was not controlled; it is conceivable that any oxygen (O_2) previously present would result in the oxidation of $FeSO_4$ to $Fe_2(SO_4)_3$ and Fe_2O_3. This explains the earlier detection of hematite when compared to hydronium jarosite.

It is often assumed that $Fe(OH)SO_4$ and $Fe_2O(SO_4)_2$ are formed during the thermal decomposition of ammoniojarosite [4, 11]. Ristić *et al.* [4] found evidence of the formation of these two iron compounds at 400 °C using Mössbauer spectroscopy. These two compounds were unable to be positively identified from synchrotron XRD due to the lack of reference patterns. Alternatively, it is possible that the $FeSO_4$ formed in the current study is due to the dehydroxylation of intermediate amorphous $Fe(OH)SO_4$ and $Fe_2O(SO_4)_2$ phases.

Fe(II) sulfate is rarely proposed as an intermediate in jarosite mineral decomposition as the Fe(III) in jarosite must be reduced and then oxidized again to form hematite. However, Fe(III) reduction to Fe(II) during thermal decomposition has been reported for ammonium fluoroferrates [39], various Fe(III) oxalates [40] and during Fe^{3+} exchange for NH_4^+ in Na^+-Fe^{3+} ZSM-5 zeolites [41]. The reduction of Fe(III) to Fe(II) for Fe(III) oxalates was also accompanied by the subsequent oxidation of Fe(II) to Fe(III) via formation of Fe(III) oxide as the temperature increased [40]. In the present study, the reduction of Fe(III) is most likely due to a redox reaction involving Fe(III) and the liberated NH_3 to form Fe(II) and N_2. The reduction could be initiated by NH_3 itself, or the result of a catalytic decomposition of NH_3 by Fe [41].

This redox reaction happens in a closed environment, for example a capillary, because the liberated NH_3 does not easily diffuse away from the sample and is available to react. It is the opinion of the current authors that an *in situ* XRD experiment performed

under both air and an inert atmosphere such as Ar or N_2 where any liberated gases are carried away from the sample surface may help to resolve these issues. Following the formation of $Fe_2(SO_4)_3$, the decomposition is straightforward and proceeds by the evolution of SO_3 ($SO_2 + O_2$) to form hematite.

In order to determine whether Fe(II) could be detected outside of the synchrotron experiment, a sample of ammoniojarosite was heated in a tube furnace under a slight positive pressure of Ar at 500 °C for 1 h. An additional sample of ammoniojarosite was heated in a capillary sealed with Blu-Tack at one end with heating (500 °C for 5 min) provided by a hot air gun, in order to recreate the conditions of the synchrotron experiment. The resultant solids from both heating regimes were digested in sulfuric acid, adjusted to pH 4 with ammonium acetate/acetic acid buffer, followed by addition to a 3 g L^{-1} 1,10-phenanthroline solution. This test is well known to be an indicator for the presence of Fe(II), with a positive result being a color change of the solution to orange [42].

The sample of ammoniojarosite heated under Ar in the tube furnace tested negative for Fe(II), whilst the sample heated with the hot air gun gave a positive test. Thus, there is evidence for the presence of Fe(II) ions in the form of Fe(II) sulfate. This experiment suggests that the Fe(II) ions are formed due to a redox reaction between iron and the liberated NH_3. No such reaction occurs in the tube furnace, TG or IES as the liberated NH_3 is free to diffuse away from the sample and into the carrier gas. In a well-packed capillary however, the NH_3 is available to interact with the sample and promote the reduction of Fe(III) to Fe(II).

CONCLUSIONS

The thermal decomposition of hydronium jarosite and ammoniojarosite has been investigated using TG/MS, in situ synchrotron XRD and IES. The crystalline intermediate compounds formed during decomposition, were in general, not positively identified. Other previously reported intermediates for ammoniojarosite and hydronium jarosite decompositions most likely exist as amorphous phases or alternate phases to what is contained in powder diffraction databases. IES data with support from TG/MS show that the hydronium ion does not persist in the crystal structure past 400-450 °C and that no water is evolved during the desulfonation stage. The evolution of ammonia and water are simultaneous in ammoniojarosite. Both Fe(II) sulfate and Fe(III) sulfate were detected in the synchrotron XRD patterns of ammoniojarosite at 421 °C and 571 °C respectively. The initial presence of Fe(II) sulfate is most likely due to a redox reaction involving Fe(III) and the liberated NH_3. The subsequent formation of Fe(III) sulfate can be explained by the reaction of Fe(II) sulfate with O_2 to also form hematite. The presence of Fe(II) ions were confirmed by the 1,10-phenanthroline test for ammoniojarosite that was heated in a similar fashion at the synchrotron, as the liberated NH_3 cannot diffuse away from the sample. It was also suggested that low Fe occupancy may change the appearance of TG/DTG curves to be more like hydronium jarosite. The utility of *in situ* X-ray diffraction for determining decomposition products is clearly demonstrated by the detection, or lack thereof, of crystalline phases that were at odds with those previously proposed. However, the positive identification of crystalline intermediates, especially of intermediate products, is more challenging.

REFERENCES

1. Dutrizac JE. Factors affecting the precipitation of potassium jarosite in sulfate and chloride media. Metall Mater Trans B. 2008;39(6):771-83.

2. Hochella Jr MF, Moore JN, Putnis CV, Putnis A, Kasama T, Eberl DD. Direct observation of heavy metal-mineral association from the Clark Fork River Superfund Complex: implications for metal transport and bioavailability. Geochim Cosmochim Acta. 2005;69(7):1651-63.

3. Kubisz J. Studies on synthetic alkali-hydronium jarosites II: thermal investigations. Mineral Pol. 1971;2:51-9.

4. Ristić M, Musić S, Orehovec Z. Thermal decomposition of synthetic ammonium jarosite. J Mol Struct. 2005;744-747:295-300.

5. Alonso M, López-Delgado A, López FA. A kinetic study of the thermal decomposition of ammoniojarosite. J Mater Sci. 1998;33:5821-5.

6. Swamy MSR, Prasad TP, Sant BR. Thermal analysis of ferrous sulphate heptahydrate in air. Part I: some general remarks and methods. J Therm Anal. 1979;15:307-14.

7. Kunda W, Veltman H. Decomposition of jarosite. Metall Trans B. 1979;10B:439-46.

8. May A, Sjoberg JJ, Baglin EG. Synthetic argentojarosite: physical properties and thermal behaviour. Am Miner. 1973;58:936-41.

9. Kotler JM, Hinman NW, Richardson CD, Scott JR. Thermal decomposition behavior of potassium and sodium jarosite synthesized in the presence of methylamine and alanine. J Therm Anal Calorim. 2010;102:23-9.

10. López-Delgado A, López FA. Thermal decomposition of ferric and ammonium sulphates obtained by bio-oxidation of water pickling liquors with *Thiobacillus ferroxidans*. J Mater Sci. 1995;30:5130-8.

11. López-Delgado A, Alguacil FJ, López FA. Recovery of iron from bio-oxidized sulphuric pickling waste water by precipitation as basic sulphates. Hydrometallurgy. 1997;45:97-112.

12. Chio CH, Sharma SK, Ming L-C, Muenow DW. Raman spectroscopic investigation on jarosite-yavapaiite stability. Spectrochim Acta A. 2010;75:162-71.

13. Drouet C, Navrotsky A. Synthesis, characterization, and thermochemistry of K-Na-H_3O jarosites. Geochim Cosmochim Acta. 2003;67(11):2063-76.

14. Xu H, Zhao Y, Vogel SC, Hickmott DD, Daemen LL, Hartl MA. Thermal expansion and decomposition of jarosite: a high-temperature neutron diffraction study Phys Chem Miner. 2010;37:73-82.

15. Vassallo AM, Finnie KS. Infrared emission spectroscopy of some sulfate minerals. Appl Spectrosc. 1992;46:1477-82.

16. Drouet C, Pass KL, Baron D, Draucker S, Navrotsky A. Thermochemistry of jarosite-alunite and natrojarosite-natroalunite solid solutions. Geochim Cosmochim Acta. 2004;68(10):2197-205. doi:DOI: 10.1016/j.gca.2003.12.001.

17. Frost RL, Wills R-A, Kloprogge JT, Martens WN. Thermal decomposition of hydronium jarosite $(H_3O)Fe_3(SO_4)_2(OH)_6$. J Therm Anal Calorim. 2006;83:213-8.

18. Hartman M, Veselý V, Jakubec K. Thermal decomposition and chemism of hydronium jarosite. Collect Czech Chem Commun. 1987;52:939-48.

19. Šolc Z, Trojan M, Brandová D, Kuchler M. A study of hydrothermal preparation of iron(III) pigments by means of thermal analysis methods. J Therm Anal. 1988;33(463-469).

20. Das GK, Anand S, Acharya S, Das RP. Preparation and decomposition of ammoniojarosite at elevated temperatures in H_2O-$(NH_4)_2$-SO_4-H_2SO_4 media. Hydrometallurgy. 1995;38:263-76.

21. Frost RL, Wills R-A, Kloprogge JT, Martens W. Thermal decomposition of ammonium jarosite $NH_4Fe_3(SO_4)_2(OH)_6$. J Therm Anal Calorim. 2006;84:489-96.

22. Basciano LC, Peterson RC. Jarosite-hydronium jarosite solid-solution series with full iron site occupancy: mineralogy and crystal chemistry. Am Mineral. 2007;92:1464-73.

23. Stoffregen RE, Alpers CN, Jambor JL. Alunite-jarosite crystallography, thermodynamics, and geochronology. Rev Mineral Geochem. 2000;40:453-79.

24. Frost RL, Vassallo AM. The dehydroxylation of the kaolinite clay minerals using infrared emission spectroscopy. Clay Clay Miner. 1996;44(5):635-51.

25. Kubisz J. Studies on synthetic alkali-hydronium jarosites III: infrared absorption study. Mineral Pol. 1972;3:23-37.

26. Grohol D, Nocera DG. Magnetic disorder in the frustrated antiferromagnet jarosite arising from the H_3O^+•••OH^- interaction. Chem Mater. 2007;19(12):3061-6. doi:10.1021/cm062793f.

27. Wilkins RWT, Mateen A. The spectroscopic study of oxonium ions in minerals. Am Mineral. 1974;59:811-9.

28. Majzlan J, Stevens R, Boerio-Goates J, Woodfield BF, Navrotsky A, Burns PC *et al.* Thermodynamic properties, low-temperature heat-capacity anomalies, and single-crystal X-ray refinement of hydronium jarosite, $(H_3O)Fe_3(SO_4)_2(OH)_6$. Phys Chem Miner. 2004;31(8):518-31.

29. Powers DA, Rossman GR, Schugar HJ, Gray HB. Magnetic behavior and infrared spectra of jarosite, basic iron sulfate, and their chromate analogs J Solid State Chem. 1975;13:1-13.

30. Pérez-Rodríguez JL, Poyato J, Jiménez de Haro MC, Pérez-Maqueda LA, Lerf A. Thermal decomposition of NH_4^+-vermiculite from Santa Olalla (Huelva, Spain) and its relation to the metal ion distribution in the octahedral sheet. Phys Chem Miner. 2004;31:415-20.

31. Nielsen UG, Heinmaa I, Samoson A, Majzlan J, Grey CP. Insight into the local magnetic environments and deuteron mobility in jarosite $(AFe_2(SO_4)_2(OD,OD_2)_6$,

A = K, Na, D_3O) and hydronium alunite ((D_3O)$Al_3(SO_4)_2(OD)_6$), from variable-temperature ^{2}H MAS NMR spectroscopy. Chem Mater. 2011;23:3176-87.

32. Nielsen UG, Majzlan J, Grey CP. Determination and quantification of the local environments in stoichiometric and defect jarosite by solid-state 2H NMR spectroscopy. Chem Mater. 2008;20(6):2234-41. doi:10.1021/cm702523d.

33. Wills AS, Harrison A. Structure and magnetism of hydronium jarosite, a model Kagomé antiferromagnet. J Chem Soc Faraday Trans. 1996;92:2161-6.

34. Frunzke J, Hansen T, Harrison A, Lord JS, Oakley GS, Visser D *et al.* Magnetic ordering in dilute kagome antiferromagnets. J Mater Chem. 2001;11:179-85.

35. Sasaki K, Tanaike O, Konno H. Distinction of jarosite-group compounds by Raman spectroscopy. Can Mineral. 1998;36:1225-35.

36. Serna CJ, Cortina CP, Garcia Ramos JV. Infrared and Raman study of alunite-jarosite compounds. Spectrochim Acta A. 1986;42A:729-34.

37. Bishop JL, Murad E. The visible and infrared spectral properties of jarosite and alunite. Am Mineral. 2005;90:1100-7.

38. Makreski P, Jovanoski G, Dimitrovska S. Minerals from Macedonia XIV. Identification of some sulfate minerals by vibrational (infrared and Raman) spectroscopy. Vib Spec. 2005;39:229-39.

39. Laptash NM, Polyshchuk SA. Thermal decomposition of ammonium fluoroferrates $(NH_4)_xFeF_{2x}$ ($2 \leq x \leq 3$). J Therm Anal. 1995;44:877-83.

40. Gallagher PK, Kurkjian CR. A study of the thermal decomposition of some complex oxalates of iron(III) using the Mössbauer effect. Inorg Chem. 1966;5:214-9.

41. Kaliaguine S, Lemay G, Adnot A, Burelle S, Audet R, Jean G *et al.* Ion exchange of Fe^{3+} in ZSM-5. Zeolites. 1990;10:559-64.

42. ASTM Standard E394. Standard test method for iron in trace quantities using the 1,10-phenanthroline method. West Conshohocken, PA: ASTM International; 2009.

CHAPTER 5 LOCATION OF HYDROGEN ATOMS IN HYDRONIUM JAROSITE

Reproduced with permission from:

Spratt, H.; Avdeev, M.; Pfrunder, M.; McMurtrie, J.; Rintoul, L.; Martens, W. *Physics and Chemistry of Minerals* 2014

© Springer-Verlag, Berlin, Heidelberg 2014

STATEMENT OF CONTRIBUTION

The authors listed below have certified* that:

1. They meet the criteria for authorship in that they have participated in the conception, execution, or interpretation, of at least that part of the publication in their field of expertise;
2. They take public responsibility for their part of the publication, except for the responsible author who accepts overall responsibility for the publication;
3. There are no other authors of the publication who meet these criteria;
4. Potential conflicts of interests have been disclosed to a) granting bodies, b) the editor or publisher of journals or other publications, and c) the head of the responsible academic unit, and
5. They agree to the use of the publication in the student's thesis and its publication on the Australasian Digital Thesis database consistent with any limitations set by the publisher requirements.

In the case of this chapter:

Location of hydrogen atoms in hydronium jarosite

Contributor	*Statement of Contribution**
Henry J. Spratt	Experimental design, conducted experiments and data analysis, wrote the manuscript,
Maxim Avdeev	Assisted experiments and data analysis, aided experimental design, major editing, supervision, aided discussion of results
Michael C. Pfrunder	Conducted experiments and data analysis (single crystal XRD), wrote a section of the manuscript (single crystal XRD)
John McMurtrie	Aided writing of manuscript (single crystal XRD), editing
Llew Rintoul	Supervision, editing
Wayde N. Martens	Overall supervisor, aided experimental design, aided experiments and data analysis, editing

Principal Supervisor Confirmation

I have sighted email or other correspondence from all co-authors confirming their certifying authorship.

Name	Signature	Date

SYNOPSIS

This chapter examines the crystal structure of hydronium jarosite by single crystal X-ray diffraction and neutron powder diffraction, with the location of all hydrogen atoms being the ultimate aim. This study was undertaken due to the uncertainty in the literature regarding the hydronium ion's hydrogen atom location and the geometry of the hydronium ion itself. Moreover, no study has addressed the possibility presented in the literature that the space group of hydronium jarosite could be lower symmetry than $R\bar{3}m$; such an assertion is merely suggested with limited proof or experimental evidence to substantiate the claim. A thorough examination of the most appropriate site symmetry for the hydronium ion has not been investigated either. Owing to the probable orientational disorder of the hydronium ion, these additional models must be investigated as incorrect site symmetry or space group choices are common causes of this problem.

Through Rietveld refinement and difference Fourier methods, all hydrogen atoms were located and numerous structural models for hydronium jarosite investigated. The most correct crystallographic description of hydronium jarosite's structure has the hydronium hydrogen atoms fractionally occupied at a C_s site and the hydronium oxygen atom at the D_{3d} site in space group $R\bar{3}m$. This means there are at least two orientations of the hydronium ion – up or down – with respect to the **c** axis. This model is the most symmetrical with the least assumptions necessary to explain all crystallographic and magnetic structural data. It was found the hydronium ion's hydrogen atoms point towards the hydroxyl groups, to which it forms the strongest hydrogen bonds. The time and spatial averaging inherent in diffraction techniques leads to the apparent D_{3d} symmetry of the C_{3v} hydronium ion. Locally, the symmetry of the ion must be lower than D_{3d}, but this cannot be accurately modelled.

LOCATION OF HYDROGEN ATOMS IN HYDRONIUM JAROSITE

Henry Spratt, Michael Pfrunder, John McMurtrie, Llew Rintoul and Wayde Martens

Chemistry, Physics and Mechanical Engineering, Science and Engineering Faculty,

Queensland University of Technology, Brisbane, QLD, 4001 Australia

Maxim Avdeev

Bragg Institute, Australian Nuclear Science and Technology Organisation, Lucas Heights,

NSW, 2234 Australia

Keywords: neutron diffraction · crystal structure · hydronium jarosite · hydrogen location · orientational disorder · Rietveld refinement

ABSTRACT

Various models for the crystal structure of hydronium jarosite were determined from Rietveld refinements against neutron powder diffraction patterns collected at ambient temperature and also single crystal X-ray diffraction data. The possibility of a lower symmetry space group for hydronium jarosite that has been suggested by the literature was investigated. It was found the space group is best described as $R\bar{3}m$, the same for other jarosite minerals. The hydronium oxygen atom was found to occupy the $\bar{3}m$ site (3a Wyckoff site). Inadequately refined hydronium bond angles and bond distances without the use of restraints are due to thermal motion and disorder of the hydronium hydrogen atoms across numerous orientations. The acquired data does not permit a precise determination of these orientations however, but the main feature, up/down disorder of hydronium is clear. Thus, the highest symmetry model with the least disorder necessary to explain all data was chosen: the hydronium hydrogen atoms were modelled to occupy an *m* (18h Wyckoff site) with 50 % fractional occupancy leading to disorder across two orientations. A rigid body description of the hydronium ion rotated by 60° with H–O–H bond angles of 112° and O–H distances of 0.96 Å was optimal. This rigid body refinement suggests that hydrogen bonds between hydronium hydrogen atoms and basal sulfate oxygen atoms are not predominant. Instead, hydrogen bonds are formed between hydronium hydrogen atoms and hydroxyl oxygen atoms. The structure of hydronium alunite is expected to be similar given that alunite supergroup minerals are isostructural.

INTRODUCTION

The alunite supergroup of minerals is a large mineral group. The supergroup is represented by the general formula $AB_3(TO_4)_2(OH)_6$. The supergroup can accommodate numerous elements at the A, B and T sites (Becker and Gasharova 2001). The A site is occupied by a monovalent or divalent cation; the B site is commonly occupied by iron(III) or aluminium, but other trivalent and some divalent cations are possible; and the T site can be occupied by sulfur, phosphorus, arsenic or chromium. Solid solutions among one or all sites are also possible (Scott 1987; Stoffregen *et al.* 2000), which leads to a vast array of minerals. Alunite supergroup minerals with sulfur at the T site and more than 50 % occupation of either iron(III) or aluminium at the B site belong to the jarosite and alunite subgroup respectively. Jarosite ($KFe_3(SO_4)_2(OH)_6$) was discovered on Mars in 2004 (Elwood Madden *et al.* 2004; Klingelhöfer 2004). This discovery provided evidence that there was once acidic, sulfate-containing water on Mars. Given the formation conditions for alunite supergroup minerals, their chemical composition can be used to determine fluid conditions in the environment (Burger *et al.* 2009).

The crystal structures of most alunite supergroup minerals are remarkably similar despite the numerous potential compositions (Stoffregen *et al.* 2000). The space group of most members is $R\bar{3}m$ in the hexagonal setting with three formula units in the unit cell (Z = 3). The a and b unit cell parameters are ~7 Å whilst the c unit cell parameter is unique at ~17 Å. Observations of pyroelectricity (Hendricks 1937) and optical second harmonic generation (Loiacono *et al.* 1982) suggest the space group is a lower symmetry polar space group, such as the maximal non-isomorphic subgroup of $R\bar{3}m$, $R3m$. However, it has been recommended that all alunite supergroup minerals be modelled as belonging to space group $R\bar{3}m$ (Menchetti and Sabelli 1976). Systematic absences for space groups $R3m$ and $R\bar{3}m$ are the same, so the space group choice is ambiguous from diffraction data. In addition, the Raman and infrared spectra are best described by space

group $R\bar{3}m$ (Serna *et al.* 1986; Arkhipenko and Bokii 1979; Breitinger *et al.* 1997). The Wyckoff sites and corresponding Schöenflies and Hermann-Mauguin notation of all atomic sites for the supergroup are given in Table 5-1.

Table 5-1: List of atomic sites for the alunite supergroup in space group $R\bar{3}m$

Atomic site	Wyckoff site	Schöenflies notation	Herman-Mauguin notation
A	3a	D_{3d}	$\bar{3}m$
B	9d	C_{2h}	$2/m$
T	6c	C_{3v}	$3m$
O (basal TO_4 oxygen)	18h	C_s	m
O (apical TO_4 oxygen)	6c	C_{3v}	$3m$
O (hydroxyl oxygen)	18h	C_s	m
H	18h	C_s	m

Hydronium jarosite ($H_3OFe_3(SO_4)_2(OH)_6$) is a jarosite mineral with the hydronium ion (H_3O^+) occupying the A site. Its crystal structure is uncertain and the hydrogen atoms have been described as "elusive" (Majzlan *et al.* 2004). The symmetry of H_3O^+ is $3m$, so should not be located at the $\bar{3}m$ site as $\bar{3}m$ is not a subgroup of $3m$; it is well known the crystallographic site of a molecule should be the same as, or, an allowed subgroup of the molecular symmetry (Jewess 1982; Petruševski *et al.* 1993; Schiebel *et al.* 2000). This stems from the fact that H_3O^+ has no inversion symmetry, yet the $\bar{3}m$ site is coincident with the inversion center of the crystal in space group $R\bar{3}m$. Thus, it has been suggested hydronium jarosite crystallizes in a lower symmetry space group (e.g. $R3m$) when compared to other alunite supergroup minerals (Szymanski 1985; Majzlan *et al.* 2004). Despite this logical conclusion, the Raman and infrared spectra of hydronium jarosite is best explained by space group $R\bar{3}m$ (Serna *et al.* 1986), as is the case for the other jarosite minerals. Hydronium jarosite does not show long range magnetic order at

low temperatures (< 70 K) like other jarosite minerals (Wills *et al.* 2000; Inami *et al.* 2000). Instead, it is a spin glass which freezes at approximately 17 K (Fåk *et al.* 2008; Wills and Harrison 1996). Various explanations have been presented to account for the lack of long range magnetic ordering in hydronium jarosite (Fåk *et al.* 2008; Frunzke *et al.* 2001; Bisson and Wills 2008; Grohol and Nocera 2007; Nocera *et al.* 2004). All explanations invoke more structural distortion of FeO_6 octahedra in other jarosite minerals, or, significant disorder and/or proton transfer involving the hydronium ion.

NMR studies have shown that H_3O^+ in jarosite minerals is mobile (Ripmeester *et al.* 1986; Nielsen *et al.* 2011; Nielsen *et al.* 2008). One particular study determined the activation energy of D_3O^+ motion to be 6.3(4) kJ mol^{-1} (Nielsen *et al.* 2011). Such a low activation energy of motion is consistent with molecular dynamic simulations based on a *P*1 unit cell, where the ion rapidly reorients between sites involving hydrogen bonding to Fe_2OH (hydroxyl groups) and sulfate oxygen atoms, and occasionally undergoes umbrella inversion (Gale *et al.* 2010). These same authors also found that hydronium may be tilted away from the crystallographic three-fold rotation axis so that more hydrogen bonds to sulfate and hydroxyl oxygen atoms can take place, leading to distribution across twelve potential orientations. Thus, disorder of the hydronium ion and/or proton mobility significantly contributes to hydronium jarosite's spin glass behaviour.

The few previous structural studies of hydronium jarosite have failed to locate hydronium hydrogen atoms (Majzlan *et al.* 2004), or determined the hydronium ion is disordered with the exact geometry unclear (Wills and Harrison 1996). A neutron diffraction study located the hydronium hydrogen atoms at an *m* site with 50 % fractional occupancy, and argued that the hydronium oxygen atom is displaced along unit cell parameter **c** to a 3*m* site with 50 % fractional occupancy (Wills and Harrison 1996). A single crystal X-ray diffraction (XRD) study located the hydronium oxygen atom at the $\bar{3}m$ site, but could not locate the hydronium hydrogen atoms (Majzlan *et al.* 2004). Further research into the crystal structure of hydronium jarosite is needed to reconcile these structural differences. In addition, the neutron diffraction study (Wills and Harrison

1996) suggested the hydronium ion is not as disordered as predicted from molecular dynamics simulations (Gale *et al.* 2010). Hence, we aim to determine the structure of hydronium jarosite, in particular, to locate the hydronium hydrogen atoms and determine its geometry. Whilst it has been mentioned hydronium jarosite could crystallize in a lower symmetry space group, no study has addressed this possibility. Therefore, we also investigate lower symmetry models for the structure of hydronium jarosite.

EXPERIMENTAL

SYNTHESIS

Hydronium jarosite single crystals were synthesized hydrothermally at 150 °C for three days. Ferric sulfate ($Fe_2(SO_4)_3 \cdot xH_2O$, x = 7) from Sigma Aldrich (0.2631 g) was weighed into a glass sample vial. The glass sample vial was then placed in a teflon lined hydrothermal pressure vessel with water (10 mL, 18.2 MΩ) surrounding the base of the sample vial. The $Fe_2(SO_4)_3$ was thus kept separate from the water. The teflon lined pressure vessel was then sealed in a stainless steel autoclave. It was found that increasing the reaction time and temperature did not significantly affect the size or quality of the obtained single crystals. The product was washed well with water and vacuum filtered. A suitable crystal was obtained for single crystal XRD. Unfortunately, the single crystals were too small for single crystal neutron diffraction. The purity was checked by grinding the sample and then collecting an X-ray powder diffraction pattern. No diffracting impurities were detected.

Hydronium jarosite powder was synthesized in a microwave hydrothermal reactor. The same ferric sulfate as used in the single crystal synthesis was weighed into a teflon lined pressure vessel (9 g) and dissolved in water (65 mL, 18.2 MΩ). The pressure vessel was then placed in the microwave reactor and heated to 150 °C with stirring for three hours under autogenous water vapour pressure (4 bar). The product was then washed well with water, filtered and dried in an oven overnight at 100 °C.

INDUCTIVELY COUPLED PLASMA – OPTICAL EMISSION SPECTROMETRY (ICP-OES)

The chemical composition was determined using a Varian inductively coupled plasma optical emission spectrometer (ICP-OES). Samples (*ca* 0.0072 g) from bulk single crystals and microwave synthesis were dissolved in concentrated nitric acid (HNO_3, 2.15 mL) at 120 °C followed by dilution to 50 mL with water (18.2 MΩ), to

result in a 3 % HNO_3 solution containing the dissolved jarosite minerals. Various iron (Fe, 500 ppm) and sulfur (S, 1000 ppm) standards made up in 3 % HNO_3 were prepared by serial dilution. The S standard was spec pure sulfuric acid (H_2SO_4) and an ACR multi element standard was used as the Fe standard. The error in the Fe and S contents are reported as the standard deviation from triplicate analyses. The S content was normalized to two in accordance with the literature for chemical formula calculations.

SINGLE CRYSTAL X-RAY DIFFRACTION

A suitable single crystal was coated in oil and mounted on a glass fiber for data collection. Data collection at 173(2) K and data reduction was performed under the software control of CrysAlis CCD and CrysAlis RED respectively (Oxford Diffraction 2007) on an Oxford Diffraction Gemini Ultra diffractometer using Mo Kα radiation generated from a sealed tube. Multi-scan empirical absorption corrections were applied using spherical harmonics which were implemented using the SCALE3 ABSPACK scaling algorithm, within CrysAlis RED.

NEUTRON POWDER DIFFRACTION

Constant-wavelength neutron powder diffraction patterns were collected on the high resolution neutron powder diffractometer (ECHIDNA) at the Australian Nuclear Science and Technology Organisation's (ANSTO) OPAL facility. The hydronium jarosite sample was loaded into vanadium (V) cans and patterns were collected at ambient temperature. The wavelength used for analysis was 1.6215 Å over a 6 – 160 °2θ range at a step size of 0.05°.

SINGLE CRYSTAL STRUCTURE REFINEMENT

Structure solution and refinement computations were carried out using the WinGX-32 graphical user interface (Farrugia 1999). The structure was solved by direct methods using SIR97 (Altomare *et al.* 1999) in space group $R\bar{3}m$ and then refined with

SHELXL-97 using a full-matrix least-squares refinement (Sheldrick 2008). All atoms were located and non-hydrogen atoms were refined with anisotropic atomic displacement parameters (ADPs). Oxygen-hydrogen bond distances were restrained to accepted values.

RIETVELD REFINEMENT OF POWDER DIFFRACTION DATA

The GSAS-EXPGUI software suite was used for structure refinement against the neutron powder diffraction patterns and Fourier density calculations (Larson and Von Dreele 2004; Toby 2001). All refinements were performed until convergence (convergence criterion of 0.01). Profile function type 4 was used for the modelling of peak shapes. The profile parameters GU, GV, GW and LX were refined, with S/L and H/L set to instrument values. A shifted Chebyshev function, with an appropriate number of terms (typically eight) was used to model the background. The model determined from the single crystal data was used as the starting model for Rietveld refinement against powder diffraction patterns, with the hydronium hydrogen atoms excluded.

RESULTS AND DISCUSSION

SINGLE CRYSTAL X-RAY DIFFRACTION

ICP-OES gave an iron content of 3.07 ± 0.02 in the chemical formula after normalization to sulfur. The single-crystal XRD data were refined in space group $R\bar{3}m$ as $R3m$ did not improve R-factors. This is consistent with previous single crystal XRD studies of other jarosite minerals (Menchetti and Sabelli 1976; Szymanski 1985; Sato *et al.* 2009). All atoms were located and their positions are in agreement with previous hydronium jarosite structure determinations (Wills and Harrison 1996; Majzlan *et al.* 2004). Atomic coordinates are given in Table 5-3. In all tables herein, numbers in parentheses are the estimated standard deviations (e.s.d.s) in the least significant digits. Wills and Harrison (1996) suggested the hydronium oxygen atom is displaced from the $\bar{3}m$ site along unit cell parameter **c**. However, our structure does not support this hypothesis. Instead, we find slight thermal displacement in the **a**-**b** plane, which is consistent with previous hydronium jarosite single crystal results (Majzlan *et al.* 2004). As the thermal ellipsoid for O4 shows little motion parallel to unit cell parameter **c** (Figure 5-1), the oxygen atom is best described occupying the $\bar{3}m$ site.

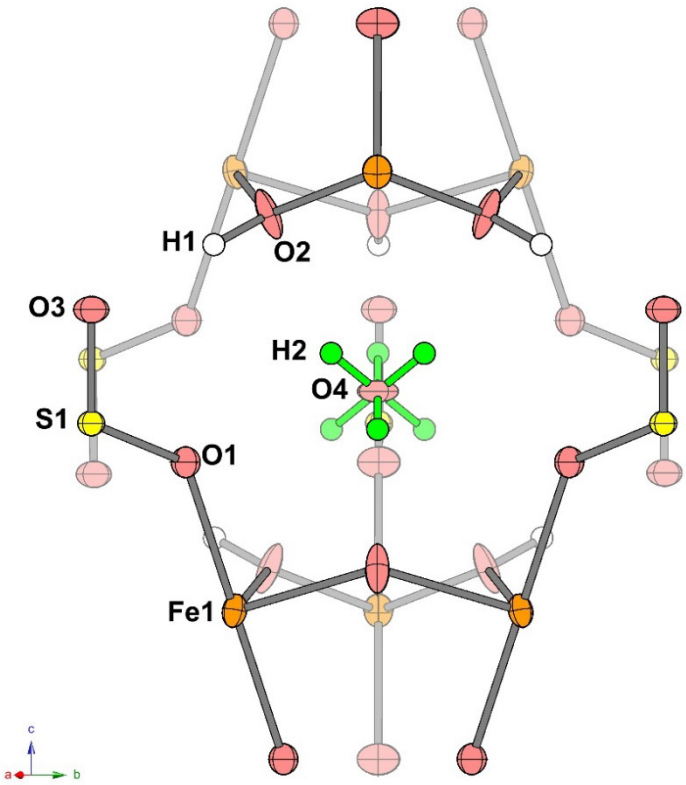

Figure 5-1: Crystal structure of hydronium jarosite refined from single crystal XRD data showing 80% thermal ellipsoids. Note the lack of thermal motion of O4 parallel to unit cell parameter c. Hydrogen bonds involving hydroxyl groups appear to restrict the disorder of the hydronium ion (green), so that regions of concentrated electron density appear in positions labelled H2

As the hydronium ion does not normally exhibit $\bar{3}m$ point group symmetry, there must be disorder in the orientation of the hydrogen atoms if the space group is $R\bar{3}m$. Any site containing the hydronium hydrogen atoms is fractionally occupied, which would result in less visible electron density in a difference Fourier map than usual. This fact, coupled with the low X-ray scattering cross section of ^{1}H, gave the expectation that the hydronium hydrogen atoms would not be located from single crystal XRD, as previously reported (Majzlan *et al.* 2004). Despite this, time-averaged positions of hydronium hydrogen atoms were located from a difference Fourier map. The model (Figure 5-1, Table 5-3) suggests the hydronium ion is disordered around the $\bar{3}m$ site such that hydronium hydrogen atoms point towards the surrounding six hydroxyl oxygen atoms.

This configuration satisfies $\bar{3}m$ symmetry requirements; the symmetry of the time-averaged structure (which is what diffraction experiments measure) is correctly described by space group $R\bar{3}m$. While this model does locate time-averaged concentrations of electron density associated with hydronium hydrogen atoms, the exact method of disorder of the hydronium ion remains unclear. It is possible the hydronium hydrogen positions are artefacts from the spatial average of a number of hydrogen atom positions in close proximity. This is an unfortunate by-product of the insensitivity of XRD to low atomic number disordered atoms. Therefore, the investigation was continued with the more hydrogen sensitive neutron diffraction.

Table 5-2: Results from the refinement of hydronium jarosite from single crystal XRD data

Formula	$Fe_3H_9O_{15}S_2$
Mass/g mol^{-1}	480.74
Crystal System	Hexagonal
Space Group	$R\bar{3}m$ (no. 166)
a/Å	7.3470(4)
c/Å	16.9299(11)
V/Å^3	791.42(8)
D_c/g cm^{-3}	3.026
Z	3
Color	Yellow
Habit	Cubic Prisms
Dimensions/mm	0.03 x 0.03 x 0.03
μ(Mo$K\alpha$)/mm^{-1}	4.559
$T_{min,max}$	0.882, 1
N_{ind} (R_{int})	269(0.037)
N_{obs} - ($I > 2\sigma(I)$)	249
N_{var}	29
$R1$[a]	0.0269
$wR2$[a]	0.0625
A, B	0.025 7.5
GoF	1.103
$\Delta\rho_{min,max}$/e$^-$ Å^{-3}	-0.614, 0.414

[a]Reflections with [$I > 2\sigma(I)$] considered observed. $R1 = \Sigma||F_o| - |F_c||/\Sigma|F_o|$ for $F_o > 2\sigma(F_o)$ and $wR2_{(all)} = \{\Sigma[w(F_o^2 - F_c^2)^2]/\Sigma[w(F_c^2)^2]\}^{/2}$ where $w = 1/[\sigma^2(F_o^2) + (\mathbf{A}P)^2 + \mathbf{B}P]$, $P = (F_o^2 + 2F_c^2)/3$.

Table 5-3: Positional and anisotropic ADPs from the single crystal XRD refinement of hydronium jarosite

Atom	Wyckoff site	*x*	*y*	*z*	Occupancy	U_{eq}/Å^2
Fe1	9d	0.5	0.0	0.5	1	0.0078(2)
S1	6c	0.0	0.0	0.30901(9)	1	0.0066(4)
O1	18h	0.5569(2)	0.1138(4)	0.61284(14)	1	0.0104(6)
O2	18h	0.7938(2)	0.2062(2)	0.46781(17)	1	0.0119(6)
O3	6c	0.0	0.0	0.3954(3)	1	0.010(1)
O4	3a	0.0	0.0	0.0	1	0.0122(14)
H1	18h	0.858(2)	0.142(2)	0.444(2)	1	0.01779 [b]
H2	18h	0.054(4)	0.108(8)	0.029(4)	0.5	0.01826 [b]

[b]Refined isotropically (U_{iso}) with restraints that did not allow reports of standard deviations

LOCATION OF HYDROGEN ATOMS FROM NEUTRON DIFFRACTION

From ICP-OES, the iron content in the chemical formula was found to be 3.13 ± 0.01. The extra 0.13 iron can be assigned to an unidentified or amorphous phase containing iron, as only peaks belonging to hydronium jarosite were identified in all diffraction patterns. Refinement of the iron occupancy after convergence did not show any evidence for significant iron vacancies. Thus, the sample was considered stoichiometric with respect to iron and the occupancy remained fixed at one. The positional parameters and isotropic ADPs were refined to convergence for all atoms before location of the hydronium hydrogen atoms by Fourier methods.

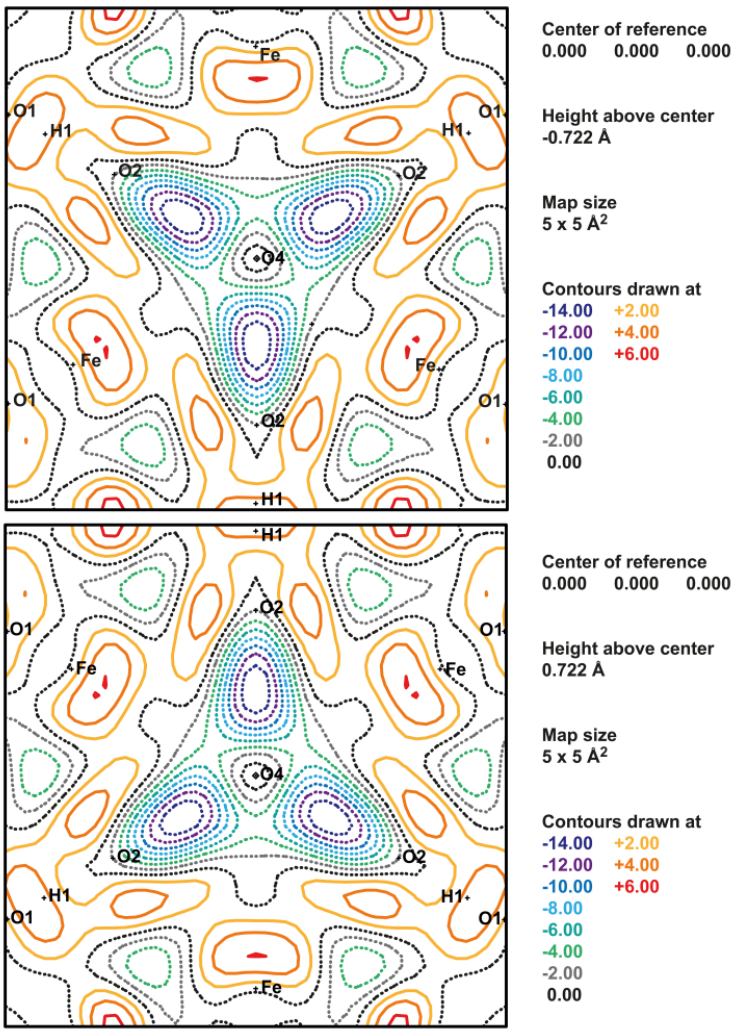

Figure 5-2: Difference Fourier maps ($F_{obs} - F_{calc}$) with F_{calc} values obtained using all atomic sites for hydronium jarosite. Solid lines show positive contours while broken lines show negative and zero contours

Figure 5-2 shows the location of the hydronium hydrogen atoms as strong, negative contours. As the neutron scattering length of hydrogen (^{1}H) is negative, it appears as negative contours in the difference Fourier map. The hydronium hydrogen atoms located both 0.722 Å below and above the center of reference are related by inversion symmetry. Thus, the hydronium hydrogen atoms are disordered across at least two orientations, as suggested from single crystal XRD. The coordinates of the missing hydrogen atoms were (0.0665, 0.1325, 0.0425) using FORSRH, which corresponds to a 1 site. However, these coordinates are marginally shifted (0.0005 along either *x* or *y*) from an *m* site for space group $R\bar{3}m$. As eighteen hydrogen atoms are expected for the site but

there are only nine in the unit cell, the hydronium hydrogen atoms are also fractionally occupied. Thus, the hydronium hydrogen atoms (designated H2) were added to the model with starting coordinates (0.0665, 0.133, 0.0425) and fractional occupancy of 0.5, and then refined without restraint to convergence (Figure 5-3). The *y* coordinate was changed to be twice that of the *x* coordinate, in keeping with the *m* site's symmetry restrictions in space group $R\bar{3}m$. The refinement results are given in Tables 5-4 and 5-5, with inter-atomic distances and angles reported in Table 5-6.

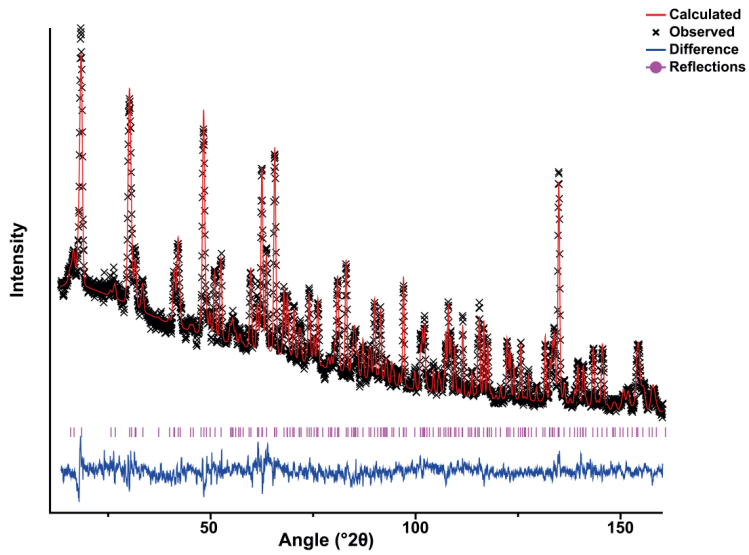

Figure 5-3: Typical Rietveld refinement profile fit (unrestrained model) against the neutron powder diffraction pattern collected from hydronium jarosite

The orientational disorder of the hydronium ion leading to at least two orientations with apparent inversion symmetry arises due to the time and structural averaging across all unit cells that is inherent in diffraction data collection. The apparent orientational disorder results in relatively large isotropic ADPs of H2 and O4 when compared to the other atomic sites. When the isotropic adp of H2 is constrained to be equal to O4, a value of 0.044 $Å^2$ is obtained, which is still large and an indicator of disorder and/or real large thermal motion. The large isotropic adp of H2 compared to the center atom (O4), suggests the dynamic disorder is librational and involves rotations

about the center of mass (Pressprich *et al.* 2002). Unfortunately, an anisotropic refinement of the ADPs was not possible as a non-positive definite result was obtained for sulfur.

The O4–O1 and O4–O2 distances are rather long at 3.003 and 2.819 Å respectively. These distances represent the upper limit for oxygen inter-atomic distances that are conducive towards hydrogen bonding (Lee and Carpenter 1959; Libowitzky 1999). Thus, any hydrogen bonds involving the hydronium ion and the surrounding oxygen atoms will be weak in strength and may not sufficiently tether H_3O^+ to the surrounding anions: it can be said that the hydronium ion is undergoing motion within the cavity surrounding the A site, assuming an analogy to hydronium perchlorate (Rahman *et al.* 2003). Such motion and dynamic disorder of the hydronium ion explains why the hydronium hydrogen atoms have not been successfully located by XRD methods.

Table 5-4: Results from the unrestrained refinement of hydronium jarosite

Space group	$R\bar{3}m$
Z	3
a/Å	7.35487(10)
c/Å	16.9983(4)
V/Å^3	796.32(2)
Data range for refinement/°2θ	13.4 – 160.35
Number of observations	2938
Number of calculated reflections	220
R_{wp} – background	0.0278
R_p – background	0.0202
$R(F^2)$	0.0990
χ^2	4.394
Parameters	34

Table 5-5: Refined positional and isotropic ADPs from the unrestrained refinement of hydronium jarosite

Atom	Wyckoff site	*x*	*y*	*z*	Occupancy	U_{iso}/Å^2
Fe	9d	0.5	0.0	0.5	1	0.0073(4)
S	6c	0.0	0.0	0.3904(4)	1	0.0058(14)
O1	18h	0.55759(17)	0.1152(3)	0.61217(14)	1	0.0119(6)
O2	18h	0.79576(18)	0.20424(18)	0.46801(15)	1	0.0143(5)
O3	6c	0.0	0.0	0.3940(3)	1	0.0145(8)
O4	3a	0.0	0.0	0.0	1	0.0322(18)
H1	18h	0.8596(3)	0.1404(3)	0.4407(3)	1	0.0295(12)
H2	18h	0.0587(12)	0.117(2)	0.0314(10)	0.5	0.085(6)

Table 5-6: Select inter-atomic distances and angles from the unrestrained refinement of hydronium jarosite

Atoms	Bond Distance/Å	Atoms	Bond Angle/°
S–O1 × 3	1.483(3)	H2–O4–H2	89.5(15)
S–O3 × 1	1.439(7)		90.4(15)
Fe–O1 × 2	2.043(2)	O1–S–O1	108.5(3)
Fe–O2 × 4	2.0041(10)	O1–S–O3	110.5(3)
O2–H1	0.936(6)	O1–Fe–O1	180.00(0)
O2–H2	1.971(17)	O1–Fe–O2	91.15(8)
O3–H1	1.958(5)		88.85(8)
O4–H2	0.919(16)	O2–Fe–O2	90.57(12)
		O2–Fe–O2	89.43

Like single crystal XRD results, unrestrained H2–O4–H2 bond angles of 89.5 and 90.4° (~90 °) are not optimal, given the ideal hydronium bond angles are approximately 112° (Begemann and Saykally 1985). All unrestrained O–H bond distances are short compared to other O – H distances determined from neutron diffraction (~0.96 Å). Apart from being a local minimum, it is known that thermal motion or disorder causes shortening of intra-molecular distances (Dunitz *et al.* 1988). Therefore, the H2–O4–H2 angles of ~90° may be due to the refinement program fitting the hydronium hydrogen atoms to the midpoint of their neutron density. Given that H_3O^+ is "highly mobile" from

NMR studies, dynamic disorder and reorientations of the ion in its cavity instead of static disorder is the cause of this inadequate geometry. Thus, a lower site symmetry for hydronium hydrogen atoms was not investigated as a split atom model (H2 occupying the general 1 site) implies the disorder is static; more atoms in close proximity decrease isotropic ADPs. In addition, side orientations of the hydronium ion are not congruent with the crystallographic symmetry imposed by the space group. Indeed, a refinement performed by the authors with the hydrogen atoms moved to a 1 site was not stable. Thus, we have adopted a more symmetrical model with higher isotropic ADPs.

On the other hand, it is possible O4 is displaced from the $\bar{3}m$ site and is located at a 3*m* site. It has been proposed for such orientationally disordered molecules, exact coincidence of all symmetry elements is not significant, and the molecules may be displaced from the higher symmetry site; only coincidence of like symmetry elements is significant (Jewess 1982). This is the model proposed by Wills and Harrison (1996) where O4 was shifted along unit cell parameter **c** so the three-fold rotation axes of the crystal and the hydronium ion were coincident (Wills and Harrison 1996). However, such a displacement from a high symmetry site was investigated for the similarly structured hydronium NASICON (Catti and Ibberson 2002), but the two situations could not be resolved. Alternatively, the space group of hydronium jarosite is lower than $R\bar{3}m$. These other models were investigated to ensure the symmetry mismatch between the hydronium ion and its site resulting in orientational disorder and large isotropic ADPs are real. Neutron diffraction, owing to its sensitivity to hydrogen, permits these models refinement compared to XRD.

INVESTIGATION OF LOWER SITE SYMMETRY FOR THE HYDRONIUM OXYGEN ATOM IN SPACE GROUP $R\bar{3}m$

From symmetry considerations, only 3*m*, 3, *m* and 1 crystallographic sites are expected for a 3*m* molecule (Farmer 1974). An examination of the entry for $R\bar{3}m$ in the

International Tables for Crystallography A, reveals that only sites 3*m* (3a), *m* (18h) and 1 (36i) are potential candidates for the hydronium ion. The coordinates of a 3*m* site are (0, 0, *z*). A Rietveld refinement with O4 moved to this site was attempted as the hydronium ion will simply be displaced along unit cell parameter **c** so the three-fold rotation axes of the crystal and hydronium will be coincident, in accordance with Jewess (1982). Note that H2 is still disordered at this site, but now 50 % fractional occupancy of O4 is induced to account for the site's multiplicity of six. Pertinent results from this refinement are presented in Tables 5-7 and 5-8.

The isotropic adp of O4 decreased to 0.026(2) but remained the same at 0.085(6) for H2, when compared to the $\bar{3}m$ model. At the lower symmetry site, O4 is shifted along unit cell parameter **c** by 0.157(19) Å. This shift results in two different O4–H2 bond distances of 0.844(18) Å and 1.03(2) Å, whose average (0.938 Å) is similar to the bond distance described by the $\bar{3}m$ model (0.919 Å). The rest of the structure is commensurate to the structure with O4 at the $\bar{3}m$ site. As R_{wp} and $R(F^2)$ slightly decrease for this model compared to the $\bar{3}m$ model, statistical tests on the *R*-factors were performed.

A Hamilton test on the crystallographic *R*-factors for these two models was performed (Hamilton 1965). The null hypothesis (H_0) is that the site symmetry of hydronium is 3*m*. The number of observations were calculated to be 1821, which is the number of observed data points greater than three standard deviations above the fitted background. The *R*-factor ratio is 0.0278/0.0275 = 1.011 and the test statistic is $\mathcal{R}_{1,\ 1786,\ 0.005}$ = 1.002. Therefore, the null hypothesis can be rejected at the 99.5 % significance level, assuming no systematic errors or serial correlations are present. A high significance level was chosen because we want to be quite sure of the correct structure. The null hypothesis can also be rejected at the 95% significance level ($\mathcal{R}_{1,\ 1786,\ 0.05}$ = 1.001). This test suggests the one additional parameter introduced by displacement of O4 from $\bar{3}m$ to 3*m* does not result in a statistically significant better fit to the data.

Table 5-7: Results from an unrestrained refinement of hydronium jarosite with O4 displaced from the $\bar{3}m$ site

Space group	$R\bar{3}m$ (no. 166)
Z	3
a/Å	7.35484(10)
c/Å	16.9982(4)
V/Å^3	796.30(2)
Data range for refinement/°2θ	13.4 – 160.35
Number of observations	2938
Number of calculated reflections	220
R_{wp} – background	0.0275
R_p – background	0.0201
$R(F^2)$	0.0974
χ^2	4.371
Parameters	35

Table 5-8: Refined positional and isotropic ADPs from the unrestrained refinement of hydronium jarosite with O4 displaced from the $\bar{3}m$ site

Atom	Wyckoff site	x	y	z	Occupancy	U_{iso}/Å^2
Fe	9d	0.5	0.0	0.5	1	0.0071(4)
S	6c	0.0	0.0	0.3092(4)	1	0.0043(15)
O1	18h	0.55771(17)	0.1154(4)	0.61203(14)	1	0.0119(6)
O2	18h	0.79570(17)	0.20430(17)	0.46819(16)	1	0.0140(5)
O3	6c	0.0	0.0	0.3940(3)	1	0.0151(8)
O4	6c	0.0	0.0	0.0092(11)	0.5	0.026(2)
H1	18h	0.8596(3)	0.1404(3)	0.4408(3)	1	0.0300(12)
H2	18h	0.0582(12)	0.116(2)	0.0329(11)	0.5	0.086(6)

The Prince test was also applied to these two models (Prince 1982). The Prince test is a comparison of the fits of two different models to the same data set; model 2 does not need to be a subset of model 1. It is a test to see whether the differences in two

models are no greater than what would normally be observed by chance alone. As the original author pointed out, the test does not prove that either model is correct as there may be another model consistent with chemistry and physics that fits the data even better (Prince 1982). A 99.5 % confidence interval for the slope of the regression line for the $3m$ model (model 1) vs the $\bar{3}m$ model (model 2) is 0.5145 ± 0.7134. The slope includes zero which suggests the difference between the two models is no greater than what would be observed by chance alone. However, at the 95 % significance level the slope does not include zero (0.5145 ± 0.4979), which suggests that the difference between the two models is significant. Statistical tests indicate the $\bar{3}m$ model is preferred over the $3m$ model.

The different models for the site symmetry of hydronium ($3m$ or $\bar{3}m$) are, in essence, similar representations of the same neutron density: one model has a lower O4 isotropic adp and more disorder, whilst the other has less disorder and a higher O4 isotropic adp. We see no reason why more disorder should be introduced to the O4 position and O4–H2 bond distances be unequal. In other words, O4 at the $\bar{3}m$ site is the best description of the time averaged structure across all unit cells and includes any small displacement with time from (0, 0, 0). Indeed, Fourier methods consistently locate the hydronium oxygen atom the $\bar{3}m$ site. In addition, the single crystal XRD results show limited evidence for hydronium oxygen displacement from the $\bar{3}m$ site. However, the highest symmetry local structure at a finite point in time for the hydronium ion must be $3m$.

INVESTIGATION OF A LOWER SYMMETRY SPACE GROUP

Refinements in a lower symmetry space group that allow fully occupied hydrogen positions were attempted as incorrect space group choice is a common cause of disorder. The hydronium jarosite structure was transposed to $P1$ symmetry, certain hydronium hydrogen atoms deleted to give a range of different orientations, and the

resulting structures' space groups and coordinates determined. $R3m$ and $P3m1$ were the only candidates, with the latter violating observed systematic peak extinctions. It was found that refinements in $R3m$: were unstable; took many more cycles to converge; needed a Marquardt damping factor of 9 on all atomic positions and isotropic ADPs; and non-ideal or variable bond distances, angles and isotropic ADPs with high e.s.d.s were obtained when compared to the $R\bar{3}m$ refinement. Results from the refinement in $R3m$ are given in Tables 5-9, 5-10, and 5-11.

Table 5-9: Results from an unrestrained refinement of hydronium jarosite in a lower symmetry space group

Space group	$R3m$ (no. 160)
Z	3
a/Å	7.35489(10)
c/Å	16.9979(4)
V/Å^3	796.30(2)
Data range for refinement/°2θ	13.4 – 160.35
Number of observations	2938
Number of calculated reflections	220
R_{wp} – background	0.0255
R_p – background	0.0187
$R(F^2)$	0.0897
χ^2	4.131
Parameters	49

No improvement in O4 or H2 isotropic ADPs were obtained in this lower symmetry space group when compared to space group $R\bar{3}m$. From Table 5-10, the refined isotropic ADPs without restraints for chemically equivalent atoms are very different and for O5, non-positive definite (but small). When these atoms were restrained to have the same isotropic ADPs, chemically equivalent bond distances became more distorted and further from ideal. Similar problems to all those aforementioned, including higher e.s.d.s and unstable refinement, are encountered when a symmetry element is

overlooked (Jones 1984; Harlow 1996; Marsh and Schomaker 1979). In addition, the coordinates of Fe (0.1666, 0.8334, 0.8173) modelled in *R*3*m* are displaced only in *z* (0.2736 Å) from the coordinates of the 2/*m* site in space group $R\bar{3}m$. Such a displacement of Fe atoms would have been observed from the single crystal X-ray data.

Table 5-10: Refined positional and isotropic ADPs from an unrestrained refinement of hydronium jarosite in space group *R*3*m*

Atom	Wyckoff site	*x*	*y*	*z*	Occupancy	U_{iso}/Å^2
S1	3a	0.0	0.0	0.2948(15)	1	0.008(7)
O1	3a	0.0	0.0	0.3785(10)	1	0.026(5)
S2	3a	0.0	0.0	0.6772(13)	1	0.002(6)
O2	3a	0.0	0.0	0.5915(7)	1	0.007(3)
O3	3a	0.0	0.0	-0.0208(13)	1	0.025(2)
Fe	9b	0.1666(5)	0.8334(5)	0.8173(4)	1	0.0085(5)
O4	9b	0.2242(8)	0.7758(8)	0.9315(5)	1	0.0076(19)
O5	9b	0.1293(5)	0.8707(5)	0.1245(5)	1	-0.0007(13)
H1	9b	0.2057(11)	0.7943(11)	0.0980(9)	1	0.039(4)
O6	9b	0.7752(9)	0.2248(9)	0.0407(6)	1	0.015(2)
O7	9b	0.8731(11)	0.1269(11)	0.8562(6)	1	0.030(3)
H2	9b	0.8143(9)	0.1857(9)	0.8820(9)	1	0.010(3)
H3	9b	0.0571(12)	0.114(2)	0.0189(10)	1	0.082(6)

Table 5-11: Select inter-atomic distances and angles from an unrestrained refinement of hydronium jarosite in space group *R*3*m*

Atoms	Bond Distance/Å	Atoms	Bond Angle/°
S1–O1 × 1	1.42(3)	O1–S1–O4	110.2(11)
S1–O4 × 3	1.481(15)	O4–S1–O4	108.8(12)
S2–O2 × 1	1.46(3)	O2–S2–O6	110.3(10)
S2–O6 × 3	1.474(15)	O6–S2–O6	108.6(10)
Fe–O4	2.073(12)	H3–O3–H3	79(2)
Fe–O5 ×2	1.981(6)	O4–Fe–O5	88.8(3)
Fe–O6	2.011(13)	O4–Fe–O6	179.1(6)
Fe–O7 ×2	2.031(7)	O4–Fe–O7	85.7(5)
O5–H1	1.072(16)	O5–Fe–O5	92.1(5)
O5–H3	2.016(17)	O5–Fe–O6	91.9(3)
O1–H1	1.858(18)	O5–Fe–O7	173.9(5)
O7–H2	0.87(2)		90.1(2)
O2–H2	2.016(12)	O6–Fe–O7	93.7(4)
O3–H3	0.99(2)	O7–Fe–O7	87.1

A Hamilton test on the crystallographic *R*-factors for the two different space group models was performed (Hamilton 1965). The null hypothesis (H_0) is that the space group of hydronium jarosite is better explained by space group *R*3*m*. The number of observations was calculated to be 1879. The *R*-factor ratio is 0.0278/0.0255 = 1.090 and the test statistic is $\mathcal{R}_{15,\ 1830,\ 0.005}$ = 1.009. Therefore, the null hypothesis can be rejected at the 99.5 % significance level, assuming no systematic errors or serial correlations are present. The null hypothesis can also be rejected at the 95 % significance level ($\mathcal{R}_{15,\ 1830,\ 0.05}$ = 1.006). This test suggests that the fifteen additional parameters introduced by refinement under space group *R*3*m* do not result in a significantly better fit to the data. However, the Prince test (Prince 1982) yields a 99.5 % confidence interval of the slope of the regression line to be 0.4048 ± 0.1778, which does not include zero. The slope does not include zero at the 95 % significance level as well (0.4048 ± 0.1241). As the slope is positive, model 1 (*R*3*m*) is preferred. The Prince test suggests that the differences in the

fits of the two models are greater than what would be observed by chance alone. Statistical tests are inconclusive.

Although better *R*-factors were obtained for refinements in *R*3*m* (0.0255 R_{wp} – background), this is not unexpected (Jones 1984; Hamilton 1965) as there are more parameters in the lower symmetry model and hence, more variables which account for unexplained neutron scattering. The nature of least squares refinement means more parameters can result in lower *R*-factors by being forced to fit the data better. Refinements in $R\bar{3}m$ rapidly converged, yet the use of excessive damping and restraints was required to achieve convergence to a sensible structure in *R*3*m* with higher e.s.d.s; it is prudent to opt for the centrosymmetric description of the structure as refinement is more efficient (Abrahams *et al.* 1998; Marsh 1986). Indeed, the centrosymmetric description of a crystal structure has been recommended even though disorder may result when compared to the non-centrosymmetric structure (Marsh 1986; Marsh and Schomaker 1981). Thus, the best space group choice appears to be $R\bar{3}m$, despite slightly higher *R*-factors. This is because the structure described $R\bar{3}m$ is the average structure of any local distortion from true centrosymmetry.

As stated earlier, previous NMR studies have shown that the hydronium hydrogen atoms are mobile. The *R*3*m* structure does not support this observation as it suggests the hydronium ion is orientated the same way (ordered) across all unit cells. The cavity that the hydronium ion resides in is surrounded by twelve oxygen atoms. It is unlikely that all hydronium ions will be directed into the cavity in one orientation, given that the other orientation and its surrounds are chemically equivalent. Such an ordered arrangement of H_3O^+ would not be deleterious to long range magnetic ordering. In fact, random disorder is a requirement for spin-glass behavior (Fåk *et al.* 2008). A model with both orientations and refinement of occupancies in *R*3*m* is the $R\bar{3}m$ structure. Thus, the time averaged structure across all unit cells is best described under space group $R\bar{3}m$

with disorder invoked on the hydronium ion. The $R\bar{3}m$ space group is the only space group choice consistent with the known magnetic and NMR data of hydronium jarosite.

INVESTIGATION OF HYDRONIUM ION GEOMETRY

The geometry of the hydronium ion was investigated further under space group $R\bar{3}m$. Whilst the unrestrained refinement in space group $R\bar{3}m$ appears satisfactory, the geometry of the hydronium ion is not ideal, as previously discussed. The geometry of hydronium from this refinement was found to be very similar to another study (Wills and Harrison 1996). Restraints on the H2–O4–H2 angle to 112° and all O–H distances to 0.96 Å will result in a more meaningful and physically sensible structure. Thus, the hydronium ion was modelled as a rigid body with H–O–H bond angles of 112° and O–H distances of 0.96 Å. The O2–H1 bond distance was also restrained to be 0.96 Å with a tolerance of 0.10 and a weight of 500. Given the site that hydronium occupies and the crystallographic symmetry of space group $R\bar{3}m$, refinement of rigid body rotation R_z seems most likely. Thus, models with 60° (RB1) and 0° (RB2) rotation around R_z were investigated. The isotropic ADPs of all atoms in the rigid body (O4, H2, H3, H4) were restrained to be equal. The use of TLS parameters using previously determined, appropriate site symmetry restraints (Schomaker and Trueblood 1968) were also investigated.

We also find a rigid body where the hydronium hydrogen atoms do not point towards basal sulfate oxygen atoms to be optimal (Wills and Harrison 1996). This particular rigid body is the one rotated by 60° (RB1). Refinement results of RB1 are given Tables 5-12 and 5-13, and the structure is shown in Figure 5-4. The geometry of hydronium is shown in Figure 5-5. The bond distances and angles are commensurate to those reported in Table 5-6 except the O2–H1 distance is now 0.944(5) Å. A TLS refinement of this structure was not stable, thus, the thermal parameters are shown as isotropic ADPs for the rigid body as a whole.

Table 5-12: Results from the Rietveld refinement of the hydronium ion described by RB1

Space group	$R\bar{3}m$ (no. 166)
Z	3
a/Å	7.35471(11)
c/Å	16.9984(4)
V/Å^3	796.29(3)
Data range for refinement/°2θ	13.4 – 160.35
Number of observations	2938
Number of calculated reflections	220
R_{wp} – background	0.0335
R_p – background	0.0233
$R(F^2)$	0.1207
χ^2	5.231
Parameters	37

Table 5-13: Refined positional and isotropic ADPs from the refinement of the hydronium ion described by RB1. Atoms O4 through H4 form the rigid body and their coordinates are reported without e.s.d.s

Atom	Wyckoff site	x	y	z	Occupancy	U_{iso}/Å^2
Fe	9d	0.5	0	0.5	1	0.0079(4)
S	6c	0.0	0.0	0.3093(4)	1	0.0044(15)
O1	18h	0.55762(19)	0.1152(4)	0.61230(15)	1	0.0119(6)
O2	18h	0.79573(17)	0.20427(17)	0.46811(16)	1	0.0130(5)
O3	6c	0.0	0.0	0.3942(3)	1	0.0147(8)
H1	18h	0.8596(3)	0.1404(3)	0.4399(3)	1	0.0322(13)
O4	3a	0.0	0.0	0.0	1	0.059(2)
H2	18h	0.07214	-0.07214	0.01633	0.1666	0.059(2)
H3	18h	-0.14428	-0.07214	0.01633	0.1667	0.059(2)
H4	18h	0.07214	0.14428	0.01633	0.1667	0.059(2)

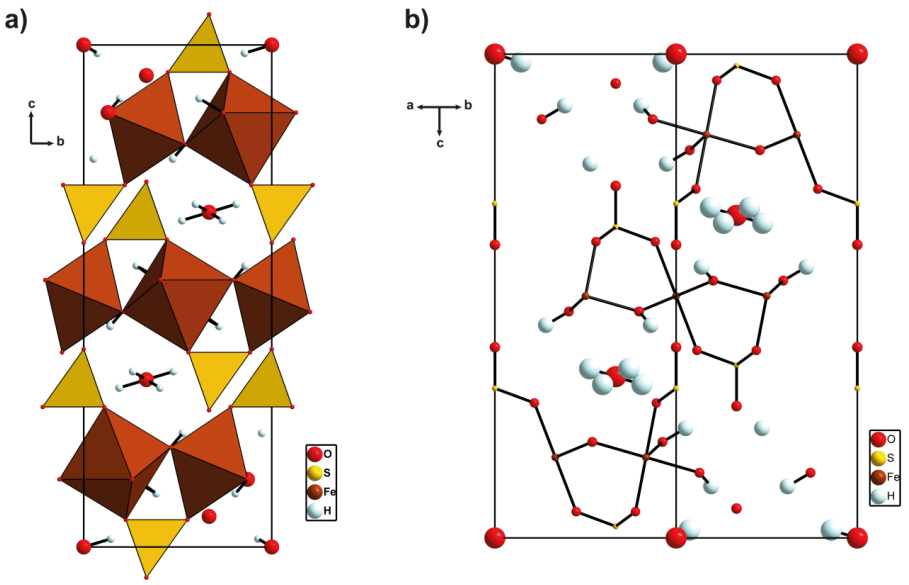

Figure 5-4: Structure of hydronium jarosite with the hydronium ion described by RB1 a) viewing direction is along **a** with FeO_6 and SO_4 groups shown as polyhedra b) viewing direction along the **[110]** axis with atoms shown as 50 % ellipsoids

RB1 results in only two orientations of the hydronium ion: the hydronium hydrogen atoms point either "up" or "down" with respect to the **c** axis. The angles of a possible side orientation, where all hydronium hydrogen atoms point towards a sulfate group is 68° (Figure 5-5). This angle is unrealistically low, because, by defining a rigid body, side orientations are not possible as the three-fold rotation axis of the crystal is destroyed. Despite the possibility of additional orientations, disorder across two orientations, coincident with all crystallographic symmetry elements, explains hydronium jarosite's magnetic and NMR behaviour. Whilst more disorder cannot be ruled out, it cannot be modelled from the acquired neutron powder diffraction data. Hence, we have opted for a more symmetrical structure with higher isotropic ADPs for the rigid body as the best representation of the diffraction data. Any deviation or displacement of hydronium hydrogen atoms from the *m* site or hydronium oxygen atoms from the $\bar{3}m$ site is accounted for by the higher isotropic adp. The structure of hydronium alunite will be essentially the same.

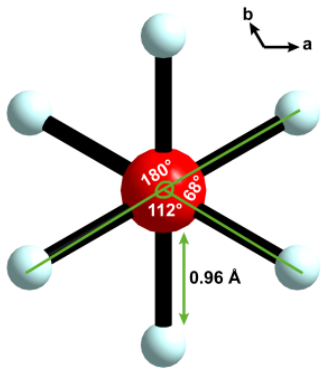

Figure 5-5: Geometry of the hydronium ion described by RB1. Viewing direction is along **c**

Although RB2 was refined to convergence, *R*-factors are significantly higher ($R(F^2)$ = 0.1395; R_{wp} – background = 0.0373; R_p – background = 0.0254) than RB1. We note that in a previous study, a rigid body with 0° rotation was not successfully refined (Wills and Harrison 1996). Slightly higher isotropic ADPs were also obtained (0.070(3) $Å^2$) for all atoms in the rigid body described by RB2. In RB2 the hydronium hydrogen atoms point towards basal sulfate oxygen atoms. In RB1, the hydronium hydrogen atoms point towards the apical sulfate oxygen atom which is further away, and the hydroxyl oxygen atom to which it most likely forms a hydrogen bond, for reasons that will be explained below.

In RB1, the O2····H2 hydrogen bond distance is 2.140 Å whilst the possible O1····H2 hydrogen bond distance is 2.280 Å. The O4–H2····O2 and O4–H2····O1 hydrogen bond angles are 126.6 and 131.4° respectively. In RB2, the O1····H2 hydrogen bond distance is shorter (2.044 Å) than the O2····H2 hydrogen bond distance (2.677 Å) with angles of 178° and 89° respectively. Note that H2 refers to all hydrogen atoms described by the rigid body, including H3 and H4 from Table 5-11. Whilst linear hydrogen bonds are energetically and statistically favorable in crystals (Hamilton 1962; Steiner 2002), linearity is not a hydrogen bond requirement (Baur 1972). Regardless of rotation about the Z axis, the O4–O2 and O4–O1 distances of 2.820 and 3.003 Å are the same; the O4–O2 distance is significantly shorter which suggests that it will form the

hydrogen bond and that this hydrogen bond will be moderate to rather weak in strength (Lee and Carpenter 1959; Libowitzky 1999). The upper limit for hydrogen bonding has been suggested to be beyond 3 Å for O–O distances (Emsley 1980). In addition, the O4–H2····O2 and O4–H2····O1 angles obtained in RB1 are in agreement with guide values for moderate hydrogen bonds (Jeffrey 1997) and long (not strong) hydrogen bonds tend to be bent (Steiner 2002). Therefore, we find no compelling diffraction evidence for hydrogen bonding to basal sulfate oxygen atoms. In addition, hydrogen bonding to hydroxyl oxygen atoms is probable given the acidity of hydronium (pKa = 0), the basicity of hydroxyl groups (pKa of water ≈ 16), and the expected strong electrostatic attraction between a positively charged and a negatively charged ion. The H_3O^+ and OH^- groups are hydrogen bonded, but this interaction does not result in complete protonation to $2H_2O$, in accordance with previous NMR studies (Nielsen *et al.* 2008).

CONCLUSIONS

Hydronium hydrogen atoms have been located in hydronium jarosite. The crystal structure of hydronium jarosite is best described in space group $R\bar{3}m$, with hydronium hydrogen atoms located at an *m* site with 50 % fractional occupancy. The hydronium oxygen atom is located at the $\bar{3}m$ site. A rigid body description of the ion was necessary for a chemically sensible geometry. The optimal rigid body structure only allows for disorder across two orientations. The high isotropic adp of all atoms in the rigid body suggests the hydrogen atoms are dynamically disordered instead of statically disordered. This particular structure is consistent with infrared and Raman spectra, previous NMR studies, and the observed lack of long range magnetic ordering at low temperature. It is also the most symmetrical model with the least assumptions. However, at a finite point in time, the hydronium ion in a particular unit cell must be 3*m* symmetry. Hydrogen bonding of the hydronium ion is with hydroxyl groups, not basal sulfate oxygen atoms.

REFERENCES

Abrahams SC, Schmalle HW, Williams T, Reller a, Lichtenberg F, Widmer D, Bednorz JG, Spreiter R, Bosshard C, Günter P (1998) Centrosymmetric or noncentrosymmetric? Case study, generalization and structural redetermination of $Sr_5Nb_5O_{17}$. Acta Cryst B54:399-416

Altomare A, Burla MC, Camalli M, Cascarano GL, Giacovazzo C, Guagliardi A, Moliterni AGC, Polidori G, Spagna R (1999) SIR97: a new tool for crystal structure determination and refinement. J Appl Crystallogr 32:115-119

Arkhipenko DK, Bokii GB (1979) Refinement of the alunite-jarosite space group by a vibrational spectroscopic method. Sov Phys Crystallogr 24:100-106

Baur WH (1972) Prediction of hydrogen bonds and hydrogen atom positions in crystalline solids. Acta Cryst B28:1456-1465

Becker U, Gasharova B (2001) AFM observations and simulations of jarosite growth at the molecular scale: probing the basis for the incorporation of foreign ions into jarosite as a storage mineral. Phys Chem Min 28:545-556

Begemann MH, Saykally RJ (1985) A study on the structure and dynamics of the hydronium ion by high-resolution infrared laser spectroscopy. I. The ν_3 band of $H_3{}^{16}O^+$. J Chem Phys 82:3570-3579

Bisson WG, Wills AS (2008) Anisotropy-driven spin glass transition in the kagome antiferromagnet hydronium jarosite, $(H_3O)Fe_3(SO_4)_2(OH)_6$. J Phys: Condens Matter 20:452204

Breitinger DK, Krieglstein R, Bogner A, Schwab RG, Pimpl TH, Mohr J, Schukow H (1997) Vibrational spectra of synthetic minerals of the alunite and crandallite type. J Mol Struct 408/409:287-290

Burger PV, Papike JJ, Shearer CK, Karner JM (2009) Jarosite growth zoning as a recorder of fluid evolution. Geochim Cosmochim Acta 73:3248-3259

Catti M, Ibberson RM (2002) Order-disorder of the hydronium ion and low-temperature phase transition of $(H_3O)Zr_2(PO_4)_3$ NASICON by neutron diffraction. J Phys Chem B 106:11916-11921

Dunitz JD, Schomaker V, Trueblood KN (1988) Interpretation of atomic displacement parameters from diffraction studies of crystals. J Phys Chem 92:856-867

Elwood Madden ME, Bodnar RJ, Rimstidt JD (2004) Jarosite as an indicator of water-limited chemical weathering on Mars. Nature 431:821-823

Emsley J (1980) Very strong hydrogen bonding. Chem Soc Rev 9:91-124

Fåk B, Coomer FC, Harrison A, Visser D, Zhitomirsky ME (2008) Spin-liquid behavior in a kagomé antiferromagnet: deuteronium jarosite. Europhys Lett 81:17006

Farmer VC, (ed.) (1974) The Infrared Spectra of Minerals. Mineralogical Society, London

Farrugia LJ (1999) WinGX suite for small-molecule single-crystal crystallography. J Appl Crystallogr 32:837-838

Frunzke J, Hansen T, Harrison A, Lord JS, Oakley GS, Visser D, Wills AS (2001) Magnetic ordering in diluted kagome antiferromagnets. J Mater Chem 11:179-185

Gale JD, Wright K, Hudson-Edwards KA (2010) A first-principles determination of the orientation of H_3O^+ in hydronium alunite. Am Mineral 95:1109-1112

Grohol D, Nocera DG (2007) Magnetic disorder in the frustrated antiferromagnet jarosite arising from the $H_3O^+ \cdots OH^-$ interaction. Chem Mater 19 (12):3061-3066

Hamilton WC (1962) The structure of solids. Annu Rev Phys Chem 13:19-40

Hamilton WC (1965) Significance tests on the crystallographic *R* factor. Acta Cryst 18:502-510

Harlow RL (1996) Troublesome crystal structures: prevention, detection and resolution. J Res Natl Inst Stand Technol 101:327-339

Hendricks SB (1937) The crystal structure of alunite and the jarosites. Am Mineral 22:773-784

Inami T, Nishiyama M, Maegawa S, Oka Y (2000) Magnetic structure of the kagomé lattice antiferromagnetc potassium jarosite $KFe_3(OH)_6(SO_4)_2$. Phys Rev B 61:12181-12186

Jeffrey GA (1997) An introduction to hydrogen bonding. Oxford University Press, Oxford

Jewess M (1982) A theoretical treatment of 'orientational' disorder for routine use. Acta Cryst B38:1418-1422

Jones PG (1984) Crystal structure determination: a critical review. Chem Soc Rev 13:157-172

Klingelhöfer GM, R. V.; Bernhardt, B.; Schröder, C.; Rodionov, D. S.; de Souza Jr, P. A.; Yen, A.; Gellert, R.; Evlanov, E. N.; Zubkov, B.; Foh, J.; Bonnes, U.; Kankeleit, E.; Gütlich, P.; Ming, D. W.; Renz, F.; Wdowiak, T.; Squyres, S. W.; Arvidson, R. E (2004) Jarosite and hematite at Meridiani Planum from Opportunity's Mossbauer spectrometer. Science 306:1740-1745

Larson AC, Von Dreele RB (2004) General Structure Analysis System (GSAS). Los Alamos National Laboratory Report LAUR 86-748.

Lee FS, Carpenter GB (1959) The crystal structure of perchloric acid monohydrate. J Phys Chem 63:279-282

Libowitzky E (1999) Correlation of O-H stretching frequencies and O-H•••H hydrogen bond lengths in minerals. Monatsh Chem 130:1047-1059

Loiacono GM, Kostecky G, White JS (1982) Resolution of space group ambiguities in minerals. Am Mineral 67:846-847

Majzlan J, Stevens R, Boerio-Goates J, Woodfield BF, Navrotsky A, Burns PC, Crawford MK, Amos TG (2004) Thermodynamic properties, low-

temperature heat-capacity anomalies, and single-crystal X-ray refinement of hydronium jarosite, $(H_3O)Fe_3(SO_4)_2(OH)_6$. Phys Chem Min 31:518-531

Marsh R (1986) Centrosymmetric or noncentrosymmetric? Acta Cryst B42:193-198

Marsh RE, Schomaker V (1979) Some incorrect space groups in *Inorganic Chemistry*, Volume 16. Inorg Chem 18:2331-2336

Marsh RE, Schomaker V (1981) Some incorrect space groups: an update. Inorg Chem 20:299-303

Menchetti S, Sabelli C (1976) Crystal chemistry of the alunite series: crystal structure refinement of alunite and synthetic jarosite. Neues Jahrbuch Mineral Monatsh 9:406-417

Nielsen UG, Heinmaa I, Samoson A, Majzlan J, Grey CP (2011) Insight into the local magnetic environments and deuteron mobility in jarosite ($AFe_2(SO_4)_2(OD,OD_2)_6$, A = K, Na, D_3O) and hydronium alunite ($(D_3O)Al_3(SO_4)_2(OD)_6$), from variable-temperature ^2H MAS NMR spectroscopy. Chem Mater 23:3176-3187

Nielsen UG, Majzlan J, Grey CP (2008) Determination and quantification of the local environments in stoichiometric and defect jarosite by solid-state ^2H NMR spectroscopy. Chem Mater 20:2234-2241

Nocera DG, Bartlett BM, Grohol D, Papoutsakis D, Shores MP (2004) Spin frustration in 2D kagomé lattices: a problem for inorganic synthetic chemistry. Chem Eur J 10:3850-3859

Oxford Diffraction (2007) CrysAlis CCD and CrysAlis RED. Oxford Diffraction Ltd, Abingdon, Oxfordshire, England

Petruševski VM, Minčeva-Šukarova B, Džorovska A (1993) The vibrational species of molecules in disordered crystals: $M(NH_3)_2$ groups at C_{4h} symmetry sites. Bull Chem Technol Macedonia 12:31-34

Pressprich MR, Bond MR, Willett RD (2002) Structures of $[(CH_3)_4P]_2CoCl_4$, $[(CH_3)_4Sb]_2CuCl_4$ and $[CH_3)_4Sb]_2ZnBr_4$ and a correlation of psuedo-antifluorite $[(CH_3)_4Pn]_2MX_4$ salts. J Phys Chem Solids 63:79-88

Prince E (1982) Comparison of the fits of two models to the same data set. Acta Cryst B38:1099-1100

Rahman AA, Usman A, Chantrapromma S, Fun H-K (2003) Redetermination of hydronium perchlorate at 193 and 293 K. Acta Cryst C59:92-94

Ripmeester JA, Ratcliffe CI, Dutrizac JE, Jambor JL (1986) Hydronium ion in the alunite - jarosite group. Can Mineral 24:435-447

Sato E, Nakai I, Miyawaki R, Matsubara S (2009) Crystal structures of alunite family minerals: beaverite, corkite, alunite, natroalunite, jarosite, svanbergite, and woodhouseite. N Jb Miner Abh 185:313-322

Schiebel P, Burger K, Büttner HG, Kearley GJ, Lehmann M, Prandl W (2000) ND_3-Density distribution in orientationally disordered $Ni(ND_3)_6Cl_2$ observed by means of neutron Laue diffraction. J Phys: Condens Matter 12:8567-8576

Schomaker V, Trueblood KN (1968) On the rigid-body motion of molecules in crystals. Acta Cryst B24:63-76

Scott KM (1987) Solid solution in, and classification of, gossan-derived members of the alunite-jarosite family, northwest Queensland, Australia. Am Mineral 72:178-187

Serna CJ, Cortina CP, Garcia Ramos JV (1986) Infrared and Raman study of alunite-jarosite compounds. Spectrochim Acta A 42:729-734

Sheldrick GM (2008) A short history of SHELX. Acta Cryst A64:112-122

Steiner T (2002) The hydrogen bond in the solid state. Angew Chem Int Ed 41:48-76

Stoffregen RE, Alpers CN, Jambor JL (2000) Alunite-jarosite crystallography, thermodynamics, and geochronology. Rev Mineral Geochem 40 (Sulfate):453-479

Szymanski JT (1985) The crystal structure of plumbojarosite. Can Mineral 23:659-668

Toby BH (2001) EXPGUI, a graphical user interface for GSAS. J Appl Cryst 34:210-213

Wills AS, Harrison A (1996) Structure and magnetism of hydronium jarosite, a model Kagomé antiferromagnet. Journal of the Chemical Society, Faraday Transactions 92:2161-2166

Wills AS, Harrison A, Ritter C, Smith RI (2000) Magnetic properties of pure and diamagnetically doped jarosites: model kagomé antiferromagnets with variable coverage of the magnetic lattice. Phys Rev B 61:6156-6169

CHAPTER 6 A NEUTRON POWDER DIFFRACTION STUDY OF THE CRYSTAL STRUCTURE OF AMMONIOJAROSITE

NEW AMMONIUM ION ORIENTATION MODEL

STATEMENT OF CONTRIBUTION

The authors listed below have certified* that:

1. They meet the criteria for authorship in that they have participated in the conception, execution, or interpretation, of at least that part of the publication in their field of expertise;
2. They take public responsibility for their part of the publication, except for the responsible author who accepts overall responsibility for the publication;
3. There are no other authors of the publication who meet these criteria;
4. Potential conflicts of interests have been disclosed to a) granting bodies, b) the editor or publisher of journals or other publications, and c) the head of the responsible academic unit, and;
5. They agree to the use of the publication in the student's thesis and its publication on the Australasian Digital Thesis database consistent with any limitations set by the publisher requirements.

In the case of this chapter:

A neutron powder diffraction study of the crystal structure of ammoniojarosite: New ammonium ion orientation model

Contributor	*Statement of Contribution**
Henry J. Spratt	Experimental design, conducted experiments, data analysis/interpretation, wrote the manuscript,
Maxim Avdeev	Supervision, editing, aided data collection and analysis and interpretation
Jasmine R. Jensen	Editing
Wayde N. Martens	Overall supervisor, aided experimental design, aided experiments and data analysis/interpretation, editing

Principal Supervisor Confirmation

I have sighted email or other correspondence from all co-authors confirming their certifying authorship.

Name	Signature	Date

SYNOPSIS

This chapter examines the crystal structure of ammoniojarosite by neutron powder diffraction at ambient temperature and also at 3 K. This study was undertaken due to the uncertainty in the literature regarding the crystal structure of ammoniojarosite, especially the position of the ammonium nitrogen atom; there are only two crystallographic studies of this mineral and they both model the nitrogen atom at a different site. Investigations of lower symmetry space groups have been performed for ammoniojarosite, and there is a wealth of evidence suggesting the true space group is the same as other jarosite minerals. Nevertheless, a re-investigation of the crystal structure of ammoniojarosite is needed, especially with regards to hydrogen atom location.

Contrary to the literature, a different site for the apical hydrogen atoms of the ammonium ion was found from difference Fourier methods. All previous literature modelled these atoms at a 3*m* site with 50 % occupancy. Instead, it was found that these atoms can be modelled at an *m* site with 16.67 % fractional occupancy. This new model offers lower *R*-factors and more reasonable refined structural parameters. Indeed, the literature model was not a good fit to the observed diffraction patterns and a 3*m* site was never observed from difference Fourier methods for this atom. Additional models for the ammonium ion were refined to make sure that the new orientation is a global minimum; other models were a worse fit to the data. The nitrogen atom is best modelled at the 3a Wyckoff site (0, 0, 0) as no compelling evidence for a lowering of symmetry to a 6c Wyckoff site (0, 0, *z*) was found. This new model implies the ammonium ion is highly disordered. The time and spatial averaging inherent in diffraction techniques leads to the apparent D_{3d} symmetry of the T_d hydronium ion. Locally, the symmetry of the ion must be lower than D_{3d}, but this cannot be accurately modelled.

A NEUTRON POWDER DIFFRACTION STUDY OF THE CRYSTAL STRUCTURE OF AMMONIOJAROSITE: NEW AMMONIUM ION ORIENTATION MODEL

Henry J. Spratt, Jasmine R. Jensen, and Wayde Martens

Chemistry, Physics and Mechanical Engineering, Science and Engineering Faculty, Queensland University of Technology, Brisbane, QLD, 4001 Australia

Maxim Avdeev

Bragg Institute, Australian Nuclear Science and Technology Organisation, Lucas Heights, NSW, 2234 Australia

Keywords: ammoniojarosite · neutron powder diffraction · crystal structure · orientational disorder · Rietveld refinement

ABSTRACT

The crystal structure of deuterated ammoniojarosite [$ND_4Fe_3(SO_4)_2(OD)_6$] was determined from Rietveld refinement against neutron powder diffraction patterns collected at 298 and 3 K. Difference Fourier methods successfully located all ^2H atoms and the crystal structure is the same at both investigated temperatures under space group $R\bar{3}m$. The ammonium nitrogen atom was located at the $\bar{3}m$ site (3a (0, 0, 0) Wyckoff site); there was limited evidence for a lowering of symmetry to 3*m* (6c (0, 0, *z*) Wyckoff site). A different site for the apical ammonium ^2H atoms was found from difference Fourier maps compared to the literature. The apical ammonium ^2H atoms can be modeled at an *m* site (18h (*x*, 2*x*, *z*) Wyckoff site) with 0.1667 fractional occupancy. The basal ^2H atoms are at the same symmetry site as the apical ^2H atoms but with 0.5 fractional occupancy, as per the literature. The $\bar{4}3m$ ammonium ion is highly disordered, and when all orientations are time and spatially averaged, can be described as having the seemingly forbidden $\bar{3}m$ symmetry. This new model suggests the ammonium ion is more disordered than previously thought.

INTRODUCTION

The jarosite subgroup of the alunite supergroup of minerals are described by the general formula $AB_3(SO_4)_2(OH)_6$, where B is predominantly iron (III). The A site can be occupied by numerous types of monovalent or divalent cations. Most jarosite minerals crystallize in space group $R\bar{3}m$ with Z = 3. There is some evidence the space group could be $R3m$ due to optical second harmonic generation of alunite (Loiacono *et al.* 1982) and observations of pyroelectricity (Hendricks 1937). A more recent study of single crystal jarosite [$KFe_3(SO_4)_2(OH)_6$] observed no pyroelectric effect (Buurma *et al.* 2012). In fact, it was suggested all jarosite minerals should be modeled in space group $R\bar{3}m$ unless there is substantial evidence to the contrary (Menchetti and Sabelli 1976).

There are myriad single and powder crystallographic studies of $R\bar{3}m$ jarosite minerals and the isostructural alunite subgroup with elemental cations at the A site (Bartlett and Nocera 2005; Groat *et al.* 2003; Hendricks 1937; Kato and Miura 1977; Majzlan *et al.* 2006; Menchetti and Sabelli 1976; Sato *et al.* 2009; Schukow *et al.* 1999; Szymanski 1985; Toumi and Tlili 2008). In most cases the A site cation occupies the $\bar{3}m$ site (3a Wyckoff site) at fractional coordinates (0, 0, 0). However, the symmetry of ammonium ions $(\bar{4}3m)$ is not a subgroup of the $\bar{3}m$ site. As a result, it has been suggested the space group of ammoniojarosite is lower than $R\bar{3}m$, with the maximal non-isomorphic subgroup $R3m$ being a promising candidate, or, the ammonium ions are disordered (Szymanski 1985). This is because no local distortion of ammonium ions can result in a center of symmetry, as required by the A site. Systematic absences for $R\bar{3}m$ and $R3m$ are the same, which complicates the correct space group choice from diffraction data.

There are few crystal structural investigations of ammoniojarosite. Recently there has been one single crystal X-ray diffraction study (Basciano and Peterson 2007a) and

one neutron powder diffraction study (Wills *et al.* 2000). The neutron powder diffraction study was part of a larger study on the magnetic structure and behavior of jarosite minerals at low temperature. Despite potential space group ambiguity, both investigations modeled the structure in space group $R\bar{3}m$. In addition, spectroscopic studies have concluded $R\bar{3}m$ is the correct space group for ammoniojarosite (Chio *et al.* 2010; Sasaki *et al.* 1998; Serna *et al.* 1986). A low temperature Raman spectroscopic study of jarosites including ammoniojarosite down to 8 K found no evidence of a phase transition or lower symmetry space group for ammoniojarosite (Chio *et al.* 2010).

The major difference between the two aforementioned crystallographic studies was the location of the ammonium nitrogen atom, which was modeled at the $\bar{3}m$ site (0, 0, 0) by Basciano and Peterson (2007a) and the 3*m* site (0, 0, *z*) by Wills *et al*. (2000). The ammonium apical and basal hydrogen atoms were modeled at a 3*m* and an *m* site respectively, both 0.5 fractionally occupied. Owing to the two hydrogen positions, the ammonium ion is disordered over at least two orientations that point up or down with respect to **c**, so when time and spatially averaged, the center of symmetry of the crystal is preserved and the space group is not lower than $R\bar{3}m$. The present study was undertaken to compare different crystallographic models for ammoniojarosite under the most likely space group $R\bar{3}m$ using neutron diffraction.

EXPERIMENTAL

SYNTHESIS

Deuterated ammoniojarosite was synthesized by the National Deuteration Facility at the Australian Nuclear Science and Technology Organisation in a similar manner to protonated ammoniojarosite described by some of the authors in another publication (Spratt *et al.* 2014). Instead of a microwave reactor, a conventional hydrothermal Parr bomb was used and the synthesis time extended to three days. The temperature remained at 423 K through the use of an oven. Deuterated reactants were used instead of their protonated forms.

CHEMICAL COMPOSITION

The nitrogen (N) content was determined from ~10 mg samples using a Leco TruSpec Micro CNH Analyser operating at a furnace temperature of 1273 K. The N standard used was acetanilide and the QC standard was a certified low organic content soil. The average nitrogen content from three replicate analyses was 2.54 % (theoretical N content 2.86 %), corresponding to 0.89 fractional occupancy of the A site. The standard deviation of the analysis is estimated to be 0.03 from the QC standard.

Iron (Fe) and sulfur (S) ratios were determined from a Perkin Elmer 8300DV Inductively Coupled Plasma Optical Emission Spectrometer (ICP-OES). Samples (*ca* 0.015 g) were dissolved in concentrated hydrochloric acid (1 mL, HCl) at room temperature then diluted to 100 mL in a volumetric flask using 3–5 % nitric acid (HNO_3). Traceable standards were acquired from Choice Analytical and serially diluted to obtain calibration. A blank was prepared by using the same 3–5 % HNO_3 spiked with 1 mL of the same HCl. Analyses indicated there was an excess of iron. An excess of iron has been reported previously for similarly synthesised jarosite minerals (Basciano and Peterson 2007a, 2007b).

POWDER X-RAY DIFFRACTION

Powder X-ray diffraction patterns were collected on a Phillips PANalytical X'Pert PRO diffractometer operating at 40 kV and 40 mA using Cu Kα incident X-rays (Kα1 = 1.5406 Å, Kα1/Kα2 = 0.5). A fixed divergence slit (0.5°) under Bragg-Brentano geometry was employed at step size of 0.017 ° 2θ. Grain averaging and counting statistics were improved by using a spinning stage and removing the incident beam monochromator respectively. Samples were ground in a mortar and pestle prior to analysis. Phase identification was performed using the American Mineralogist Crystal Structure Database (April 2010 version) (Downs and Hall-Wallace 2003) and the PDF-2 database of the International Center for Diffraction Data (ICDD).

NEUTRON POWDER DIFFRACTION

Constant wavelength neutron powder diffraction patterns were collected on the high resolution neutron powder diffractometer (ECHIDNA) at the Australian Nuclear Science and Technology Organisation's (ANSTO) OPAL facility. The ammoniojarosite sample was loaded into a vanadium (V) can and patterns were collected at ambient temperature (~298 K) and 3 K at a step size of 0.05°. A temperature of 3 K was achieved by using a top loading AS Scientific cryofurnace. The wavelength used for data collection was 1.6215 Å obtained from the (335) reflection of a germanium (Ge) crystal monochromator.

RIETVELD REFINEMENT OF NEUTRON POWDER DIFFRACTION PATTERNS

The GSAS-EXPGUI software suite (Larson and Von Dreele 2004; Toby 2001) was used for Rietveld refinement and difference Fourier methods. In all refinements, an 8th order Chebyshev function was used to model the background with profile function type 4 (GU, GV, GW, and LX were refined). Profile parameters for the nuclear and magnetic phases were constrained to be equal. Starting structural parameters, and magnetic unit cell atomic positions and magnetic moment constraints for refinement at 3

K were taken from Wills *et al*. (2000). The refined structural and profile parameters at 298 K were used as the starting values for the refinement at 3 K. For refinement at 3 K the magnetic **a** and **b** axes were constrained to the nuclear **a** and **b** axes. Owing to the antiferromagnetic type of ordering of iron in the magnetic phase, the magnetic **c** axis was constrained to be double the nuclear **c** axis.

The isotropic atomic displacement parameter (adp) of all Fe atoms from both nuclear and magnetic phases were constrained to be equal. The nitrogen content was fixed to CN analyser results and the rest of the A site was assumed to be occupied by oxygen as a hydronium impurity. The O4 and N isotropic ADPs were constrained to be equal. Accounting for incomplete deuteration was not required as refinement of the D1 fractional occupancy at 3 K after convergence of all other parameters yielded 0.968 (97 % deuteration), which is close to the purity of the used D_2O. In addition, no significant change in refined parameters or difference Fourier map peaks were found by including ^1H atoms with the appropriate fractional occupancies and equivalent isotropic ADPs and positional parameters as the corresponding ^2H atoms. Thus, ^2H occupancies were fixed to 1.0 for all refinements. In all tables and the text hereafter, estimated standard deviations (e.s.d.s) are reported as numbers in parentheses and refer to the least significant digit/s. Refinement of the Fe occupancy of the nuclear phase after convergence gave a fractional occupancy of 0.99, indicating a fully occupied iron site, which is consistent with the results of the chemical analysis.

WHOLE POWDER PATTERN DECOMPOSITION

Whole powder pattern decomposition (Pawley method) was employed in TOPAS version 4.1 software. A 5th order Chebyshev was used to model the background. Peaks were described by the PV-TCHZ profile function where X, U, V, and W were refined. Unit cell parameters were allowed to refine, along with the zero error. The simple axial model was used to model axial divergence. Continue after convergence was used in order to avoid false minima.

RESULTS AND DISCUSSION

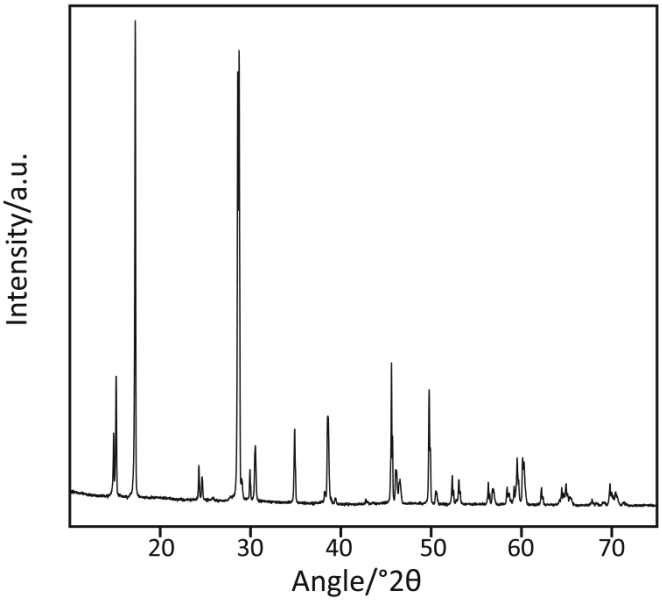

Figure 6-1: Powder X-ray diffraction pattern (Cu Kα1 and Kα2) of the deuterated ammoniojarosite

Powder X-ray diffraction patterns matched ammoniojarosite (00-026-1014) and the pattern is show in Figure 6-1. Significant crystalline impurities were not detected. Calculated reflections of the ammoniojarosite phase are in strong agreement with the observed neutron powder diffraction pattern (Figure 6-2). This fact, combined with the refined Fe fractional occupancy of the nuclear phase to 0.99 (see Experimental section), means the excess iron determined from ICP-OES can be assigned to an amorphous iron containing phase.

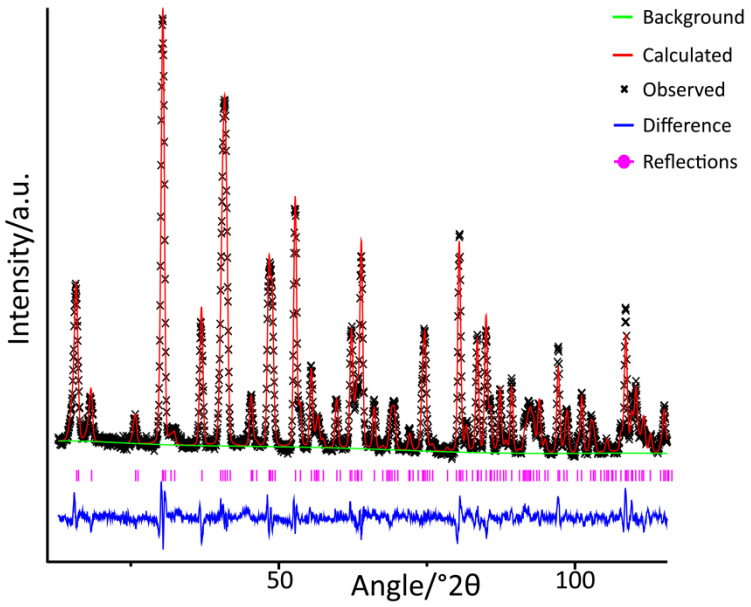

Figure 6-2: Typical Rietveld refinement profile fit to the deuterated ammoniojarosite (unconstrained model at 298 K)

Starting coordinates and unit cell parameters from Wills *et al.* (2000) were refined to convergence for both 298 and 3 K diffraction patterns. However, the N/O4 atoms were shifted from the lower symmetry 3*m* site in the original publication to the $\bar{3}m$ site. The ammonium ^{2}H atoms were successfully located at both temperatures as strong positive contours in difference Fourier maps (Figure 6-3). In all cases, the missing ^{2}H atoms were the most intense peaks. The first missing ^{2}H atom was located at fractional coordinates of (0.0639, 0.128, 0.0485) at 3 K, which corresponds to a general position (36i Wyckoff site). However, these coordinates are very close to an *m* site (*x*, 2*x*, *z*), so a ^{2}H atom (D2) was added to the model with fractional coordinates (0.064, 0.128, 0.049), a fractional occupancy of 0.5, and then refined to convergence. The second missing ^{2}H atom following refinement of D2 was located in a similar fashion and was also found to be close to an *m* site. From Figure 6-3, it appears to be disordered over six orientations. This peak was added to the model as D3 and refined to convergence with a fractional occupancy of 0.1667 to ensure charge balance and stoichiometry. This particular site for apical ammonium ^{2}H atoms is different to the literature and has hitherto not been

reported. No difference Fourier map contours with coordinates that matched a 3*m* site could be successfully refined as the apical ^{2}H ammonium atom. Final refinement results are given in Table 6-1, while structural information is given in Tables 6-2 and 6-3. Discussion of the structure refers to the refinement results at 3 K.

Table 6-1: Unconstrained refinement results of deuterated ammoniojarosite

T/K	298	3
Space group	$R\bar{3}m$	$R\bar{3}m$
Z	3	3
a = *b*/Å	7.3213(2)	7.31278(5)
c/Å	17.5530(8)	17.4049(9)
V/Å^3	814.81(5)	806.06(4)
Sublattice moment/μ_B	-	3.51(5)
Data range/°2θ	12.7 – 115.64	12.89 – 115.64
Number of observations	2058	2054
R_{wp} – background (R_{wp})	4.55 % (4.55 %)	5.69 % (5.57 %)
R_p – background (R_p)	3.69 % (3.54 %)	4.60 % (4.34 %)
$R(F^2)$	7.12 %	6.49 %
Number of parameters	37	38

We find limited evidence for shifting N/O4 atoms to a lower symmetry 3*m* site as per the study by Wills *et al.* (2000). Apart from being more difficult to refine and diverging often, the one extra variable this refinement induces yields *R*-factors only 0.01 % better than the $\bar{3}m$ model when successfully converged. Indeed, the Prince test (Prince 1982) on these two models suggests they are equally good fits to the data, as a 95 % confidence interval for the regression slope includes zero. Furthermore, N/O4 isotropic ADPs refine to non-positive definite values at a 3*m* site. The shift in real space along *c* at the 3*m* site from 0.0 is 0.07(5) Å (refined *z* = 0.004(3)), which is only ~1.3 e.s.d.s away from the ideal position. Therefore, we conclude the N/O4 atoms are located at fractional coordinates (0, 0, 0) as allowing the *z* coordinate to refine does not result in a statistically

or crystallographically better refinement. In fact, the two models are slightly different ways of explaining the same neutron density; more atoms with lower U_{iso} or less atoms with higher U_{iso}. The $\bar{3}m$ site for the N/O4 atoms are consistent with numerous single crystal X-ray diffraction studies of jarosite minerals where the A site cation is located at (0,0,0); see for example Sato *et al.* (2009), Menchetti and Sabelli (1976), and Bartlett and Nocera (2005) . The similarly disordered hydronium jarosite also shows limited evidence for a lower symmetry site of the hydronium oxygen atom from single crystal X-ray diffraction at liquid nitrogen temperature (Majzlan *et al.* 2004).

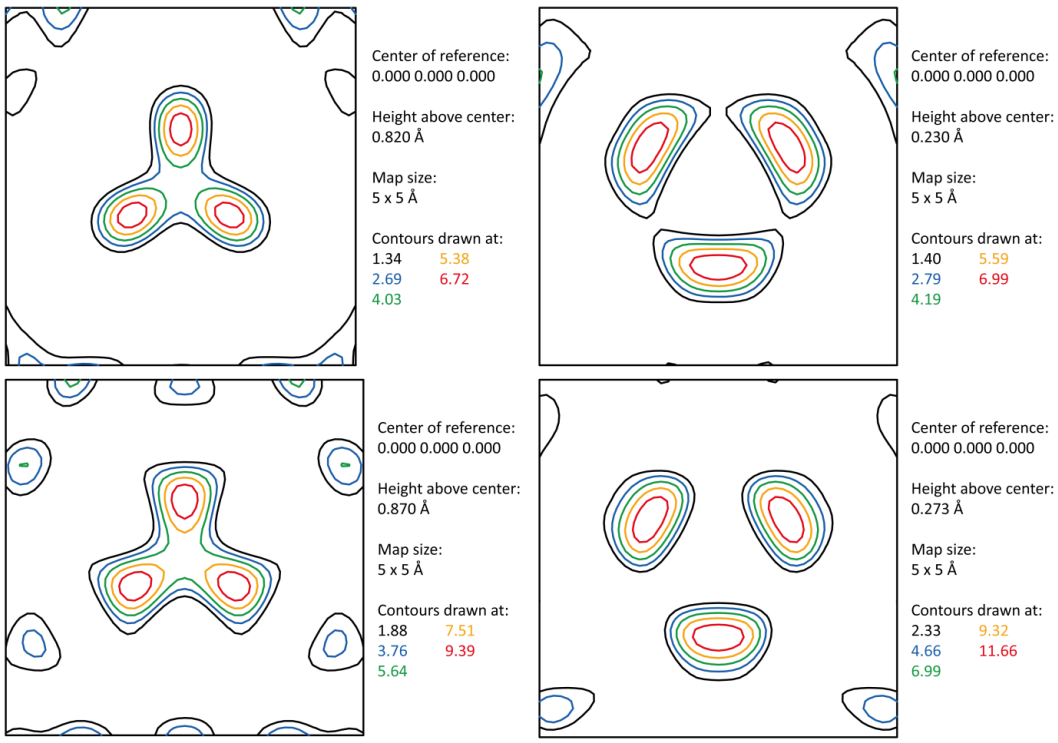

Figure 6-3: Difference Fourier maps at 298 K (top) and 3 K (bottom) at approximately +1σ contour levels. Cuts taken after refinement of the jarosite framework with no ammonium ^{2}H atoms (left), and after refinement to convergence including the previously found ^{2}H atoms (right)

Alternative models were refined for the ammonium ^{2}H atoms as the current structure is different to those previously reported. The possibility of the two ^{2}H atoms positions simply being due to separate basal ammonium and hydronium impurity ^{2}H atoms was investigated by restarting the search for ^{2}H atoms, but as they were found,

changing the fractional occupancy of D2 to 0.445 and D3 to 0.055 and vice versa. Apart from refining to higher *R*-factors, the isotropic ADPs of either ^{2}H atoms was large non-positive definite, and the missing apical ^{2}H atom position could not be successfully located from difference Fourier methods. Thus, it is concluded that the impurity hydronium ^{2}H atoms and the basal ammonium ^{2}H atoms share the same site, while the apical ammonium ^{2}H atoms are at an additional *m* site.

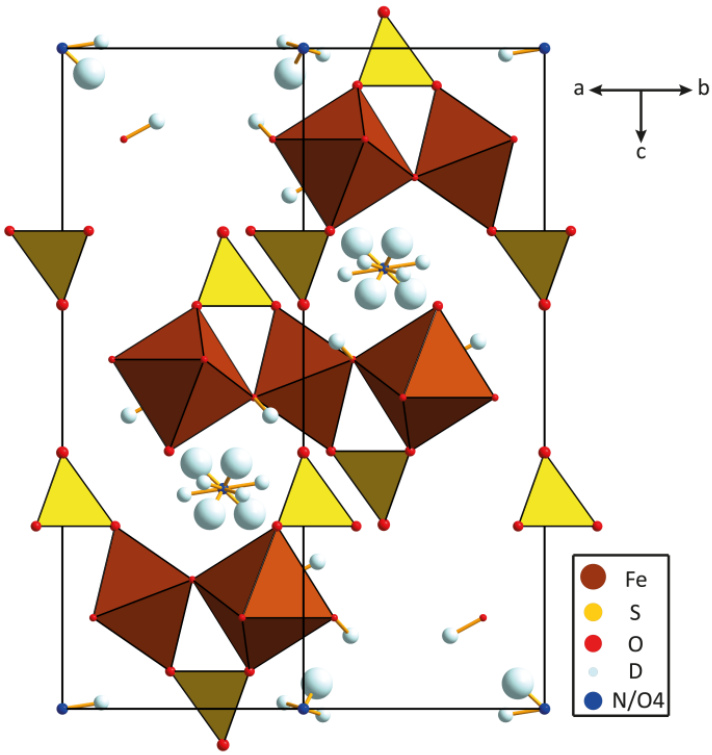

Figure 6-4: Crystal structure of deuterated ammoniojarosite at 3 K viewed down **[110]**. All atoms are shown as 50 % probability ellipsoids. FeO_6 and SO_4 are shown as polyhedra

It is also possible the previously refined basal ammonium ^{2}H atoms are the apical ammonium ^{2}H atoms. When the occupancies of D2 and D3 are reversed, *R*-factors are slightly higher (R_{wp} = 5.59 % and R_p = 4.39 % vs R_{wp} = 5.57 and R_p = 4.34), but more importantly, numerous isotropic ADPs refine to non-positive definite values (D2, O4/N, and S). Hence, it is concluded D2 is 0.5 fractionally occupied and is the basal ammonium ^{2}H atom, while D3 is 0.1667 fractionally occupied and is the apical ammonium ^{2}H atom.

We also investigated the structure refined by Basciano and Peterson (2007a) for ammoniojarosite where the apical ^{2}H atom is located at a 3*m* site with 50 % fractional occupancy and N/O4 occupies the $\bar{3}m$ site. While this model could be refined to convergence, *R*-factors were significantly higher with R_{wp} = 5.94 % and R_p = 4.54%, the isotropic adp of D3 was excessively large at 0.43(10) Å^2, the isotropic adp of D2 was larger at 0.116(7) Å^2, and the N–D3 bond distance was too short at 0.80(13) Å. When the isotropic ADPs of D2 and D3 are restrained to be equal in this model, the N–D3 bond distance is more reasonable at 0.95(4) Å but U_{iso} is still quite large at 0.137(6) Å^2, and *R*-factors show no improvement. It is concluded that in the present case, the apical ammonium ^{2}H atom is more reasonably modeled at an *m* site, not a 3*m* site, as shown in Figure 6-4. This *m* site is the only site consistent with the difference Fourier maps in Figure 6-3. The difference Fourier maps do not support a 3*m* site for the apical ammonium hydrogen atom.

Table 6-2: Unconstrained refined positional parameters and isotropic ADPs (× 10^2) of deuterated ammoniojarosite at 3 K. Isotropic ADPs at 298 K are shown for comparison

					U_{iso}/Å^2	
Atom	*x*	*y*	*z*	Occupancy	3 K	298 K
Fe	0.5	0	0.5	1.0	0.19(7)	0.82(6)
S	0.0	0.0	0.3102(9)	1.0	0.2(2)	0.26(19)
O1	0.0	0.0	0.3879(4)	1.0	1.14(16)	2.06(15)
O2	0.2240(3)	-0.2240(3)	-0.05684(19)	1.0	0.82(10)	1.41(9)
O3	0.1274(3)	-0.1274(3)	0.13782(19)	1.0	0.40(9)	1.15(8)
D1	0.1957(3)	-0.1957(3)	0.11068(17)	1.0	1.96(11)	3.03(10)
N	0.0	0.0	0.0	0.89	0.02(17)	1.35(15)
O4	0.0	0.0	0.0	0.11	0.02(17)	1.35(15)
D2	0.0544(8)	0.1107(16)	0.0384(8)	0.50	7.5(4)	10.5(5)
D3	0.161(4)	0.081(2)	0.0092(13)	0.1667	1.7(6)	2.2(5)

Although unlikely, another possibility is that the space group of ammoniojarosite is lower symmetry than $R\bar{3}m$. It has been shown that iron vacancies can order in jarosite minerals and lower the space group to monoclinic *C*2/*m* (Scarlett *et al.* 2010). We used whole powder pattern decomposition (Pawley) methods to compare these space groups for the acquired data. Refinement in $R\bar{3}m$ was fast and rapidly converged. Refinement in *C*2/*m* was slow and took much longer to converge. Space group $R\bar{3}m$ gave R_{wp} – background = 9.46 (R_{wp} = 3.79) and R_p – background = 9.21 (R_p = 2.93), while space group *C*2/*m* gave R_{wp} – background = 14.81 (R_{wp} = 5.82) and R_p – background = 12.18 (R_p = 3.74). On the basis of *R*-factors there is little profit investigating the monoclinic space group further. Such structural refinements were not attempted. In addition, these results indicate that there is no evidence for significant iron vacancies, as alluded to earlier. Of course, the higher resolution of 0.9523 Å synchrotron radiation used by Scarlett *et al.* (2010) compared to the current 1.6215 Å neutrons, means that subtler peak splitting indicative of monoclinic symmetry may not be observed in our data. However, these effects cannot be modeled if present as the data does not support it. Thus, we conclude the space group of our ammoniojarosite is not lower than $R\bar{3}m$ within the limits of the data collection strategy employed.

Table 6-3: Select inter-atomic distances and angles from the unconstrained refinement of ammoniojarosite at 3 K. Hydrogen bonds shown as dotted lines

Atoms	Distance/Å	Atoms	Angle/°
Fe–O2 × 2	2.045(3)	O2–Fe–O2	180.00
Fe–O3 × 4	1.9763(13)	O2–Fe–O3	89.82(10)
Fe–Fe (nearest neighbor)	3.65639(2)		90.18(10)
		O3–Fe–O3	90.02(17)
			180.00
			89.99(17)
S–O1 (apical)	1.352(15)	O1–S–O2	113.0(5)
S–O2 × 3 (basal)	1.504(7)	O2–S–O2	105.8(6)
N/O4–D2 (basal)	0.969(12)	D2–N–D2	77.7(11)
			180.00
			102.3(11)
N–D3 (apical)	1.03(2)	D2–N–D3	62.3(10)
			127.5(11)
			117.7(10)
			52.5(11)
O3–D1	0.986(4)	O3–D1···O1	179.4(3)
D1···O1	1.998(5)	N/O4–D2···O3	161(1)
D2···O3	1.956(13)	N–D3···O2	164.4(19)
D3···O2	2.00(2)		

From Table 6-3, the two different N–D bond distances refined implies the local structure of one ammonium ion at a finite point is a distorted 3*m* symmetry tetrahedron. It cannot be said from powder diffraction data alone whether the disorder of the ammonium ion is static or dynamic in nature as both types of disorder increase isotropic ADPs. Due to the time and spatial averaging inherent in diffraction techniques these two types of disorder, for all intents and purposes, are indistinguishable. Given the very low temperature used for NPD data collection (3 K), significant libration of ND_4^+ is unlikely. However, rotational tunnelling which is known to persist in ammonium compounds to very low temperatures cannot be ruled out, see for example (Verdal *et al.* 2011). It can

also be said the disorder, regardless of whether it is static or dynamic, is certainly not complete free rotation leading to spherical symmetry for the ammonium ion, as such a situation often results in spherical missing electron density (Schiebel *et al.* 1996). Indeed, excessive smearing of the electron density is not seen in Figure 6-3 nor in any difference Fourier map; distinct contours corresponding to missing ^{2}H nuclei were resolved. A nuclear magnetic resonance study and/or incoherent inelastic neutron scattering study of ammoniojarosite or the isostructural ammonialunite is required to further investigate proton/deuteron dynamics. Such studies have not been undertaken on ammonium containing alunite supergroup minerals, but have been performed on hydronium analogs (Lager *et al.* 2001; Nielsen *et al.* 2008; Nielsen *et al.* 2011).

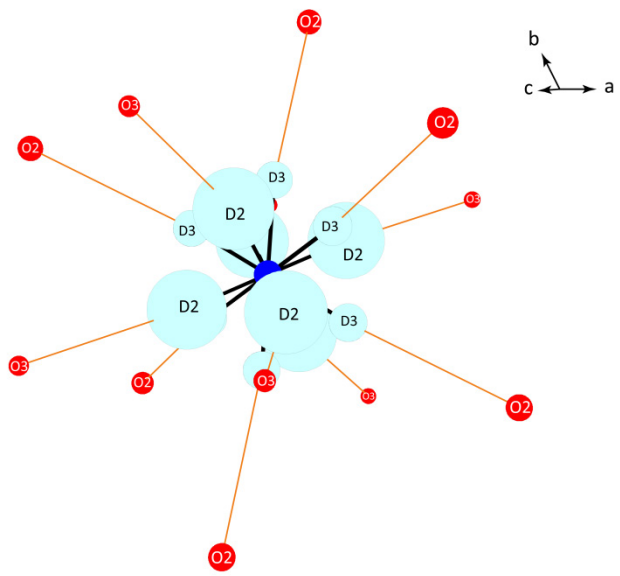

Figure 6-5: Hydrogen bonding scheme involving the ammonium ion. Hydrogen bonds are shown as thin orange lines

One possible reason for our structure being different to the literature is in hydrogen bonding. In the literature structures, D3 atoms are hydrogen bonded to the hydroxyl oxygen atoms (O3) and the D3···O3 bond distance is significantly long at 2.24 Å. In the presently refined structure, D3 appears to be hydrogen bonded to basal sulfate oxygen atoms (O2) and the D3···O2 distance is shorter at 2.00(2) Å and closer to 180˚.

Thus, a potentially stronger and more directional hydrogen bond is formed between D3 and O2 when compared to D3 and O3. When averaged over time and space, more and lower energy configurations (greater entropy) are possible if D3 is hydrogen bonded to O2 instead of O3 (Figure 6-5).

IMPLICATIONS

All ammonium ^{2}H nuclei were located from difference Fourier methods. A new model for the crystal structure of ammoniojarosite was successfully refined and shown to be a better fit to the data than the established literature structure. There was no evidence for the apical ^{2}H atom occupying a $3m$ site. Unlike prior investigations, we find the apical ammonium ^{2}H atom is disordered over at least six orientations in a single unit cell due to its 0.1667 fractional occupancy at an m site. The nitrogen atom is adequately modeled at the $\bar{3}m$ site like other jarosite minerals. The ammonium ion does not destroy the jarosite $\bar{3}m$ axis and does not lower the space group symmetry, due to the time and spatial averaging inherent in diffraction based techniques.

REFERENCES CITED

Bartlett, B. M., and D. G. Nocera, 2005: Long-range magnetic ordering in iron jarosites prepared by redox-based hydrothermal methods. *Journal of the American Chemical Society*, **127,** 8985-8993.

Basciano, L. C., and R. C. Peterson, 2007a: The crystal structure of ammoniojarosite, $(NH_4)Fe_3(SO_4)_2(OH)_6$ and the crystal chemistry of the ammoniojarosite-hydronium jarosite solid-solution series. *Mineralogical Magazine*, **71,** 427-441.

——, 2007b: Jarosite-hydronium jarosite solid-solution series with full iron site occupancy: mineralogy and crystal chemistry. *American Mineralogist*, **92,** 1464-1473.

Buurma, A. J. C., I. P. Handayani, N. Mufti, G. R. Blake, P. H. M. van Loosdrecht, and T. T. M. Palstra, 2012: Spin-lattice coupling in iron jarosite. *Journal of Solid State Chemistry*, **195,** 50-54.

Chio, C. H., S. K. Sharma, L.-C. Ming, and D. W. Muenow, 2010: Raman spectroscopic investigation on jarosite-yavapaiite stability. *Spectrochimica Acta*, **A75,** 162-171.

Downs, R. T., and M. Hall-Wallace, 2003: The American Mineralogist Crystal Structure Database. *American Mineralogist*, **88,** 247-250.

Groat, L. A., J. L. Jambor, and B. C. Pemberton, 2003: The crystal structure of argentojarosite, $AgFe_3(SO_4)_2(OH)_6$. *Canadian Mineralogist*, **41,** 921-928.

Hendricks, S. B., 1937: The crystal structure of alunite and the jarosites. *American Mineralogist*, **22,** 773-784.

Kato, T., and Y. Miura, 1977: The crystal structures of jarosite and svanbergite. *Mineralogical Journal*, **8,** 419-430.

Lager, G. A., G. A. Swayze, C.-K. Loong, F. J. Rotella, J. W. Richardson Jr, and R. E. Stoffregen, 2001: Neutron spectroscopic study of synthetic alunite and oxonium-substituted alunite. *Canadian Mineralogist*, **39,** 1131-1138.

Larson, A. C., and R. B. Von Dreele, 2004: General Structure Analysis System (GSAS).

Loiacono, G. M., G. Kostecky, and J. S. White, 1982: Resolution of space group ambiguities in minerals. *American Mineralogist*, **67,** 846-847.

Majzlan, J., S. Speziale, T. S. Duffy, and P. C. Burns, 2006: Single-crystal elastic properties of alunite, $KAl_3(SO_4)_2(OH)_6$. *Physics and Chemistry of Minerals*, **33,** 567-573.

Majzlan, J., and Coauthors, 2004: Thermodynamic properties, low-temperature heat-capacity anomalies, and single-crystal X-ray refinement of hydronium jarosite, $(H_3O)Fe_3(SO_4)_2(OH)_6$. *Physics and Chemistry of Minerals*, **31,** 518-531.

Menchetti, S., and C. Sabelli, 1976: Crystal chemistry of the alunite series: crystal structure refinement of alunite and synthetic jarosite. *Neues Jahrbuch für Mineralogie Monatshefte*, **9,** 406-417.

Nielsen, U. G., J. Majzlan, and C. P. Grey, 2008: Determination and quantification of the local environments in stoichiometric and defect jarosite by solid-state ^2H NMR spectroscopy. *Chemistry of Materials*, **20,** 2234-2241.

Nielsen, U. G., I. Heinmaa, A. Samoson, J. Majzlan, and C. P. Grey, 2011: Insight into the local magnetic environments and deuteron mobility in jarosite ($AFe_2(SO_4)_2(OD,OD_2)_6$, A = K, Na, D_3O) and hydronium alunite ($(D_3O)Al_3(SO_4)_2(OD)_6$), from variable-temperature ^2H MAS NMR spectroscopy. *Chemistry of Materials*, **23,** 3176-3187.

Prince, E., 1982: Comparison of the fits of two models to the same data set. *Acta Crystallographica*, **B38,** 1099-1100.

Sasaki, K., O. Tanaike, and H. Konno, 1998: Distinction of jarosite-group compounds by Raman spectroscopy. *Canadian Mineralogist*, **36,** 1225-1235.

Sato, E., I. Nakai, R. Miyawaki, and S. Matsubara, 2009: Crystal structures of alunite family minerals: beaverite, corkite, alunite, natroalunite, jarosite, svanbergite, and woodhouseite. *Neues Jahrbuch für Mineralogie - Abhandlungen*, **185,** 313-322.

Scarlett, N. V. Y., I. E. Grey, and H. E. A. Brand, 2010: Ordering of iron vacancies in monoclinic jarosites. *American Mineralogist*, **95,** 1590-1593.

Schiebel, P., W. Prandl, R. Papoular, and W. Paulus, 1996: Amost free rotation of NH_3 molecules in crystals: observation from a maximum-entropy reconstruction of the proton density in $[Co(NH_3)_6](PF_6)_2$. *Acta Crystallographica*, **A52,** 189-197.

Schukow, H., D. K. Breitinger, T. Zeiske, F. Kubanek, J. Mohr, and R. G. Schwab, 1999: Localization of hydrogen and content of oxonium cations in alunite via neutron diffraction. *Zeitschrift für Anorganische und Allgemeine Chemie*, **625,** 1047-1050.

Serna, C. J., C. P. Cortina, and J. V. Garcia Ramos, 1986: Infrared and Raman study of alunite-jarosite compounds. *Spectrochimica Acta*, **A42,** 729-734.

Spratt, H., L. Rintoul, M. Avdeev, and W. Martens, 2014: The thermal decomposition of hydronium jarosite and ammoniojarosite. *J Therm Anal Calorim*, **115,** 101-109.

Szymanski, J. T., 1985: The crystal structure of plumbojarosite. *Canadian Mineralogist*, **23,** 659-668.

Toby, B. H., 2001: EXPGUI, a graphical user interface for GSAS. *Journal of Applied Crystallography*, **34,** 210-213.

Toumi, M., and A. Tlili, 2008: Rietveld refinement and vibrational spectroscopic study of alunite from El Gnater, central Tunisia. *Russian Journal of Inorganic Chemistry*, **53,** 1845-1853.

Verdal, N., T. J. Udovic, J. J. Rush, V. Stavila, H. Wu, W. Zhou, and T. Jenkins, 2011: Low-temperature tunneling and rotational dynamics of the ammonium cations in $(NH_4)_2B_{12}H_{12}$. *Journal of Chemical Physics*, **135,** 094501.

Wills, A. S., A. Harrison, C. Ritter, and R. I. Smith, 2000: Magnetic properties of pure and diamagnetically doped jarosites: model kagomé antiferromagnets with variable coverage of the magnetic lattice. *Physical Review*, **B61,** 6156-6169.

CHAPTER 7 ON THE ORIENTATIONAL DISORDER OF HYDRONIUM JAROSITE AND AMMONIOJAROSITE IN COMPARISON TO JAROSITE

A VIBRATIONAL SPECTROSCOPIC STUDY

STATEMENT OF CONTRIBUTION

The authors listed below have certified* that:

1. They meet the criteria for authorship in that they have participated in the conception, execution, or interpretation, of at least that part of the publication in their field of expertise;
2. They take public responsibility for their part of the publication, except for the responsible author who accepts overall responsibility for the publication;
3. There are no other authors of the publication who meet these criteria;
4. Potential conflicts of interests have been disclosed to a) granting bodies, b) the editor or publisher of journals or other publications, and c) the head of the responsible academic unit, and
5. They agree to the use of the publication in the student's thesis and its publication on the Australasian Digital Thesis database consistent with any limitations set by the publisher requirements.

In the case of this chapter:

On the orientational disorder of hydronium jarosite and ammoniojarosite in comparison to jarosite: A vibrational spectroscopic study

Contributor	*Statement of Contribution**
Henry J. Spratt	Experimental design, conducted experiments and data analysis/interpretation, wrote initial draft of manuscript
Llew Rintoul	Supervision, aided experimental design, aided data collection and data analysis/interpretation, major editing
Maxim Avdeev	Supervision, editing of drafts
Wayde N. Martens	Overall supervisor, aided experimental design, aided experiments and data analysis, editing of drafts

Principal Supervisor Confirmation

I have sighted email or other correspondence from all co-authors confirming their certifying authorship.

Name	Signature	Date

SYNOPSIS

This chapter reports the vibrational spectra of both protonated and deuterated forms of hydronium jarosite and ammoniojarosite in comparison to jarosite. Vibrational spectroscopy gives structural information at the molecular level, and is a compliment to powder diffraction and single crystal diffraction studies of hydronium jarosite and ammoniojarosite (Chapters 5 and 6). Structural nuances which may not be easily recognised by diffraction can be apparent from a thorough vibrational spectroscopic study as time averaging does not occur. Reconciliation of hydronium jarosite and ammoniojarosite's crystal structure with their vibrational spectra via a symmetry analysis was the major aim of this study. If successful, this would allow for the proposal of general principles for the symmetry analysis of other orientationally disordered molecules in crystals at symmetry forbidden sites; a problem which has been largely ignored in the literature. In addition, band assignments in jarosite vibrational spectra differ amongst studies with assignments in the lattice mode region (< 700 cm^{-1}) varying the most.

This study found the most appropriate site symmetry of hydronium and ammonium ions for vibrational spectroscopic purposes is C_{3v} with 50 % fractional occupancy, instead of D_{3d} as determined from diffraction. This is the highest symmetry of one orientation at a finite point in time. Spectra were interpreted based on a symmetry analysis using a C_{3v} site of hydronium and ammonium ions, and also no Davydov splitting to account for the fractional occupancy of both oxygen/nitrogen and hydrogen atoms. Owing to deuteration and its ability to distinguish vibrations involving hydrogen, bands were assigned correctly and some assignments differ to the current literature. The spectra suggest hydrogen bonds involving the hydronium ion are towards hydroxyl groups, and these bonds are weaker in ammoniojarosite. This is a contributing factor to the spin glass behaviour of hydronium jarosite. Using jarosite minerals as a basis, a new procedure for the symmetry analysis of disordered molecules in ordered crystals is proposed.

ON THE ORIENTATIONAL DISORDER OF HYDRONIUM JAROSITE AND AMMONIOJAROSITE IN COMPARISON TO JAROSITE: A VIBRATIONAL SPECTROSCOPIC STUDY

Henry J. Spratt, Llew Rintoul and Wayde N. Martens

Chemistry, Physics and Mechanical Engineering, Science and Engineering Faculty,

Queensland University of Technology, Brisbane, QLD, 4001 Australia

Maxim Avdeev

Bragg Institute, Australian Nuclear Science and Technology Organisation, Lucas Heights,

NSW, 2234 Australia

Keywords: hydronium jarosite · ammoniojarosite · jarosite · normal mode determination · factor group analysis · vibrational spectroscopy · orientational disorder

ABSTRACT

The Raman spectra of jarosite, ammoniojarosite and hydronium jarosite were studied at 298 and 82 K; the Raman, mid-infrared and far-infrared spectra of protonated and deuterated forms were studied at 298 K. Band assignments were similar to the literature with some notable exceptions. These exceptions were only obvious through deuteration and careful consideration of the appearance of bands: the band at ~450 cm^{-1} is $\nu_2(SO_4)$; the band at 570 cm^{-1} is not γ(OH) but rather a lattice mode of the iron octahedra; γ(OH) is a shoulder at 540 cm^{-1} of the 570 cm^{-1} band but occurs at 512 cm^{-1} for hydronium jarosite; the MIR band at ~1020 cm^{-1} is due to δ(OH); and lastly, a band at ~1000 cm^{-1} in the MIR spectra is the $\nu_1(SO_4)$ vibration. A symmetry analysis for hydronium jarosite and ammoniojarosite is proposed where the hydronium and ammonium ions are located at a C_{3v} site with 50 % fractional occupancy in space group $R\bar{3}m$ leading to no Davydov splitting of $\nu(H_3O^+/NH_4^+)$. General principles for the factor group analysis of non-linear orientationally disordered molecules located at sites that are not a subgroup of their molecular symmetry are also outlined.

INTRODUCTION

The alunite supergroup of minerals are a large hydroxy-sulfate mineral group described by the general formula $AB_3(TO_4)_2(OH)_6$. The jarosite subgroup, which is the focus of this paper, is characterized by Fe^{3+} at the B site and sulfur at the T site. The A site cation is typically monovalent with K^+, Na^+, H_3O^+, NH_4^+ and Ag^+ being the most common, but divalent cations such as Pb^{2+} may also substitute at this site. In 2004, the Mars Exploration Rover Opportunity detected jarosite on the Martian surface at Meridiani Planum (Elwood Madden *et al.* 2004; Klingelhöfer *et al.* 2004). This discovery gave strong evidence the Martian surface was once wet and aqueous processes occurred on the planet.

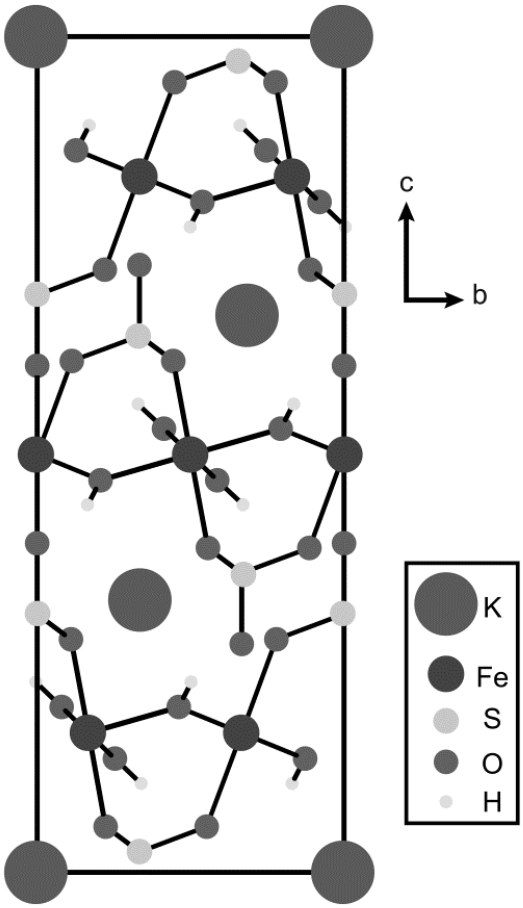

Figure 7-1: Crystal structure of jarosite projected down the **a** axis

The space group of most jarosite minerals is $R\bar{3}m$, in the hexagonal setting with $Z = 3$. The structure is shown in Figure 7-1 for jarosite, using data taken from a previous single crystal refinement (Menchetti and Sabelli 1976). The symmetry of each atomic site based on this study is given in Table 7-1. The structure can be described as alternating layers of FeO6 octahedra and SO_4 tetrahedra. The A site cation is located in the sulfate layer in a cavity formed by a framework of 12 surrounding sulfate and hydroxyl oxygen atoms. Hydrogen bonds between apical sulfate oxygen atoms and the hydroxyl hydrogen atoms connect the layers.

Table 7-1: Symmetry of atomic sites for jarosite minerals in space group $R\bar{3}m$

Atom	Wyckoff site	Hermann-Mauguin notation	Schöenflies notation
A site cation	3a	-3*m*	D_{3d}
Fe^{3+}	9d	2/*m*	C_{2h}
S	6c	3*m*	C_{3v}
O (basal SO_4 oxygen)	18h	*m*	C_s
O (apical SO_4 oxygen)	6c	3*m*	C_{3v}
O (hydroxyl oxygen)	18h	*m*	C_s
H (hydroxyl hydrogen)	18h	*m*	C_s

Only a few spectroscopic and crystallographic studies have noted the symmetry mismatch between the hydronium and ammonium ions and their crystallographic site (Majzlan *et al.* 2004; Serna *et al.* 1986; Szymanski 1985); the molecular symmetry C_{3v} (H_3O^+) and T_d (NH_4^+) are not subgroups of the D_{3d} site symmetry. Factor group analysis is challenging as vector tables for molecular correlation (Farmer (ed.) 1974) and the unit cell method (Bhagavantam and Venkatarayudu 1939) cannot be employed. Since hydronium and ammonium ions lack the inversion centre required by the three-fold roto-inversion axis of $R\bar{3}m$ it has been suggested (see for example Serna *et al.*, 1986; Majzlan *et al.*, 2004) that the structure of hydronium jarosite and ammoniojarosite is slightly

distorted to a lower symmetry space group such as $R3m$. A molecule, or structural unit, occupying a site whose symmetry is not a subgroup of its point group is not a unique problem (Boyle 1972; Catti and Ibberson 2002; Halford 1946; Jewess 1982; Mookherjee *et al.* 2002; Oxton *et al.* 1976; Petruševski *et al.* 1993; Plaza *et al.* 1996; Rudolf *et al.* 1985; Schiebel *et al.* 2000). In most of these situations the molecule of interest is orientationally disordered; that is, the molecule is statistically distributed either dynamically or statically across numerous orientations such that the time averaged structure is of the otherwise forbidden higher symmetry. This is the case for hydronium jarosite and ammoniojarosite where there are two orientations, of equal probability, with respect to the **c** axis in space group $R\bar{3}m$ (Basciano and Peterson 2007; Wills and Harrison 1996; Wills *et al.* 2000). The two orientations are modelled by 50 % fractional occupancy of the hydronium and ammonium ion hydrogen atoms. The location of the oxygen/nitrogen atom is contentious.

Due to the orientational disorder, a factor group analysis and normal mode determination for hydronium jarosite and ammoniojarosite has not been previously attempted; indeed to our knowledge, no protocol for the factor group analysis of similarly disordered molecules occupying seemingly forbidden sites in other crystals has been published. There are also many problems in the spectral assignment of these jarosites, despite numerous spectroscopic studies (Frost *et al.* 2006b; Kubisz 1972; Maubec *et al.* 2012; Sasaki *et al.* 1998; Serna *et al.* 1986), band assignment, particularly below 700 cm^{-1}, remains contentious. Hence, in this paper we aim to report and assign bands in the Raman, MIR and FIR spectra of these jarosite minerals. We also propose a protocol for the factor group analysis of hydronium jarosite and ammoniojarosite that can be easily applied to other similarly disordered systems. Given the current interest in this group prompted by the Mars discoveries and the fact that the hydronium and ammonium hydrogen atoms have been difficult to model by X-ray diffraction, a thorough vibrational spectroscopic study is appropriate and long overdue.

EXPERIMENTAL

SYNTHESIS

A microwave hydrothermal method was employed using a microwave reactor and Teflon lined pressure vessels. The synthesis conditions were 150 °C for 3 hours at 4 bar autogenous water vapor pressure with constant stirring. The starting solution consisted of 6.688 × 10^{-3} mol of the relevant A site chloride (KCl or NH_4Cl), ferric chloride ($FeCl_3$, 1.23 M, 7.5 mL), saturated lithium chloride (LiCl, 18 mL) and ferric sulfate ($Fe_2(SO_4)_3 \cdot 6H_2O$, 9 g) dissolved in water (18.2 MΩ, 37.5 mL). Hydronium jarosite was synthesized in a similar fashion, but with chlorides excluded; only a 138 g L^{-1} solution of the same $Fe_2(SO_4)_3$ was used. All products were washed well with water, filtered and dried overnight at 100 °C. Deuterated samples were prepared by the National Deuteration Facility (NDF) by substituting D_2O for H_2O and using ^2H analogues of the relevant chemicals, with heating provided by a conventional hydrothermal pressure vessel (Parr bomb) for 3 days.

POWDER X-RAY DIFFRACTION

Powder X-ray diffraction patterns between 3 and 75 °2θ were collected on a Phillips PANalytical X'Pert PRO diffractometer operating at 40 kV and 40 mA using Cu Kα incident X-rays (Kα1 = 1.5406 Å, Kα1/Kα2 = 0.5) and a fixed divergence slit (0.5°) under Bragg-Brentano geometry. A step size of 0.017 °2θ was employed. A spinning stage was used and the incident beam monochromator was removed to improve grain averaging and intensity respectively. Samples were ground in a mortar and pestle prior to analysis.

FOURIER TRANSFORM INFRARED ABSORBANCE SPECTROSCOPY

FIR absorbance spectra in the 700 to 50 cm^{-1} region were collected using a Nicolet Nexus 870 FTIR (mirror velocity 0.6329 cm s^{-1}) that was equipped with a Smart

Orbit single bounce diamond ATR accessory and a DTGS polyethylene detector. In all cases, the reported spectra are the result of the co-addition of 256 scans at a resolution of 4 cm^{-1}. Spectra below about 100 cm^{-1} were found to be noisy and are not reported. MIR absorbance spectra in the 4000 to 565 cm^{-1} region were collected using a Nicolet Nexus 5700 FTIR (mirror velocity 0.6329 cm^{-1}) that was equipped with a Smart Endurance single bounce diamond ATR accessory and a DTGS KBr detector. In all cases, the reported spectra are the result of the co-addition of 64 scans at a resolution of 4 cm^{-1}.

Low Temperature and Room Temperature Raman Spectroscopy of Hydronium Jarosite, Jarosite and Ammoniojarosite

Low temperature Raman spectroscopy (~82 K) was performed using a Renishaw 1000 Raman microscope system that was equipped with an Olympus BHSM microscope. Raman spectra were acquired from a Melles-Griot He-Ne laser with an output of 633 nm at a resolution better than 4 cm^{-1} in the range between 100 and 4000 cm^{-1}. Spectra were calibrated using the 520.5 cm^{-1} line of a silicon wafer. Spectra were co-added using the 50x objective in order to improve the signal to noise ratio. A Linkam thermal stage (Scientific Instruments, Waterfield, Surrey, UK) was used for cooling the sample with liquid nitrogen. To facilitate a comparison of bandwidths and band positions upon cooling and to gauge the effects of hydronium or ammonium ion substitution, the low temperature spectra were compared to spectra taken at room temperature (~298 K) using the same spectrometer for hydronium jarosite and potassium jarosite. The laser power, number of accumulations and the acquisition time were optimized according to the sample being analyzed.

Raman Spectroscopy at Room Temperature in Comparison to Deuterated Analogues

Raman spectra of various jarosites and their deuterated analogues were acquired with a Renishaw inVia Raman microscope in the range between 100 and 4000 cm^{-1}.

Spectra were calibrated to the 520.5 cm^{-1} line of a silicon wafer. Excitation was provided by a 785 nm laser (100 to 1500 cm^{-1} region) and a 532 nm laser (1500 to 4000 cm^{-1} region) using a 50x objective (Leica) lens. Spectra were co-added to improve signal to noise. The laser power, acquisition time and number of scans were optimized according to the sample being analyzed.

SPECTRAL MANIPULATION AND ANALYSIS

Baseline correction of spectra was performed using the GRAMS (Thermo Fisher Scientific Inc.) software package. Band component analysis was performed using the PeakFIT (Systat Software Inc.) software package in order to more accurately determine peak positions such as shoulders. A minimum number of bands, defined by a Lorentz-Gaussian cross-product function with a Gaussian-Lorentzian ratio greater than 0.7, were used to model the peak shapes. The fitting procedure was deemed complete when squared correlations of r^2 were greater than or equal to 0.995 and the general shape of the spectral shape was adequately fit. Where appropriate, bandwidths are reported as the full width at half maximum (FWHM, cm^{-1}).

RESULTS AND DISCUSSION

PHASE IDENTIFICATION

XRD patterns (Figures 7-2a, b) show that the synthesized jarosites have no diffracting impurities and match the respective reference patterns from the PDF-2 database of the International Center for Diffraction Data (ICDD) of jarosite (01-071-1777), hydronium jarosite (00-031-0650) and ammoniojarosite (00-026-1014). Thus the jarosite mineral phase of the samples is confirmed and the amorphous content appears minimal given the lack of a broad background.

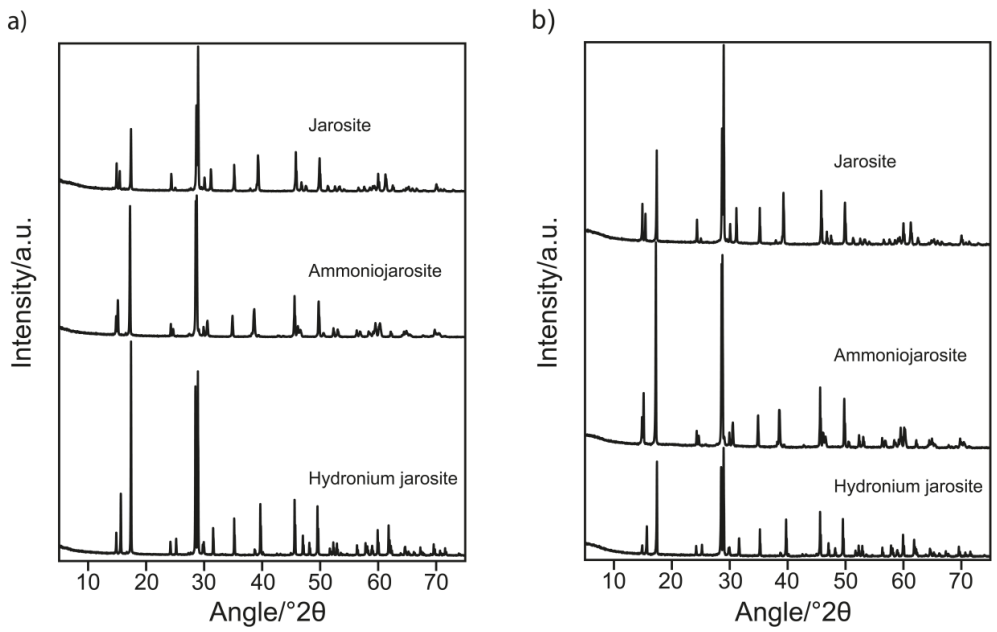

Figure 7-2: a) XRD patterns of hydronium jarosite, ammoniojarosite and jarosite, b) XRD patterns of their respective deuterated analogs

SPECTROSCOPIC SPACE GROUP CHOICE

Low temperature Raman spectroscopy was used to compare the structure of hydronium jarosite and ammoniojarosite to jarosite. The full spectra are shown in Figure 7-3. To understand these spectra a factor group analysis must be performed, the first step

being to identify the correct space group. There is strong evidence that the space group of all jarosite minerals is $R\bar{3}m$ (Basciano and Peterson 2007; Majzlan *et al.* 2004; Menchetti and Sabelli 1976; Wills and Harrison 1996). As mentioned earlier, the space group of hydronium jarosite and ammoniojarosite could be lower, with $R3m$ being the most promising candidate. Space group $R3m$ is the result when inversion symmetry is removed from $R\bar{3}m$. However, $R3m$ and $R\bar{3}m$ have the same systematic absences, making identification of the true structure from diffraction methods difficult. Under $R\bar{3}m$ symmetry standard factor group analysis is not possible with the hydronium and ammonium ions on the D_{3d} site. The spectroscopic space group can be different to the crystallographic space group (Buttery *et al.* 1969; Hollebone and Lever 1972; Kettle *et al.* 1984), but, as Serna *et al.* (1986) indicated, the number of room temperature Raman spectra bands is best explained by space group $R\bar{3}m$.

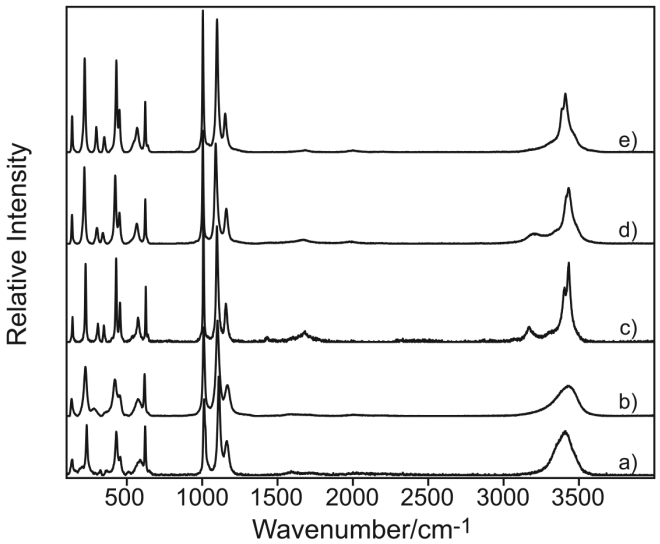

Figure 7-3: Raman spectra collected with 633 nm excitation of a) hydronium jarosite at 82 K, b) hydronium jarosite at 298 K, c) ammoniojarosite at 82 K, d) ammoniojarosite at 298 K and e) jarosite at 298 K

Inspection of Figure 7-3 reveals a great similarity between the spectra of the orientationally disordered hydronium jarosite and ammoniojarosite compared to that of

the ordered titular jarosite. It can therefore be inferred that the basic structure of the three minerals is the same, and that the orientationally disordered hydronium and ammonium ions have minimal impact on the rest of the jarosite framework. Additional bands are not observed at low temperature which means no phase transition occurred and that there is no significant change in the site symmetry or geometry of the ammonium or hydronium ions. This is in agreement with a previous low temperature Raman study of jarosite, natrojarosite and ammoniojarosite where lower temperatures were achieved (Chio *et al.* 2010). Thus, we conclude hydronium and ammonium ions do not destroy the three-fold roto-inversion axis and the spectroscopic space group is $R\bar{3}m$.

HYDRONIUM AND AMMONIUM ION SPECTROSCOPIC SITE SYMMETRY

An NMR study of deuteron mobility in jarosites and alunites found D_3O^+ motion freezes at 125 ± 10 K on the NMR time scale (Nielsen *et al.* 2011). Our Raman spectra at 82 K are below this temperature range which suggests motion of the ammonium and hydronium ions is minimal. Thus, for the purposes of this paper, when orientational disorder is mentioned, it is meant that the disorder is more dynamic in nature at room temperature but more static in nature at lower (82 K) temperatures. The problem is to assign the appropriate spectroscopic site symmetry to ammonium and hydronium ions in space group $R\bar{3}m$. In essence, the crystal itself and the repeat unit are not disordered, only the hydronium and ammonium ions. For disordered molecules that can be linear assuming free rotation, correlation between the molecular symmetry and the forbidden site symmetry is possible with infinite ($C_{\infty v}$ or $D_{\infty h}$) point groups (Petruševski *et al.* 1993), but this does not apply to the ammonium and hydronium ions and so a different theoretical method of analysis is needed.

The spectroscopic site symmetry of a molecule is not always the same as that deduced from diffraction, and may be lower, because small displacements that are absorbed into the temperature factor can be important during vibrational spectroscopic

lifetimes (English and Heyns 1984). The spectroscopic site symmetry of ammonium and hydronium ions in jarosite minerals must be lower than the time averaged symmetry of D_{3d}. See for example, the structures determined by Wills and Harrison (1996) and Wills *et al.* (2000) where, the ammonium and hydronium ions obey D_{3d} symmetry when time averaged across all unit cells. Jewess (1982) proposed the crystallographic site for orientationally disordered molecules is a minor displacement in space along one crystallographic direction from the symmetry disallowed site so that like principal crystallographic and molecular rotation axes are coincident. The highest effective symmetry, i.e. the symmetry when one orientation is considered at a finite point in time, is C_{3v}, which in space group $R\bar{3}m$ accommodates both hydronium and ammonium ions. Factor group analysis is trivial if this were the case but too many modes would be predicted since the multiplicity of the C_{3v} site is six. To maintain charge balance the oxygen and nitrogen atoms would be fractionally occupied (50 %). The three ammonium or hydronium ions in a single unit cell can be of any orientation and the inversion operation is destroyed locally which leads to a break down of the factor group splitting.

The so called site group approach can be used to predict the modes when there is effectively no coupling between symmetry-related molecules in a unit cell (Kettle 1971). This is the case for hydronium jarosite and ammoniojarosite as fractionally occupied molecules cannot vibrationally couple. The ammonium and hydronium ions are only affected by C_{3v} site symmetry and less so the factor group symmetry. Table 7-2 shows the expected internal modes for hydronium and ammonium ions in the alunite supergroup while Table 7-3 shows the expected lattice/librational and translational modes. Note that full factor group splitting to the crystal symmetry $\left(D_{3d}^{5}\right)$ is shown for completeness. Our analysis is supported by an oriented single crystal Raman study of disordered ammonium perovskites (Auglló-Rueda *et al.* 1988) that found that the ammonium vibrations followed those of the site symmetry predictions. Unfortunately, jarosite minerals do not often form

single crystals (Nocera *et al.* 2004) and as yet we are unable to undertake a single crystal study.

Table 7-2: Splitting of hydronium and ammonium ion internal modes in the alunite supergroup at a C_{3v} site

Hydronium		
Molecular Symmetry (C_{3v})	Site Symmetry (C_{3v})	Crystal Symmetry (D_{3d})
($\nu_{1,2}$) $2A_1$	$2A_1$	$2A_{1g} + 2A_{2u}$
($\nu_{3,4}$) $2E$	$2E$	$2E_g + 2E_u$
Ammonium		
Molecular Symmetry (T_d)	Site Symmetry (C_{3v})	Crystal Symmetry (D_{3d})
(ν_1) A_1	A_1	$A_{1g} + A_{2u}$
(ν_2) E	E	$E_g + E_u$
($\nu_{3,4}$) $2T_2$	$2E + 2A_1$	$2E_g + 2A_{1g} + 2E_u + 2A_{2u}$

Table 7-3: Lattice modes of hydronium and ammonium ions in the alunite supergroup at a C_{3v} site

Hydronium and Ammonium	
Site Symmetry (C_{3v})	Crystal Symmetry (D_{3d})
(T_z) A_1 (IR + R)	$A_{1g} + A_{2u}$
(R_z) A_2 (-)	$A_{2g} + A_{1u}$
(T_{xy}, R_{xy}) $2E$ (IR + R)	$2E_g + 2E_u$

Using this approach, modes are predicted for hydronium and ammonium with symmetries not expected by the factor group, i.e. A_1, A_2 and E. The appropriate character table, C_{3v}, was used to determine mode activity; A_2 modes should be inactive, while A_1 and E modes should be both Raman and IR active. The polarizability tensors of the Raman active modes governed by the site symmetry, C_{3v}, take the same from as those of equivalent symmetry under space group symmetry, D_{3d}. (Turrell 1972):

$$A_{1g} / A_1 = \begin{pmatrix} a & 0 & 0 \\ 0 & a & 0 \\ 0 & 0 & b \end{pmatrix} \qquad E_g / E = \begin{pmatrix} c & 0 & 0 \\ 0 & -c & d \\ 0 & d & 0 \end{pmatrix} \begin{pmatrix} 0 & -c & -d \\ -c & 0 & 0 \\ -d & 0 & 0 \end{pmatrix}$$

Therefore single crystal studies can still be used to determine the symmetry of the modes governed by site the same as those governed by crystal class.

For hydronium on a C_{3v} site the irreducible representation including lattice modes is:

$$\Gamma_{irred} = 3A_1(R, IR) + A_2(-) + 4E(R, IR)$$

The irreducible representation for the rest of the jarosite structure is:

$$\Gamma_{irred} = 8A_{1g}(R) + 3A_{2g}(-) + 11E_g(R) + 4A_{1u}(-) + 9A_{2u}(IR) + 13E_u(IR)$$

Combining these gives a total of 84 modes for hydronium jarosite which is the number of modes expected based on the number of atoms in the Bravais cell (Adams 1973). A similar calculation gives 87 modes for ammoniojarosite. By adopting this "site symmetry only" approach for the disordered polyatomic ion sites, the correct number of modes are predicted unlike the case when the full factor group splitting is applied which results in 96 modes for hydronium jarosite and 102 for ammoniojarosite. These results show that vibrational spectroscopy and symmetry considerations provide important insights into the correct space group choice and the local symmetries of polyatomic ions when diffraction methods are ambiguous.

SPECTRAL INTERPRETATION AND ANALYSIS

An expanded view of the high wavenumber region of the Raman spectra of the low temperature study is shown in Figure 7-4. The peak maxima of ν(OH) bands of the analyzed jarosites are similar and in the range of 3360 – 3430 cm^{-1}. Low intensity and broad shoulder bands at ~3450 and ~3310 cm^{-1} for ammoniojarosite and jarosite have been assigned to either $\nu(H_2O)$ due to H_2O occupation of vacant Fe^{3+} sites or $\nu_{1,3}(H_3O^+)$ arising from hydronium substitution at the A site (Chio *et al.* 2010). The lack of a

substantial difference in the ν(OH) stretching vibrations suggests that the hydrogen bond strength for hydronium jarosite, ammoniojarosite, and jarosite are comparable (Libowitzky 1999). This is consistent with diffraction studies where the N···O3 and O4···O3 distances are ~2.8 Å leading to an H···O bond distance of ~1.9 Å, where O3 is the hydroxyl oxygen atom and O4 is the hydronium oxygen atom (Basciano and Peterson 2007; Wills and Harrison 1996; Wills *et al.* 2000). In all jarosite minerals, the hydroxyl hydrogen atom is hydrogen bonded to the apical sulfate oxygen atom; the relevant O···O distance in this case is also ~2.8 Å which results in an H···O bond length of ~1.9 Å (Menchetti and Sabelli 1976; Sato *et al.* 2009; Xu *et al.* 2010). The O···O distance and H···O distance in all cases are indicative of only moderate to weak hydrogen bonds (Emsley 1980; Libowitzky 1999).

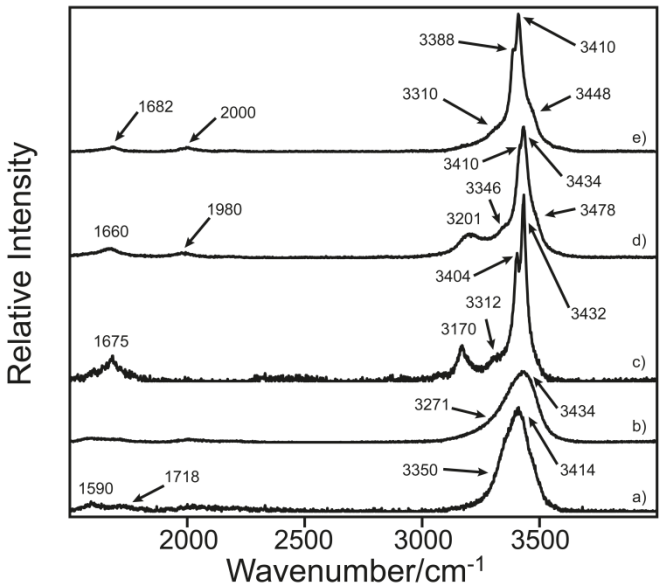

Figure 7-4: Raman spectra collected with 633 nm excitation in the 1500 to 4000 cm^{-1} region of a) hydronium jarosite at 82 K, b) hydronium jarosite at 298 K, c) ammoniojarosite at 82 K, d) ammoniojarosite at 298 K and e) jarosite at 298 K

For hydronium jarosite at room temperature, ν(OH) manifest in the Raman spectrum as a broad band at 3434 cm^{-1} with an indistinct shoulder at 3270 cm^{-1} (Figures 7-4 and 7-5) and in the MIR at 3360 cm^{-1} with a shoulder at 3212 cm^{-1} (Figure 7-5). No

further bands are resolved in either case, even at 82K. A broad and weak tail at 2575 cm^{-1} in the MIR spectrum could be due to $\nu_1(H_3O^+)$ (Kubisz 1972). Two sharp bands near 3430 and 3390 cm^{-1} in the Raman and MIR spectra are observed in both jarosite and ammoniojarosite. A contributing factor to the broadness and no observable Davydov splitting in hydronium jarosite is orientational disorder (either dynamic or static) (Bertie 1968; Besbes *et al.* 1999; Dharmasena and Frech 1995; Fernandes *et al.* 1979; Lutz 1988; Pham-Thi *et al.* 1987; Taylor and Vidale 1956). However, it is not the only factor.

Although the hydrogen bond distance to the hydroxyl oxygen is the same for both H_3O^+ and NH_4^+ ions, it is only in hydronium jarosite that this interaction is significant. This is because the O–H of H_3O^+ is more polar than the N–H of NH_4^+, thus the hydronium H is more attracted to an OH^- group than the ammonium H. In addition, the strongly acidic pKa of -1.74 for H_3O^+ (Taft *et al.* 1978) means hydronium Hs are likely more mobile than the weakly acidic ammonium Hs. Hence, it is primarily a strong hydrogen bond, not orientational disorder, that leads to such broad ν(OH) bands.

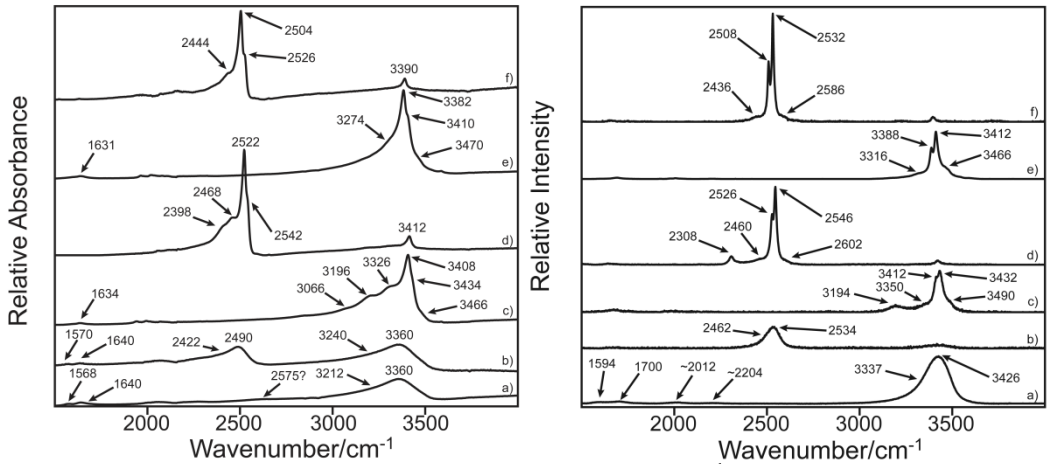

Figure 7-5: MIR (left) and 532 nm Raman (right) in the 1500 to 4000 cm^{-1} region for a) hydronium jarosite, b) deuteronium jarosite, c) ammoniojarosite, d) deuterated ammoniojarosite, e) jarosite and f) deuterated jarosite

The $\nu(NH_4^+)$ Raman band at 3194 cm^{-1} is easily assigned, but $\nu(NH_4^+)$ MIR bands are harder to assign due to Fermi-resonance with the bending mode overtones and

combinations, see for example Mookherjee *et al.* (2002). The $\nu(NH_4^+)$ bands are located at 2838 (very weak), 3066 (weak), 3196 and 3326 cm^{-1} in the MIR spectra. The weak broad band at 3066 cm^{-1} is the component made stronger by Fermi resonance. The very weak band at 2838 cm^{-1} agrees well to $2\nu_4(NH_4^+)$. Hydronium bands are harder to locate due to overlapping modes. However, a weak band at ~1580 cm^{-1} in both Raman and MIR spectra is assigned to $\nu_4(H_3O^+)$ (Mazej *et al.* 2012; Taylor and Vidale 1956; Yukhnevich 1963). This band has been observed in other hydronium jarosite studies (Kubisz 1972; Wilkins *et al.* 1974) and found to be correlated with hydronium occupancy (Grohol and Nocera 2007). This band is very weak or absent in jarosite and ammoniojarosite vibrational spectra. This suggests the band is correlated to the hydronium ion. Thus, the $\nu_4(H_3O^+)$ mode at ~1580 cm^{-1} is the only readily identifiable hydronium vibration in jarosite minerals. The $\nu_2(NH_4^+)$ mode at ~1660 cm^{-1} (Chio *et al.* 2010) is not readily assigned in either Raman or MIR as it overlaps with the $\delta(H_2O)$ at ~1640 cm^{-1} that is observed in nearly all jarosite mineral spectra.

Orientational disorder and hydrogen bond strength, the two main mechanisms that lead to broadness and the presence or not of Davydov splitting of $\nu(OH)$, $\nu(H_3O^+)$ and $\nu(NH_4^+)$, are congruent with the magnetic behavior of jarosite minerals. Most alunite supergroup minerals with magnetic ions at the B site undergo long-range magnetic ordering at low temperature and are a text book example of the Kagomé lattice (Grohol *et al.* 2003). At approximately 70 K, all jarosite minerals except for hydronium jarosite, exhibit long range magnetic ordering with the q = 0 structure (Wills *et al.* 2000). With a freezing temperature at 17 K, hydronium jarosite is characterized as a spin glass (Fåk *et al.* 2008). If orientational disorder, possible proton mobility, and large thermal motion or reorientations are major mechanisms for the spin glass behavior of hydronium jarosite, then ammoniojarosite should also be a spin glass. The stronger hydrogen bonds in hydronium jarosite could communicate the disorder of the hydronium ion to, and perturb the FeO_6 octahedra in hydronium jarosite more so than the ammonium ion. By this it is meant that at a finite point in time, only half of the oxygen atoms of the FeO_6 octahedra in

the unit cell are hydrogen bonded to the hydronium ion. A similar argument involving proton mobility and strong interactions between hydronium and the surrounding hydroxyl groups leading to broadness of O–H stretches was proposed by Grohol and Nocera (2007) and our spectra are consistent with this study. NMR studies of deuterated and protonated ammonioalunite and ammoniojarosite in comparison to hydronium jarosite are required as no such studies exist. Such a study would reveal the $^{1}H/^{2}H$ environments in ammoniojarosite and could determine the activation energy for the motion of the ammonium ion.

All bands in the high wavenumber region shift upon deuteration to lower wavenumbers (Figures 7-5 and 7-6) as expected. The isotopic shifts for the stretching modes are given in Table 7-4. The observed shifts are in agreement with previous deuterated studies (Kubisz 1972; Powers *et al.* 1975). The hydronium jarosite appears to be only partially deuterated from the MIR spectra. The weak and broad band at 1580 cm^{-1} which was attributed to $\nu_4(H_3O^+)$ disappears upon deuteration in the Raman spectrum and weakens in intensity in the MIR, giving further credence to this assignment. Given the isotopic shifts, this band is expected at ~1170 cm^{-1} in the deuterated spectra where it is presumably lost beneath the stronger $\nu_3(SO_4)$ band.

Table 7-4: Raman and MIR isotopic shifts upon deuteration

Mineral	Raman Band		MIR Band		$\nu(R–^{1}H)/\nu(R–^{2}H)^{a}$	
	Protonated	Deuterated	Protonated	Deuterated	Raman	MIR
Jarosite	3412	2532	3410	2526	1.35	1.35
	3388	2508	3382	2504	1.35	1.35
Ammoniojarosite	3432	2546	3434	2542	1.35	1.35
	3412	2526	3408	2522	1.35	1.35
	3194	2308	3196	2398	1.38	1.33
Hydronium Jarosite	3426	2534	3360	2490	1.35	1.35

[a]R is either oxygen or nitrogen where appropriate

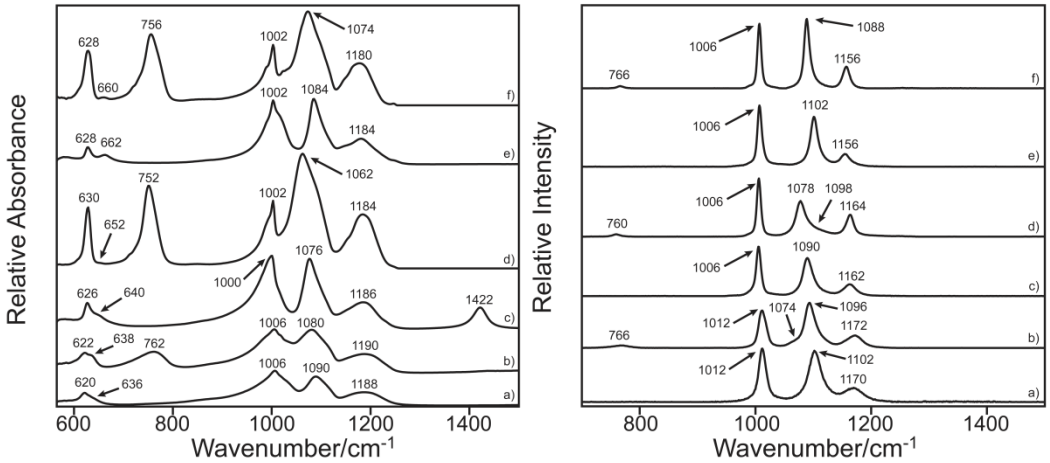

Figure 7-6: MIR (left) and 785 nm Raman (right) spectra in the 600 to 1500 cm^{-1} region for a) hydronium jarosite, b) deuteronium jarosite, c) ammoniojarosite, d) deuterated ammoniojarosite, e) jarosite and f) deuterated jarosite

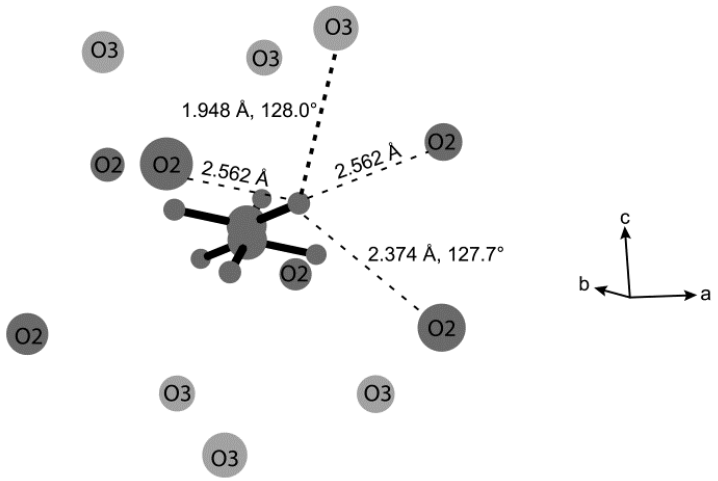

Figure 7-7: Hydronium ion surrounding environment, showing possible hydrogen bonds to hydroxyl oxygen atoms (O3) or basal sulfate oxygen atoms (O2). Structural data from Wills and Harrison (1996)

Figure 7-6 shows the IR and Raman spectra in the region 600 – 1400 cm^{-1} which is dominated by sulfate modes. Strong Davydov splittings of the sulfate internal modes in hydronium and ammoniojarosite can be seen and provides further evidence that hydrogen bonding to the sulfate ion is not a predominate interaction. Even so, the sulfate fundamentals are distinctly broader in the case of hydronium jarosite. This shows there is

some interaction between the hydronium and sulfate ions, but it is not as strong as that between the hydronium and hydroxyl groups. It is proposed that this weaker interaction takes the form of numerous, but very weak, hydrogen bonds between basal sulfate oxygen atoms and the hydronium hydrogen atoms, as shown in Figure 7-7. These interactions are negligible for ammoniojarosite. Not all of the hydrogen bonds to basal sulfate oxygen atoms are the same despite their constant O···O distance. Although free rotation of the hydronium ion is possible, the surrounding hydroxyl groups provide stability and essentially restrict the number of orientations to two: "up" or "down" with respect to the **c** axis. However, the ammonium ion has weaker hydrogen bonds and is expected to oscillate around its equilibrium position, or "rattle" in its cage so to speak, more than the hydronium ion. Whether this can be classed as true free rotation as found in the gas phase is debatable.

A very weak band, not observed in previous studies (Chio *et al.* 2010; Sasaki *et al.* 1998) can be seen at 1430 cm^{-1} in the low temperature Raman spectrum of ammoniojarosite (Figure 7-8). It corresponds to a sharper and more intense band at 1422 cm^{-1} in the MIR spectra which, on inspection of Figure 7-6, is observed to disappear on deuteration to overlap with $\nu_3(SO_4)$. We assign these bands to the $\nu_4(NH_4^+)$. Although two Raman and IR active $\nu_4(NH_4^+)$ bands ($E + A_1$) are expected by site symmetry (Table 7-5), only one is observed. The two components could overlap or they may be resolved at low temperature in the MIR. It is possible that the ammonium ion is not perturbed enough in jarosite minerals to show significant site splitting; this being the corollary to the situation where some molecules in crystals do not show Davydov splitting, despite no disorder or fractional occupancy (Kettle 1971).

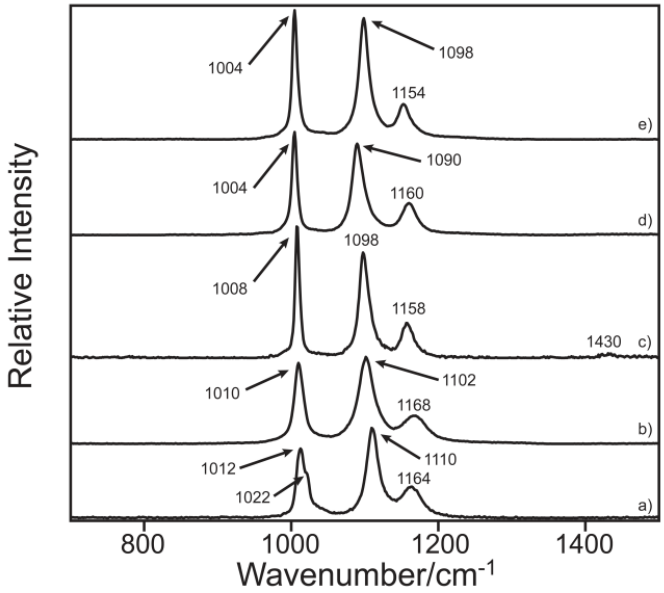

Figure 7-8: Raman spectra collected with 633 nm excitation in the 1500 to 4000 cm^{-1} region of a) hydronium jarosite at 82 K, b) hydronium jarosite at 298 K, c) ammoniojarosite at 82 K, d) ammoniojarosite at 298 K and e) jarosite at 298 K

The sharp intense Raman bands at 1006 cm^{-1} (1012 cm^{-1} in hydronium jarosite) are assigned to $\nu_1(SO_4)$. The two Raman bands near1100 and 1160 cm^{-1} are assigned to the Davydov split $\nu_3(SO_4)$ modes. Upon cooling to 82 K, a shoulder of hydronium jarosite $\nu_1(SO_4)$ is visible at 1022 cm^{-1} (Figure 7-8). This position does not correspond to any expected hydronium bands and an assignment to a hydronium mode is precluded by the fact that it can also be seen as minor asymmetry to $\nu_1(SO_4)$ in jarosite and ammoniojarosite. A weak δ(OD) Raman mode (Figure 7-6) appears at ~760 cm^{-1} for jarosite, ammoniojarosite, and hydronium jarosite which would corresponds to a band at ~1030 cm^{-1} in the protonated spectra. Thus the δ(OD) band position supports the assignment of the band at 1022 cm^{-1} in the 82 K Raman spectrum of hydronium jarosite to δ(OH). Furthermore this is its approximate position as assigned in some MIR studies (Kubisz 1972; Sasaki *et al.* 1998; Serna *et al.* 1986) which will be discussed if further detail in a later section. The lower wavenumber and more intense component of $\nu_3(SO_4)$ at ~1100 cm^{-1} shifts slightly to lower wavenumbers upon deuteration while the other

component and $\nu_1(SO_4)$ remain unchanged. The origin of broad shoulders at 1074 cm^{-1} in deuterated hydronium jarosite and at 1098 cm^{-1} in deuterated ammoniojarosite is unclear. The $\nu_2(H_3O^+)$ mode is expected at about 1150–1175 cm^{-1} and although it is the only hydronium mode that cannot be easily confused with water or hydroxyl groups (Wilkins *et al.* 1974), it is still not observed, presumably because is it obscured by $\nu_3(SO_4)$.

The MIR spectra in this region are more complex than the Raman spectra due to the manifestation of numerous shoulder bands of the ν_1 and $\nu_3(SO_4)$ modes. Hydronium jarosite has a rather long tail below 1000 cm^{-1}. Peak fitting analysis revealed it comprises two broad and weak shoulders at 750 and 860 cm^{-1}. The band at 750 cm^{-1} is unique to hydronium jarosite, butthe band at 850 – 870 cm^{-1} is also observed in the MIR spectra of jarosite and ammoniojarosite. Kubisz (1972) assigned the band at ~860 cm^{-1} to a librational H_3O^+ mode, however this band does not shift upon deuteration for any jarosite mineral, so we tentatively assign the band at 750 cm^{-1} to a librational H_3O^+ mode instead. The band at 620 – 630 cm^{-1} in all MIR spectra is a component of the $\nu_4(SO_4)$ mode. In the deuterated spectra, there is a weak shoulder at ~610 cm^{-1}. The other component of the $\nu_4(SO_4)$ due to Davydov splitting is observed at 660 cm^{-1} for jarosite, 640 cm^{-1} for ammoniojarosite and 636 cm^{-1} for hydronium jarosite.

A MIR band at 1006 cm^{-1} for hydronium jarosite and 1002 cm^{-1} for jarosite and ammoniojarosite do not shift upon deuteration and are therefore assigned to $\nu_1(SO_4)$. The shoulder at ~1020 cm^{-1} for all jarosites is assigned to $\delta(OH)$ as it disappears upon deuteration to be replaced by a strong band at ~756 cm^{-1} at the expected isotopic shift. This interpretation does not agree with some studies (Bishop and Murad 2005; Chio *et al.* 2010; Powers *et al.* 1975) in which the shoulder at ~990 cm^{-1} is assigned to $\nu_1(SO_4)$ and the sharper band at 1004 cm^{-1} to $\delta(OH)$ or the band at 1020 cm^{-1} to $\nu_1(SO_4)$. Our assignment for $\nu_1(SO_4)$ and $\delta(OH)$ in the MIR is in agreement with Kubisz (1972), Sasaki *et al.* (1998) and Serna *et al.* (1996). The origin of the shoulder at 990 cm^{-1} is less certain as it does not shift upon deuteration and is better resolved in the deuterated spectra. We

note that either the band at 990 cm^{-1} or the previously assigned $\nu_1(SO_4)$ at 1002 cm^{-1} could be overtones.

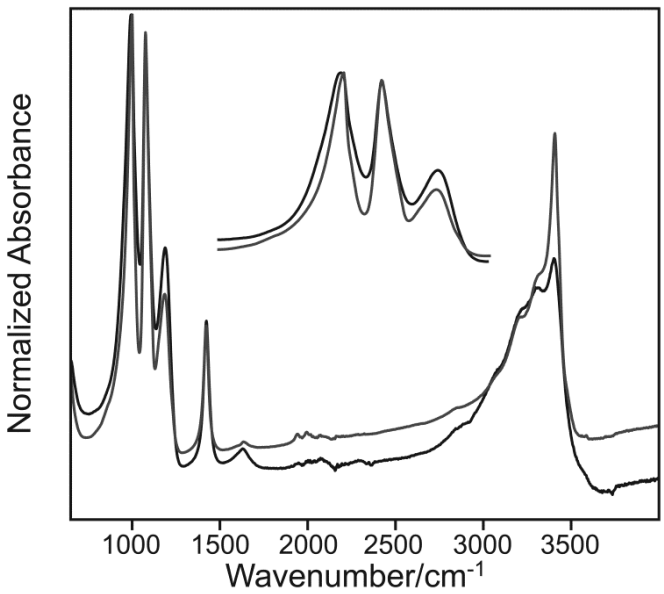

Figure 7-9: MIR spectra of low iron ammoniojarosite (black) compared to the ammoniojarosite previously analyzed (grey). Inset shows an expanded view of the sulfate stretching mode region

Asymmetry of the $\nu_3(SO_4)$ MIR bands is tentatively attributed to a confluence of two main structural features: $\nu_2(H_3O^+)$ which is expected at 1175 cm^{-1} (Kubisz 1972); and iron vacancies that are charge balanced by water (Nielsen *et al.* 2011). Sulfates adjacent to iron vacancies (water) are perturbed sufficiently to shift slightly in wavenumber compared to those that are not. The effect Fe vacancies have on the MIR spectrum can be seen in Figure 7-9 where spectra of an ammoniojarosite with low iron as synthesised (Frost *et al.* 2006a), is compared to the sample from the current study. Besides the expected dramatic increase in the intensity of the $\delta(H_2O)$ mode at 1640 cm^{-1} and a reduction in the $\nu(OH)$ intensity at ~3410 cm^{-1}, the $\nu_1(SO_4)$ region in the low iron ammoniojarosite spectrum is much broader and the $\nu_3(SO_4)$ bands are also broader and show more asymmetry on the high wavenumber side.

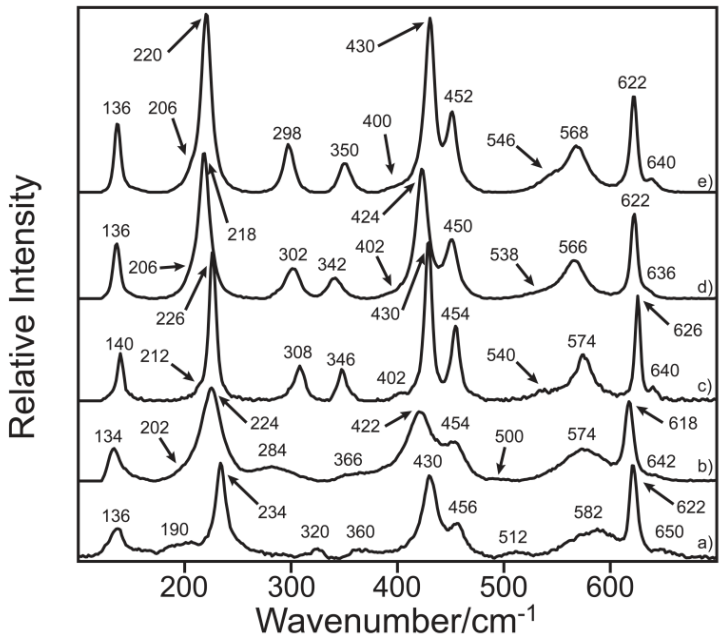

Figure 7-10: Raman spectra collected with 633 nm excitation in the 100 to 700 cm^{-1} region of a) hydronium jarosite at 82 K, b) hydronium jarosite at 298 K, c) ammoniojarosite at 82 K, d) ammoniojarosite at 298 K and e) jarosite at 298 K

The lattice region of the Raman spectra of these minerals are shown at 298 K and 82 K in Figure 7-10. The Raman lattice modes for hydronium jarosite, jarosite and ammoniojarosite are similar. This shows there is no significant structural change upon cooling that is a result of orientational disorder of hydronium and ammonium ions. In general, bands in this region are broader for hydronium jarosite than jarosite and ammoniojarosite. This is due to either the stronger interaction between hydronium and hydroxyl groups or orientational disorder. The only significant changes on cooling are observed in the hydronium jarosite spectra, where two broad and weak bands at 284 and 366 cm^{-1} shift and sharpen to 320 and 360 cm^{-1} such that they adopt a similar appearance to their counterparts in the jarosite and ammoniojarosite spectra at ~300 and ~346 cm^{-1}. In addition broad and weak bands at 500 and 202 cm^{-1} in the 298 K spectra shift on cooling to 512 cm^{-1} and 190 cm^{-1}, respectively, and are better resolved.

The $\nu_4(SO_4)$ mode is assigned to the doublet observed in all Raman spectra at ~620 and 640 cm^{-1}. The component at 640 cm^{-1} is weak, and only well resolved for

jarosite at 298 K. Identification of $\nu_2(SO_4)$ is challenging as it is either the Raman band at ~450 cm^{-1} (Arkhipenko and Bokii 1979; Kubisz 1972; Sasaki *et al.* 1998; Serna *et al.* 1986) or ~430 cm^{-1} (Bishop and Murad 2005; Chio *et al.* 2010; Maubec *et al.* 2012). As noted by Maubec et al. (2012), the assignment of both bands to $\nu_2(SO_4)$ (Frost *et al.* 2006b; Murphy *et al.* 2009) is not consistent with factor group analysis, nor is supported by any crystallographic study of jarosite minerals as no lowering of sulfate symmetry has ever been observed . The other possible assignment for these two Raman bands is an FeO_6 lattice mode (Chio *et al.* 2010; Maubec *et al.* 2012; Sasaki *et al.* 1998; Serna *et al.* 1986). We note that Chio *et al.* (2010) assigned the band at 450 cm^{-1} to γ(OH), but the spectra in Figure 7-11 show that this band [1] is upshifted by ~10 cm^{-1} upon deuteration and is therefore a good candidate for $\nu_2(SO_4)$ instead. The band at 430 cm^{-1} downshifts by only ~ 10 cm^{-1} and so is assigned here to an FeO_6 lattice vibration.

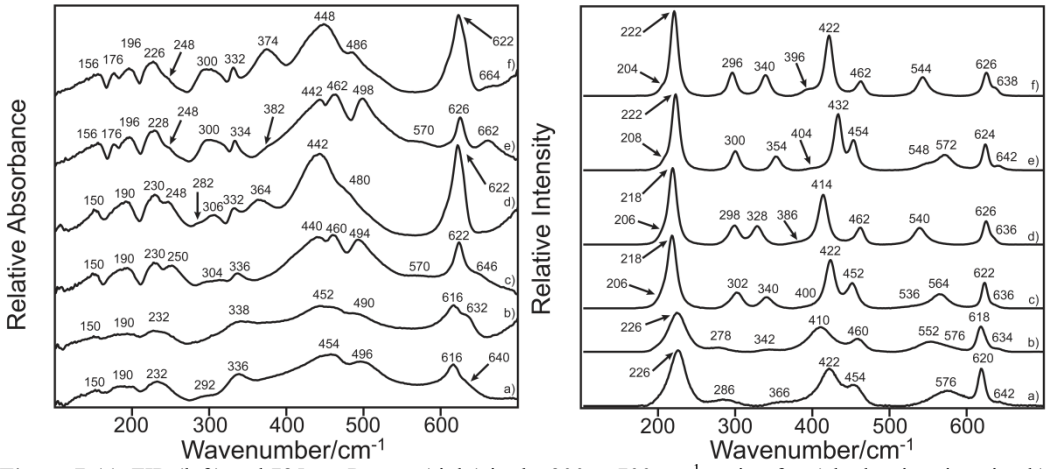

Figure 7-11: FIR (left) and 785 nm Raman (right) in the 200 to 700 cm^{-1} region for a) hydronium jarosite, b) deuteronium jarosite, c) ammoniojarosite, d) deuterated ammoniojarosite, e) jarosite and f) deuterated jarosite

Previous studies have assigned Raman bands of medium intensity near 570 cm^{-1} and low intensity near 540 cm^{-1} to either γ(OH) or FeO_6 lattice vibrations (Chio *et al.* 2010; Maubec *et al.* 2012; Sasaki *et al.* 1998; Serna *et al.* 1986). In hydronium jarosite the higher wavenumber band is broader than in the other jarosites and the low wavenumber band appears at 500 cm^{-1} at 298 K shifting to 512 cm^{-1} at 82 K. The

broadness the hydronium jarosite bands indicates they are related to OH^- groups, as previously discussed. If the band near 570 cm^{-1} was due to γ(OH) it would shift to lower wavenumbers by about 150 cm^{-1} on deuteration, but it appears to shift only ~25 cm^{-1} which rather favours its assignment to an FeO_6 lattice mode. The band that was previously around 540 cm^{-1} is, after deuteration, either lost under the stronger shifted band or has itself shifted to much lower wavenumbers. If the latter were the case it could be assigned to γ(OH) but there are many overlapping bands in the 400 cm^{-1} region so it is difficult to be certain.

The Raman bands at 284 cm^{-1} and 366 cm^{-1} for hydronium jarosite appear to correspond to those at ~300 and ~346 cm^{-1} for ammoniojarosite and jarosite, respectively. These bands are broad at 298 K for hydronium jarosite owing to the potential increased proton mobility of hydronium and the stronger attraction of hydronium hydrogen atoms to the surrounding hydroxyl groups. Upon deuteration the higher wavenumber band in all spectra shifts by ~12 cm^{-1}, except for hydronium jarosite where the shift is 24 cm^{-1}. The lower wavenumber band for all spectra does not shift significantly upon deuteration. Both of these bands have been attributed to the FeO_6 octahedra in previous studies. The band that shifts must be influenced more by the OH groups. Other Raman bands (136, 202, 222 and 400 cm^{-1}) are assigned to lattice modes and show limited isotopic substitution effects. However, the shoulder at ~200 cm^{-1} for hydronium jarosite shifts to 190 cm^{-1} at 82 K and becomes more resolved than its counterpart in the spectra of jarosite and ammoniojarosite.

In the FIR spectra, the $\nu_4(SO_4)$ doublet has one intense component from 616 – 626 cm^{-1} and a weaker component from 640 – 660 cm^{-1}. There is a weak band at 570 cm^{-1} except in hydronium jarosite spectra. If this band were γ(OH), it could be expected to be more intense in the infrared spectra. A more likely assignment it is the infrared complement to the more intense band Fe–O observed in the Raman. A stronger band at ~500 cm^{-1} in all spectra disappears upon deuteration and shifts to give rise to a band at 374 cm^{-1} (jarosite) and 364 cm^{-1} (ammoniojarosite). Therefore, the band at ~500 cm^{-1} is

the γ(OH) vibration in MIR spectra. The band at 440 – 454 cm^{-1} is assigned to $\nu_2(SO_4)$ and overlaps with an FeO_6 lattice mode at 460 cm^{-1} which shifts upon deuteration. Bands at ~156, ~190 (very broad for ammoniojarosite and hydronium jarosite), ~230, ~334 and 300 cm^{-1} are unaffected by deuteration and are assigned to lattice modes not involving hydrogen atoms. Bands at 250 cm^{-1} in jarosite and ammoniojarosite, and at 176 cm^{-1} in jarosite, may be obscured by the broadness of hydronium and ammoniojarosite bands at 230 and 190 cm^{-1} respectively.

IMPLICATIONS

There is no panacea for the spectroscopic problems caused by orientational disorder as a result of molecules occupying sites not allowed by their point group; each situation should be treated on a case-by-case basis. However, based on the presented symmetry analysis, the following general principles can be extended to similar situations in other minerals and crystals:

1. Disordered molecules that are satisfactorily described by an infinite point group ($C_{\infty v}$ or $D_{\infty h}$) assuming free rotation of all or part of the molecule can be dealt with according to the methods outlined by Petruševski *et al.* (1993).

2. The correct spectroscopic space group is the space group that best explains the Raman and IR spectra. This space group can be either higher or lower symmetry than the crystallographic space group due to small structural distortions or pseudo-symmetry.

3. The effective symmetry of a disordered molecule at a site that is not a subgroup of its molecular symmetry must be determined. This is the symmetry when only one orientation of the disordered molecule is considered; the disordered symmetry is only applicable in diffraction based methods due to time and spatial averaging. The principles of Jewess (1982) should be applied. Alternatively, the effective symmetry can be derived by removing the "forbidden" symmetry elements with respect to the disordered molecule.

4. The spectroscopic site symmetry selected in the preceding point must be a subgroup of the point group symmetry and the spectroscopic space group (factor

group). If there is no such site, then the trivial point group C_1 is the spectroscopic site symmetry.

5. If fractional occupancy at the spectroscopic site eventuates, then only site symmetry effects are relevant for predicting internal modes as Davydov splitting cannot occur. However, splitting due to the spectroscopic site may not be observed depending on the molecule and its surrounding environment.

6. Mode activity and Raman tensors will follow that of the spectroscopic site symmetry. This is because the symmetry species of the factor group cannot be employed.

The spectra presented in this study are suggestive of more hydrogen bonding in hydronium jarosite compared to ammoniojarosite. This hydrogen bonding perturbs the ν(OH) bands such that they appear to coalesce into one broad band. Despite this disorder in spectroscopic terms, ammoniojarosite appears more similar to jarosite than hydronium jarosite and also undergoes long range magnetic ordering at low temperature. This is attributed to hydrogen bonding involving the hydroxyl groups and the ammonium ion being of lesser consequence than the respective hydrogen bonds in hydronium jarosite. Therefore, orientational disorder is not the only cause of the spurious magnetic behaviour of hydronium jarosite. An NMR study to determine the activation of energy of motion of ammonium in ammoniojarosite and/or ammonioalunite could provide further illumination on this issue. Finally, vibrational spectroscopy coupled with factor group analysis is a powerful tool for the study of minerals, especially where the structure is ambiguous from diffraction methods.

REFERENCES

Adams, D. M., 1973: A descriptive introduction to analysis of the vibrational spectra of solids. *Coordination Chemistry Reviews*, **10,** 183-193.

Arkhipenko, D. K., and G. B. Bokii, 1979: Refinement of the space group of alunite-jarosite by means of vibrational spectroscopy. *Soviet Physics - Crystallography*, **24,** 100-106.

Auglló-Rueda, F., J. M. Calleja, and J. Bartolomé, 1988: Raman spectroscopy of the ammonium ion in NH_4MnF_3 and NH_4ZnF_3 perovskites: temperature dependence. *Journal of Physics C: Solid State Physics*, **21,** 1287-1297.

Basciano, L. C., and R. C. Peterson, 2007: The crystal structure of ammoniojarosite, $(NH_4)Fe_3(SO_4)_2(OH)_6$ and the crystal chemistry of the ammoniojarosite-hydronium jarosite solid-solution series. *Mineralogical Magazine*, **71,** 427-441.

Bertie, J. E., 1968: Far-infrared spectra of the ices. *Applied Spectroscopy*, **22,** 634-640.

Besbes, H., T. Mhiri, and A. Daoud, 1999: Disorder study in triammonium hydrogen disulphate $(NH_4)_3H(SO_4)_2$ and its solid solutions $(NH_4)_{3-x}M_xH(SO_4)_2$. *Phase Transitions*, **70,** 183-195.

Bhagavantam, S., and T. Venkatarayudu, 1939: Raman effect in relation to crystal structure. *Proceedings of the Indian Academy of Science, A*, **9,** 224-258.

Bishop, J. L., and E. Murad, 2005: The visible and infrared spectral properties of jarosite and alunite. *American Mineralogist*, **90,** 1100-1107.

Boyle, L. L., 1972: The method of ascent in symmetry-III application to lattice vibrations. *Spectrochimica Acta*, **A28,** 1355-1360.

Buttery, H. J., G. Keeling, S. F. A. Kettle, I. Paul, and P. J. Stamper, 1969: Correlation between crystal structure and carbonyl-bond stretching vibrations of

methyl benzene transition metal tricarbonyls. *Discussions of the Faraday Society*, **47,** 48-52.

Catti, M., and R. M. Ibberson, 2002: Order-disorder of the hydronium ion and low-temperature phase transition of $(H_3O)Zr_2(PO_4)_3$ NASICON by neutron diffraction. *Journal of Physical Chemistry B*, **106,** 11916-11921.

Chio, C. H., S. K. Sharma, L.-C. Ming, and D. W. Muenow, 2010: Raman spectroscopic investigation on jarosite-yavapaiite stability. *Spectrochimica Acta*, **A75,** 162-171.

Dharmasena, G., and R. Frech, 1995: Orientational disorder in lithium sodium sulfate. *Journal of Chemical Physics*, **102,** 6941-6945.

Elwood Madden, M. E., R. J. Bodnar, and J. D. Rimstidt, 2004: Jarosite as an indicator of water-limited chemical weathering on Mars. *Nature*, **431,** 821-823.

Emsley, J., 1980: Very strong hydrogen bonding. *Chemical Society Reviews*, **9,** 91-124.

English, R. B., and A. M. Heyns, 1984: An infrared, Raman, and single-crystal X-ray study of cesium hexafluorophosphate. *Journal of Crystallographic and Spectroscopic Research*, **14,** 531-540.

Fåk, B., F. C. Coomer, A. Harrison, D. Visser, and M. E. Zhitomirsky, 2008: Spin-liquid behavior in a kagomé antiferromagnet: deuteronium jarosite. *Europhysics Letters*, **81,** 17006.

Farmer (ed.), V. C., 1974: *The Infrared Spectra of Minerals*. Mineralogical Society.

Fernandes, J. R., S. Ganguly, and C. N. R. Rao, 1979: Infrared spectroscopic study of the phase transitions in $CsNO_3$, $RbNO_3$ and NH_4NO_3. *Spectrochimica Acta*, **A35,** 1013-1020.

Frost, R. L., R.-A. Wills, J. T. Kloprogge, and W. Martens, 2006a: Thermal decomposition of ammonium jarosite $NH_4Fe_3(SO_4)_2(OH)_6$. *Journal of Thermal Analysis and Calorimetry*, **84,** 489-496.

Frost, R. L., R.-A. Wills, M. L. Weier, W. Martens, and S. Mills, 2006b: A Raman spectroscopic study of selected natural jarosites. *Spectrochimica Acta*, **A63,** 1-8.

Grohol, D., and D. G. Nocera, 2007: Magnetic disorder in the frustrated antiferromagnet jarosite arising from the H_3O^+•••OH^- interaction. *Chemistry of Materials*, **19,** 3061-3066.

Grohol, D., Q. Huang, B. H. Toby, J. W. Lynn, Y. S. Lee, and D. G. Nocera, 2003: Powder neutron diffraction analysis and magnetic structure of kagomé-type vanadium jarosite $NaV_3(OD_6)(SO_4)_2$. *Physical Review B*, **68,** 094404.

Halford, R. S., 1946: Motions of molecules in condensed systems: I. Selection rules, relative intensities, and orientation effects for Raman and infrared spectra. *Journal of Chemical Physics*, **14,** 8-15.

Hollebone, B. R., and A. B. P. Lever, 1972: The application of symmetry ascent selection rules to a factor group analysis of red mercuric iodide. *Inorganic Chemistry*, **11,** 1158-1160.

Jewess, M., 1982: A theoretical treatment of 'orientational' disorder for routine use. *Acta Crystallographica*, **B38,** 1418-1422.

Kettle, S. F. A., 1971: Molecular vibrational spectra in the solid state. *Conférences plénières: présentées à Krakow-Zakopane, Pologne, 14-22 Septembre 1970*, 113-125.

Kettle, S. F. A., U. A. Jayasooriya, and L.-J. Norrby, 1984: Reinterpretation of the internal mode vibrational spectra of ammonium sulfate (phase I). *Journal of Physical Chemistry*, **88,** 5971-5975.

Klingelhöfer, G., and Coauthors, 2004: Jarosite and hematite at Meridiani Planum from Opportunity's Mossbauer spectrometer. *Science*, **306,** 1740-1745.

Kubisz, J., 1972: Studies on synthetic alkali-hydronium jarosites III: infrared absorption study. *Mineralogia Polonica*, **3,** 23-37.

Libowitzky, E., 1999: Correlation of O–H stretching frequencies and O–H•••O hydrogen bond lengths in minerals. *Monatshefte für Chemie*, **130,** 1047-1059.

Lutz, H. D., 1988: Bonding and structure of water molecules in solid hydrates. Correlation of spectroscopic and structural data. *Structure and Bonding*, **69,** 97-124.

Majzlan, J., and Coauthors, 2004: Thermodynamic properties, low-temperature heat-capacity anomalies, and single-crystal X-ray refinement of hydronium jarosite, $(H_3O)Fe_3(SO_4)_2(OH)_6$. *Physics and Chemistry of Minerals*, **31,** 518-531.

Maubec, N., A. Lahfid, C. Lerouge, G. Wille, and K. Michel, 2012: Characterization of alunite supergroup minerals by Raman spectroscopy. *Spectrochimica Acta*, **A96,** 925-939.

Mazej, Z., E. Goreshnik, and Z. Jagličić, 2012: Syntheses and crystal structures of $[H_3O]^+/M^{2+}$ (M = Fe, Zn, Cu, Hg) salts with $[AsF_6]^-$. *European Journal of Inorganic Chemistry*, **2012,** 1734-1741.

Menchetti, S., and C. Sabelli, 1976: Crystal chemistry of the alunite series: crystal structure refinement of alunite and synthetic jarosite. *Neues Jahrbuch für Mineralogie Monatshefte*, **9,** 406-417.

Mookherjee, M., S. A. T. Redfern, M. Zhang, and D. S. Harlov, 2002: Orientational order-disorder of ND_4^+/NH_4^+ in synthetic ND_4/NH_4-phlogopite: a low temperature infrared study. *European Journal of Mineralogy*, **14,** 1033-1039.

Murphy, P. J., A. M. L. Smith, K. A. Hudson-Edwards, W. E. Dubbin, and K. Wright, 2009: Raman and IR spectroscopic studies of alunite-supergroup compounds containing, Al^{3+}, Cr^{3+} Fe^{3+} and V^{3+} at the B site. *Canadian Mineralogist*, **47,** 663-681.

Nielsen, U. G., I. Heinmaa, A. Samoson, J. Majzlan, and C. P. Grey, 2011: Insight into the local magnetic environments and deuteron mobility in jarosite ($AFe_2(SO_4)_2(OD,OD_2)_6$, A = K, Na, D_3O) and hydronium alunite ($(D_3O)Al_3(SO_4)_2(OD)_6$), from variable-temperature ^2H MAS NMR spectroscopy. *Chemistry of Materials*, **23,** 3176-3187.

Nocera, D. G., B. M. Bartlett, D. Grohol, D. Papoutsakis, and M. P. Shores, 2004: Spin frustration in 2D kagomé lattices: a problem for inorganic synthetic chemistry. *Chemistry A European Journal*, **10,** 3850-3859.

Oxton, I. A., O. Knop, and M. Falk, 1976: Determination of the symmetry of the ammonium ion in crystals from the infrared spectra of the isotopically dilute NH_3D^+ species. *Journal of Physical Chemistry*, **80,** 1212-1217.

Petruševski, V. M., B. Minčeva-Šukarova, and A. Džorovska, 1993: The vibrational species of molecules in disordered crystals: $M(NH_3)_2$ groups at C_{4h} symmetry sites. *Bulletin of the Chemists and Technologists of Macedonia*, **12,** 31-34.

Pham-Thi, M., P. Colomban, A. Novak, and R. Blinc, 1987: Vibrational spectra and phase transitions in caesium hydrogen sulphate. *Journal of Raman Spectroscopy*, **18,** 185-194.

Plaza, I., J. Rubín, M. A. Laguna, and J. Bartolomé, 1996: Optical spectroscopy of the NH_4^+ internal vibrations in the orthorhombic phase of NH_4MF_3 (M is Mn, Zn) perovskites. *Spectrochimica Acta*, **A52,** 57-67.

Powers, D. A., G. R. Rossman, H. J. Schugar, and H. B. Gray, 1975: Magnetic behavior and infrared spectra of jarosite, basic iron sulfate, and their chromate analogs. *Journal of Solid State Chemistry*, **13,** 1-13.

Rudolf, P. R., M. A. Subramanian, A. Clearfield, and J. D. Jorgensen, 1985: The crystal structures of the ion conductors $(NH_4^+)Zr_2(PO_4)_3$ and $(H_3O^+)Zr_2(PO_4)_3$. *Solid State Ionics*, **17,** 337-342.

Sasaki, K., O. Tanaike, and H. Konno, 1998: Distinction of jarosite-group compounds by Raman spectroscopy. *Canadian Mineralogist*, **36,** 1225-1235.

Sato, E., I. Nakai, R. Miyawaki, and S. Matsubara, 2009: Crystal structures of alunite family minerals: beaverite, corkite, alunite, natroalunite, jarosite, svanbergite, and woodhouseite. *Neues Jahrbuch für Mineralogie Abhandlungen*, **185,** 313-322.

Schiebel, P., K. Burger, H. G. Büttner, G. J. Kearley, M. Lehmann, and W. Prandl, 2000: ND_3-density distribution in orientationally disordered $Ni(ND_3)_6Cl_2$ observed by means of neutron Laue diffraction. *Journal of Physics: Condensed Matter*, **12,** 8567-8576.

Serna, C. J., C. P. Cortina, and J. V. Garcia Ramos, 1986: Infrared and Raman study of alunite-jarosite compounds. *Spectrochimica Acta*, **A42,** 729-734.

Szymanski, J. T., 1985: The crystal structure of plumbojarosite. *Canadian Mineralogist*, **23,** 659-668.

Taft, R. W., J. F. Wolf, J. L. Beauchamp, G. Scorrano, and E. M. Arnett, 1978: Solvent effects of water and fluorosulfuric acid on proton transfer equilibria and the energies of solvation of gaseous onium ions. *Journal of the American Chemical Society*, **100,** 1240-1249.

Taylor, R. C., and G. L. Vidale, 1956: The vibrational spectrum of the hydronium ion in hydronium perchlorate. *Journal of the American Chemical Society*, **78,** 5999-6002.

Turrell, G., 1972: *Infrared and Raman spectra of crystals.* Academic Press.

Wilkins, R. W. T., A. Mateen, and G. W. West, 1974: The spectroscopic study of oxonium ions in minerals. *American Mineralogist*, **59,** 811-819.

Wills, A. S., and A. Harrison, 1996: Structure and magnetism of hydronium jarosite, a model Kagomé antiferromagnet. *Journal of the Chemical Society, Faraday Transactions*, **92,** 2161-2166.

Wills, A. S., A. Harrison, C. Ritter, and R. I. Smith, 2000: Magnetic properties of pure and diamagnetically doped jarosites: model kagomé antiferromagnets with variable coverage of the magnetic lattice. *Physical Review B*, **61,** 6156-6169.

Xu, H., Y. Zhao, S. C. Vogel, D. D. Hickmott, L. L. Daemen, and M. A. Hartl, 2010: Thermal expansion and decomposition of jarosite: a high-temperature neutron diffraction study. . *Physics and Chemistry of Minerals*, **37,** 73-82.

Yukhnevich, G. V., 1963: Advances in the use of infrared spectroscopy for the characterisation of OH bonds. *Russian Chemical Reviews*, **32,** 619-633.

CHAPTER 8 CONCLUSIONS

PREFACE

The overarching aim of this thesis was to account for the differing magnetic behaviour of the orientationally disordered hydronium jarosite [$H_3OFe_3(SO_4)_2(OH)_6$] and ammoniojarosite [$NH_4Fe_3(SO_4)_2(OH)_6$] minerals, by determining the most appropriate model for their crystal structures that are also consistent with vibrational spectra. The location of hydronium and ammonium ion hydrogen atoms was integral to this aim. By thoroughly studying the crystal structure and vibrational spectra of hydronium jarosite and ammoniojarosite in comparison to jarosite [$KFe_3(SO_4)_2(OH)_6$], additional insight into the spurious magnetic behaviour of ammoniojarosite was obtained, and the structural effects of the ammonium and hydronium ions elucidated. Hydronium jarosite and ammoniojarosite in deuterated and protonated forms were synthesised and studied via thermogravimetric analysis, Raman and infrared spectroscopy at varying temperatures, infrared emission spectroscopy, single crystal and powder X-ray diffraction, and neutron powder diffraction. An improved method for symmetry analysis that predicts the normal modes of vibration was developed for orientationally disordered non-linear molecules in crystals. This chapter places the findings of the preceding chapters in context through a general discussion, which shows each chapter leads to the same conclusions regarding the presence of hydronium and ammonium ions in jarosite minerals. Avenues for future work directly related to the work reported in this thesis are also suggested.

8.1 ORIGINAL CONTRIBUTION

This thesis has expanded the knowledge of jarosite minerals. This thesis has made the following original contributions to the literature:

1. *The thermal decomposition of ammoniojarosite and hydronium jarosite was clarified.*
    a. Water and ammonia were lost simultaneously for ammoniojarosite between 300 – 400 °C.
    b. For both ammoniojarosite and hydronium jarosite, evolution of the NH_4^+ and H_3O^+ ions occurred via protonation of a surrounding hydroxyl group which evolved $NH_3 + H_2O$ and $2H_2O$, respectively.
    c. Hydrogenated sulfurous oxide compounds were not evolved. Instead, all hydrogen were lost before desulfonation began.
    d. Crystalline decomposition intermediate compounds, in general, were not identified.
    e. Control of the atmosphere during *in situ* heating stage XRD measurements is important as a curious iron(III) to iron(II) to iron(III) redox cycle was observed. This redox cycle was attributed to the presence of NH_3 in the capillary during *in situ* XRD data collection.

2. *The crystal structure of hydronium jarosite was solved from neutron powder diffraction and Rietveld refinement.*
    a. All hydronium hydrogen atoms were located from difference Fourier methods.

b. The hydronium hydrogen atoms were most adequately modelled at a C_s/m site (x, $2x$, z) with 50 % occupancy, leading to a minimum of two orientations, "up" or "down" with respect to the **c** axis.

c. Numerous lower symmetry models were refined and statistically compared for the first time.

d. The hydronium ion's presence did not result in a lowering of the space group symmetry when temporally averaged. The space group is $R\bar{3}m$.

e. The hydronium oxygen atom occupies the $D_{3d}/\bar{3}m$ site (0, 0, 0) when temporally averaged. Minimal evidence for displacement from this site was found based on statistical tests.

f. A poor geometry of the hydronium ion resulted (O–H = 0.919 Å, H–O–H = 90°) if the ion was not modelled as a rigid body with O–H distances of 0.96 Å and H–O–H angles of 112°. This poor geometry suggests more orientations are possible, but are beyond the resolution of the neutron diffraction experiment employed.

g. The hydronium ion preferentially forms hydrogen bonds to hydroxyl groups.

3. *A new crystal structure for ammoniojarosite was determined from neutron powder diffraction and Rietveld refinement.*

a. The established literature model was a poor fit to the data, and did not agree with difference Fourier maps. Alternative models were investigated to ensure the new model was a global minimum.

b. All ammonium hydrogen atoms were located from difference Fourier methods.

c. All ammonium hydrogen atoms were most adequately modelled at a C_s/m site (x, $2x$, z) with 50 % and 16.67 % occupancy, leading to a minimum of six orientations.

d. The ammonium ion's presence does not result in a lowering of the space group symmetry when temporally averaged. The space group is $R\bar{3}m$.

e. The ammonium nitrogen atom occupies the $D_{3d}/\bar{3}m$ site (0, 0, 0) when temporally averaged. Statistical tests found limited evidence for the nitrogen atom being displaced from this site.

f. The ammonium ion preferentially hydrogen bonds to hydroxyl groups.

4. *The vibrational spectra of ammoniojarosite and hydronium jarosite were reinterpreted in comparison to jarosite.*

a. Similar ν(OH) band positions meant that all hydrogen bonds in the jarosite minerals investigated are of a similar strength.

b. Broader hydronium jarosite hydroxyl bands, and no observable Davydov splitting of ν(OH) modes, means the hydroxyl groups are more perturbed in this mineral. This was attributed to more significant hydrogen bonds between the hydroxyl groups and the hydronium ion when compared to the ammonium or potassium ions and hydroxyl groups.

c. Broader ν(SO_4) bands in hydronium jarosite means the hydronium ion experiences some interaction with sulfate groups. However, Davydov splitting is still observed so the interaction is less significant than its interaction with hydroxyl groups.

d. A band at 570 cm^{-1} which has been attributed to γ(OH) in the literature, is actually an Fe–O / Fe–OH type vibration. This conclusion was reached by careful consideration of the appearance of bands, isotopic shifts, and intensity of bands in Raman and MIR spectra.

e. The δ(OH) mode overlaps with $\nu_1(SO_4)$, not $\nu_3(SO_4)$ as some literature argues. This assignment was easily reached from isotopic shifts upon deuteration. In addition, the cold stage Raman spectrum of hydronium jarosite clearly showed a shoulder of $\nu_1(SO_4)$.

5. *An improved protocol for the symmetry analysis of disordered non-linear molecules in otherwise ordered crystals was proposed for the first time.*

a. The proposed symmetry analysis is in agreement with the number of vibrations expected that is calculated from the number of atoms in the Bravais unit cell of a crystal ($3N_B - 3$ where N_B is the number of atoms in the Bravais unit cell). This is the number of vibrational modes available to any crystal.

b. The proposed symmetry analysis means the vibrational spectra of hydronium jarosite and ammoniojarosite can be understood from a theoretical stand point for the first time.

c. The proposed symmetry analysis is based on determining the highest effective allowed symmetry of the disordered molecule at a finite point in time. This circumvents the assertion that disordered molecules are “spherical” or “behave as a point,” and that a subsequent symmetry analysis for their vibrational modes is not possible.

d. The symmetry analysis is easily extended to other similarly disordered crystals to check whether the structure containing

orientational disorder is correct, for vibrational spectroscopic purposes.

6. *Structural nuances involving hydrogen bonds are the most significant structural effects of ammonium and hydronium in jarosite minerals.*
    a. Due to the acidity of hydronium compared to ammonium, and the polarity of O–H bonds compared to N–H bonds, hydrogen bonds involving the hydronium ion are stronger than those involving the ammonium ion. Thus, hydronium jarosite is a spin glass because its FeO_6 octahedra are significantly perturbed by the hydronium ion. Although hydrogen bonding seems a likely cause for this perturbation, the exact orientational disorder mechanism of the hydronium and ammonium ions cannot be elucidated by the methods used in this thesis.

8.2 GENERAL DISCUSSION

This thesis investigated the spectroscopy and crystal structure of jarosite minerals containing hydronium and ammonium ions at low, ambient and elevated temperatures. This thesis has fundamentally increased the knowledge of jarosite minerals, in particular, the structural effects of hydronium and ammonium ions via a thorough interpretation of spectroscopic and crystallographic data. These studies provide evidence that hydrogen bonding is strongly linked to the differing magnetic behaviour of ammoniojarosite and hydronium jarosite. This conclusion was reached after a reinterpretation of the neutron powder diffraction patterns and vibrational spectra of these two minerals in comparison to titular jarosite.

In Chapter 4 it was shown that hydrogen atoms do not persist in the jarosite structure past about 400 °C, and H_2O is evolved in tandem with NH_3 for ammoniojarosite. This means the hydronium and ammonium ions experience more of an attraction to the surrounding hydroxyl groups than the sulfate groups, as there was no evidence for the loss of protonated sulfur compounds during thermal decomposition. Dehydroxylation temperatures for hydronium jarosite are lower than ammoniojarosite, which suggests hydronium hydrogen atoms are more mobile and/or more strongly attracted to the surrounding hydroxyl groups compared to ammonium hydrogen atoms.

Numerous models for the crystal structures of hydronium jarosite and ammoniojarosite were determined and compared in Chapters 5 and 6 respectively. Rietveld refinement reveals the space group is the same as for other jarosite minerals $\left(R\bar{3}m\right)$, and there is limited evidence for the displacement of hydronium and ammonium cations from the $\bar{3}m$ site that has been invoked in some prior studies. Orientational disorder of the hydronium and ammonium ions leads to fractional occupancy of the hydrogen atoms over at least two orientations. A new structural model for ammoniojarosite was proposed, whereby the apical ammonium hydrogen atom is located at an *m* site with 16.67 % fractional occupancy. This new structure was the only model

that was consistent with difference Fourier maps; the literature structure was not a good fit to the data as the hydrogen positions do not agree with those found via difference Fourier methods.

When time and spatially averaged, the two orientations (or more) are related by inversion symmetry and allow the hydronium and ammonium ions to occupy an otherwise symmetry forbidden crystallographic site. The isotropic adps of hydronium and ammonium hydrogen atoms are significantly larger than other atoms in the proposed crystal structure models. While the exact nature of the disorder cannot be determined from diffraction data alone, this result is suggestive of dynamic disorder around the centre of mass, i.e. the oxygen and nitrogen atom of hydronium and ammonium respectively, or a high degree of static disorder. Further evidence for hydrogen bonds between hydronium and ammonium ions and the surrounding hydroxyl groups were revealed from the modelled structures. These chapters have clarified the crystal structures of hydronium jarosite and ammoniojarosite, and are the first to rigorously compare different models.

However, when considering vibrational spectra as in Chapter 7, it was found the temporal averaged symmetry of the crystal structures determined from Rietveld refinement was not adequate. This is because structural averaging does not occur, and small structural distortions are more relevant during vibrational spectroscopic lifetimes. Therefore, the highest allowed effective or local symmetry of one orientation at a finite point in time for an orientationally disordered molecule must be determined for vibrational spectroscopic purposes. Thus, an improved method for the symmetry analysis of orientationally disordered non-linear molecules that are consistent with their crystal structures were proposed, using hydronium jarosite and ammoniojarosite as a case study. The symmetry analysis involves the following steps:

1. The most appropriate space group that accounts for the vibrational spectra is chosen. It can be different to the diffraction determined space group.

2. Determine the highest symmetry of one orientation of the disordered molecule at a finite point in time that is both a subgroup of the molecular symmetry and the space group symmetry.

3. Determine the multiplicity of the site that corresponds to this symmetry. If fractional occupancy results in order to maintain charge balance and stoichiometry, Davydov splitting cannot occur and modes follow site symmetry selection rules.

Chapter 7 also gave spectroscopic evidence the hydronium and ammonium ions are orientationally disordered, hydrogen bonding in hydronium jarosite is stronger or of more consequence than in ammoniojarosite, and hydrogen bonds are predominantly towards hydroxyl groups. These structural conclusions were reached by careful consideration of the broadness, position and appearance of bands. For example, certain bands in hydronium jarosite were much broader than their ammoniojarosite and jarosite counterparts. This can be attributed to perturbed molecular groups arising from stronger hydrogen bonds and/or orientational disorder. However, ν(OH) bands occurred at approximately the same position for all minerals, which means any hydrogen bonding is of the same strength, no matter the A site cation in the jarosite structure.

The conclusions from each chapter clearly support the argument the magnetic behaviour of hydronium jarosite and ammoniojarosite is related to hydrogen bonding. Such an argument has been previously conceived but with little further expansion or evidence from the literature (Grohol and Nocera 2007; Wills 2001). Grohol and Nocera (2007) noted the magnetic ordering temperature of jarosite minerals was dependent on the concentration of H_3O^+ at the A site. This thesis has presented structural evidence consistent with this hypothesis; primarily from vibrational spectroscopy, thermal analysis, and neutron diffraction. Overall, it can be said the hydronium ion induces more magnetic disorder than the ammonium ion in jarosite minerals, and this magnetic disorder arises

from a stronger hydrogen bond with Fe–OH groups and hydronium compared to Fe–OH and ammonium. The nature of this interaction means that at any given point in time, half the Fe–OH groups in the unit cell are hydrogen bonded, but the other half are not. In other words, the FeOH groups are more perturbed in hydronium jarosite. Unlike Grohol and Nocera (2007), the data in this thesis is consistent with NMR data from Nielsen *et al.* (2008 & 2011) whereby the strength of this interaction is such that complete neutralisation to water via $H_3O^+ + OH^- \rightarrow 2H_2O$ is not permanent. The weaker hydrogen bonds involving the ammonium ion mean that is less tightly bound to the framework compared to hydronium and thus, the ammonium ion can librate/rotate or "rattle" in its cavity more than hydronium. For instance, the ammonium basal hydrogen atom isotropic ADPs are significantly larger than the hydronium hydrogen atoms at ambient temperature. This is in addition to the high degree of orientational disorder owing to the six apical ammonium hydrogen positions.

The **c** axis of hydronium jarosite is significantly shorter than ammoniojaorsite, and as such, the Fe–O bond distances are different. It has been proposed that a more disordered FeO_6 octahedra results in a higher antiferromagnetic transition temperature (Bisson and Wills 2008) as observed in all jarosite minerals except hydronium jarosite. Indeed, in Chapters 5 and 6 the Fe–O bond distances in hydronium jarosite (2.043 and 2.0041 Å at 298 K) show less variation from 2.0 Å compared to ammoniojarosite (2.053 and 1.9848 Å at 298 K). It is argued by the author that the explanation offered by Bisson and Wills (2008) occurs in confluence with hydrogen bonding effects, and may in fact, be due to the differing hydrogen bond strength in hydronium jarosite and ammoniojarosite. For instance, the disorder of the hydronium ion is around the principal three-fold roto-inversion axis when considering the highest symmetry model; this particular axis is parallel to the crystallographic **c** axis. Therefore, any structural differences between the hydronium ion and ammonium ion due to hydrogen bonding will have a greater affect upon the **c** axis than the **a** and **b** axes.

As a result of the work reported in this thesis, three pertinent structural effects of the hydronium and ammonium ions in jarosite minerals can be stated:

- Hydronium and ammonium ions are both orientationally disordered with numerous orientations available in the unit cell of the jarosite structure. However, many of these orientations are beyond the resolution of neutron powder diffraction.

- Hydronium and ammonium ions do not destroy the three-fold roto-inversion axis of the jarosite structure when temporally averaged. However, considering the hydronium and ammonium ions locally and at a finite point in time, it is destroyed.

- Hydronium and ammonium ions are hydrogen bonded to hydroxyl groups. However, this interaction is more significant in hydronium jarosite such that it is a spin glass at low temperature due to more perturbed hydroxyl groups.

8.3 IMPLICATIONS

The improved symmetry analysis presented in this thesis is in agreement with the theoretically calculated number of modes for crystals, which is based on the number of atoms (N_B) in the Bravais unit cell ($3N_B - 3$). This is the major attraction and advantage of this method: it is based in reality on an immutable physical law and has no seemingly arbitrary assumptions underpinning it. It can be easily extended to other similarly disordered systems, i.e. orientationally disordered non-linear molecules in an ordered crystal. For example, it not only predicts the normal modes of hydronium and ammonium end-members in the rhombohedral zirconium alkali metal orthophosphates family, often called the sodium super ionic conductors (NASICON), it determines their true structure at a finite point in time is an entirely different space group to the current literature (Catti and Ibberson 2002; Rudolf *et al.* 1985).

NASICON materials can be described by the general formula $A^{I}M^{IV}{}_{2}(PO_4)_3$ where A is a monovalent cation and M^{IV} is an octahedrally coordinated tetravalent transition metal (Alamo 1993). In general, the crystal structure is defined by space group $R\bar{3}c$ (no. 167) with $Z = 6$ (Alamo 1993; Kurazhkovskaya *et al.* 2000; Tarte *et al.* 1986). The structure is built up of vertex-sharing ZrO_6 octahedra and PO_4 tetrahedra. The A site, like jarosite materials, is best described as a cavity and is surrounded by oxygen atoms. Hydronium and ammonium NASICON can be prepared, and both hydronium and ammonium ions are disordered across two orientations at the $\bar{3}$ (S_6) site while the hydrogen atoms are fractionally occupied at a 1 (C_1) site (Catti and Ibberson 2002; Rudolf *et al.* 1985). A similar problem to hydronium and ammonium jarosite arises for hydronium and ammonium NASICON: the observed S_6 site symmetry is not a subgroup of C_{3v} or T_d molecular symmetries. Factor group analysis cannot be performed in the usual way.

The theoretically calculated number of modes for hydronium NASICON and ammonium NASICON are given by:

$$3N_B(H_3O^+) - 3 = 3 \times \left(\frac{21 \times 6}{3}\right) - 3 = 123$$

$$3N_B(NH_4^+) - 3 = 3 \times \left(\frac{22 \times 6}{3}\right) - 3 = 129$$

If one considers the general principles outlined in the preceding chapter, the effective symmetry of only one S_6 orientation can be described by the C_3 point group. The C_3 point group is the site symmetry that results when the coordinates of the S_6 site (0, 0, 0) are displaced in the z direction, and, when the inversion operation is removed from S_6. This displacement to a C_3 site (0, 0, z) ensures the principle molecular and crystallographic three-fold rotation axes are coincident (Jewess 1982). More importantly, the C_3 point group is also a subgroup of both the space group symmetry and the molecular symmetries of hydronium and ammonium. Thus, the highest symmetry local structure at a finite point in time has the hydronium oxygen or ammonium nitrogen atom fractionally occupied (50 %) at a C_3 site, while the hydrogen atoms will remain at the C_1 site. Due to the disorder and subsequent fractional occupancy of the ammonium and hydronium ions, no Davydov splitting is to be expected for ammonium and hydronium internal modes in NASICON materials. Only site symmetry effects are necessary to describe the spectra for hydronium and ammonium vibrations. The factor group analysis and mode determination for hydronium and ammonium in NASICON is now a trivial undertaking. Unfortunately, to the best of the author's knowledge, the vibrational spectra of hydronium and ammonium NASICON have not been reported.

Applying the principles of the new symmetry analysis, the following irreducible representations are calculated:

$$\Gamma_{irred}(H_3O^+) = 8A_{1g} + 9A_{2g} + 8A_{1u} + 8A_{2u} + 17E_g + 16E_u + 4A + 8E$$

Where $\Gamma(H_3O^+) = 4A + 8E$

$$\Gamma_{irred}(NH_4^+) = 8A_{1g} + 9A_{2g} + 8A_{1u} + 8A_{2u} + 17E_g + 16E_u + 5A + 10E$$

Where $\Gamma(NH_4^+) = 5A + 10E$

Clearly the irreducible representations do not agree with the calculated number of modes: 119 modes instead of 123 for hydronium jarosite, and 124 modes instead of 129 for ammoniojarosite. This means the spectroscopic space group of ammonium and hydronium NASICON is not $R\bar{3}c$. The proposed spectroscopic structures are incorrect. It is well known that the spectroscopic space group does not have to be the same as the space group determined from diffraction, particularly if one is only a small distortion of the other. This appears to be the case for hydronium and ammonium NASICON. Indeed, Catti and Ibberson (2002) state that the local structure of hydronium NASICON is possibly monoclinic, similar to the observed low temperature phase ($C2/c$ at 4.5 K). This particular structure is also disordered. The hydronium and ammonium ions are now fractionally occupied at a general (C_1 or 1) site, so no Davydov splitting is expected. The irreducible representations can then be calculated, giving:

$$\Gamma_{irred}(H_3O^+) = 28A_g + 29B_g + 27A_u + 27B_u + 12A$$

Where $\Gamma(H_3O^+) = 12A$

$$\Gamma_{irred}(NH_4^+) = 28A_g + 29B_g + 27A_u + 27B_u + 15A$$

Where $\Gamma(NH_4^+) = 15A$

The calculated numbers of modes are in agreement with the symmetry analysis. The proposed spectroscopic space group is correct. The only difference this time being that the spectroscopic space group was different to the diffraction space group (step 1 of the procedure). The other steps of the procedure were applied: C_1 is a subgroup of both molecular symmetries T_d and C_{3v}, and the space group $C2/c$ (C_{2h}^6); and this C_1 site results in fractional occupancy so no Davydov splitting is expected.

The implication of this improved symmetry analysis is profound: it can detect when a seemingly reasonable disordered structure is correct or incorrect for *spectroscopic purposes*, i.e. the local structure at a finite point in time. What it cannot do is determine the correct structure or space group *ab initio* for spectroscopic purposes: it is a method to *verify* a proposed structure when orientational disorder of a non-linear molecule is present or suspected. The tenant of this theory is that a normal mode determination must agree with the expected normal modes of a crystal, namely, the $3N_B - 3$ rule. If a normal mode determination of a structure modelled from diffraction does not agree with this rule, the true local structure at a finite point in time must be different. This is due to the structural averaging inherent in diffraction techniques where such distortions can be "mopped up" by the atomic displacement parameters; or, refinement in the lower symmetry structure is not possible due to instrumental resolution limitations, a poor data to parameter ratio, or simply too many parameters that are highly correlated. The jarosite and NASICON groups are not the only materials that benefit from this method of symmetry analysis: organic molecules, metal-organic framework structures, and extended oxides are frequently disordered. The developed method is a way to rationalise the temporally averaged forbidden symmetry of orientationally disordered molecules with the local symmetry at a finite point in time.

The improved symmetry analysis, and the work contained in this thesis, shows that vibrational spectroscopy and factor group analysis should never be overlooked for structure determination, as they are sensitive to true local distortions. Indeed, it clearly highlights that diffraction and spectroscopic techniques although sensitive to the structure of crystals, are not necessarily complementary and may give different results when orientational disorder is present. Mitigating orientational disorder is complex, and no two situations are the same (hydronium jarosite and hydronium NASICON for instance): each situation needs to be addressed on a case by case basis. It is only when both methods of analysis are analysed in tandem that an accurate picture of disorder can be painted.

8.4 FUTURE WORK

There are numerous unresolved questions surrounding the jarosite group of minerals which could be investigated further (see Chapter 2). However, the following areas are directly related to the work presented in this thesis and are recommended for future investigation. Note that alunite analogues would be appropriate for all these suggested studies as jarosite and alunite minerals are isostructural. This thesis has shown that hydronium jarosite and ammoniojarosite should be investigated in tandem owing to their similar but also unique properties.

1. *An ammoniojarosite (^{1}H and ^{2}H) nuclear magnetic resonance study*

All NMR studies of alunite supergroup minerals have been concerned with the analysis of hydronium end members in comparison to potassium (jarosite) and sodium (natrojarosite) end members (Nielsen *et al.* 2008; Nielsen *et al.* 2011; Ripmeester *et al.* 1986). It is suggested that ammoniojarosite should be studied by NMR and compared to hydronium jarosite as the $^{1}H/^{2}H$ environments are well known in jarosite and natrojarosite. Such a study would allow for the activation energy of motion for the ammonium ion in jarosite minerals to be determined.

2. *A single crystal Raman spectroscopic study of hydronium jarosite compared to jarosite*

An oriented single crystal Raman study under various polarisation regimes would give definitive proof of whether the symmetry analysis presented in Chapter 7 is adequate. The question of whether a fractionally occupied orientationally disordered molecule, such as hydronium and ammonium in jarosites, is actually affected by the orientation of its crystal is not extensively studied, with the author only finding one

example in the literature (Auglló-Rueda *et al.* 1988). In addition, bands in the Raman and infrared spectra of jarosite minerals have not been assigned according to their symmetry species. The assignment of bands according to their symmetry species can help clarify band identification. This is necessary for jarosite minerals in the low wavenumber region. For instance, $\nu_2(SO_4)$ is an E_g mode and should be visible under cross polarisation. The main problem of a single crystal Raman study would be the synthesis of suitable (euhedral and easily indexed) single crystals, and whether the ammonium and hydronium bands would be detected under the various polarisation regimes. The most suitable bands to use for this study would be $\nu_4(H_3O^+)$ at 1580 cm^{-1} and the various ammonium N–H stretching bands at ~3200 cm^{-1} as other vibrations due to ammonium and hydronium are not readily observed and very weak.

3. *A low temperature and isotopically dilute deuterated hydronium jarosite and ammoniojarosite MIR study*

A low temperature MIR study of hydronium jarosite and ammoniojarosite would serve as a complement to the low temperature Raman study presented in this thesis. Hydronium and ammonium vibrations are stronger in the MIR than Raman, and different/additional bands may be visible at low temperature. Low temperature MIR spectroscopic studies of isotopically dilute ions can help determine the disordered ion's symmetry (Oxton *et al.* 1976). Isotopically dilute deuterated hydronium jarosite and ammoniojarosite, to the best of the author's knowledge, have not been studied. By isotopically dilute, it is meant that a small proportion of the A site is populated, taking hydronium jarosite for example, by DH_2O^+ or D_2HO^+ instead of D_3O^+/H_3O^+. Due to the different molecular symmetries of the dilute ions, at low temperature in the MIR different splitting patterns of bands is observed when compared to the fully deuterated/protonated ions. The observed splitting can be correlated to the symmetry of the isotopically dilute

ion, and thus, the symmetry of H_3O^+ and NH_4^+ can be determined as this symmetry must be a subgroup of the dilute ion's symmetry and the site symmetry.

4. *A single crystal neutron diffraction study of hydronium jarosite and ammoniojarosite*

Single crystal diffraction offers data in three dimensions, compared to only two dimensions from powder diffraction; it can be said that loss of data is inherent to the powder diffraction technique. Fourier maps generated from powder data are more diffuse than those from single crystal data. Thus, the question of whether a contour corresponds to a real missing atom or to misfit of the model is more ambiguous as more atoms are found by difference Fourier methods. Difference Fourier maps are also model biased, and even more so from powder data as both the phases and intensity portioning are determined from the model (McCusker *et al.* 1999). This is one reason why the simplest, highest symmetry model, i.e. the model of minimal assumption that explains all data was chosen by the author in Chapters 5 and 6.

A single crystal neutron diffraction study of both hydronium jarosite and ammoniojarosite at various temperatures would offer a more complete description of their crystal structures than what can be determined from powder neutron diffraction. Neutron techniques are more sensitive to ^1H and ^2H and would offer additional information than what can be obtained from single crystal X-ray diffraction. However, to achieve this aim, significant research effort would have to be devoted to the synthesis of adequately sized single crystals (mm dimensions at least) owing to the low flux of neutron diffraction techniques and the small crystal sizes obtained from current jarosite single crystal syntheses. The tendency for jarosite minerals to form powders and small single crystals has vexed many a jarosite researcher, including this one.

5. *An IINS study of hydronium jarosite and ammoniojarosite in comparison to jarosite*

Although the only previous IINS study of hydronium alunite in comparison to alunite was largely inconclusive with respect to any structural effect of the hydronium ion (Lager *et al.* 2001), this work did not also study ammonioalunite. A thorough IINS study of these three minerals, across a wide range of temperatures, should allow for the determination of the degree of band narrowing as a function of temperature, and may offer more insight into the disorder mechanism than a similar vibrational spectroscopic study.

6. *A detailed vibrational spectroscopic study of hydronium NASICON and ammonium NASICON in comparison to sodium NASICON.*

Vibrational spectra for hydronium NASICON and ammonium NASICON have not been reported. In addition, this particular group of materials represents an ideal case study for further confirmation of the symmetry analysis procedure presented in this thesis. Raman and MIR spectra collected at both ambient and low temperature of ^{1}H and ^{2}H forms of hydronium NASICON and ammonium NASICON in comparison to sodium NASICON will allow for accurate band assignment. A single crystal study would be ideal. This is because the polarisability tensors of the A_{1g} and E_g modes in factor group D_{3d} are very different to the tensors of A_g and B_g modes in factor group C_{2h} (Turrell 1972):

$$A_{1g} = \begin{pmatrix} a & & \\ & a & \\ & & b \end{pmatrix} \qquad E_g = \begin{pmatrix} c & -c & -d \\ -c & -c & d \\ -d & d & \end{pmatrix}$$

$$A_g = \begin{pmatrix} a & & d \\ & b & \\ d & & c \end{pmatrix} \qquad B_g = \begin{pmatrix} & e & \\ e & & f \\ & f & \end{pmatrix}$$

In addition, more modes in total are expected for C_{2h}. Since $\nu_1(PO_4)$ splits to $1A_{1g}$ + $1E_g$ (D_{3d}) or $2A_g$ + $1B_g$ (C_{2h}), the splitting and tensors of this mode alone should determine the factor group.

8.5 REFERENCES

Alamo, J., 1993: Chemistry and properties of solids with the [NZP] skeleton. *Solid State Ionics*, **63-65,** 547-561.

Auglló-Rueda, F., J. M. Calleja, and J. Bartolomé, 1988: Raman spectroscopy of the ammonium ion in NH_4MnF_3 and NH_4ZnF_3 perovskites: temperature dependence. *J. Phys. C.*, **21,** 1287-1297.

Bisson, W. G., and A. S. Wills, 2008: Anisotropy-driven spin glass transition in the kagome antiferromagnet hydronium jarosite, $(H_3O)Fe_3(SO_4)_2(OH)_6$. *J. Phys.: Condens. Matter*, **20,** 452204.

Catti, M., and R. M. Ibberson, 2002: Order-disorder of the hydronium ion and low-temperature phase transition of $(H_3O)Zr_2(PO_4)_3$ NASICON by neutron diffraction. *J. Phys. Chem. B.*, **106,** 11916-11921.

Grohol, D., and D. G. Nocera, 2007: Magnetic disorder in the frustrated antiferromagnet jarosite arising from the H_3O^+•••OH^- interaction. *Chem. Mater.*, **19,** 3061-3066.

Jewess, M., 1982: A theoretical treatment of 'orientational' disorder for routine use. *Acta Cryst.*, **B38,** 1418-1422.

Kurazhkovskaya, V. S., A. I. Orlova, V. I. Petkov, D. V. Kemenov, and L. N. Kaplunnik, 2000: IR study of the structure of rhombohedral zirconium and alkali metal orthophosphates. *J. Struct. Chem.*, **41,** 61-66.

Lager, G. A., G. A. Swayze, C.-K. Loong, F. J. Rotella, J. W. Richardson Jr, and R. E. Stoffregen, 2001: Neutron spectroscopic study of synthetic alunite and oxonium-substituted alunite. *Can. Mineral.*, **39,** 1131-1138.

McCusker, L. B., R. B. von Dreele, D. E. Cox, D. Louër, and P. Scardi, 1999: Rietveld refinement guidelines. *J. Appl. Cryst.*, **32,** 36-50.

Nielsen, U. G., J. Majzlan, and C. P. Grey, 2008: Determination and quantification of the local environments in stoichiometric and defect jarosite by solid-state ^{2}H NMR spectroscopy. *Chem. Mater.*, **20,** 2234-2241.

Nielsen, U. G., I. Heinmaa, A. Samoson, J. Majzlan, and C. P. Grey, 2011: Insight into the local magnetic environments and deuteron mobility in jarosite ($AFe_2(SO_4)_2(OD,OD_2)_6$, A = K, Na, D_3O) and hydronium alunite ($(D_3O)Al_3(SO_4)_2(OD)_6$), from variable-temperature ^{2}H MAS NMR spectroscopy. *Chem. Mater.*, **23,** 3176-3187.

Oxton, I. A., O. Knop, and M. Falk, 1976: Determination of the symmetry of the ammonium ion in crystals from the infrared spectra of the isotopically dilute NH_3D^+ species. *J. Phys. Chem.* , **80,** 1212-1217.

Ripmeester, J. A., C. I. Ratcliffe, J. E. Dutrizac, and J. L. Jambor, 1986: Hydronium ion in the alunite-jarosite group. *Can. Mineral.*, **24,** 435-447.

Rudolf, P. R., M. A. Subramanian, A. Clearfield, and J. D. Jorgensen, 1985: The crystal structures of the ion conductors $(NH_4^+)Zr_2(PO_4)_3$ and $(H_3O^+)Zr_2(PO_4)_3$. *Solid State Ionics*, **17,** 337-342.

Tarte, P., A. Rulmont, and C. Merckaert-Ansav, 1986: Vibrational spectrum of nasicon-like, rhombohedral orthophosphates $M^IM_2^{IV}(PO_4)_3$. *Spectrochim. Acta*, **A42,** 1009-1016.

Turrell, G., 1972: *Infrared and Raman spectra of crystals.* Academic Press.

Wills, A. S., 2001: Conventional and unconventional orderings in the jarosites. *Can. J. Phys.*, **79,** 1501-1510.